To Develop Techniques that will Enhance Dermal Cell and Tissue Attachment in Order to Create a Seal and Prevent Infection of Implant Biomaterials used for ITAP

Robert Peter Dowling

Submitted for the degree of Doctorate of Philosophy

Department of Biomedical Engineering
University College London

May 2014

John Scales Centre for Biomedical Engineering
Institute of Orthopaedics and Musculoskeletal Science
University College London
Royal National Orthopaedic Hospital
Brockley Hill, Stanmore
Middlesex HA7 4LP

I, Robert Peter Dowling, confirm that the work presented in this thesis is my own. Where information has been obtained from other sources, they have been duly referenced.

Contents

Chapter 3- Understanding of the

Loading and Release Kinetics of Biological Functionalisation of Titanium Alloy Substrates, *in vitro*

Chapter 4- Optimal

Abstract

Failure modalities of bone anchoring and skin penetrating devices, such as Intraosseous Transcutaneous Amputation Prosthesis (ITAP), stem from the lack of dermal cell and tissue attachment at the skin implant interface. As a result the implant shaft offers a direct route for harmful pathogens into the body. The aim of my thesis is to develop techniques that will enhance dermal cell and tissue attachment, in order to create a tight biological seal of implant biomaterials currently used for ITAP.

I compared the effects of fibronectin against its cell binding region- a 3-amino-acid region know as Arginine-Glycine-Aspartic Acid (RGD)- on human dermal fibroblast (HDF) attachment to ITAP substrates. Silanization of RGD-polypeptides provided a durable biological functionalisation technique that significantly increased HDF attachment compared with controls. No significant difference was observed between fibronectin and RGD-polypeptide functionalised substrates *in vitro.*

I then investigated the effects of porosity (as a function of pore and strut diameter) on soft fibrosis tissue in-growth and vascularisation. Electron Beam Manufacturing (EBM) provided an effective method of creating precise 3-dimensional porous structures. Porosity as a function of pore and strut diameter led to optimal soft fibrosis tissue in-growth with 700μm pore and 300μm strut diameters exhibiting significantly increased vascularisation over other implants groups after 4 weeks *in vivo*.

The development of these functionalisation techniques, which utilised porous structures and silanization of RGD sequences, were combined and applied to the ITAP device. An EBM porous flange, of 700μm pore and 300μm strut diameters, were silanised with RGD-polypeptide and compared with the current clinical standard ITAP device. Implants were tested in a trans-tibial, transcutaneous ovine model for 5-months. Functionalisation techniques employed in this study did not eradicate the failure modalities of ITAP devices,

however they did not detrimentally affect the formation of a stable transcutaneous interface compared with current clinical standards. Significant positive effects were observed, with the biological functionalisation, using silanised RGD-polypeptides, significantly increasing dermal tissue infiltration and porous structures, manufactured by EBM, significantly increasing vascularisation.

Functionalisation with silanised RGD-polypeptides to porous structures may provide an opportunity to enhance the skin implant interface and tight biological seal for bone anchoring and skin penetrating devices, such as ITAP, clinically.

Acknowledgement

I would like to express my sincere gratitude to Professor Gordon Blunn for the opportunity to be a part of his world-leading department over the last four years. His belief in me has given me huge confidence.

I would also like to thank Dr Catherine Pendegrass (AKA Sheels) for her tireless support, patience, high standards and sense of humour throughout my time at UCL. Sheels, it has been a wonderful experience learning from you, your zeal for life is truly infectious. Thank you for all your help!

Thank you to all my colleagues, past and present, in BME and IOMS. Special gratitude must go to; Gill for her help in animal husbandry, Henry for his wide ranging discussions, Josie for her kindness, Keith for his colourful language and engineering knowledge, Mukai for her clinical know-how, Rebecca for her expertise in cell culture and Yazan for his positive outlooks on all matters science. I wish you all success with your own endeavours.

On a personal level this thesis is the summation of my academic education, from school through to university. This point would have been unattainable without the love and support of my parents. I am truly grateful for everything they have done for me. Mum, Dad; thank you for being there when it has mattered most.

To Mum and Dad

List of Figures

	hophysiology-Of-Healing.html
Fig 1.06.	Schematic representation of Amniopropylated substrates. 1) Implant substrates. 2) Coupling of 3-aminopropyl-triethooxysiane (APTES) containing saline complex to the substrate. 3) Coupling glutaraldehyde to saline complex. 4) Covalent bond formation between a functional group and spacer complex.
Fig 1.07.	Schematic representation of the outline of my thesis.
Fig 2.01.	Box and Whisker plot demonstrating FA Density on adsorbed (green) RGD polypeptide functionalised titanium alloy substrates compared with controls (red) at 24 hours.
Fig 2.02.	Box and Whisker plot demonstrating FA Density on silanised Linear (dark green) and silanised Cyclic (light green) RGD functionalised titanium alloy substrates compared with controls (red) at 24 hours.
Fig 2.03.	Box and Whisker plot demonstrating FA Density on adsorbed (green) and silanised (yellow) RGD functionalised titanium alloy substrates, adsorbed (blue) and silanised (purple) fibronectin functionalised

	titanium alloy substrates compared with controls (red) at 24 hours.
Fig 2.04.	Box and Whisker plot demonstrating HDF attachment on adsorbed RGD functionalised titanium alloy substrates (green) compared with controls (red) at 24 hours.
Fig 2.05.	Box and Whisker plot demonstrating HFD attachment on adsorbed (green) and silanised (yellow) RGD functionalised surfaces, adsorbed (blue) and silanised (purple) fibronectin functionalised titanium alloy substrates compared with controls (red) at 1-hour.
Fig 2.06.	Box and Whisker plot demonstrating HDF attachment on adsorbed (green) and silanised (yellow) RGD functionalised titanium alloy substrates, adsorbed (blue) and silanised (purple) fibronectin functionalised titanium alloy substrates compared with controls (red) at 4-hours.
Fig 2.07.	Box and Whisker plot demonstrating HDF attachment on adsorbed (green) and silanised (yellow) RGD functionalised titanium alloy substrates, adsorbed (blue) and silanised (purple) fibronectin functionalised titanium alloy substrates

	compared with controls (red) at 24-hours.
Fig 2.08.	Box and Whisker plot demonstrating HDF attachment on adsorbed (green) and silanised (yellow) RGD functionalised titanium alloy substrates, adsorbed (blue) and silanised (purple) fibronectin functionalised titanium alloy substrates compared with controls (red) at 96-hours.
Fig 2.09.	Fig 2.09. Immunolocalisation of vinculin in HDFs attached to titanium alloy substrates at 4-hours; A) image: Control, B) Functionalised with adsorbed RGD-polypeptide.
Fig 2.10.	Immunolocalisation of vinculin in HDFs attached to titanium alloy substrates at 24-hours. A) Control. B) Functionalised with adsorbed RGD-polypeptide.
Fig 2.11.	Immunolocalisation of vinculin in HDFs attached to titanium alloy substrates at 24-hours. A) Control. B) Functionalised with adsorbed RGD-polypeptide.
Fig 3.01.	Schematic representation of the silanization reaction. Taken from http://www.intechopen.com/books/nanowires-implementations-and-applications/organic-surface-modification-of-silicon-

	nanowire-based-sensor-devices
Fig 3.02.	Box and Whisker plot demonstrating FA Density on adsorbed Linear (green) RGD functionalised titanium alloy substrates compared with controls (red) at 24 hours.
Fig 3.03.	Calibration curve for I^{125}YRGD in Counts per Million (CPM)
Fig 3.04.	Calibration curve for I^{125}fibronectin in Counts per Million (CPM)
Fig 3.05.	Box and Whisker plot of changes in concentration of I^{125}YRGD-polypetptides remaining adsorbed to titanium alloy substrates with increasing concentrations of I^{125}YRGD-polypeptides.
Fig 3.06.	Box and Whisker plot of changes in concentration of I^{125}YRGD-polypeptides remaining silanised to titanium alloy substrates with increasing concentrations of I^{125}YRGD-polypeptides
Fig 3.07.	Box and Whisker plot of changes in amount of I^{125}fibronectin remaining silanised to titanium alloy substrates with increasing amounts of I^{125}fibronectin.
Fig 3.08.	Box and Whisker plot of changes in concentration of silanised (yellow) and adsorbed (green) I^{125}YRGD functionalised titanium alloy

	substrates were washed in PBS after 5mins, 2, 20 and 140 hours.
Fig 3.08.	Box and Whisker plot of changes in concentration of silanised (purple) and adsorbed (blue) I^{125}fibronectin functionalised titanium alloy substrates were washed in PBS after 5mins, 2, 20 and 140 hours.
Fig 3.10.	Box and Whisker plot of changes in concentration of silanised (yellow) and adsorbed (green) I^{125}YRGD functionalised titanium alloy substrates when soaked in FCS for 5mins, 2, 20 and 140-hours.
Fig 3.11.	Box and Whisker plot of changes in concentration of silanised (purple) and adsorbed (blue) I^{125}fibronectin functionalised titanium alloy substrates when soaked in FCS for 5mins, 2, 20 and 140-hours.
Fig 3.12.	Box and Whisker plot of changes in concentration of silanised (yellow) and adsorbed (green) I^{125}YRGD functionalised titanium alloy substrates when soaked in PBS for 5mins, 2, 20 and 140-hours.
Fig 3.13.	Box and Whisker plot of changes in concentration of silanised (purple) and adsorbed (blue)

	infiltration of each porous implant group from Zone 2.
Fig 4.06.	Box plot demonstrating the percentage of tissue infiltration of each porous implant group from inner most zone, Zone 3.
Fig 4.07.	Box plot demonstrating the cell nuclei density/mm^2 of each porous implant group from the outer most zone, Zone 1.
Fig 4.08.	Box plot demonstrating the number of cell nuclei density/mm^2 of each porous implant group from Zone 2.
Fig 4.09.	Box plot demonstrating the number of cell nuclei density/mm^2 of each porous implant group from inner most zone, Zone 3.
Fig 4.10.	Box plot demonstrating the blood vessels density/mm^2 of each porous implant group from outer most zone, Zone 1.
Fig 4.11.	Box plot demonstrating the blood vessels density/mm^2 of each porous implant group from Zone 2.
Fig 4.12.	Box plot demonstrating the blood vessels density/mm^2 of each porous implant group from inner most zone, Zone 3
Fig 4.13.	Light microscopy image sections stained with Toluidine blue of a Group 4 implant at Zone 1. High magnification image of dense, well-ordered soft

	tissue infiltration.
Fig 4.14.	Light microscopy image sections stained with Toluidine blue of a Group 4 implant at Zone 1. High magnification image of dense, well-ordered soft tissue infiltration.
Fig 4.15.	Light microscopy image sections stained with Toluidine blue of a Group 1 implant at Zone 2. High magnification image of dense, well-ordered soft tissue infiltration with intimate contact (arrows) between pore edge and soft tissues.
Fig 4.16.	Light microscopy image sections stained with Toluidine blue of a Group 2 implant at Zone 3. Low magnification imagine of dense, well-ordered soft tissue preferentially depositing collagen around interconnecting struts (arrows).
Fig 4.17.	Light microscopy image sections stained with Toluidine blue of a Group 3 implant at Zone 1. Dense, well-ordered soft tissue, preferentially depositing collagen around interconnecting struts (arrows) with distinct cell nuclei populating the implant pore.
Fig 4.18.	Light microscopy image sections stained with

	Toluidine blue of a Group 4 implant at Zone 1. High magnification image of dense, well ordered soft tissue with extensive blood vessel formation (arrows).
Fig 4.19.	Light microscopy image sections stained with Toluidine blue of a Group 7 implant at Zone 2. High magnification image of less dense soft tissue with poor contact (arrows) between pore edge and soft tissues.
Fig 4.20.	Light microscopy image sections stained with Toluidine blue of a Group 7 implant at Zone 1. Low magnification image of less dense soft tissues with poor contact (arrows) between pore edge and soft tissues.
Fig 5.01.	Functionaliseed Implant Groups; A) Flange Control at intra-operative, B) Flanged RGD pre-silanization, C) Porous Control intra-operative (Right), Porous RGD at intra-operative (Left) and D) Porous RGD pre-silanization.
Fig 5.02.	Box and Whisker plot demonstrating the length of Downgrowth (μm) for functionalised ITAP flanges by drilling (red), drilling and silanised with RGD-polypeptides (green), porous (blue) and porous silanised

	with RGD-polypeptide (yellow).
Fig 5.03.	Box and Whisker plot demonstrating the percentage of Epidermal Attachment for functionalised ITAP flanges by drilling (red), drilling and silanised with RGD-polypeptides (green), porous (blue) and porous silanised with RGD-polypeptide (yellow).
Fig 5.04.	Box and Whisker plot demonstrating the blood vessel density of soft tissue with functionalised ITAP flanges by drilling (red), drilling and silanised with RGD-polypeptides (green), porous (blue) and porous silanised with RGD-polypeptide (yellow).
Fig 5.05.	Box and Whisker plot demonstrating cell nuclei density of soft tissue with functionalised ITAP flanges by drilling (red), drilling and silanised with RGD-polypeptides (green), porous (blue) and porous silanised with RGD-polypeptide (yellow).
Fig 5.06.	Box and Whisker plot demonstrating percentage of dermal tissue infiltration with functionalised ITAP flanges by drilling (red), drilling and silanised with RGD-polypeptides (green), porous (blue) and porous silanised

	with RGD-polypeptide (yellow).
Fig 5.07.	Light microscopy image of a transcutaneous section stained with Toluidine blue of a Group 4 implant at Zone 1. Low magnification image of epidermal downgrowth and sinus track formation along the implant shaft (arrows).
Fig 5.08.	Light microscopy image of a transcutaneous section stained with Toluidine blue of a Group 4 implant at Zone 1. Low magnification image of wound debris impeding epidermal attachment, forcing the cell sheet underneath the blockage before interfacing with the implant.
Fig 5.09.	Light microscopy image of a transcutaneous section stained with Toluidine blue of a Group 3 implant. Low magnification image of epidermal attachment, with limited downgrowth.
Fig 5.10.	Light microscopy image (split in two) of a transcutaneous section stained with Toluidine blue of a Group 1 implant. Low magnification image of epidermal attachment taking place at the flange (red arrows).
Fig 5.11.	Light microscopy image of a transcutaneous section stained with Toluidine blue of a Group 4 implant. Low

	magnification image of dermal tissue infiltration within a porous flange.
Fig 5.12.	Light microscopy image of a Group 3 transcutaneous section stained with Toluidine blue. High magnification image of dense, well-ordered dermal tissue with a number of blood vessels formed within a pore.
Fig 5.13.	Light microscopy image of a Group 4 transcutaneous section stained with Toluidine blue. High magnification image of dense, well-ordered dermal tissue with a number of blood vessels formed within a pore.
Fig. 5.14.	Light microscopy image of a transcutaneous section stained with Toluidine blue of a Group 1 implant. Low magnification image of dermal tissue infiltration within a drilled flange, poor contact at dermal tissue implant interface (red arrow).
Fig 6.01.	PerFiTS device (Percutaneous Fixation To Skeleton) courtesy of Fitzbionics (Patents PCT/GB2013/052639 and 1317782.9).

List of Tables

Chapter 1- The Introduction

Chapter 1

1.1- Thesis Outline

I intend to review the background literature and current knowledge to develop relevant research questions around a research theme associated with improving the soft tissue interface adjacent to intraosseous transcutaneous amputation prostheses (ITAP). As a result I have developed the following research hypothesis: Soft tissue attachment to ITAP devices will be improved by functionalisation, using a protein coated porous implant, compared with surfaces that are currently used for ITAP. I have investigated this hypothesis in a series of experimental chapters aligned to specific research questions. The outline of my thesis is presented below.

Chapter 1- The Introduction

This chapter aims to review the overall subject area of bone anchored transcutaneous implant biomaterials, from a clinical standpoint through to biomedical engineering techniques designed to enhance tissue attachment through to new areas such as innervated prostheses, which may well become more of a possibility once a reproducible and long lasting transcutaneous device can be engineered. From reviewing the literature I will present my thesis aim and general hypothesis and relevant research questions, which will be experimentally tested and explored in the following chapters. A schematic diagram showing these questions is shown at the end of the introduction in Figure 1.06.

Chapter 2- Enhancement of Human Fibroblast Attachment Using RGD-polypeptide and Fibronectin Coatings.

This chapter aims to compare the effects of the synthetic Arg-Gly-Asp (RGD)-polypeptides and fibronectin coatings on human dermal fibroblast (HDF) attachment strength *in vitro*. In this chapter the development of a functionalisation technique involving surface modification of titanium alloy that affects the attachment of HDF will be investigated.

Chapter 3- Optimal Chemical Covalent Attachment of Fibronectin and RGD-polypeptide coatings.

This chapter aims to develop a full understanding of the loading and release kinetics of linear RGD-polypeptides compared with fibronectin on titanium alloy substrates, using adsorbed and covalently attached moieties. A methodology to create a durable and robust biologically active functionalisation technique that ultimately increases HDF attachment to titanium alloy substrates *in vitro* will be investigated.

Chapter 4- Optimal Structure of Porous Implants for Soft Tissue Integration into ITAP.

This chapter aims to determine the effect of porous structures for an ITAP device by varying the pore and strut sizes and assessing tissue infiltration and vascularisation throughout the implant, *in vivo.*

Chapter 5- Functionalisation of the ITAP Flange *in vivo.*

This chapter aims to biologically functionalise a porous ITAP device based on information learnt in previous chapters and to limit epithelial downgrowth and create a tight biological seal between the dermal and epidermal tissues with the implant biomaterial.

Chapter 6- General Discussion.

This chapter will discuss the results of the thesis in its entirety and relate the findings to the wider setting of bone-anchored transcutaneous devices for clinical use.

1.2- Background

1.2i- Amputation

The word amputate' originates from the Latin L. *amputates,* pp of amputare literally meaning to "cut off" or "to prune" (Compact Oxford English Dictionary 2005). Amputation can be a treatment for traumatic injury, infection, vascular disease, cancer and congenital defects. Surgical dismemberment of the diseased limb or extremity removes the affliction, permanently (Branemark et al. 2001).

Between 1997 and 2007 there have been, on average, 5,456 new amputation referrals to prosthetic service centres per annum in the United Kingdom. By gender, two thirds of all new referrals were male. As a function of time, figures remained constant. Of these new referrals, the vast majority of amputations were lower limb, mostly at either the trans-tibial or trans-femoral level (Luff, 2007). The epidemiology surrounding amputation is difficult, as there are many factors to consider. Data can come from a variety of sources, which may be dependent on the type, level of resection or reason for amputation. The above referral figures fit in to the incidence figures for amputation published in 2000 for Europe, North America and East Asia of 2.8-43.9 per 100,000 individuals (GLEASG 2000). Recent war-zones in Iraq and Afghanistan have attributed to an increase in traumatic amputation of limbs. UK forces personnel have suffered over 250 amputations between 2006-2011. US forces suffered 1,407 traumatic limb amputations during the Iraq war and in Afghanistan from the beginning of the conflict to September 2010 (Wallace, 2012). These figures suggest amputation is a considerable health burden.

1.2ii- Conventional Treatment

Current treatments for amputation use prosthetic devices that work on a modular suspension system, where a cup or socket fits over the residual stump. The prosthetic limb and cup articulates using an exoskeleton for support (Lyon et al 2000).

Modern materials and cutting edge techniques have led to the use of highly sophisticated artificial prosthetic limbs which are benefiting amputees but still rely on external fixation of cups or sockets around the stump (Thurston, 2007).

The motion of lower limb endoprosthetic joints, have been subject to much research, in an attempt to mimic the mechanisms of normal limb form and function. Load bearing applications continue to be problematic as the finite control of lower limb prostheses appears difficult to achieve, despite advances in weight, cosmetic design and appeal (Cochrane et al 2001).

The principles of prosthetic treatment that forms the basis of design today are routed in the past (Thurston, 2007). Malone et al. (1981) suggested that a multi-faceted approach from the time of surgery could increase rehabilitation rates, decrease morbidity and mortality rates making lower limb amputation a successful treatment option. Despite this approach, Lyon et al. (2000) indicated the importance of the integrity of the skin on the stump of amputees as a critical factor.

1.2iii- Problems Implicated by Conventional Treatment

The stump-socket interface is the site of many of the problems associated with conventional stump-socket designs. It has been reported that 40.7% of lower extremity amputees tested suffered from a dermatological condition of the stump (Dudek et al 2005).

DesGroseiliers et al. (1978) and Lyon et al. (2000) agree that the importance of dermatological conditions of the stump is paramount for a successful amputation, however problems with the soft tissues account for 34% of all complications. Specific dermatological conditions in these studies ranged in both diagnosis and extent. There was high prevalence of contact dermatitis, resulting from both chemical and physical stimuli (Koc et al 2008), callus, ulcer formation, keloid scarring, epidermoid cyst formation and bacterial infections (DesGroseilliers et al 1978, Dudek et al 2005, Koc et al 2008 and Lyon et al 2000).

The catalyst for many problems associated with these conventional treatments stem from the level of locomotion. Factors namely the fit of prosthetic device, alignment between the stump and prosthesis, anatomy of the stump, age of amputee and position of level of resection all relate to dermatological conditions. The severity of which are dependent upon the level of activity of the user.

The stump is made up of soft tissue with underlying bone. Irregularities in pressure distribution are exacerbated during locomotion compared to low or no levels of locomotion. The soft tissues of the stump are not designed to tolerate such pressures. This can cause focal point trauma in the soft tissue of the stump from pointed calcified osteophytes outcropping from the residual bone (Dudek et al 2005 and Portnoy et al 2009).

Koc et al. (2008) found that 73.9% of participants presented with at least a single dermatological condition of the residuum. Reasons for this high prevalence of dermatological issues (Dudex et al 2005, Lyon et al 2000) were found in young, active patients. An increase in activity can therefore increase the likelihood of skin complications associated with the stump socket interface.

Pressure to the anatomy of the soft tissue surrounding the stump can impact on the vascular and lymphatic flow, further compromising the stumps health (Levy, 1980). If the skin becomes compromised by a dermatological disorder, however trivial, limb disuse is inevitable. Small lesions to the cutaneous portion of the stump can develop into an extensive disorder. Treatment of these problems, such as relieving the pressure on the soft tissues means protracted period of limb disuse. This not only impacts on the amputee's locomotive ability but also more broadly on work, social and psychological status (Levy, 1956).

A further challenge is one of alignment and subsequent fitting between stump and socket component. Continual changes in size and shape around the stump cause fitting issues for trans-tibial amputees. It has be reported that

users require new sockets for their prosthetic devices every 4-years to account for these changes in soft tissue volume (Portnoy, 2009).

New prosthetic users can experience tissue re-modelling as a result of un-natural pressures. Biopsies of soft tissue from lower extremity amputee's stumps had increased formation of fibrotic tissue (Levy, 1956). This can detrimentally affect the biology of the soft tissues leading to breakdown and tissue remodelling (Le Gros Clark, 1946). Poor fitting of the socket around the stump may lead to strangulation of the soft tissues, starving the skin of a blood supply (Levy, 1956), leading to skin surface Infections, which can be common around the stump. The closed environment becomes warm and humid, conducive for bacterial proliferation and this unnatural environment can disrupt the normal bacterial flora (Kohler et al 1989).

The anatomy of the residual limb is not that of a specialised joint. Dissipated forces that result from load bearing functions adversely affect the health of the stump (Pendegrass et al 2006). Furthermore, all citations make reference to the social, economic and psychological implications of medical complications associated with conventional treatment for amputations (DesGroseilliers et al 1978, Dudek et al 2005, Koc et al 2008 and Lyon et al 2000). These may present in something as apparently simple as the every day problems of fastening or removing prosthesis (Kang et al 2010) or referred pain in contralateral limbs, joints or lower backs during or as a result of ambulation (Pohjolainen et al 1990). These difficulties can translate into significant energy consumption requirement (25-65%- depending on level of lower limb amputation) compared with non-amputees whilst ambulating (Schmalz et al 2002). If a miss-match in alignment exists at the stump-socket interface exists, muscular correction further increases energy consumption, which, intensifies if cadence changes (Schmalz et al 2002).

Top athletes overcome these issues by frequently changing their prosthetic devices to maintain the best possible fit. However, this is not achievable within the general population (Webster et al 2001).

1.2iv- The Proposed Solution

The conventional prosthetic devices are flawed in design because they all conduct and dissipate forces through an unnatural load bearing structure. One author even makes light of the situation, by referencing bionics as the solution to the stump-socket issue (DesGroseilliers et al 1978).

It was suggested by Winter (1974) that a skeletally attached prosthesis could alleviate these issues observed at stump-socket interface. Several research groups have clinical experience in using a bone anchored transcutaneous device that provides a platform for prosthetic attachment (Pitkin, 2013). The crucial feature of these devices allows the user the transfer load through their skeletal system to the prosthesis without undue force on soft tissue of the stump.

Intraosseous Transcutaneous Amputation Prosthesis (ITAP) is a concept where an implantable device anchors into a host's bone and protrudes through the overlaying soft-tissue and skin. If stable fixation is achieved, a solid platform allows the transfer of load from the skeletal system through the ITAP device to a prosthesis, promoting functionality of load bearing activities (Pendegrass et al 2006). Kang et al. (2010) reported clinical usage of ITAP in a two-year follow up study for a trans-humeral amputee. Radiographs suggested stable bone anchorage in the residual humeral medullary canal of the patient. Furthermore, the patient's own account was well documented. The range of motion of the shoulder joint was stated as being comparable to near-normal movements, these accounts were supported by Disabilities of the Arm, Shoulder and Hand (DASH) scores pre and post surgery. No clinical concerns were reported. Fitzpatrick et al. (2011) reported further clinical experience with ITAP implanted into distal limb amputation stumps in dogs. Loading bearing functionality was observed in 4-animal subjects. Stable integration between the implant and skin appeared to form by 3-weeks, which was retrospectively confirmed with histology, post mortem. Authors noted a high degree of dermal fibroblasts and epidermal keratinocytes interacting with the implant, suggesting biological integration.

Branemark and Albrektsson (1982) were the first to use implantation of skin penetrating titanium implants in human subjects. Their results were varied. Where implants were allowed free movement with the skin, histological analysis of the interface and surrounding tissue showed an active inflammatory response. Where implants were stabilised with connective elements on the hypodermis and dermis, no evidence of an inflammatory response was observed. Where implants were anchored into the temporal bone on the lateral aspect of the skull, macroscopically there were no obvious signs of an inflammatory up to a period of 50-months).

Aschoff et al. (2010) (2011) have 10 years of clinical experience of bone-anchored transcutaneous implants. They refer to these implants as the Exo-Endo Prosthesis. In their early attempts, development of hyper-granulation tissue frequently occurred. It was attributed to a rough implant surface at transcutaneous portion. Later designs to the Exo-Endo Prosthesis incorporated a smooth surface finish that has been reported to support a stable soft tissue interface.

A study by Sullivan et al. (2003) assessed clinical performance of 11 trans-femoral amputees who had bone-anchored transcutaneous devices implanted for prosthetic attachment. Their findings, 2 years post implantation, suggested over 80% of recipients had functional implants.

Lundberg et al. (2011) in a study of bone-anchored transcutaneous devices described the effects of functionality on quality on life. Profoundly positive impacts were observed on physical activity, emotional and psychological relationships. However the authors declined to discuss the complications that their patient cohort experienced.

Disrupting the naturally continuous skin with a transcutaneous device compromises the primary function of the skin (Von Recum, 1984). Winter (1974) provided histological evidence of disruption to the natural wound healing process caused by transcutaneous devices. He observed that re-

epithelization of a wound could occur if the structures could support an influx of dermal fibroblast to support wound healing through the structure of the implant. Without such events, the upper layers of the skin would migrate downwards. This migration or marsupilization is a biological attempt to extrude the device and keep the skin continuous (Von Recum, 1984). Such observations have been observed clinically with the use of bone-anchored transcutaneous implant devices (Sullivan et al 2003).

1.2v The Anatomy of the Skin

Bone anchored transcutaneous devices, such as ITAP, do overcome the issues surrounding conventional treatment of amputees (Kang et al 2010). In turn, their use creates a new set of biological complications principally surrounding the natural, dynamic action of the skin and its response to a foreign body (Von Recum, 1984). A detailed understanding of the anatomy and physiology of the human skin may better direct my experimental research in the development of a potential solution to the failure modalities of bone anchored transcutaneous devices.

Collections of solitary cells, similar in morphology are held together in a scaffold, structure known as the extra-cellular matrix (ECM). Soft tissues such as the dermis and epidermis are formed by distinct structures known as cell-cell and cell-matrix junctions. This allows cells to anchor and organise within connective ECM or basement membrane and maintain form and function (Alberts et al 2002 and Lanza et al 2000).

Human skin is an organ that surrounds the entire body, without interruption. At natural openings or orifices it joins seamlessly with mucosal membranes. Skin can be separated into distinct layers, comprising of different cells (Fig 1.01).

The outermost layer, the epidermis, is rich in epidermal keratinocytes, stratified in layers or strata that anchor to a basement membrane, the basal lamina (Fig 1.02). Keratinocytes continually migrate up the strata towards the surface. During this time the cells mature and morph into flatter, a-nucleate

corneocytes and at the upper most strata exuviate from the body. Keratinocytes deposit keratin, a structural protein that assembles into an ECM. This process occurs over a month, maintains structural integrity and provides a physical barrier between the body and outside environment. The epidermis is a stratified layer with distinct molecular components referred to as the epithelium. The well-ordered and organised nature of the keratinocyte cell layer is evident when observing the function performed by human skin. The keratinocytes strata interconnect via cell junctions that physically stabilise the tissue, aid and facilitate communication between neighbouring cells and the ECM. There are various classes of anchoring cellular junctions that comprise of intra and extracellular domains and on interaction form dense molecular plaques (Le Gros Clark, 1946, Gardner and Osburn 1973, Hess and Kirsner 2003, Kanitakis, 2002, Alberts et al 2002 and Lodish et al 2008).

Adherens junctions link neighbouring epidermal keratinocytes on the lateral aspect to the actin cytoskeleton. Transmembranous cadherin proteins project out into the cytoplasm and homodimerise with an adjacent cadherins. Intracellular components anchor each cadherin protein to the actin cytoskeleton. A cadherin/catinin complex forms through the physical interaction between alpha, beta and gamma catinin and vinculin (Albert et al 2002 and Niessen, 2007).

Desmosomal junctions perform cell-cell anchoring roles but to keratin containing intermediate filaments of the cytoskeleton rather than actin filaments. Transmembranous desmosomal cadherins, desmocollin and desmoglien, project into the extracellular space from the lateral aspect of the cell and interact with corresponding projections on adjacent keratinocytes. The extra-cellular domains of both desmosomal and cadherin glycoproteins are highly conserved regions. Dense intracellular plaques anchor cadherin components to keratin elements of the cytoskeleton. These anchoring plaques consist of gamma-catinin (often referred to as plakaglobin) and desmosplakin. The desmosomal homophillic interaction fluctuates between two adhesive states, mediated by Ca^{2+} binding in the extra-cellular domain (Albert et al 2002 and Green and Jones 1996).

Below this thin and avascular layer of the skin lies the thicker and fibrous dermis, separated via a basement membrane, the dermal-epidermal junction (Fig 1.02).

The dermal-epidermal junction compartmentalises the two distinct layers, providing mechanical anchorage and a portal for metabolic communication. In skin epithelia, the junction is referred to the basal lamina in which immature keratinocytes anchor through cell-matrix junctions known as hemidesmosomes. These anchoring cell-matrix junctions link to the keratin elements of tonofilaments in the cytoskeleton, in the same manner as desmosomal junctions.

Hemidesmosomal junctions permit the transmission of tensile strength across the extracellular junction and are thus similar in function to desmosomal junctions, which distribute forces to neighbouring cells. This helps promote an even distribution of trans-cellular tensile force (Alberts et al 2002).

Hemidesmosomes act through a distinct class of cell surface receptors, integrins. Integrins are a distinct group of membrane spanning proteins with separate alpha and beta subunits that heterodimerise during ligand binding. Cytoplasmic plaques of anchoring proteins link the intracellular portion of the beta subunit of the integrin protein receptor with the actin cytoskeleton (Alberts et al 2002). These molecular junctions, project into the extra cellular cytoplasm with the same transmembranous desmosomal cadherins that the full desmosome uses. The intracellular plaque of the hemidesmosome involves protein associations between Plectin and Bullous Pemphigoid Antigen 230 (BP230) to keratin elements of the cytoskeleton. Bullous Pemphigoid Antigen 180 (BP180) spans the cellular membrane in conjunction with the integrin receptors. This binds Laminin-5, an ECM protein component, to which keratinocytes can anchor to the basal lamina (Jones et al 1998).

The dermis differs from epidermal anatomy and is considered a connective tissue rather than an epithelial tissue. Dermal fibroblasts, the cellular

component of the dermis, secrete collagen and elastin proteins that form structural matrices giving the integrity and flexibility to the dermis. Blood and lymphatic vessels are rooted in the soft tissue for protection but also provide nutrients and fluid exchange. Hair follicles, sebaceous, eccrine and apocrine glands are all embedded within the dermis and regulate protection, sensation, thermoregulation, excretion, metabolism and immunoregulation (Le Gros Clark, 1946, Gardner and Osburn 1973, Hess and Kirsner, 2003 and Kanitakis, 2002).

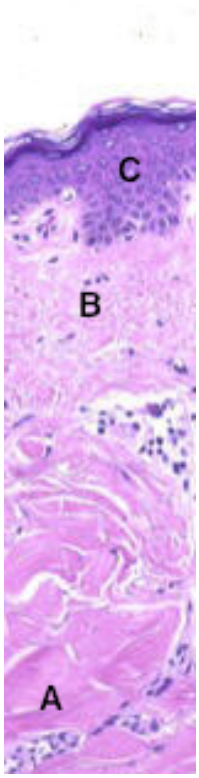

Fig 1.01. Light microscopic section of human skin. A) Subdermal layer, the hypodermis consisting mainly of adipose tissue. B) Dermal layer, the dermis consisting mainly of connective tissue. C) Epidermal layer, keratized rich strata. Taken from http://missinglink.ucsf.edu/lm/dermatologyglossary/img/Dermatology%20Glossary/Glossary%20Histo%20Images/normal_skin_not_of_a_special_site.jpg.

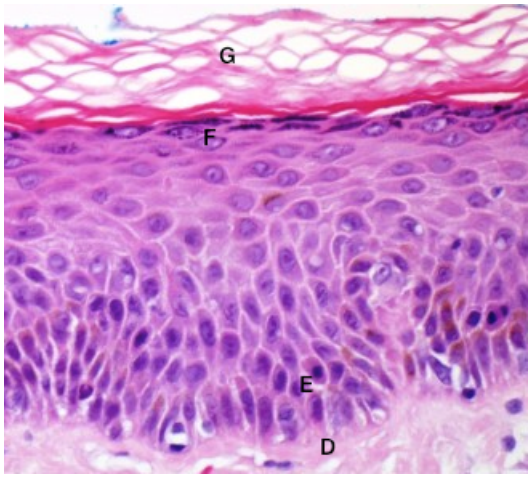

Fig 1.02. Light microscopic section of the upper most layer of human skin. D) Stratum Basale E) Stratum Spinosum F) Stratum Granulosum G) Stratum Corneum. Taken from http://tissupath.com.au/medical-student-subjects-skin/

Focal Adhesions (FA) establish a bridge between the actin cytoskeleton of fibroblasts (Singer et al 1988) and endothelial cell (Fath et al 1988) and the underlying substrata through the association of intra and extra cellular protein components, clustering, forming dense plaques (Fig.1.03).

Fibronectin was first described as an “exfoliate” of chicken fibroblasts (Ruoslahti et al 1973). It was of high molecular weight, separated into two distinct subunits and soon after this the presence of the protein was confirmed in human fibroblasts (Ruoslahti et al 1974). The protein, fibronectin, was subject to extensive research and the proteins interaction with fibroblasts and extra-cellular collagen matrices has been described (Klebe, 1974 and Ruoslahti, 2003). Fibronectin has a central role in the ECM. In addition to binding to the cell surface, it binds many other macromolecules such as collagens, fibrin, heparin and actin, implicating it in cell attachment, cell motility, wound healing and cell morphology. It is ubiquitous within many tissues including skin and underlying connective tissues (Alberts et al 2002). Morphology of attached fibroblasts within an ECM are well spread (Pearlstein, 1976) with projected cellular processes (Yamada et al 1976) (Fig.1.04).

Anchorage of fibroblasts through fibronectin depends on the affinity of a tri-peptide binding domain consisting of Arginine-Glycine-Aspartic acid or RGD

(Pierschbacher and Ruoslahti 1984). This small polypeptide fragment promotes cell attachment by providing anchoring points (Alberts et al 2002). Attachment can be inhibited if stable presentation of the RGD-polypeptide is not achieved (Yamada and Kennedy 1984). The relationships of flanking residues to the RGD-polypeptide, in native fibronectin, take the form of a secondary structure. Hydrogen bonds form within a hexa-peptide fragment, which contains the RGD-polypeptide binding domain (Glycine-ArginineGlycine-Aspartic acid-Serine-Proline). Within fibronectin, this sequence is highly conserved, exhibiting a curved or cyclic structure. Beta-turns add structural specificity in the native conformation in fibronectin compared with primary linear polypeptides of the same binding sequence (Reed et al 1988).

Molecular mechanisms involved in fibroblast attachment involve a complimentary cell surface receptor with specific affinity for fibronectin (Pytela et al 1985a). A second cell-surface receptor was soon discovered that also had affinity for RGD-polypeptide (Pytela et al 1985b). Both receptors bound different ligands (fibronectin and vitronectin respectively), but each acted through the same basic amino acid sequence, RGD. A family of receptors were soon established and are known as integrins. They induced signal recognition system dependent of cell attachment to the ECM (Ruoslahti and Pierschbacher 1987). To date, 24 combinations of various alpha and beta subunits make up the integrin family (Alberts et al 2002).

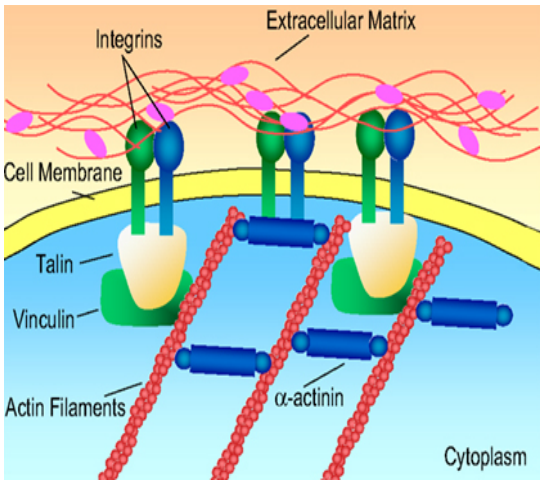

Fig 1.03. Schematic representation of the Focal Adhesion complex (Rao and Winter 2009).

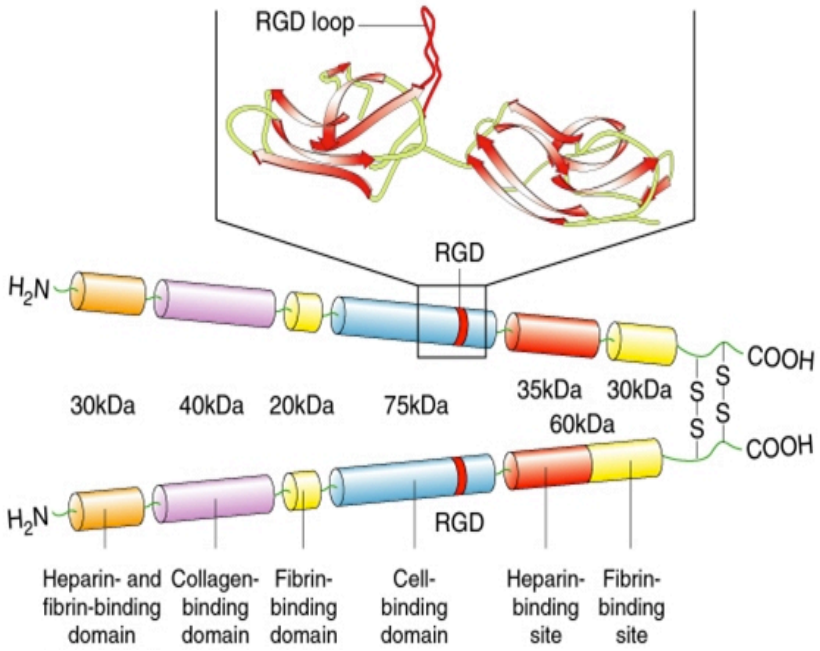

Fig 1.04. Schematic representation of fibronectin,
http://www.zoology.ubc.ca/~alorch/ecm/gallery2.htm

1.2vi- Wound Healing

Six functional aspects make up the dynamic response to the skin being broken, known as the wound healing process, although these are broadly classed into three phases. Platelets migrate, through the vascular system and leak into the wound space. Thrombosis and coagulation plugs the space with a three-dimensional latticework of ECM components; fibronectin, fibrinogen, thrombospondin and platelets. This is part of the inflammatory response and primarily serves to maintain integrity and protective properties by sealing the wound, blocking the entry of pathogens and preventing blood loss. Infection control begins with the mobilization of neutrophils to the wound site. The wound is debrided of dead cellular material and foreign bodies by monocytes, enzymatic degradation and toxic oxygen products, which also initiate the anabolic stage by secreting growth factors. In the anabolic stage, fibroblasts move up into the wound space from the sub-dermis. The initiation of the tissue-repairing phase is thought to result from monocyte metamorphosis to wound macrophages, which in turn secrete a variety of growth factors into the wound space and stimulate growth. Fibroblasts contract and form granulation tissue, synthesize collagen and proteoglycans in an effort build a new ECM and remodel tissue, which is nutritionally supported by endothelial cells. Endothelial cells migrating form the sub-dermis, re-vascularising the area. Keratinocytes from the wound edges, spread and migrate downwards, using the fibrin latticework to re-epithelise and form an epidermal layer. Fibroblasts continue to move through the fibrin network and thicken the dermal cell layer. This process is swift and fulfills the vital role of knitting the layers back together. Connective tissue of the sub-dermis often leaves fibrous scars as a result of dense collagen bundles being deposited. Fig 1.05. Represents the wound-healing cascade on a logarithmic timescale. Secondary homeostatic functions of the skin are often lost due to the regenerated skin being unable to support structures such hair follicles usually found in normal adult skin. Due the skins' ability to re-generate, skin grafting can be achieved at a superficial level because of the stratum germinativums high mitotic proliferative capacity (Le Gros Clark, 1946, Grinnel, 1984, Pollack, 1984, Martin, 1997 and Lanza et al 2000).

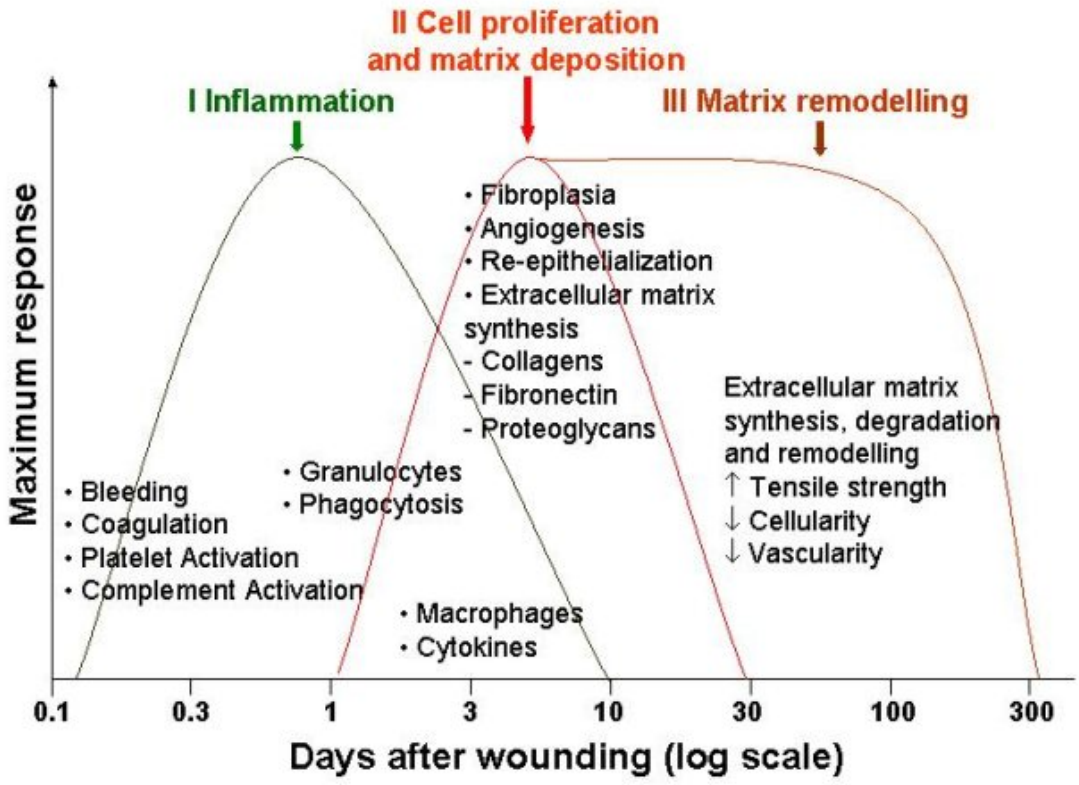

Fig1.05. The phases of wound healing cascade represented in a logarithmic timescale. Taken from http://www.worldwidewounds.com/2004/august/Enoch/Pathophysiology-Of-Healing.html

1.2vii- Natural Transcutaneous Appendages

At first glance it may appear that nature has many examples of transcutaneous structures. Fingernails, hair or horns may be seen as such examples. Grosse-Siestrup and Affled (1984) make the distinction that such structures are in fact “organs of the skin”. A layer of epithelial cells separates the appendages and skin and therefore should not be considered a transcutaneous structure, as they do not break skin continuity.

Bone-anchored transcutaneous devices, including ITAP, do disrupt skin continuity. Cellular downgrowth is the critical determinant of the success or failure of bone-anchored, skin-penetrating devices, such as ITAP (Pendegrass et al 2006).

ITAP devices were modelled on deer antlers, which are a natural analogue to a bone-anchored transcutaneous device (Pendegrass et al 2006). Deer antlers are of bony protuberances that out-crop from the frontal portion of the skull via a permanent bony pedicle. Anatomy of the frontal bones and pedicles are the same, both made up of trabecular bone. It is easier to think of the pedicle as simply an extension of the frontal bones. The structural architecture of the pedicle changes as the deer increases with age, becoming thicker as bone is deposited evenly around the structure (Landete-Castillejos et al 2012).

Winter (1974) noted that the tooth created a “natural” and “permanent” disruption in the epithelial membrane lining the mouth cavity. Cellular downgrowth of the gingival epithelia can not re-establish continuity because of a physical blockade of collagen fibres arranged in a peridontal membrane that interact with the bony socket and cementum of the tooth. Here, a natural example exists of an interface created when the epithelial layer is disrupted. Hemidesmosomes bridge the soft-hard tissue interface, linking the gingival epithelia with the collagen fibres that interact with the tooth (Grosse-Siestrup and Affled 1984). The anatomy structurally stabilises the gingival epithelia to the hard tissue of the tooth but critically, minimises the effect of breaking the skin seal (Sauberlich et al 1999). Maintenance of a healthy environment is sustained by the action of the saliva, washing away cell debris and promoting normal flora (Grosse-Siestrup and Affled 1984). No free movement between the gingival epithelia and tooth exists, which may play a role in permitting and maintaining soft tissue interface formation (Branemark and Albrektsson 1982).

During the developmental stage, antlers are covered by a Velvet- an adapted layer of skin that is shed as and when the bones grow. The Velvet and connective tissue consists of large bundles of collagen fibres and extensive vasculature. This epidermis is thicker than that of normal epidermis (Chapman, 1975). At the point of breaking the transcutaneous continuity collagen fibres, or Sharpey’s fibres, bridge the soft hard tissue gap by anchoring into the porous trabecular bone with the surrounding connective tissues. The interaction of Sharpey’s fibre between the bony pedicle and dermal tissue physically block marsupilisation and create a tight biological seal. This

supports the development of the epithelium and ties the soft tissue into the bone so that there is little movement between the two tissues (Pendegrass et al 2006).

Early *in vivo* development of ITAP saw straight titanium alloy pins skeletally anchored into a trans-tibial goat model (*Capra hircus*) for 4-weeks (Pendegrass, 2005). The implant shaft provided an opportunity for epithelial downgrowth and the formation a dead space between the implant and skin interface. Dermal and epidermal cellular attachment was limited (Pendegrass, 2005 and Pendegrass et al 2006). In an attempt to increase the surface area for dermal tissue to attach to, novel engineering structures were incorporated in later ITAP designs based on deer antler histology, however, epithelial downgrowth was not fully eradicated (Pendegrass et al 2006 and Pendegrass et al 2006).

1.2viii- Implant Biomaterials

Materials that are used to aid or restore natural function of tissue are described as biomaterials. Biomaterials have to satisfy two aspects and as suggested by Black (1992), requirements for implantable biomaterials should not be absolute but should be seen to have a “minimum requirement” of biocompatibility. He also suggested that given the body’s dynamic environment, performance of an implant biomaterial should be classed in terms of the host response and a greater understanding of the host responses is key in the development of successful biomaterials. Some of the most obvious successes of the implant biomaterial can be seen in the hard tissue replacement area, with vast numbers of joint replacement arthroplasty surgeries being performed each year alone (Liu et al 2000). The challenge is clear; a non-living, foreign material must interface with a living material on a long-term basis (Van Noort,1987).

Commercially pure titanium (cp.Ti) was first described as “tolerated” in reference to direct contact between native bone and implant surface by Bothe et al. (1940). Cp.Ti does not invoke an adverse tissue response and due to its

material properties lends itself as an ideal material for bony fixation (Leventhal and Gottlied 1951). The metal forms a very stable oxide of titanium dioxide (TiO_2), referred to as a passivation layer, and as a result the material is far less likely to corrode in its local environment. The material strength of cp.Ti can be increased when the metallic hexagonal crystalline structure is stabilised with additions of aluminium and vanadium. The desired characteristics for orthopaedic applications require a low elastic modulus (so the ratio of stiffness between implant and bone are a close as possible), mechanical strength (to withstand forces in load-bearing activities) and tissue compatibility to resist corrosion. By matching the Young's modulus to that of the anchoring point, the stress shielding effect can be limited and bio-fixation can be supported. $TiAl_6V_4$ is an alloy of cp.Ti and has increased structural and tensile strength, which is important for load-bearing activities, necessary for ITAP devices. This makes the metallic alloy a more appropriate material to use for orthopaedic implant device manufacturing. A mismatch in Young's modulus still exist between bone and titanium alloy (Wang 1996 and Liu et al 2004).

Electron beam manufacturing (EBM) is a rapid type of powder metallurgical processing that fabricates highly specific microstructures for medical implantation. It is a layer-by-layer single process that is CAD-directed and occurs under vacuum. Atomized Titanium alloy powder is homogeneously applied layer-by-layer and a directed electron beam fuses the powder to form struts, which when the residual powder is removed produces a 3-dimensional porous structures. The EBM process also has a greater energy density compared to laser manufacturing techniques. High scanning speeds and position accuracy are achieved by focusing the E-beam through electromagnetic lenses, meaning this single step process has shorter build times and lower manufacturing costs (Heinl et al 2007, Heinl et al 2008 and Parthasarathy et al 2010).

Porous structures can act as a mechanical scaffold to aid cell attachment for implant biomaterials. Inter-pore connections allow cells to grow through implants. This benefits load-bearing implants as bio-fixation and mechanical

attachment of osteoblastic cells can be achieved. Current joint replacement implants utilize these principles. High volumetric porosity of implants can also positively influence biological tissue integration at the soft tissue level. The permeability of an open structure can facilitate transport of body fluid through the implant promoting in-growth of well vascularised soft tissue in a short period of time. As a result the tissue-implant interface can be integral. By modifying the porosity as a function of pore and strut size the functionality and longevity of the implant are increased (Heinl et al 2007, Heinl et al 2008 and Parthasarathy et al 2010).

ITAP's long-term success relies upon dermal attachment to prevent epithelial downgrowth. A flange increases the surface area for soft tissue attachment and decreases epithelial downgrowth (Pendegrass et al 2006). If the porosity of this structure could be increased, soft tissue attachment could be optimized to promote a skin seal around ITAP.

Branemark led the cross-disciplinary research from the 1950s with the aim of understanding and establishing direct bone-implant interfaces. This principal, of establishing bony contact onto a foreign surface, without rejection or fibrous encapsulation was termed osseointegration. (Branemark et al 1969) Albrektsson et al (1981) postulate the interface could be as a result of chemical integration between cell and TiO_2 layer as opposed to direct contact with the solid metal. In turn, this evidence was seen as the pre-requisite for a stable bio-fixation to allow load-bearing activities to be performed.

Titanium alloy's structural characteristics, in relation to implant materials, have been well established (discussed earlier). To better serve the host, implant substrates can be functionalised, adapting to the biology of the host and attempting to develop a biologically stable interface.

Cellular interactions with an implant biomaterial are challenging, as the environment is dynamic. Functionalisation can involve the physical structure such as topographical changes to better suit cell attachment. Biological elements can be incorporated on an implant substrate to aid cellular

attachment or hinder bacterial colonisation. Research has focused on attempting to meet the demands of an implant's intended function within a specific biological environment thereby increasing longevity *in* situ and clinical success (Kasemo and Gold 1999).

Hall et al. (1975) suggested that a smooth, non-textured surface of a transcutaneous device, such as a cannula, would increase the opportunity for marsupilisation to create a portal between the skin and device. He also observed the maturation rate of the cells involved in playing a critical roll for long-term transcutaneous device to be *in situ*. Burnette et al. (1986) substantiated implant surface research *in vivo* (Albrektsson et al 1981 and Branemark and Albrektsson 1982), when epithelial cells ordered themselves within surface crevices of titanium-coated substrates. Cell projections, such as lamella and filopodia, were observed, "bending" over topographical features.

Others argue that increasing the surface roughness decreases the surface area available for epithelial cell attachment, spreading and proliferation leading to flattened cells and the successful development of a monolayer (Elisenbarth et al 1996 and Pendegrass et al 2008).

The longer-term effect of micro-machined surfaces on transcutaneous implants suggested an optimal surface topography could limit bacterial colonisation and positively aid soft tissue integration (Chehroudi and Brunette 2002). Smooth surfaces presented a 7-fold increase in susceptibility to infection compared with porous-coated transcutaneous implant devices *in vivo*. Topographical features of the implant surface aided attachment of cutaneous and subcutaneous soft tissues (Isckson et al 2011).

Three different cellular responses occur when a device breaks the skin barrier, which induces a cascade of events. Disruption of the well-ordered anatomy of the skin changes the mechanical forces between the individual components. The introduction of a foreign substrate disrupts normal stresses exerted by soluble biological material. This adversely affects the cell matrix assembly and links to the cellular cytoskeleton. So called "contaminated air" and the lack of

cellular attachment cause a build up of cellular debris and wound exudate. Cells migrate along the interface and the skin surrounding the foreign body invaginates in an attempt to re-establish the continuity of the skin often forming pockets or recesses (Grosse-Siestrup and Affled 1984 and Balaban et al 2001).

Holgers et al. (1995) observed no physical interaction between extra-oral epithelia and cpTi bone anchored dental implant devices. SEM analysis was unable to establish hemidesmosome formation or organised collagen bundles linking the epidermis to implant surface in implants retrieved from 14 human subjects.

Lundborg et al. (1996) insist the critical factor for successful skin penetrating devices is stabilising the skin around the implant, this can be achieved by pinning to the underlying bone. Surface topography needs to enhance epithelial cell attachment *in vivo* for successful integration between skin and implant, and this is the critical determinant for the clinical success of ITAP (Kang et al 2010).

Roy and Linnehan (1974) suggested that hydroxyapitite (HA) possessed potential as an implant material as a result of its native structure. HA, a major component of hard tissue in humans was prepared using hydrothermal exchange reactions from coral skeletal carbonate samples. The bone implant interface could form a strong chemical bond (Jarcho et al 1977). Ducheyne et al. (1980) compared HA functionalised steel sintered fibres with uncoated controls *in vivo*. Osseointegration with the HA functionalised substrates demonstrates a strong stable interface as measured by mechanical tests, indicating greater bio-fixation.

HA soft tissue integration is also achievable, when porous HA blocks supported soft tissue infiltration and revascularisation throughout the structure within 21 day *in vivo* (Butts et al 1989). Solid implants, in combination with HA coatings are successful as endoprostheses where bony fixation is necessary,

however these implants do not promote soft tissue attachment or infiltration (Gupta et al 2006).

Biological functionalisation of implant biomaterials are used to better meet the functional requirements of the cells involved in the host biological composition (Kasemo and Gold 1999). The principle of using native, non-rigid, biological materials bridging the interface between the host's tissue and implant biomaterial fits in with Black's statement referencing a host response to an implantable biomaterial (Black, 1992).

Cells must be attached to a substratum in order to function (Stoker et al 1968). Components for the ECM and connective tissue are aimed at cell surfaces receptors to induce molecular interaction between the host and implant material. Recognition of molecular substrates supports contact guidance, in which cells deposit a fibrous layer that acts as a scaffold to promote cellular morphogenesis (Weiss, 1945). ECM constituents readily adsorb onto biomaterial substrates, on entering a biological environment, but exposure to such environments is not specific and cannot be regulated to elicit the desired cellular interactions (Shin et al 2003). Proteins in aqueous solution, when in the presence of a solid surface, will non-covalently interact with that solid surface to produce a monolayer. For the desired cellular response (anchorage dependent) this protein layer is critical (Wilson et al 2005). Non-covalent forces of attraction allow the physical attachment of proteins to titanium alloy surfaces. Functionality of the adsorbed protein can be maintained and quantifiable increases in anchorage dependent cell growth mechanisms have been well established using ECM components. The performance of fibronectin has been established within the biomaterial field. Yang et al. (2003) showed the use of a simple adsorption method (relying upon surface energy of a cp.Ti surface) to bind and present fibronectin as a coating. This fibronectin coating functionalised titanium surfaces and significantly increased osteoblast attachment.

Laminin-5 is implicated in hemidesomsome formation (Jones et al 1998). It can be adsorbed on to titanium alloy substrates and up-regulate

hemidesmosome formation and cell spreading of epidermal keratinocytes (El-Ghannam et al. 1997). Well-spread, viable and attached gingival fibroblasts have been observed (to a significantly greater degree) on collagen coated cpTi substrates compared with uncoated substrates *in vitro* (Nagai et al 2002).

The dynamic environment created *in vivo* means physical and chemical aspects affect cellular attachment (Hormia and Kononen 1994). Implant biomaterials are subject to blood and serum on entering an *in vivo* environment. Attachment of specific cells have to compete for the surface with an active immune response, which involves protein adsorption and the attachment of cells such as macrophages and neutrophils, associated with the immune system (Baier and Dutton 1969 and Nygren et al 1997). Chemical coupling of a biological molecule to a biomaterial substrate can be engineered to control and enhance the subsequent cell and tissue response (Davis et al 2002). Covalent bonding of a protein to the substrate surface can provide a stronger and more stable immobilization. Jose et al. (2005) utilized the reactive oxide layer of titanium to couple antibiotics to self protect their implant devices against infection.

Cell attachment functional groups have been explored in the same manner in order to promote osseointegration (Nanci et al 1997) and soft tissue integration (Middleton et al 2007 and Chimutengwende-Gordon et al 2011).

All the referenced examples above rely on comparable methodologies utilizing the same intermediary between metal and protein. Aminopropylated substrates provide a spacer between implant and protein, coupling via unpaired electrons (Fig 1.05). An increase in the number of chemical bonds between the metal and protein mean greater distance amid the two components, facilitating biological activity of the protein functionaliseation (Jose et al 2005, Nanci et al 1997, Middleton et al 2007 and Chimutengwende-Gordon et al 2011).

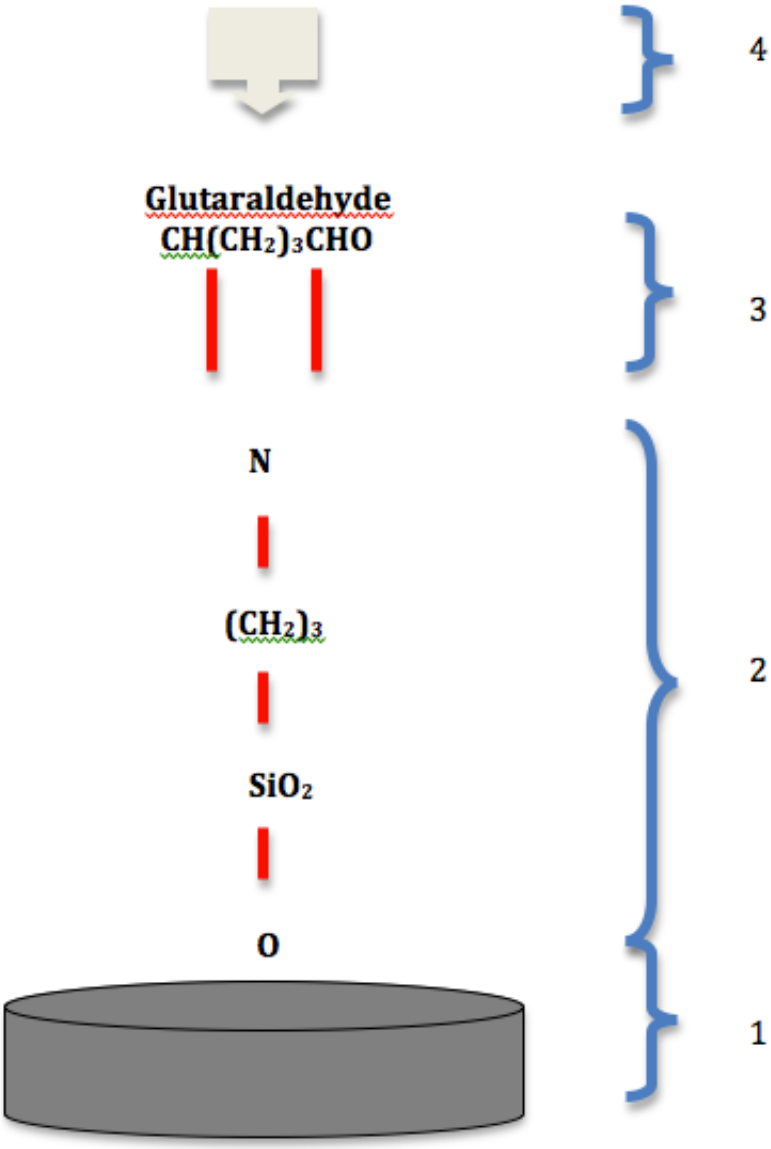

Fig 1.06. Schematic representation of Aminopropylated substrates.
1) Implant substrates. 2) Coupling of 3-aminopropyl-triethooxysiane (APTES) containing saline complex to the substrate. 3) Coupling glutaraldehyde to saline complex. 4) Covalent bond formation between a functional group and spacer complex.

These cited examples suggest a good rationale for the use of biological functionalisation for biomaterials. Cellular responses can be influenced and as such, physical attachment may be increased by the up-regulation of the formation of contacts points between host and substrate. This can act as the prerequisite in the development of a tight biological interface between host tissues and implant biomaterial.

In vitro studies are one-dimensional. Exposure to serum that creates a competitive environment to the biologically functionalised surfaces is often withheld so only specific cellular responses can be observed. The challenge is to establish a functionalised substrate and demonstrate that it works in an *in vivo* model. These coatings have been shown to be effective in a number of in vivo models (Chimutengwende-Gordon et al 2011, Elmengaard et al 2005 and Ferris et al 1997).

Elmengaard et al. (2005) reports RGD-polypeptide functionalised porous coated titanium alloy substrates *in vivo.* Fibrous tissue formation was reduced yet new bone formation in the experimental groups was not as advanced as hypothesised.

Bone thickness increased around rat femurs when RGD-polypeptide substrates were implanted *in vivo* yet results did not significantly increase the strength of osseointegration (Ferris et al 1997).

Fibronectin has shown promise as a protein coat both *in vitro* and *in vivo* (Middleton et al 2007 and Chimutengwende-Gordon et al 2011). Established methodologies show the positive up-regulatory effect fibronectin has on dermal fibroblast attachment and attachment strength on materials used for ITAP devices, by fluorescently tagging vinculin within the FA (Middleton et al 2007 and Pendegrass et al 2008).

Early Immunocytochemistry methodologies for intra-cellular FA components demonstrate that these complexes, which are composed partly of vinculin and actin, differentiate into a mature form in attached fibroblasts, and appear as

intracellular ‘dashes’ and ‘dots’ respectively under fluorescent microscopy. Vinculin and Actin localisation were observed in both mature and immature forms of FAs, with the mature dash contacts associated with actin microfilament bundles (Bershadsky et al 1985). Both Hunter et al. (1994) and Middleton et al. (2007) appear not to discriminate between maturity of FAs when assessing dermal fibroblast attachment to titanium alloy substrates.

The relationship between vinculin localisation, as a function of cell area and the biophysical forces necessary for fibroblast detachment from a metallic surface, positively correlate. It is therefore possible to calculate the force of a single FA. Cells cultured on fibronectin functionalised titanium alloy surface response by producing more FA per unit area without increasing their cell area (Pendegrass et al 2009). Morphology characterised under microscopy, be it at a micro or nanoscale, of attached fibroblasts to titanium alloy substrates appear consistent. Cellular projections extend outwards of the cell body creating a stellate shape and morph into a discoid shape, attached to a surface (Hunter et al 1994 and Middleton et al 2007).

Earlier work by Truskey and Pirone (1990) used laminar fluid flow through parallel plates to theoretically quantify detachment of murine fibroblasts attached to glass substrates, functionalised with or without Fibronectin.

Well spread fibroblast cells (of human or murine lineage) are less susceptible to laminar hydrodynamic forces coupled to a greater number of physical contacts (fibronectin mediated) between cell and substrate results in a greater force required to detach the cells (Truskey and Pirone 1990 and Pendegrass et al 2009).

I now strive to develop functionalisation techniques for ITAP devices that can withstand *in vivo* implantation support a tight biological seal at the transcutaneous interface and can feasibly be applied in the clinical setting. I aim to develop techniques to functionalise titanium alloy, which will up-regulate human dermal fibroblast attachment strength. In a previous study the number of FAs per unit cell area (termed FA density) has been shown directly

to correlate with the strength of attachment of fibroblasts to substrates (Middleton et al 2007 and Pendegrass et al 2009). Hence, throughout my thesis, FA density will be used as a measure of human dermal fibroblast attachment strength.

1.3- Thesis Aim

My overall aim is **to develop techniques that will enhance dermal and epidermal cell and tissue attachment, in order to create a seal and prevent infection of implant biomaterials used for ITAP**. The general hypothesis for my thesis is that **soft tissue attachment to ITAP will be improved using a protein coated porous implant compared with surfaces that are currently used for ITAP.**

Fig 1.06 illustrates a breakdown of my thesis. It aims to schematically represent how the experimental work in this thesis has been dictated by a central axis. It starts with the overall aim for the experimental work, followed by a brief outline of the problem this research wishes to address. My research bifurcates into *in vitro* (Chapter 2 and 3) and *in vivo* (Chapter 4) experimental chapters, each addressing the overall aim but by differing methods. Each chapter is dictated by a research question, highlighted in red italics in the flow diagram. The final experimental chapter, Chapter 5, brings the two branches of my thesis together in one final experimental study.

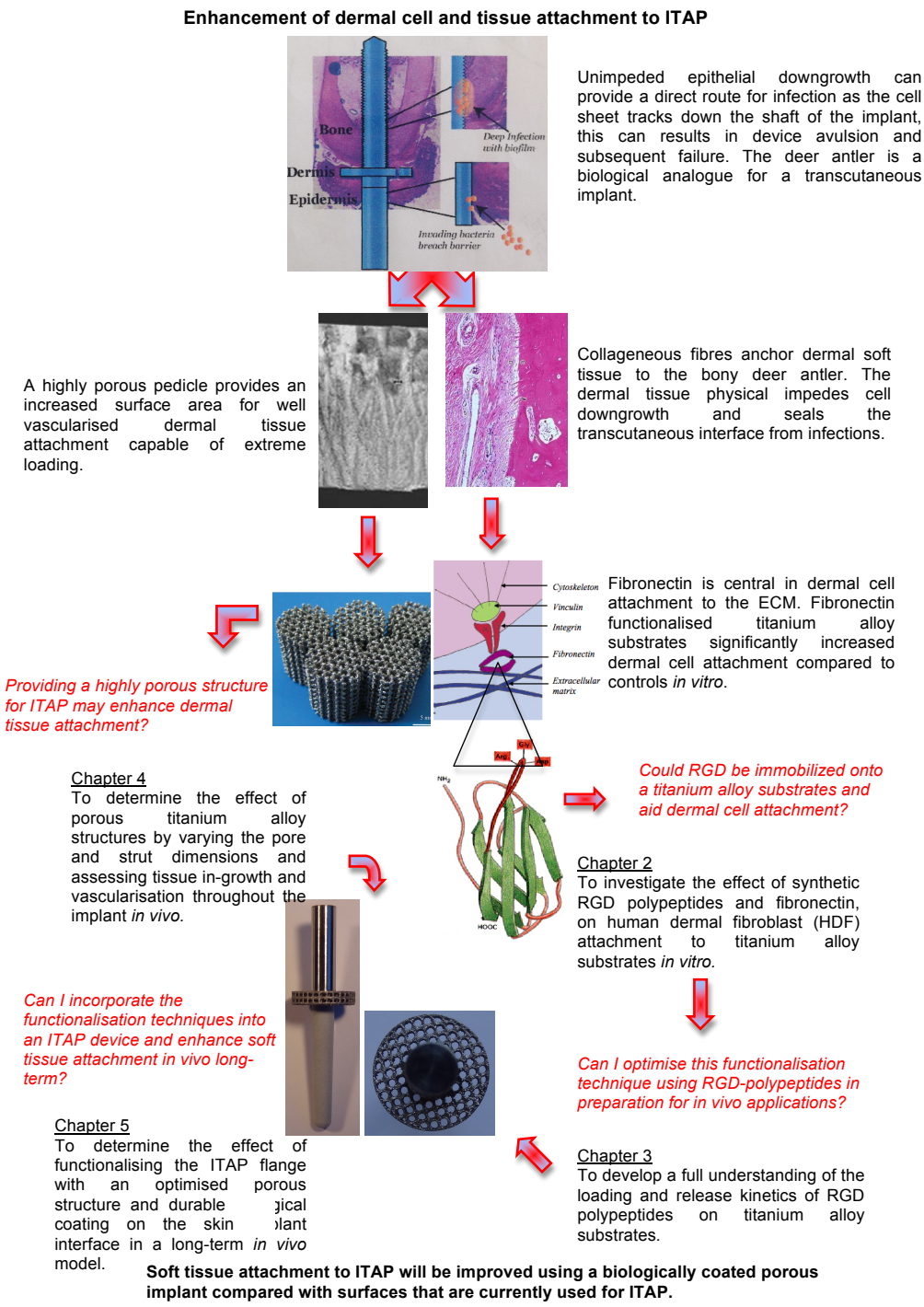

Fig 1.07 Schematic representation of the outline of my thesis. Text in red indicate my main research questions and are related to experimental chapters of my thesis

Chapter 2- Enhancement of Human Fibroblast Attachment using Fibronectin and RGD-polypeptide coatings.

Chapter 2

2.1-Introduction

Fibronectin is a critical component within the ECM. In addition to binding to the cell surface, fibronectin facilitates the binding of many macromolecules such as collagens, fibrin, heparin and actin, implicating it in cell attachment, cell motility, wound healing and cell morphology. It is ubiquitous within many tissues including skin and underlying connective tissues (Alberts et al 2002).

Fibronectin has been shown to improve cell attachment to titanium alloy substrates, with increases in vinculin expression being observed as early as 1-hour (Yang et al 2003 and Middleton et al 2007). Functionalisation of titanium alloy using fibronectin increases the FA density per cell area, which correlates with an increase in force required to detach dermal cell from the substrate (Middleton et al 2007 and Pendegrass et al 2009). For the purpose of the thesis functionalisation techniques of titanium alloy substrates are aimed at increasing human dermal fibroblast attachment strength.

The minimum amino acid sequence in fibronectin required to initiate cell attachment via integrin binding is arginine-glycine-aspartic acid (RGD) (Pierschbacher and Ruoslahti 1984a).

Independently of fibronectin, the RGD-polypeptide can bind many different integrin receptors with low affinity (Ruoslahti, 1996). However, high affinity is observed with the whole fibronectin molecule, which is only observed to bind the alpha5 beta1 integrin receptor (Hautanen et al 1989).

This native alpha5 beta1 integrin binding may occur because fibronectin exposes the RGD-polypeptide in a specific orientation, thus increasing cell attachment (Ruoslahti, 1996).

The RGD-polypeptide in fibronectin exists as a looped structure, which is held together by hydrogen bonds and forms a beta turn. This creates the specific orientation that increases integrin affinity (Reed et al 1988 and Main et al

1992). In addition, there is evidence to suggest that further regulation of integrin binding could be achieved in native fibronectin by a second synergistic site, remote from the RGD sequence, which may play a role in increasing specific interaction between integrin receptors and the RGD binding domain in fibronectin (Obara et al 1988).

Individual amino acids within the RGD-polypeptide can also significantly impact on integrin binding affinity. Substituting L-aspartic with D-aspartic acid down-regulates integrin binding, and this has been shown to decrease cell attachment (Pierschbacher and Ruoslahti, 1987).

In addition, the amino acids that flank the RGD-polypeptide can impact upon orientation, and hence integrin binding; therefore cell attachment (Ruoslahti, 1996). For example, cysteine residues flanking the RGD-polypeptide can form di-sulphide bonds causing the polypeptide structure to loop. This can result in increased affinity to specific integrin receptors compared with linear RGD-polypeptide structure (Koivunen et al 1994). If Proline flanks the aspartic acid, integrin affinity is completely inhibited (Pierschbacher and Ruoslahti, 1987).

RGD-polypeptides flanked by long chains of amino acids show greater integrin binding affinity compared with the RGD sequence alone. Some evidence suggests that increasing length stabilizes the RGD binding domain, which holds the polypeptide in a formation that supports specific integrin binding. However the precise mechanism has not been determined (Ruoslahti, 1996). Irrespective of the mechanism by which this occurs, longer chain RGD-containing polypeptides with specific flanking residues that can induce a cyclic structure may confer increased integrin binding affinity compared with linear forms, hence may increase cell attachment. There is some evidence to support this because the cyclic forms of RGD-containing polypeptides can bind specific integrin receptors with high affinity, which is known to increase cell attachment compared with the ubiquitous weaker integrin binding seen with linear forms. It may be possible to use lower concentrations of cyclic RGD-containing polypeptides. Patel et al (2012) have shown that the same

degree of cell attachment can be achieved with significantly less cyclic RGD-containing polypeptides compared with linear forms.

For ITAP to be successful, it is critical to up-regulate cell attachment at the skin-implant interface as early as possible. Biological functionalisation of the titanium alloy used in ITAP may achieve this, irrespective of whether fibronectin or an RGD-containing polypeptide is used.

ITAP is designed for load bearing activities and osseointegration must be achieved. Titanium Alloy is the material that is used clinically for ITAP (Kang et al 2010). This is because it's Young's Modulus is closer to that of bone (compared with other implant materials, such as alloys of cobalt) reducing the potential for stress shielding, and it is highly biocompatible (discussed in Chapter 1.2). Titanium's material properties can influence functionalisation techniques. Proteins can be absorbed onto the amorphous oxide layer on the surface of titanium. Immobilization of the absorbed proteins is achieved via electrostatic forces, which hold the proteins in place (Yang et al 2003). RGD-polypeptides could be immobilized in the same way.

Covalent tethering of fibronectin to titanium alloy using silanization (Chapter 1.2, Fig 1.05) has been shown to provide a stronger, and more durable bond compared with adsorption and maintains significant positive effects on cell attachment compared with non-functionalised controls (Middleton et al 2007). It therefore may be possible to silanise RGD-containing peptides to titanium alloy substrates to up-regulate HDF attachment.

The clinical use of fibronectin is highly regulated because it is sourced from humans or animals and hence may induce an inflammatory response due to an immune reaction. However, sterilization techniques denature proteins rendering them inactive. RGD may provide a possible solution because it can be artificially synthesized avoiding potential regulatory complications and may be less susceptible to sterilization damage.

Some studies have demonstrated increasing cell attachment-dependent processes on RGD-containing polypeptide functionalised material substrates (Kantlehner et al 2000 and Kammerer et al 2011). However, there are no studies investigating cell attachment strength on RGD-functionalised substrates, comparing linear and cyclic RGD-containing polypeptides with fibronectin. This chapter aims to develop a functionalised titanium alloy substrates, which act to increase human dermal cell attachment strength to titanium alloy substrates.

2.2- Aims and Hypotheses

This chapter aims to **investigate the effect of synthetic RGD polypeptides and fibronectin, on human dermal fibroblast (HDF) attachment to titanium alloy substrates *in vitro.***

To achieve this aim, I will determine whether there is a difference in HDF attachment to functionalised titanium alloy substrates with either linear or cyclic RGD-polypeptides compared with fibronectin. In addition, I will investigate whether silanisation effects HDF attachment *in vitro* compared with adsorption, and whether attachment will be increased at earlier time points on functionalised substrates compared with controls.

This chapter aims to test the following specific hypotheses:

1. Linear RGD-polypeptide functionalised titanium alloy substrates will significantly increase HDF attachment compared with controls.
2. There will be no significant difference between HDF attachment on linear RGD-, compared with cyclic RGD-polypeptide functionalised titanium alloy substrates.
3. Attachment of HDFs will be RGD-polypeptide concentration dependent.
4. Titanium alloy substrates functionalised with Fibronectin or RGD will significantly increase HDF attachment at 1, 4, 24 and 96 hours compared with controls.
5. There will be no significant difference in HDF attachment between silanised and adsorbed fibronectin- or RGD-functionalised substrates.

2.3- Materials and Methods

2.3i- Study Design

This chapter is broken down into individual experiments to address a series of questions to test my hypotheses.

Study 1

The first research question was whether titanium alloy adsorbed with RGD-polypeptides increases HDF attachment? Secondly, regarding optimal adsorption duration, linear (A8052, Sigma Aldrich, UK) and cyclic (ANA63785-1, Cambridge Bioscience, UK) RGD-containing polypeptides were adsorbed for 1 and 4 hours prior to assessing HDF attachment to establish the adsorption duration for HDF attachment protocols for Studies 2-5. Table 2.01 outlines the groups assessed (2.41), their specific functionalisations and details of the experiment performed.

Table 2.01- Study 1 Description

Group.	Substrate Functionalisation.	Study details.
Control.	Polished titanium alloy (2.3ii).	n=3 and cell attachment assay (2.3vii) performed at 24-hours.
0.1mM L RGD 1h.	0.1mM linear RGD-polypeptide adsorbed for 1-hour to titanium alloy substrates (2.3iii).	n=3 and cell attachment assay (2.3vii) performed at 24-hours.
0.1mM L RGD 4h.	0.1mM linear RGD-polypeptide adsorbed for 4-hour to titanium alloy substrates (2.3iii).	n=3 and cell attachment assay (2.3vii) performed at 24-hours.
0.1mM C RGD 1h.	0.1mM cyclic RGD-polypeptide adsorbed for 1-hour to titanium alloy substrates (2.3iii).	n=3 and cell attachment assay (2.3vii) performed at 24-hours.
0.1mM C RGD 4h.	0.1mM cyclic RGD-polypeptide adsorbed for 4-hour to titanium alloy substrates (2.3iii).	n=3 and cell attachment assay (2.3vii) performed at 24-hours.

Study 2

The second research question was to determine whether silanised linear or cyclic RGD-polypeptides significantly improved HDF attachment to titanium alloy. Cell attachment assays were performed at 24-hours on titanium alloy substrates, which were silanised with linear or cyclic RGD-polypeptides and compared with controls. Table 2.01 outlines the groups assessed (2.42), their specific functionalisations and details of the experiment performed.

Table 2.02- Study 2 Description

Group.	Substrate Functionalisation.	Study Details.
Control.	Polished titanium alloy (2.3ii).	n=3 and cell attachment assay (2.3vii) performed at 24-hours.
siLinear RGD.	0.1mM linear RGD-polypeptide silanised to titanium alloy substrates (2.3iv).	n=3 and cell attachment assay (2.3vii) performed at 24-hours.
siCyclic RGD.	0.1mM cyclic RGD-polypeptide silanised to titanium alloy substrates (2.3iv).	n=3 and cell attachment assay (2.3vii) performed at 24-hours.

Study 3

Study 3 was performed using linear RGD-polypeptides only. This was based on the results from studies 1 and 2, which demonstrate its significantly greater positive effects of HDF attachment (2.41 and 2.42). This study compared the effects of silanised and adsorbed linear RGD-polypeptides with those of fibronectin (F2006, Sigma Aldrich, UK) on HDF attachment to titanium alloy *in vitro*, a methodology that has been established by Middleton et al. (2007). Table 2.03 outlines the groups assessed (2.43), their specific functionalisations and details of the experiment performed.

Table 2.03- Study 3 Description

Group	Substrate Functionalisations	Study Details.
Control.	Polished titanium alloy (2.3ii).	n=3 and cell attachment assay (2.3vii) performed at 24-hours.
Adsorbed RGD.	0.1mM linear RGD-polypeptide adsorbed to titanium alloy substrates (2.3iii).	n=3 and cell attachment assay (2.3vii) performed at 24-hours.
Adsorbed fn.	10.0μg/ml Fibronectin adsorbed to titanium alloy substrates (2.3iii).	n=3 and cell attachment assay (2.3vii) performed at 24-hours.
Silanised RGD.	0.1mM linear RGD-polypeptide silanised to titanium alloy substrates (2.3iv).	n=3 and cell attachment assay (2.3vii) performed at 24-hours.
Silanised fn.	10.0μg/ml Fibronectin silanised to titanium alloy substrates (2.3iv).	n=3 and cell attachment assay (2.3vii) performed at 24-hours.

Study 4

The research question was whether increasing the number of RGD-polypeptides increases HDF attachment? The aim was to determine an optimal concentration of RGD-polypeptide for HDF attachment at 24-hours. Table 2.04 outlines the groups assessed (2.44), their specific functionalisations and details of the experiment performed.

Table 2.04- Study 4 Description

Group	Substrate Functionalisation	Study Details
Control.	Polished titanium alloy (2.3ii).	n=3 and cell attachment assay (2.3vii) performed at 24-hours.
5mM.	5mM linear RGD-polypeptide adsorbed to titanium alloy substrates (2.3iii).	n=3 and cell attachment assay (2.3vii) performed at 24-hours.
10mM.	10mM linear RGD-polypeptide adsorbed to titanium alloy substrates (2.3iii).	n=3 and cell attachment assay (2.3vii) performed at 24-hours.
25mM.	25mM linear RGD-polypeptide adsorbed to titanium alloy substrates (2.3iii).	n=3 and cell attachment assay (2.3vii) performed at 24-hours.
50mM.	50mM linear RGD-polypeptide adsorbed to titanium alloy substrates (2.3iii).	n=3 and cell attachment assay (2.3vii) performed at 24-hours.
100mM.	100mM linear RGD-polypeptide adsorbed to titanium alloy substrates (2.3iii).	n=3 and cell attachment assay (2.3vii) performed at 24-hours.

Study 5

To determine the degree of HDF attachment over time, functionaliseed RGD-polypeptides and fibronectin titanium alloy substrates were prepared by both adsorption and silanization and HDF attachment assessed at 1, 4, 24 and 96-hour time-points. Table 2.05 outlines the groups assessed (2.45), their specific functionalisations and details of the experiment performed.

Table 2.05- Study 5 Description

Group	Substrate Functionalisation	Study Details
Control 1h.	Polished titanium alloy (2.3ii).	n=3 and cell attachment assay (2.3vii) performed at 1-hour.
Control 4h.	Polished titanium alloy (2.3ii).	n=3 and cell attachment assay (2.3vii) performed at 4-hours.
Control 24h.	Polished titanium alloy (2.3ii).	n=3 and cell attachment assay (2.3vii) performed at 24-hours.
Control 96h.	Polished titanium alloy (2.3ii).	n=3 and cell attachment assay (2.3vii) performed at 96-hours.
AdRGD 1h.	5mM linear RGD-polypeptide adsorbed to titanium alloy substrates (2.3iii).	n=3 and cell attachment assay (2.3vii) performed at 1-hour.
AdRGD 4h.	5mM linear RGD-polypeptide adsorbed to titanium alloy substrates (2.3iii).	n=3 and cell attachment assay (2.3vii) performed at 4-hours.
AdRGD 24h.	5mM linear RGD-polypeptide adsorbed to titanium alloy substrates (2.3iii).	n=3 and cell attachment assay (2.3vii) performed at 24-hours.
AdRGD 96h.	5mM linear RGD-polypeptide adsorbed to titanium alloy substrates (2.3iii).	n=3 and cell attachment assay (2.3vii) performed at 96-hours.
Adfn 1h.	10.0μg/ml Fibronectin adsorbed to titanium alloy substrates (2.3iii).	n=3 and cell attachment assay (2.3vii) performed at 1-hour.
Adfn 4h.	10.0μg/ml Fibronectin adsorbed	n=3 and cell attachment

	to titanium alloy substrates (2.3iii).	assay (2.3vii) performed at 4-hours.
Adfn 24h.	10.0μg/ml Fibronectin adsorbed to titanium alloy substrates (2.3iii).	n=3 and cell attachment assay (2.3vii) performed at 24-hours.
Adfn 96h.	10.0μg/ml Fibronectin adsorbed to titanium alloy substrates (2.3iii).	n=3 and cell attachment assay (2.3vii) performed at 96-hours.
SiRGD 1h.	5mM linear RGD-polypeptide silanised to titanium alloy substrates (2.3.iv).	n=3 and cell attachment assay (2.3…) performed at 1-hour.
SiRGD 4h.	5mM linear RGD-polypeptide silanised to titanium alloy substrates (2.3.iv).	n=3 and cell attachment assay (2.3vii) performed at 4-hours.
SiRGD 24h.	5mM linear RGD-polypeptide silanised to titanium alloy substrates (2.3.iv).	n=3 and cell attachment assay (2.3vii) performed at 24-hours.
SiRGD 96h.	5mM linear RGD-polypeptide silanised to titanium alloy substrates (2.3iv).	n=3 and cell attachment assay (2.3vii) performed at 96-hours.
Sifn 1h.	10.0μg/ml Fibronectin silanised to titanium alloy substrates (2.3iv).	n=3 and cell attachment assay (2.3vii) performed at 1-hour.
Sifn 4h.	10.0μg/ml Fibronectin silanised to titanium alloy substrates (2.3iv).	n=3 and cell attachment assay (2.3vii) performed at 4-hours.
Sifn 24h.	10.0μg/ml Fibronectin silanised to titanium alloy substrates (2.3iv).	n=3 and cell attachment assay (2.3vii) performed at 24-hours.
Sifn 96h.	10.0μg/ml Fibronectin silanised to titanium alloy substrates (2.3iv).	n=3 and cell attachment assay (2.3vii) performed at 96-hours.

The following methods were performed for Studies 1-5.

2.3ii- Substrate Preparation

Surgical grade titanium alloy (Ti_6V_4Al) discs, 10mm in diameter and 2mm thick were manufactured. Substrates were prepared by grinding down one surface

using P400, P800, P1200 and P2500 Silicon Carbide Abrasive Papers (Buehler, Germany). Substrates were polished to orthopaedic grade standard (surface roughness (Ra) value <0.03) using P4000 Silicon Carbide Grit Paper (Buehler, Germany) followed by polishing with a pad lubricated with AP-A Suspension, a 5μm agglomerate α alumina suspension (Struers, Germany). Method validation was confirmed by surface profilometry analysis, examples of which are published in Appendix 1.

All substrates were cleaned ultrasonically with 10% Decon 90 (Decon Laboratories Ltd., UK) for 10-minutes, thoroughly rinsed under running water and distilled water for 5-minutes respectively and ultrasonically cleaned using acetone for a further 10-minutes. All substrates were autoclaved at 126^0C and 1.4 bar for 25-minutes (PriorClave Ltd, UK).

2.3iii- Functionalisation via Adsorption

Substrates for peptide or protein coatings were individually placed in a well-plate under aseptic conditions. A 50μl droplet of protein solution (at the concentrations stated in Tables 2.01-2.05) was placed onto each substrate, covering the entire surface, using a Gilson pipette. This droplet was left for 4-hours (unless otherwise stated- 2.3i) at 37^0C to adsorb on the surface. Substrates were washed with sterile phosphate buffered saline (PBS) 3 times to remove any unbound protein.

2.3iv- Functionalisation via silanisation

Substrates for peptide or protein silanisation were individually placed in a 10:1 solution of acetone and 3-aminopropyltriethooxysilane (APTES, Sigma-Aldrich, UK) for 2-hours at room temperature and pressure (RTP). Substrates were washed in acetone and air-dried overnight at 37^0C. Substrates were immersed in 1% glutaraldehyde (Agar Scientific, UK) solution in 0.172M PBS for 2-hours at RTP, washed in PBS and air-dried. Proteins were pipetted onto the surfaces of the substrates according to the protocol stated in 2.3iii.

2.3v- Cell Culture

Human dermal fibroblasts (1BR.3.G 90020507, Culture Collections, Public Health England, UK) were sub-cultured in vented flasks at 37^{o}C and 5% CO_2 using Dulbecco's Modified Eagle's Medium (DMEM) with 4500mg/L glucose, supplemented with 1% Penicillin/Streptomycin and 10% Fetal Calf Serum (FCS). Adherent cell populations were trypsinised (10% trypsin in PBS) after reaching 80% confluence. The number of cells was counted in a haemocytometer using a vital dye, Trypan Blue (Sigma-Aldrich, UK). Population numbers were calculated by N=M x D x 10^4 V cells, where N is the number of cells, M is the average number of cells counted from each of the four quadrants in the haemocytometer, D is the dilution factor between cell volume and Trypan Blue dye and V is the volume of the original cell population. Cells were re-suspended in DMEM to give a concentration of 200,000/ml.

2.3vi- Cell Seeding

Substrates were individually placed in well-plates under aseptic conditions. 10,000 cells were seeded onto each disc in a 50µl droplet of DMEM, which covered the entire substrate surface. The substrates were incubated for 1-hour at 37^{o}C and 5% CO_2 prior to the wells being flooded with media and returned to the incubator for a further study-dependent incubation period (2.3i).

2.3vii- Cell Attachment Assay- Immunocyochemistry

Excess media was removed from the wells and the substrates were washed 3 times for 5-minutes with PBS. Cells were fixed with 10% formal saline for 5-minutes, prior to 4, 5-minute washes in PBS. A 50µl droplet of primary antibody (Primary anti-vinculin mouse monoclonal Antibody (v9131, Sigma-Aldrich, UK), dilution of 1:200 with PBS and 0.0025% Triton X) was used to cover the entire surface of each substrate according to the protocol 2.3iii and incubated at RTP for 1-hour. Unbound primary antibody was removed with 3,

10-minute PBS washes. The secondary antibody (Alexa Fluor 488 chicken anti-mouse IgG antibody (A21200, Invitrogen, UK), dilution 1:1000 with PBS) was applied in a 50µl droplet according to protocol 2.3iii and substrates were incubated at RTP for 2-hours in the dark. Unbound secondary antibody was removed with 3, 10-minute PBS washes in the dark.

Samples were stored in PBS at 4^0C, analyses were performed within 24 hours using a Carl Zeiss photomicroscope (KS300, Zeiss, Germany). Six, randomly selected cells were photographed per disc. Cell area was measured, the number of focal adhesion were determined by counting the individual vinculin markers within each cell. The FA density (the number of vinculin markers per cell) was calculated using digital image processing software (Axiovision Rel 4.5, Zeiss, Germany). FA density data were used as a method of assessing HDF attachment strength. Cell area, vinculin count and vinculin density were measured on attached HDFs and compared between substrates. Previously published research has shown that FA density per cell area directly correlates with cell attachment strength in HDFs (Pendegrass et al 2009).

2.3viii- Assessment

Fluorescent Microscopy was used to assess HDF morphology. Cell area and the number of vinculin markers and were both measured under fluorescent microscopy, with FA density calculated from these figures.

2.3ix- Statistics

Data are presented graphically in box and whisker plots where the X-axis represents the substrate groups and the Y-axis represents FA Density/per unit cell area. Data is presented as median (with 95% confidence intervals) and outliers are plotted as individual points outside the box and whiskers. The data did not meet the assumptions required for parametric testing. Non-parametric statistical analyses were performed. Kruskal-Wallis tests of each data set, consisting of one nominal variable and one measurable variable, were performed to determine whether multiple groups were from the same population distribution. Where data sets were not observed to be in the same

population distribution (Kruskal-Wallis $p < 0.05$), pair-wise Mann-Whitney (MWU) tests were used to determine differences between groups on a pair-wise basis. These tested were performed using SPSS version 19.0 (IMB Inc, USA) (McDonald 2008) and significance results were considered significant at the 0.05 level. Pair-wise comparisons (MWU) are presented in tables for each study. Significant values are highlighted in yellow.

2.4- Results

2.41- Study 1

HDF attachment was observed on all substrates. A Kruskal-Wallis test demonstrated that the data were not from the same population distribution (p <0.05).

There were no significant differences in HDF attachment with either linear or cyclic RGD-polypeptide functionalised titanium alloy substrates compared with controls when substrates were prepared with a 1-hour adsorption time (MWU p >0.05; Fig 2.01, Table 2.06).

HDF attachment significantly increased on RGD-polypeptide functionalised titanium alloy substrates compared with controls when substrates were prepared with a 4-hour adsorption time (MWU p <0.05; Fig 2.01, Table 2.06).

No difference in HDF attachment was observed with linear or cyclic RGD-polypeptide functionalised substrates at either 1 or 4-hours (MWU p >0.05; Fig 2.01, Table 2.06).

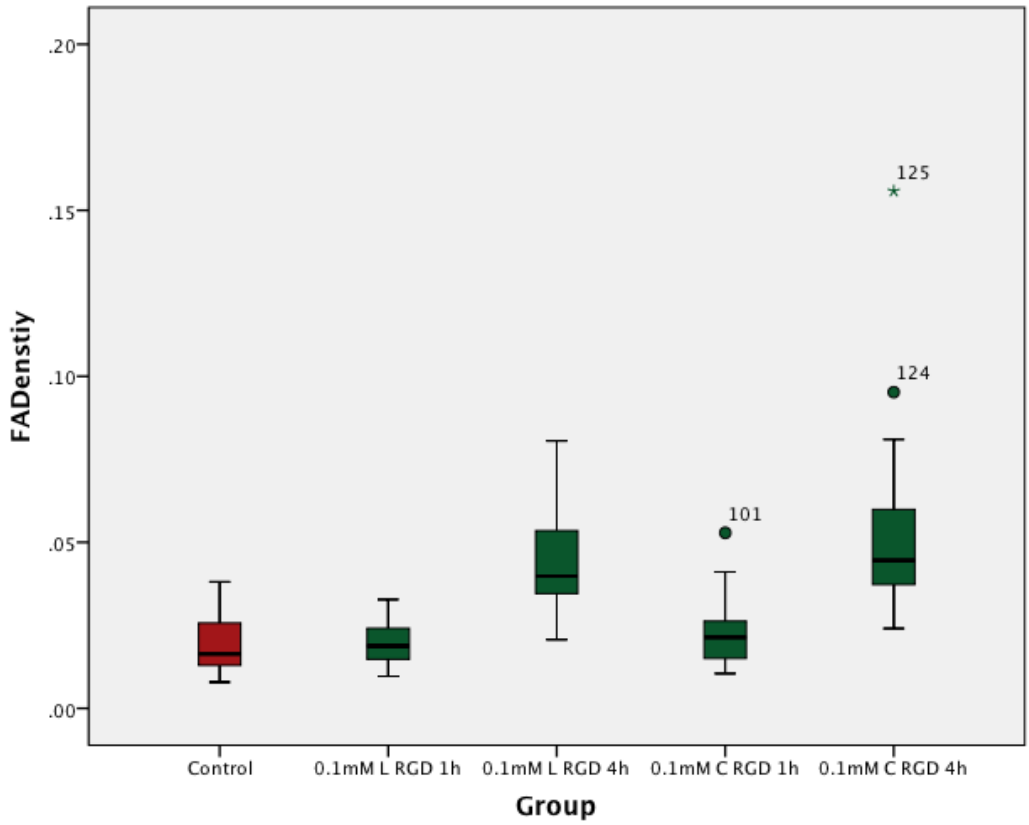

Fig 2.01 Box and Whisker plot demonstrating FA Density on adsorbed (green) RGD polypeptide functionalised titanium alloy substrates compared with controls (red) at 24 hours.

Table 2.06- Pair-wise MWU comparisons

	Control	**0.1mM L RGD 1h.**	**0.1mM L RGD 4h.**	**0.1mM C RGD 1h.**	**0.1mM C RGD 4h.**
Control		0.515	0.000	0.069	0.000
0.1mM L RGD 1h.			0.000	0.261	
0.1mM L RGD 4h.					0.322
0.1mM C RGD 1h.					0.000

2.4ii- Study 2

Statistical analysis using Kruskal-Wallis test suggested data were not normally distributed (p <0.05).

HDF attachment was highest on titanium alloy substrates functionalised with silanised linear RGD-polypeptides, median value 0.0439 (CI 0.0363-0.0476). These data were significantly higher compared with controls (MWU p <0.05; Fig 2.02, Table 2.08) and substrates functionalised with silanised cyclic RGD-polypeptide (MWU p <0.05; Fig 2.02, Table 2.07).

No significant difference was observed in HDF attachment between cyclic RGD-polypeptide functionalised titanium alloy substrates and controls (MWU p >0.05; Fig 2.02, Table 2.07).

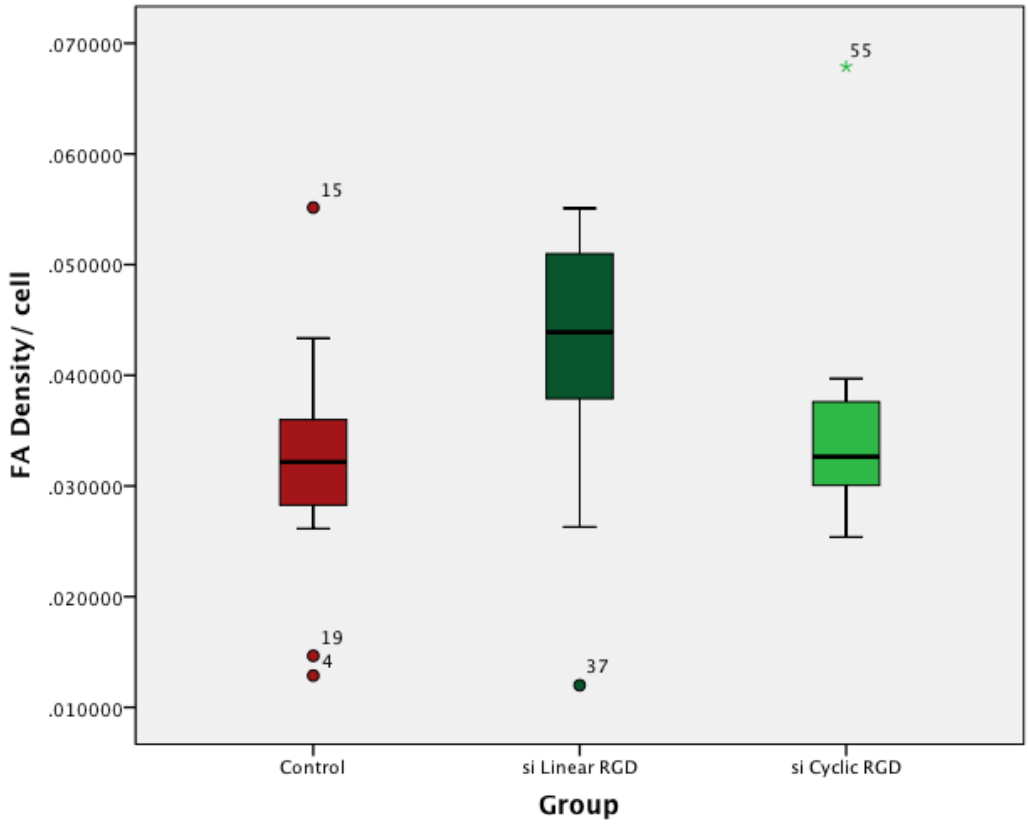

Fig 2.02 Box and Whisker plot demonstrating FA Density on silanised Linear (dark green) and silanised Cyclic (light green) RGD functionalised titanium alloy substrates compared with controls (red) at 24 hours.

Table 2.07- Pair-Wise MWU Comparisons

	Control	siLinear RGD	siCyclic RGD
Control		0.007	0.411
siLinear RGD			0.007

2.4iii- Study 3

A Kruskal-Wallis test of normality demonstrated that the data were not from the same population distribution (p <0.05).

All functionalised substrates, whether with fibronectin or RGD polypeptide, prepared through adsorption or silanization, significantly increased HDF attachment when compared with controls (MWU p <0.05; Fig 2.03, Table 2.08).

Attachment of HDF peaked on silanised fibronectin substrates with a median value of 0.0428 (CI 0.0357-0.0454). These data were significantly higher than HDF attachment on substrates functionalised with silanised RGD polypeptides (MWU p <0.05; Fig 2.03, Table 2.08).

There was no significant difference in HDF attachment between the adsorbed and silanised fibronectin functionalised titanium alloy substrates (MWU p >0.05; Fig 2.03, Table 2.08).

There was no significant difference in HDF attachment between the adsorbed and silanised RGD-polypeptide functionalised titanium alloy substrates (MWU p >0.05; Fig 2.03, Table 2.09), nor when comparing RGD with fibronectin functionalised substrates, using the adsorbed protocol (MWU p >0.05; Fig 2.03, Table 2.08).

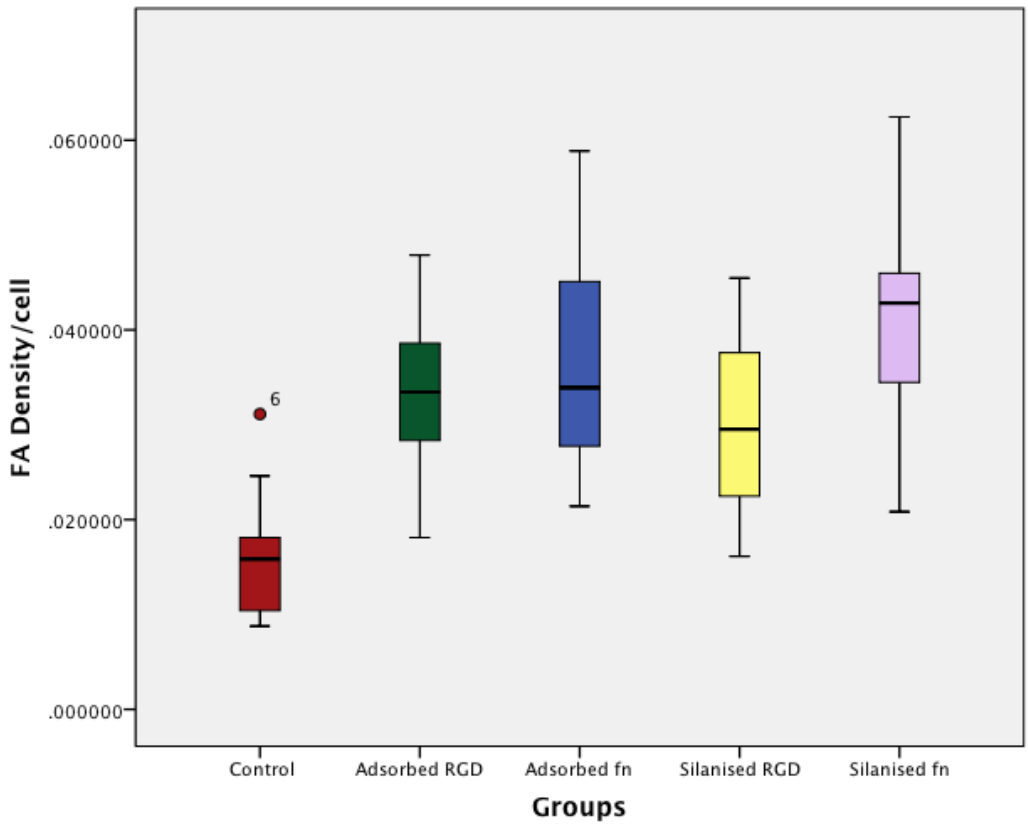

Fig 2.03 Box and Whisker plot demonstrating FA Density on adsorbed (green) and silanised (yellow) RGD functionalised titanium alloy substrates, adsorbed (blue) and silanised (purple) fibronectin functionalised titanium alloy substrates compared with controls (red) at 24 hours.

Table 2.08- Pair-wise MWU Comparisons

	Control	AdRGD	Adfn	SiRGD	Sifn
Control		0.000	0.000	0.000	0.000
AdRGD			0.591	0.164	
Adfn					
SiRGD					0.002

2.4iv- Study 4

Data in Study 4 were not normally distributed as demonstrated by Kruskal-Wallis test (p <0.05).

HDF attachment was significantly increased on all RGD-polypeptide functionalised titanium alloy substrates compared with controls (MWU p <0.05; Fig 2.04, Table 2.09).

HDF attachment was highest on 10mM RGD-polypeptide functionalised titanium alloy substrates (median value: 0.0344, CI 0.0286-0.0389). However this was not significantly higher than HDF attachment observed on either 5mM but significantly higher than 25mM RGD-polypeptide functionalised substrates (MWU p >0.05; Fig 2.04, Table 2.09).

5mM RGD-polypeptide functionalised titanium alloy substrates significantly increased HDF attachment compared with all other RGD-polypeptide functionalised titanium alloy substrates (MWU p <0.05; Fig 2.04, Table 2.09).

HDF attachment was significantly increased on 25mM RGD-polypeptide functionalised titanium alloy substrates compared with 50mM substrates (MWU p <0.05; Fig 2.04, Table 2.09).

There was no significant difference observed in HDF attachment between 50mM and 100mM RGD-polypeptide functionalised substrates (MWU p >0.05; Fig 2.04, Table 2.09).

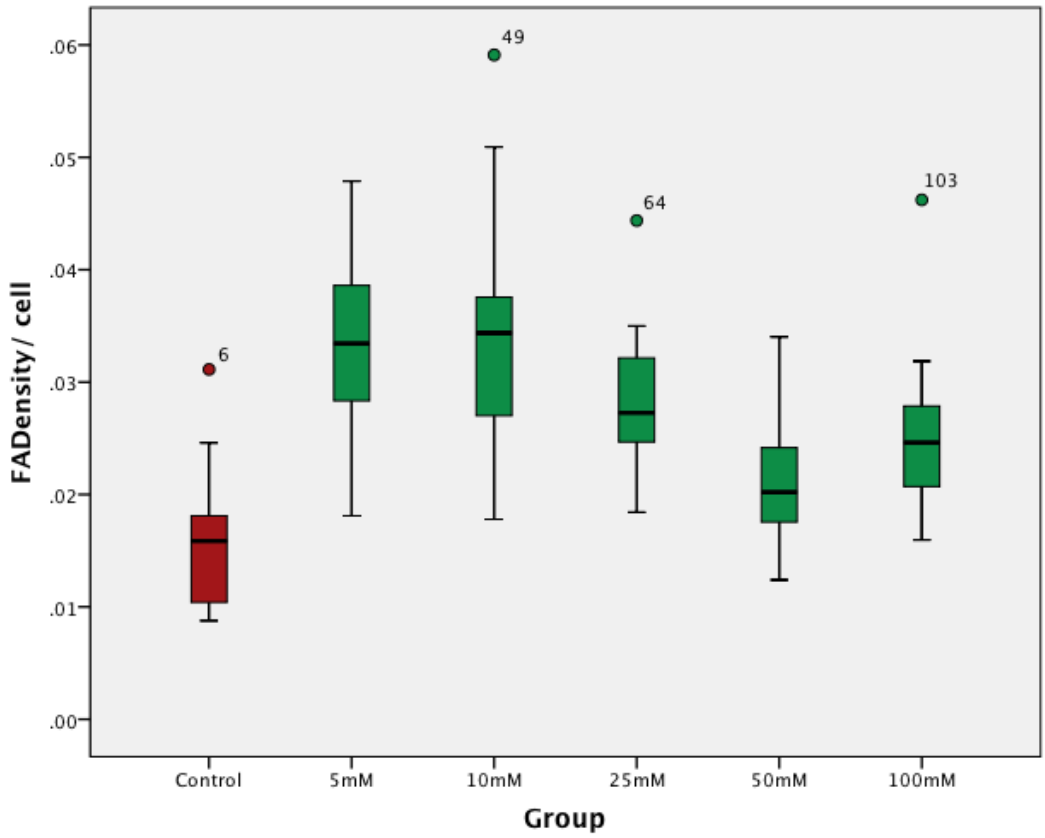

Fig 2.04 Box and Whisker plot demonstrating HDF attachment on adsorbed RGD functionalised titanium alloy substrates (green) compared with controls (red) at 24 hours.

Table 2.09- Pair-wise MWU Comparisons

	Control	5mM	10mM	25mM	50mM	100mM
Control		0.000	0.000	0.000	0.008	0.000
5mM			0.728	0.021	0.000	0.001
10mM				0.054	0.000	0.006
25mM					0.004	0.155
50mM						0.112

2.4v- Study 5

Analysis using the Kruskal-Wallis test showed that data in this study were not normally distributed (p <0.05).

HDF attachment was significantly increased on all functionalised titanium alloy substrates compared with controls at 1-hour (MWU p <0.05; Fig 2.05, Table 2.11), with the exception of silanised RGD-polypeptide functionalised substrates (MWU p >0.05; Fig 2.05, Table 2.10).

HDF attachment was highest on adsorbed RGD-polypeptide functionalised titanium alloy substrates with a median value of 0.0195 (CI 0.0174-0.021). This HDF attachment was significantly higher compared with silanised RGD-polypeptide functionalised substrates (MWU p <0.05; Fig 2.05, Table 2.10).

No significant difference in HDF attachment was observed between RGD-polypeptide and fibronectin functionalised titanium alloy substrates, when compared with either adsorbed or silanised fibronectin (MWU p >0.05; Fig 2.05, Table 2.10).

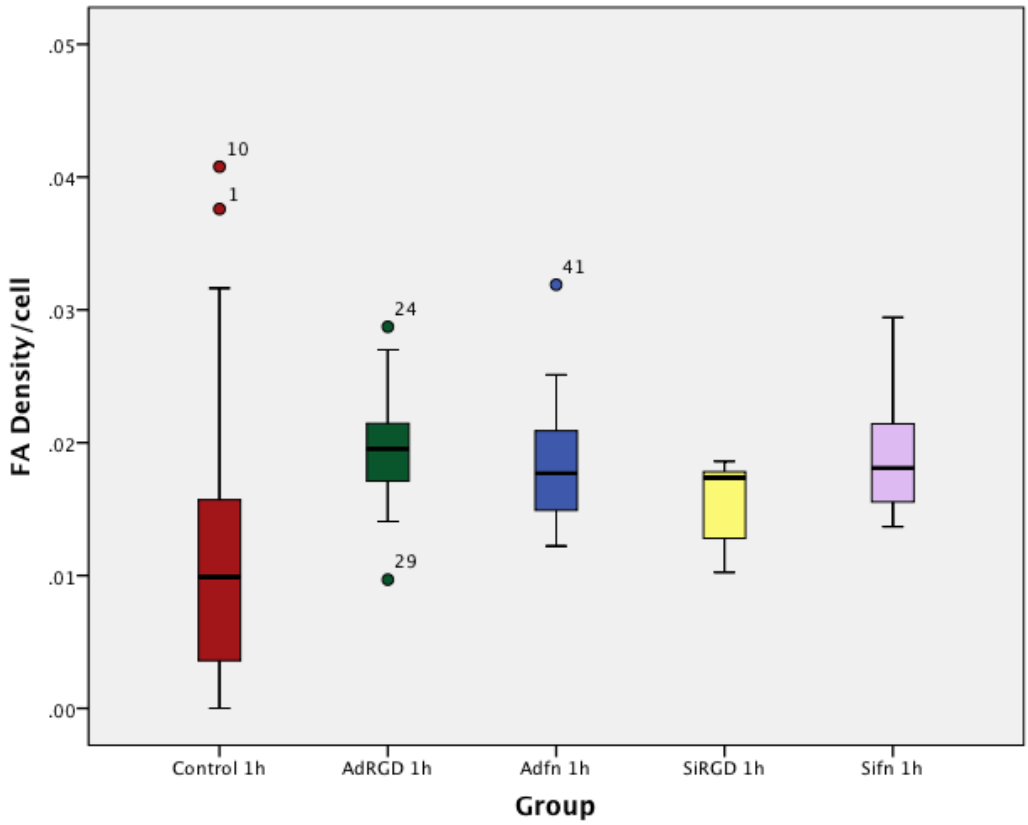

Fig 2.05 Box and Whisker plot demonstrating HFD attachment on adsorbed (green) and silanised (yellow) RGD functionalised surfaces, adsorbed (blue) and silanised (purple) fibronectin functionalised titanium alloy substrates compared with controls (red) at 1-hour.

Table 2.10- Pair-wise MWU Comparisons

	Control	**AdRGD 1h**	**Adfn 1h**	**siRGD 1h**	**Sifn 1h**
Control		0.000	0.000	0.161	0.016
AdRGD 1h			0.395	0.049	
Adfn 1h					0.496
siRGD 1h					0.188

HDF attachment was significantly increased on adsorbed RGD-polypeptide functionalised titanium alloy substrates compared with controls at 4-hours (MWU p <0.05; Fig 4.06, Table 2.11). The highest HDF attachment was observed on this substrate at this time point with a median value of 0.0285 (CI 0.0238-0.0329). (Fig 4.06, Table 2.11)

No significant difference existed between functionalised titanium alloy substrates adsorbed with RGD-polypeptides and absorbed fibronectin (MWU p >0.05; Fig 4.06, Table 2.11).

There was a significant increase in HDF attachment on silanised RGD-polypeptide functionalised substrates compared with silanised fibronectin functionalised substrates (MWU p <0.05; Fig 4.06, Table 2.11).

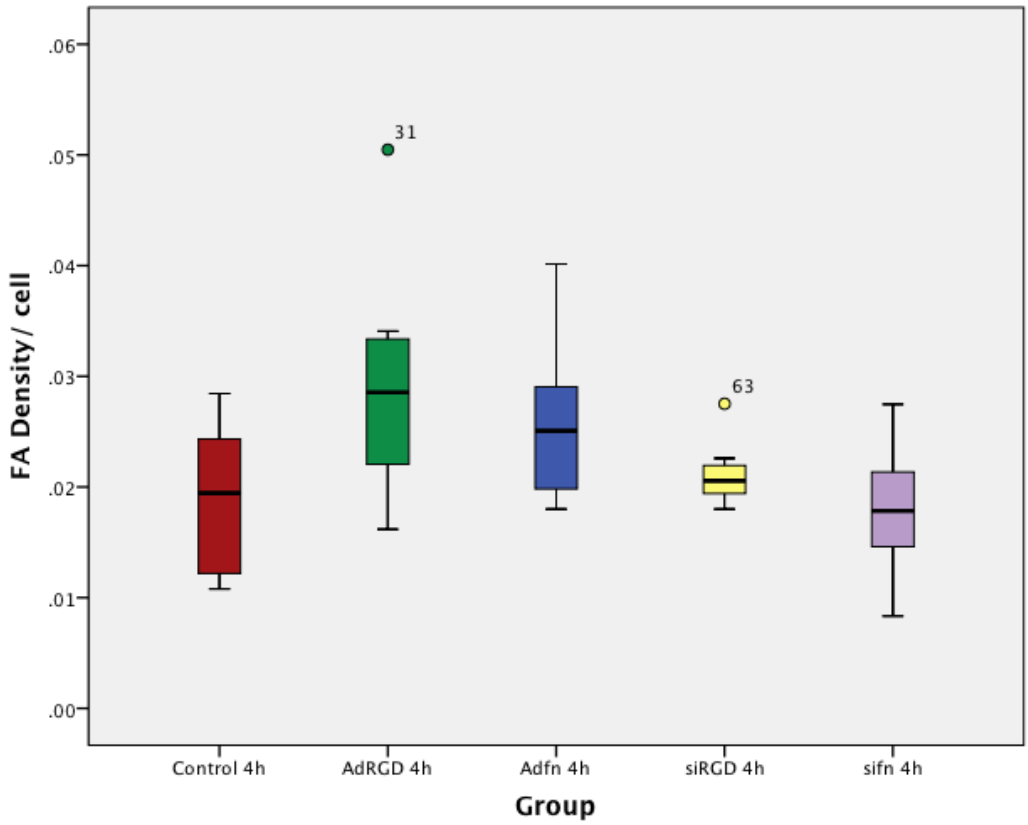

Fig 2.06 Box and Whisker plot demonstrating HDF attachment on adsorbed (green) and silanised (yellow) RGD functionalised titanium alloy substrates, adsorbed (blue) and silanised (purple) fibronectin functionalised titanium alloy substrates compared with controls (red) at 4-hours.

Table 2.11- Pair-wise MWU Comparisons

	Control	**AdRGD 4h**	**Adfn 4h**	**siRGD 4h**	**Sifn 4h**
Control		0.013	0.057	0.342	0.572
AdRGD 4h			0.430	0.018	
Adfn 4h					0.001
siRGD 4h					0.039

HDF attachment was significantly increased in all functionalised titanium alloy substrates compared with controls at 24-hours (MWU p <0.05; Fig 2.07, Table 2.12)

Highest levels of HDF attachment were observed on adsorbed RGD-polypeptide functionalised titanium alloy substrates; with a median value of 0.0333 (CI 0.0303-0.0391) and silanised RGD-polypeptide functionalised titanium alloy substrates, (median value 0.0325; CI 0.0292-0.0421). There was no significant difference in HDF attachment between these functionalised substrates (MWU p >0.05; Fig 2.07, Table 2.12).

No significant difference in HDF attachment was observed when a comparison was made between adsorbed and silanised fibronectin functionalised substrates (MWU p >0.05; Fig 2.07, Table 2.12).

RGD-polypeptide functionalised titanium alloy substrates significantly increased HDF attachment compared with fibronectin functionalised titanium alloy substrates, when either adsorbed or silanised (MWU p <0.05; Fig 2.07, Table 2.12).

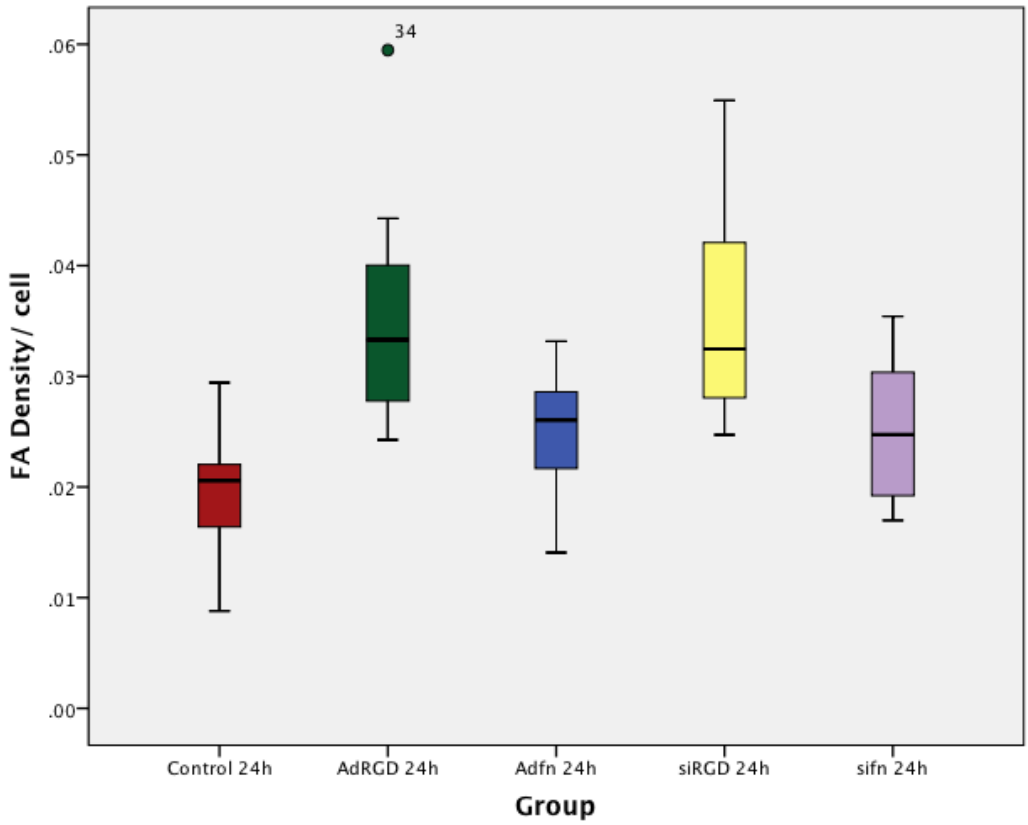

Fig 2.07 Box and Whisker plot demonstrating HDF attachment on adsorbed (green) and silanised (yellow) RGD functionalised titanium alloy substrates, adsorbed (blue) and silanised (purple) fibronectin functionalised titanium alloy substrates compared with controls (red) at 24-hours.

Table 2.12- Pair-wise MWU Comparisons

	Control	AdRGD 24h	Adfn 24h	siRGD 24h	Sifn 24h
Control		0.000	0.007	0.000	0.044
AdRGD 24h			0.002	0.933	
Adfn 24h					0.885
siRGD 24h					0.010

HDF attachment was significantly increased in all functionalised titanium alloy substrates compared with controls at 96-hours (MWU p <0.05; Fig 2.08, Table 2.13).

Highest levels of HDF attachment were observed on adsorbed RGD polypeptide functionalised titanium alloy substrates (median value 0.0734; CI 0.0668-0.0785). HDF attachment was significantly higher than those on adsorbed fibronectin functionalised substrates (MWU p <0.05; Fig 2.08,Table 2.13) and silanised RGD-polypeptide functionalised titanium alloy substrates, (MWU p <0.05; Fig 2.08,Table 2.13).

No significant difference in HDF attachment existed between fibronectin functionalised titanium alloy substrates when either adsorbed or silanised (MW p >0.05; Fig 2.08, Table 2.13).

No significant difference in HDF attachment existed between silanised fibronectin and silanised RGD-polypeptide functionalised titanium alloy substrates (MWU p >0.05; Fig 2.08, Table 2.13).

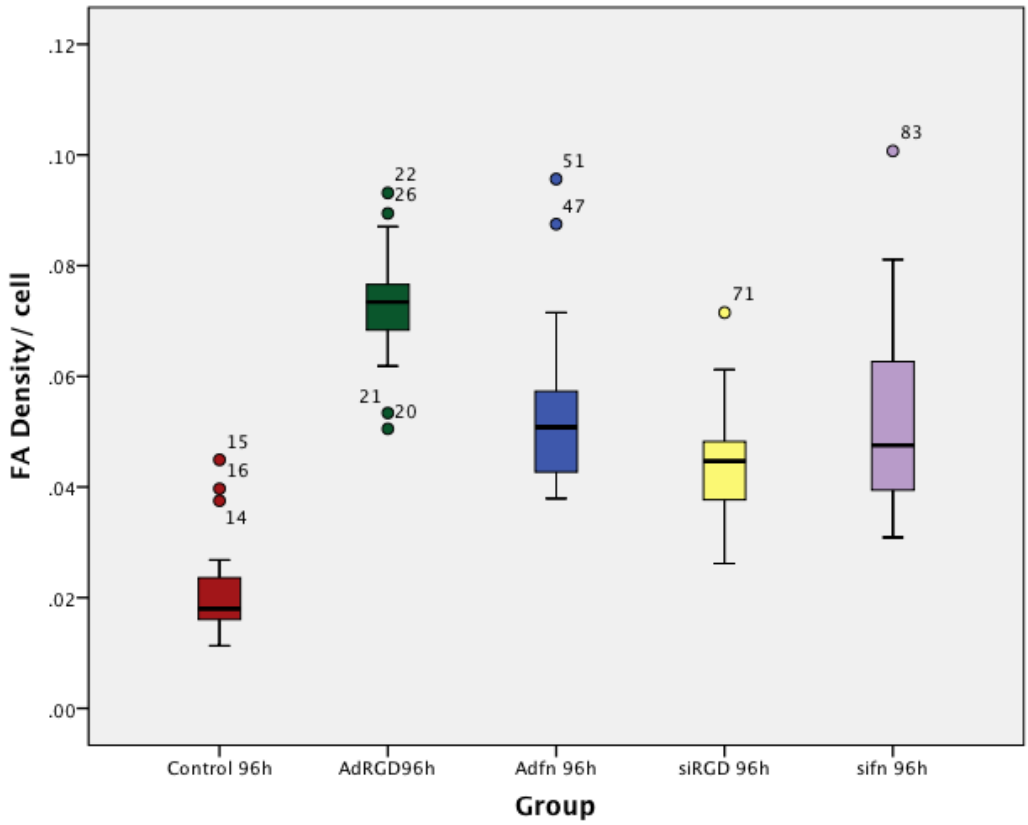

Fig 2.08 Box and Whisker plot demonstrating HDF attachment on adsorbed (green) and silanised (yellow) RGD functionalised titanium alloy substrates, adsorbed (blue) and silanised (purple) fibronectin functionalised titanium alloy substrates compared with controls (red) at 96-hours

Table 2.13- Pair-wise MWU Comparisons

	Control	**AdRGD 96h**	**Adfn 96h**	**siRGD 96h**	**Sifn 96h**
Control		0.000	0.000	0.000	0.000
AdRGD 96h			0.002	0.000	
Adfn 96h					0.626
siRGD 96h					0.204

2.4vi-Qualitative Assessment

At 1-hour, HDF morphology on control substrates were rounded and compact with no cellular processes evident. Vinculin markers were few and appeared as small dots at the periphery of the cell. HDF morphology was consistent on functionalised titanium alloy substrates. However more vinculin markers were observed at the cell periphery and also more spicule shaped markers were observed on these substrates.

At 4-hours HDF morphology on control substrates appeared to be the same as their appearance at 1-hour. However there was evidence of bi-polar elongation of the vinculin markers at the cell periphery as HDF processes began to emanate from the cell body. HDF morphology on functionalised titanium alloy substrates exhibited polygonal spreading with multiple processes emanating from the HDF body (Fig 2.09).

At 24-hours HDF morphology on control substrates exhibited bi-polar elongation from the cell body. HDFs were less round and more spread out with an increase in vinculin markers, distinct as dashes at the cell periphery compared with earlier time-points (Fig 2.09). HDF morphology on functionalised titanium alloy substrates also exhibited increased spreading at this time-point. However, cells were more symmetrical and exhibited a discoid shape, as spreading appeared to occur in multiple directions. Vinculin markers were also clearly evident at the cell periphery and throughout the cell (Fig 2.10).

At 96-hours HDF morphology on controls were well spread and elongation could be observed in multiple directions. HDFs were often observed in a stellate shape compared with discoid morphologies observed on functionalised titanium alloy substrates. Vinculin markers were evident, concentrated in the periphery in HDFs on control substrates. A greater number of vinculin markers were observed in HDFs on functionalised titanium alloy substrates. These were evident throughout the attached HDFs, with clusters still observed in leading edges. Observations at 96-hours using a

lower magnification suggested functionalised titanium alloy substrates appeared to have an increased number of attached cells compared with control substrates (Fig 2.11).

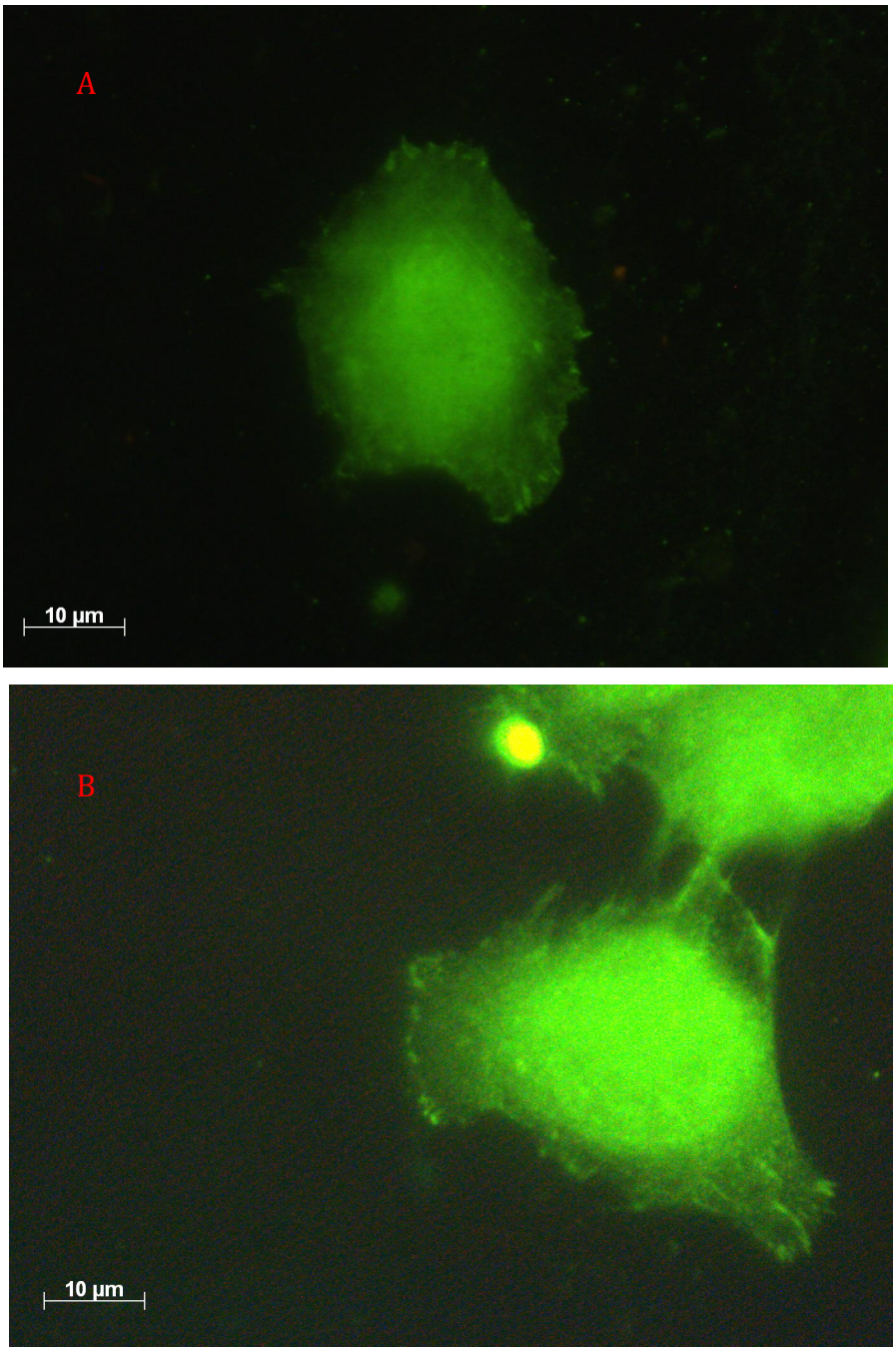

Fig 2.09. Immunolocalisation of vinculin in HDFs attached to titanium alloy substrates at 4-hours; A) image: control, B) functionalised with adsorbed RGD-polypeptide.

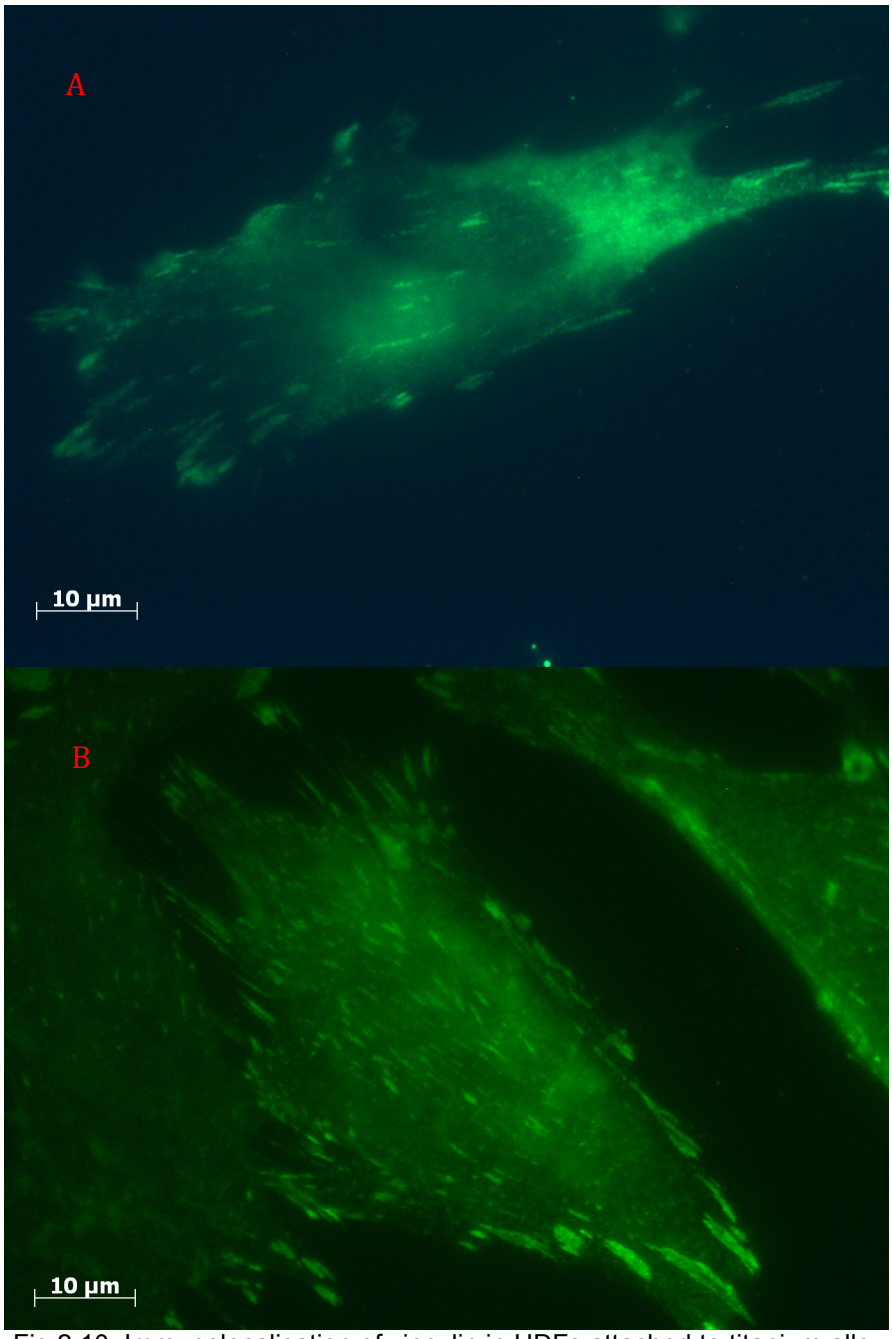

Fig 2.10. Immunolocalisation of vinculin in HDFs attached to titanium alloy substrates at 24-hours; A) image: control, B) functionalised with adsorbed RGD-polypeptide.

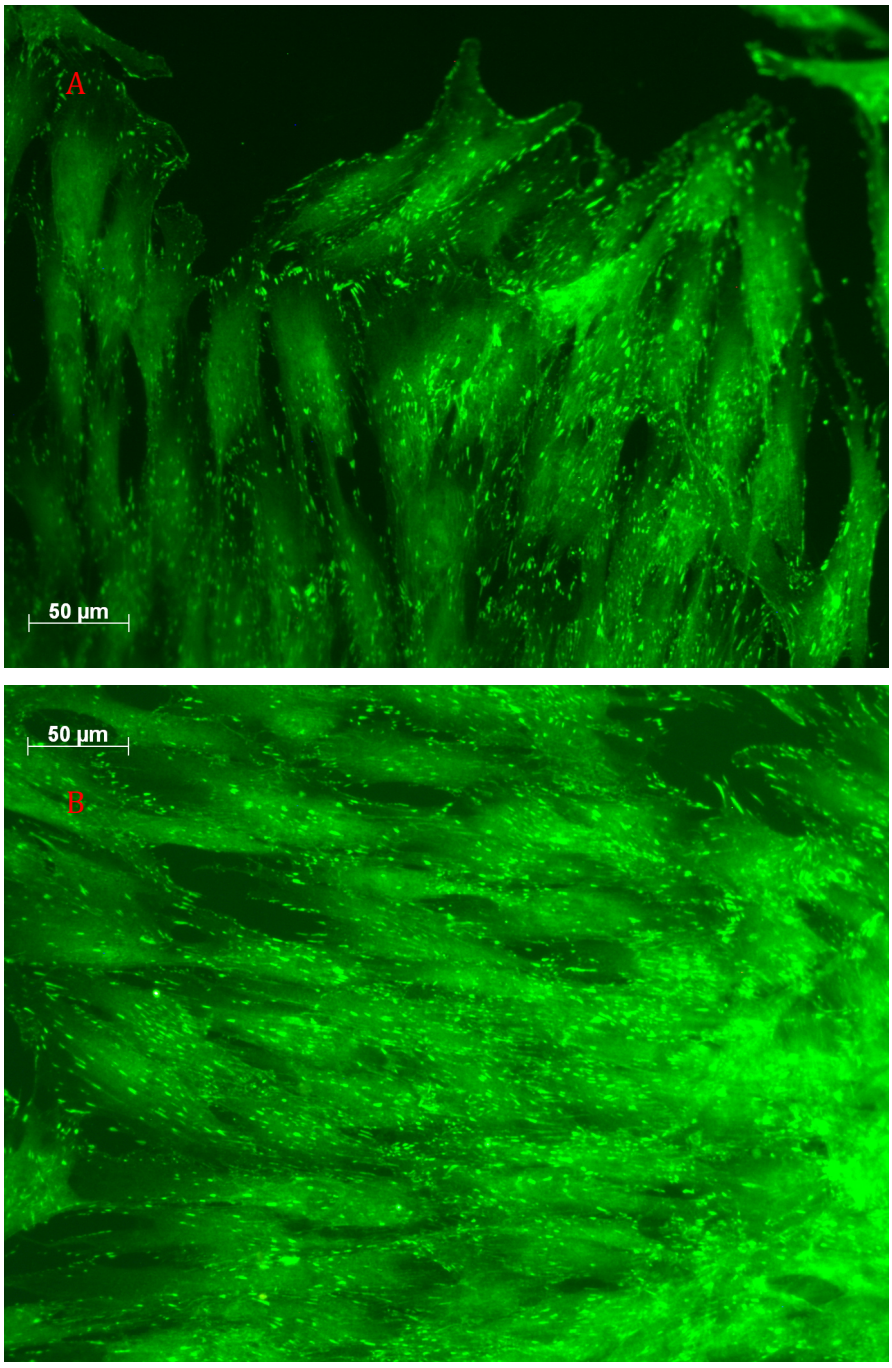

Fig 2.11. Immunolocalisation of vinculin in HDFs attached to titanium alloy substrates at 96-hours; A) image: control, B) functionalised with adsorbed RGD-polypeptide.

2.5- Discussion

Study 1

Adsorption for 1 hour with either linear or cyclic RGD-polypeptides, had no positive influence on cell attachment compared with controls. To positively influence cell attachment the polypeptide would need to be immobilized onto the substrate and remain biologically active. At 4 hours, the polypeptides demonstrated bioactivity by significantly increasing cell attachment. At 1-hour RGD-polypeptides had no significant effect on HDF attachment. Adsorption of biological material to a metallic substrate relies on the formation of electrostatic bonds between the two (Wilson et al 2005). RGD-polypeptides would need to form electrostatic bonds, such as dipole-dipole or Hydrogen bonds, with the titanium alloy substrate. I propose an insufficient number of bonds had formed between the RGD-polypeptides (irrespective of the structure) and the titanium oxide layer had 1-hour. Immobilization of RGD-polypeptides was not achieved and as a consequence, they were able to dissociate from the substrate during the washing phase of the protocol. Passivation of my titanium alloy substrates may have induced an amorphous oxide layer to form and therefore increased the formation of electrostatics bonds between RGD-polypeptides and the substrates. However, this technique can detrimentally affect the structural properties of titanium alloy, which in turn may compromise its' performance in load bearing situations, such as ITAP devices *in vivo* (Chimutengwende-Gordon et al 2011). Yang et al. (2003) demonstrated fibronectin adsorption to titanium substrates was dependent on time, with significant increases in protein adsorption between 15-minutes and 3-hours.

No significant difference in HDF attachment existed between substrates functionalised with linear and cyclic RGD-polypeptides I suggest that linear RGD-polypeptide functionalised titanium alloy substrates, in my study, were able to bind a greater variety of integrin receptors, which has counterbalanced the added preferential affinity of the cyclic polypeptide to the $alpha_V beta_3$ integrin receptor, accounting for the lack of significant difference in HDF attachment observed.

The primary amino-acid sequence RGD, can bind many integrin receptors with low affinity compared with the high affinity to integrin $alpha_v beta_3$ possessed by cyclic RGD-polypeptides. (Ruoslahti, 1996)

The linear polypeptide in this study is zwitterionic, meaning the opposing charges on Arginine (positive) and Aspartic Acid (negative) counterbalance each other. This small, linear polypeptide sequence can be flexible in an aqueous environment as the polar water molecules can interact with the charged arginine and aspartic acid residues. Immobilized on a substrate surface, this flexibility may provide a greater degree of freedom to bind integrin receptors, as there is less emphasis on a highly conserved secondary structure and precise orientation (Reed et al 1988 and Chen et al 2009).

The cyclic polypeptide structure is more rigid due to the presence of stabilising Beta turns (Reed et al 1988). If immobilized onto a substrate surface the structure must be presented to the specific integrin $alpha_v beta_3$ in order to bind. With less flex in the structure, free movement is limited which may decrease receptor affinity. Kammerer et al. (2009) and Patel et al. (2012) both observed significant differences between linear and cyclic RGD-polypeptides on functionalised titanium and PMMA substrates respectively.

Study 2

Silanised linear RGD-polypeptides significantly increased HDF attachment compared with controls. The RGD-polypeptide increased HDF attachment by binding integin receptors on the cell surface. Silanization of biological coatings uses an APTES/Glutaraldhyde complex to act as a spacer between the metallic substrate and, in this case, RGD-polypeptides. This adds rigidity and stability to the coating (Wilson et al 2005) allowing stable presentation of the binding domain to the cell surface receptors.

Davis et al. (2002) confirmed immobilisation of RGD-polypeptides with X-ray Photoelectron Spectroscopy elemental analysis (XPS) before observing

biological activity on his substrates. Myocardial fibroblasts were observed to significantly increase, in number, when cultured on silanised RGDC-polypeptides functionalised silicone substrates compared silicone controls.

No significant difference was observed in HDF attachment when cyclic RGD-polypeptides were silanised to titanium alloy substrates compared with controls. I have already discussed the orientation requirements of the cyclic structure; and these may have contributed to non-significant differences in HDF attachment with the linear structure, when coatings were adsorbed.

Covalent bonding may reduce the flex of the cyclic structure even more, rendering the polypeptide less able to interact with specific integrins, required hence further effecting HDF attachment. Porte-Durrieu et al. (2004) showed successful silanization with both linear and cyclic RGD-polypeptides to titanium alloy substrates. Moreover, osteoprogenitor cell attachment on both linear and cyclic RGD-polypeptide functionalised substrates dramatically improved at 3 and 24-hours time-points compared with titanium alloy controls. Their observed cell attachment results, on the cyclic RGD-polypeptide functionalised substrates, do not support the findings of this experiment, although no statistical evidence was presented.

Kammerer et al. (2011) also observed significant increases in endothelial cell, attachment-dependent processes at 24-hours on titanium substrates silanised with linear RGD-polypeptides. Cyclic RGD-polypeptide functionalised titanium did not have an effect at this time-point, in accordance with my study.

At 72-hours, cyclic RGD-polypeptide functionalised titanium substrates significantly increased endothelial cell proliferation compared with both controls and linear RGD-functionalised substrates (Kammerer et al 2011).

It is possible that HDF attachment could be significantly increased by silanised cyclic RGD-polypeptides at later time points. However, as soft tissue attachment to ITAP *in vivo* is critical within the first 24-hours after implantation,

I have chosen to perform research that looks for a functionalisation strategy to optimise attachment at this time point.

Study 3

Functionalised titanium alloy substrates either with fibronectin or RGD-polypeptide and prepared through adsorption or silanisation, saw a significant up-regulation in HDF attachment compared with controls.

HDF attachment on substrates functionalised with fibronectin was not significantly different, irrespective of coating methodology. This is in accordance with Middleton et al (2007), who demonstrated both adsorbed and silanised fibronectin could significantly enhance HDF attachment.

Adsorbing RGD-polypeptides had no significant effect on HDF attachment compared with silanisation. This suggests the additional surface chemistry associated with silanization does not detrimentally affect the presentation of linear RGD-polypeptides to integrin receptors. Furthermore silanization provides a more favourable functionalisation technique for *in vivo* applications due to the formation of a more durable coating (Middleton et al 2007). In this study, and in opposition to Middleton et al (2007), the silanisation of titanium alloy substrates was performed without a passivation stage. The result of this study supports earlier work performed by Chimutengwende-Gordon et al (2011), who demonstrated enhanced dermal fibroblast attachment to titanium alloy substrates *in vitro* and *in vivo* without this harsh substrate treatment preceding silanisation.

No significant difference in HDF attachment was observed on either absorbed RGD-polypeptide or fibronectin, however silanisation of fibronectin significantly increased attachment compared with RGD-polypeptides.

A true comparison between RGD-polypeptides and fibronectin is difficult, because the numbers of binding domains can never be controlled for.

However the overall aim for ITAP is to develop a functionalised substrate that up-regulates HDF attachment to the greatest degree.

Obara et al. (1988) suggest that differences in fibronectin-mediated attachment and RGD-mediated attachment may be due to a loss of a synergistic site when immobilising the RGD-polypeptide as a biological coating. Results from site-directed mutagenesis experiments suggest the plausibility of fibronectin's mode to encompass positive allosteric modulation through the interaction of a second domain, which may interact with integrin subunits (Obara and Yoshizato 1995). Fibronectin's proposed allosteric modulation of cell attachment compared with increasing the number of bindings domains using RGD-polypeptide functionalisations may counterbalance one other.

Based on a substantially larger relative molecular mass, fibronectin has a superior adsorption capacity compared with RGD-polypeptides, (Yang et al 2003) which, may be more readily removed from the substrates during the preparatory phases of the experiment. However, as no significant difference was observed in HDF attachment between the coatings, it is possible that the number of increased number of binding domains on the RGD-polypeptide compensated for the reduced amount retained on the surface.

RGD-polypeptides in aqueous solution may begin to fold or bend as hydrogen bonds form between flanking residues, therefore decreasing the likelihood of successful receptor affinity as presentation of the binding domain is obstructed compared with fibronectin. However, the linear RGD-polypeptide has the ability to bind various integrin receptors compared with specific integrin affinity associated with binding domain of fibronectin.

Holland et al. (1996) demonstrated a significant increase in percentage of endothelial cell attachment using both fibronectin and RGD-containing polypeptide coated polystyrene substrates compared with control substrates at 1-hour.

Despite these possible differences, functionalisation with RGD-polypeptides or fibronectin is favourable for ITAP as they both significantly up-regulate HDF attachment compared with controls.

Study 4

RGD-polypeptide functionalisation significantly increased HDF attachment in a concentration dependent manner compared with controls.

5mM and 10mM RGD-polypeptide significantly increased HDF attachment compared with all other concentrations. Increasing the number of binding domains with 25, 50 and 100mM of RGD-polypeptides may result in polypeptide aggregation, inhibiting presentation and subsequent binding to integrin receptors, and resulting in the decrease in HDF attachment. The addition of more binding domains may have promoted a non-uniform surface topography and inhibited HDF attachment compared to lower concentrations of RGD-polypeptide. Holland et al. (1996) suggests a uniform surface of RGD-containing polypeptide functionalised polystyrene substrates significantly increases endothelial cell attachment-dependent processes. Integrin receptor clustering in response to the RGD-polypeptides would support the significant increased in HDF attachment observed in substrates functionalised with 5mM and 10mM (Irvine et al 2002).

Maheshwari et al. (2000) demonstrated that increasing the number of RGD-polypeptides covalently bound to glass substrates increased murine fibroblast attachment. However their results suggested receptor saturation at high ligand densities, which may account for my results with concentrations above 10mM of RGD-polypeptides.

Holland et al. (1996) showed significant increases in endothelial cell attachment with RGD-containing polypeptide functionalisation. However, the data did not indicate whether a concentration dependent increase in cell attachment was observed.

In my study a concentration dependent increase was observed up to 10mM and despite a larger number of RGD-polypeptides being made available to the HDF with 25, 50 and 100mM concentrations of RGD polypeptides, failure to see a continued increase in HDF attachment may be due to the cells reaching a maximum level of integrin expression.

This study has shown that HDF attachment to RGD-polypeptides is a concentration dependent process up to 10mM. Further investigation to optimise RGD concentration for HDF attachment is required.

Study 5

Adsorbed RGD-polypeptide functionalisation significantly increased HDF attachment compared with controls at 1, 4, 24 and 96-hours. Middleton et al. (2007) demonstrated similar findings in HDF attachment with silanised and adsorbed fibronectin. In my study, at some time points, 5mM RGD-polypeptides significantly increased HDF attachment compared with fibronectin. This pattern was not observed at 24 hours in Study 3 at 24 hours, where there was no significant difference in HDF attachment on RGD-polypeptide or fibronectin functionalised substrates. This may be due to the decreased concentration on 0.1mM in Study 3, which was insufficient to observe a significant difference. The inconsistency between the studies necessitates further investigation, which is the subject of Chapter 3.

The cell density appeared to be greater under FM, on RGD-functionalised substrates compared with controls, which would indicate higher proliferative capacity of cells on these surfaces. This was not quantified, however it is a finding that is in agreement with Middleton et al. (2007), who, demonstrated a significant increase in dermal cell metabolism with fibronectin functionalised titanium alloy substrates compared with controls. My observations, in conjunction with these data, suggest that coating a titanium substrate with a functional ligand (such as RGD-polypeptide or fibronectin) may positively influence cell attachment dependent processes such as an up-regulation in

cell proliferation, ECM formation and cell differentiation. However, further work would be needed to investigate this.

2.6- Conclusion

The aim of this chapter was to **investigate the effect of synthetic RGD-polypeptides and fibronectin, on human dermal fibroblast (HDF) attachment to titanium alloy substrates *in vitro.***

My experiments have shown that linear RGD-polypeptides can up-regulate HDF attachment to substrates and may be used for ITAP devices to enhance early cell attachment. Such techniques have functionalised titanium alloy substrates as demonstrated by increased HDF attachment strength data. It is critical for soft tissues to attach to ITAP devices within the first 24-hours of implantation *in vivo. In vitro* HDF attachment increases with increasing concentration of linear RGD-polypeptides, up to 10mM, provided they have had sufficient time to adsorb onto the substrate surface or have been covalently tethered to it using silanization.

If functionalisation with RGD-polypeptides is to be considered for *in vivo* applications the durability of the coating must be tested. Silanisation may confer a more beneficial method for functionalising ITAP devices *in vivo* but the use of RGD-polypeptides with this method requires further experimental study to observe whether the functionalised titanium alloy substrates remain functionalised *in vivo*, as demonstrated in this chapter *in vitro*.

Sterilization process combined with regulatory requirements may limit the clinical use of fibronectin as a functionalisation technique. My experiments have shown the adsorption or silanization of RGD-polypeptides can up-regulate HDF attachment to a similar degree to that of fibronectin. This may provide an opportunity to use RGD-polypeptides clinically. Linear RGD-polypeptides can be synthesized from non-human or animal sources and may be less susceptible to harsh sterilization techniques that can denature quaternary structured proteins, such as fibronectin.

A full understanding of the loading and release kinetics for the preparation of a functionalised titanium alloy substrate with RGD-polypeptides is required. I conclude that the RGD biomimetic functionalisation technique in this chapter shows promise for a possible substrate for ITAP but the preparation protocol must be optimized first *in vitro*.

Chapter 3- Understanding of the Loading and Release Kinetics of Biological Functionalisation to Titanium Alloy Substrates, *in vitro*

Chapter 3

3.1- Introduction

Functionality of ITAP devices *in vivo* rely upon a tight skin seal at the transcutaneous interface forming as early after implantation as possible.

In Chapter 2, I demonstrated that RGD-polypeptide functionalised titanium alloy substrates can up-regulate HDF attachment compared with controls. My results suggested HDF attachment on adsorbed and silanised RGD-polypeptide functionalised substrates was concentration dependent. However, the amount of RGD-polypeptide coupled to the titanium alloy substrates needs to be quantified so cell attachment can be optimised and be more strongly attached to titanium alloy substrate.

In the development of other biological functionalisation techniques, fibronectin and laminin have been successfully iodinated to quantify loading and release kinetics to titanium alloy substrates (Middleton et al 2007 and Gordon et al 2009). These techniques rely on the coupling of the ligand with a gamma-emitting Iodine^{125} (I^{125}) isotope.

Others have successfully iodinated RGD-containing polypeptides by the same method and maintained integrin affinity (Jin et al 2010). However, successful RGD-polypeptide iodination required the addition of a Y residue (Tyrosine amino acid) to support isotope coupling. This can be achieved by the established Chloroamine-T method (Jin et al 2010 and advice from PerkinElmer).

The Chloroamine-T method of coupling is rapid and efficient; it minimizes structural changes to the polypeptide and decreasing changes related to bioactivity (Hunter,1962). The reaction utilizes an enzyme to increase the power of oxidation and therefore lower the concentration of potential damaging oxidizing agents (Marchalonis, 1969).

This technique should allow the successful quantification of RGD-polypeptides in order to develop an optimal functionalisation protocol.

Flanking residues adjacent to RGD can influence integrin affinity (Pierschbacher and Ruoslahti, 1987). Tyrosine is a neutral amino acid with a polar hydroxyl side group (Alberts et al 2002). Its addition and possible influence on HDF attachment to titanium alloy substrates will need to be observed before further study to the protocol is undertaken.

As outlined in Chapter 1.2viii, aminopropylated substrates can functionalise implant surfaces by covalently bonding ligands that remain biologically active. This functionalisation technique has been referred to as silanisation (Davis et al 2002, Chimutengwende-Gordon et al 2011, Jose et al 2005, Middleton et al 2007, Nanci et al 1997 and Puleo, 1995). A schematic representation of the silanisation reaction is presented below (Fig 3.01), which has been adapted from others (Puleo, 1995 and Middleton et al 2007). The silane complex provides a ductile spacer arm that covalently bonds to oxygen provided by free surface hydroxyl groups on the substrate (Jose et al 2005), in my case titanium alloy. The ductility of the silane complex may provide the mechanical properties to better withstand the physical stresses associated with receptor interaction during cell attachment (Hersel et al 2003). Hydroxyl groups form on the surface of titanium alloy substrates in an amorphous layer. This layer can be experimentally induced by passivation (Davis et al 2002, Chimutengwende-Gordon et al 2011, Jose et al 2005, Middleton et al 2007, Nanci et al 1997) however, as previously indicated, it compromises the structural properties of titanium alloy, which is critical for ITAP *in vivo* (Chimutengwende-Gordon et al 2011). Substrate analysis on silanised implants has been used to demonstrate the covalent reaction has taken place (Davis et al 2002, Jose et al 2005, Nanci et al 1997 and Puleo, 1995) and functional analysis has been used to confirm the biological activity of tethered ligands (Davis et al 2002, Chimutengwende-Gordon et al 2011, Jose et al 2005, Middleton et al 2007, Nanci et al 1997 and Puleo, 1995).

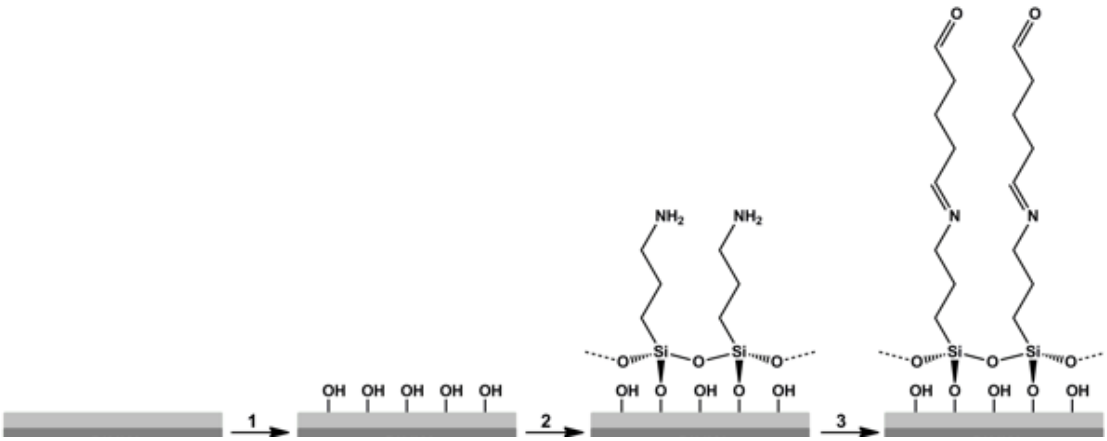

Fig 3.01 Schematic representation of the silanisation reaction in the biological functionalisation of titanium alloy substrates using RGD-polypeptides. Taken from http://www.intechopen.com/books/nanowires-implementations-and-applications/organic-surface-modification-of-silicon-nanowire-based-sensor-devices

RGD-polypeptides (or other ligands) used to functionalise implant surfaces must remain immobilized to the substrate in dynamic environments to have a positive effect. It has been hypothesized that adsorbed proteins are displaced *in vivo* (Middleton et al 2007), so a durable covalent bond between RGD-polypeptides and titanium alloy must be developed. Functionalisation of the bone implant interface using RGD-polypeptides has been established *in vivo* (Ferris et al 2005, Elmengaard et al 2005 and Kroese-Deutman et al 2005), whilst silanisation, rather than adsorption, of fibronectin to titanium alloy implants has been shown to increase soft tissue attachment *in vivo* (Chimutengwende-Gordon et al 2011). However, the environment *in vivo* is far removed from that of *in vitro* experiments.

Other methods of covalently coupling biological ligands to material substrates exist. 2,2,2-trifluoroethanesulfonyl chloride (Tresyl chloride) has been used to hydroxylate titanium and covalently bond fibronectin to the substrate. This method, which does not require a solvent, has not been validated by functionally testing the biological activity of the tethered fibronectin (Hayakawa et al 2003). Nylon functionalisation has been achieved with the covalent attachment of oligodeoxynucleotides. Substrates were coated with poly(ethyleneimine) and 2,4,6-trichloro-1,3,5-triazine (cyanuric chloride),

which allowed the covalent attachment of biologically functional oligodeoxynucleotide ligands (Van Ness et al 1991).

Despite the variety of published methodologies describing the covalent attachment of functional ligands to substrates (Hersel et al 2003), I have decided to use silanisation because significant increases in HDF attachment strength to titanium alloy substrates were observed in Chapter 2 using this particular method. To build upon those initial results, it is important to optimize the methodology in preparation for the *in vivo* development of functionalised ITAP substrates. To achieve this I will use methodologies established by Middleton et al. (2007), in which functionalised substrates were exposed to a competitive environment, mimicking that observed *in vivo,* using protein rich serum and measuring the amount of fibronectin remaining bound over time. The steps taken to optimize this RGD-polypeptide functionalisation technique must positively influence HDF attachment *in vitro*. If my protocol can be optimised I may be able to develop a functionalised ITAP substrate for *in vivo* use.

3.2- Aims and Hypotheses

This chapter aims **to develop a full understanding of the loading and release kinetics of linear RGD polypeptides on titanium alloy substrates, through adsorption and silanisation, and to compare their effects on HDF attachment *in vitro* with those of fibronectin.**

To achieve this, I have devised more specific experimental aims. First, because the addition of a Y residue to the RGD polypeptide is necessary, my initial aim is to establish the effect of YRGD-polypeptide functionalisation on HDF attachment. Secondly, to determine the maximum amount of RGD-polypeptide and fibronectin, that can be adsorbed or silanised, to titanium alloy, and observe how much remains immobilized over time. Thirdly, I aim to assess the durability of my functionalisation techniques by measuring how much RGD-polypeptides and fibronectin remains bound to the substrates when they are exposed to competitive environments which a more realistic in terms of the *in vivo* application. Finally, I will use my optimised functionalisation protocol, which will be determined in these experiments, and assess the outcome of this on HDF attachment *in vitro*.

This Chapter will test the following hypotheses:

1. The Y addition to RGD-polypeptides will have no effect on its ability to up-regulate HDF attachment on titanium alloy surfaces.
2. Silanisation of RGD-polypeptide or fibronectin will create a more durable coating compared with substrates functionalised by adsorption protocols.
3. HDF attachment at 1, 4, 24 and 96 hours will be significantly greater on RGD and fibronectin functionalised substrates compared with controls.

3.3- Material and Methods

3.3i- Study Design

Each study was directed by a specific research question to test my hypotheses, outlined previously.

Study 1

The first research question was whether the addition of a Y residue would alter the effects of the RGD-polypeptide on HDF attachment? Substrates were prepared by adsorption of either RGD-polypeptides or YRGD-polypeptides (HQ809608, AltaBioscience, UK and outlined in 3.3iii). HDF attachment assays were subsequently performed. Table 3.01 outlines the groups assessed (3.41), their specific functionalisations and details of the experiment performed.

Table 3.01- Study 1 Description

Group.	**Substrate Functionalisation.**	**Study Details.**
Control.	Polished titanium alloy (2.3ii).	n=3 and cell attachment assay (2.3vii) performed at 24-hours.
5mM adYRGD.	5mM linear YRGD-polypeptide adsorbed to titanium alloy substrates (2.3iii).	n=3 and cell attachment assay (2.3vii) performed at 24-hours.
5mM adRGD.	5mM RGD-polypeptide adsorbed to titanium alloy substrates (2.3iii).	n=3 and cell attachment assay (2.3vii) performed at 24-hours.

Study 2

This study asked whether there were any errors in the iodination of either ligand, relating to half life or radiolysis. A concentration gradient was set up for I^{-125}YRGD-polypetides and I^{-125}fibronectin respectively and calibration curves were generated. I^{-125}YRGD-polypetides ranged from 1-10mM and I^{-125}fibronectin ranged 0.02μg/mL-20μg/mL, ligands were always dissolved in 50μL droplet of PBS. Assays were repeated three times and the radioactivity was analysed for beta radiation in counts per minute (CPM) using a Tricarb 2900 TR Liquid Scintillation Analyser (PerkinElmer LAS (UK) Ltd), a full methodology is discussed in 3.3iv.

Study 3

The first aspect of understanding the loading and release kinetics of YRGD was to determine the maximal amount of YRGD polypeptide that could be adsorbed and silanised to titanium alloy substrates. I^{-125}YRGD-polypetides substrates were prepared by adsorption (2.3iii) or silanisation (2.3iv) protocols using a range of concentration of 1, 2, 3, 4, 5, 6, 7, 8, 9 and 10mM in 50μL PBS solutions. I^{-125}fibronectin substrates were prepared by silanisation using a range of concentrations, namely 0.2, 2, 5, 10, 15, 20, 40 and 60, 80 and 100μg/mL. These equated to weights of 10, 100, 250, 500, 750, 1000, 2000, 3000, 4000, 5000ng per 50μL droplet of PBS. Radioactivity levels of each substrate were read (3.3iv) and plotted against the original concentrations or weights.

Study 4

This study was performed to determine the time required to couple either YRGD or fibronectin to titanium alloy substrates. Functionalised substrates were prepared through adsorption or silanisation with I^{-125}YRGD-polypetides and I^{-125}fibronectin. Initial concentrations of I^{-125}YRGD-polypetides were **increased to 7mM**, based on results from Study 3. Ligands were allowed to

couple to substrates for 5-min, 2-hour, 20-hour and 140-hour time-points before being washed with PBS. Radioactivity levels of the substrates were read to evidence the amount of ligand remaining bound to the substrates.

Study 5

The aim of this study was to determine the durability of coatings. I^{-125}YRGD-polypetides and I^{-125}fibronectin substrates were prepared. Adsorption and silanisation protocols were amended on the basis of the previous Study's results and the coupling time during silanisation of I^{-125}YRGD-polypetides was increased to 20-hours. In order to measure the durability of adsorbed or silanised proteins substrates were soaked in either PBS or FCS for 5-mins, 2-hours, 20-hours and 140-hours. At each time interval substrates were washed in PBS three times and analysed for radioactivity levels. Assays were repeated three times.

Study 6

To determine the degree of HDF attachment over time, functionalised RGD-polypeptides and fibronectin substrates were prepared by both adsorption and silanisation and HDF attachment assessed at 1, 4, 24 and 96-hour time-points. Protocols used in the preparation of functionalised substrates were based upon 2.3iii and 2.3iv but specific alterations were made based on the findings of Studies 2 and 3 of this chapter (3.4). Table 2.05 outlines the groups assessed (2.45), their specific functionalisations and details of the experiment.

Table 3.02- Study 6 Description

Group	Substrate Functionalisations	Study Details
Control 1h.	Polished titanium alloy (2.3ii).	n=3 and cell attachment assay (2.3vii) performed at 1-hour.
Control 4h.	Polished titanium alloy (2.3ii).	n=3 and cell attachment assay (2.3vii) performed at 4-hours.
Control 24h.	Polished titanium alloy (2.3ii).	n=3 and cell attachment

		assay (2.3vii) performed at 24-hours.
Control 96h.	Polished titanium alloy (2.3ii).	n=3 and cell attachment assay (2.3vii) performed at 96-hours.
AdYRGD 1h.	7mM linear RGD-polypeptide adsorbed to titanium alloy substrates (Based on 2.3iii).	n=3 and cell attachment assay (2.3vii) performed at 1-hour.
AdYRGD 4h.	7mM linear RGD-polypeptide adsorbed to titanium alloy substrates (Based on 2.3iii).	n=3 and cell attachment assay (2.3vii) performed at 4-hours.
AdRGD 24h.	7mM linear RGD-polypeptide adsorbed to titanium alloy substrates (Based on 2.3iii).	n=3 and cell attachment assay (2.3vii) performed at 24-hours.
AdRGD 96h.	7mM linear RGD-polypeptide adsorbed to titanium alloy substrates (Based on 2.3iii).	n=3 and cell attachment assay (2.3vii) performed at 96-hours.
Adfn 1h.	10.0μg/ml Fibronectin adsorbed to titanium alloy substrates (Based on 2.3iii)	n=3 and cell attachment assay (2.3vii) performed at 1-hour.
Adfn 4h.	10.0μg/ml Fibronectin adsorbed to titanium alloy substrates (Based on 2.3iii)	n=3 and cell attachment assay (2.3vii) performed at 4-hours.
Adfn 24h.	10.0μg/ml Fibronectin adsorbed to titanium alloy substrates (Based on 2.3iii).	n=3 and cell attachment assay (2.3vii) performed at 24-hours.
Adfn 96h.	10.0μg/ml Fibronectin adsorbed to titanium alloy substrates (Based on 2.3iii).	n=3 and cell attachment assay (2.3vii) performed at 96-hours.
SiYRGD 1h.	7mM linear YRGD-polypeptide silanised, left to couple to substrate for 20-hours, to titanium alloy substrates (Based on 2.3.iv).	n=3 and cell attachment assay (2.3…) performed at 1-hour.
SiYRGD 4h.	7mM linear YRGD-polypeptide silanised, left to couple to substrate for 20-hours, to titanium alloy substrates (Based on 2.3.iv).	n=3 and cell attachment assay (2.3vii) performed at 4-hours.

SiYRGD 24h.	7mM linear YRGD-polypeptide silanised, left to couple to substrate for 20-hours, to titanium alloy substrates (Based on 2.3.iv).	n=3 and cell attachment assay (2.3vii) performed at 24-hours.
SiYRGD 96h.	7mM linear YRGD-polypeptide silanised, left to couple to substrate for 20-hours, to titanium alloy substrates (Based on 2.3.iv).	n=3 and cell attachment assay (2.3vii) performed at 96-hours.
Sifn 1h.	10.0μg/ml Fibronectin silanised to titanium alloy substrates (2.3iv).	n=3 and cell attachment assay (2.3vii) performed at 1-hour.
Sifn 4h.	10.0μg/ml Fibronectin silanised to titanium alloy substrates (2.3iv).	n=3 and cell attachment assay (2.3vii) performed at 4-hours.
Sifn 24h.	10.0μg/ml Fibronectin silanised to titanium alloy substrates (2.3iv).	n=3 and cell attachment assay (2.3vii) performed at 24-hours.
Sifn 96h.	10.0μg/ml Fibronectin silanised to titanium alloy substrates (2.3iv).	n=3 and cell attachment assay (2.3vii) performed at 96-hours.

The following methods were performed for Studies 1-6.

3.3ii- Substrate Preparation

Surgical grade titanium alloy (Ti_6V_4Al) discs were prepared in accordance with the methodology described in Chapter 2.3ii.

3.3iii- Polypeptide Synthesis

YRGD-polypeptide synthesis was outsourced to AltaBiosciences (Birmingham, UK). Peptide synthesis was achieved by solid phase synthesis from the C-terminal to the N-terminal. High Performance Liquid chromatography (HPLC) and Mass Spectroscopy data confirmed purity. Full spectra data is published in Appendix 2.

3.3iv- Radio-labeling of Ligands

YRGD-polypeptides and fibronectin were radiolabeled by Perkin Elmer (PerkinElmer LAS (UK) Ltd). Iodination of YRGD was performed with oxidizing agent Chloroamine-T. Fibronectin was iodinated by Lactoperoxidase method. Radioactive purity was determined by chromatography before use and was >95% in both instances. (Appendix 2)

Experimental work described from this point was completed in accordance with University College London's Rules for the Uses of Ionizing Radiation (http://www.ucl.ac.uk/estates/safetynet/guidance/radiation/ionising/index.htm).

3.3v- Assessment of Radioactivity

Functionalised substrates were individually placed into 5ml tubes along with 4ml of Ultima Gold XR scintillant (PerkinElmer LAS (UK) Ltd) and analysed for beta radiation in counts per minute (CPM) using a Tricarb 2900 TR Liquid Scintillation Analyser (PerkinElmer LAS (UK) Ltd). Three readings were performed each time. In the case of Study 2, where no substrate was present, a 50ul droplet of dissolved ligand of was pipetted directly into 5ml tubes and follows the same protocol.

3.3vi- Functionalisation via Adsorption

Functionalised substrates were prepared by adsorption of radio-labeled ligands according to 2.3iii, unless otherwise stated.

3.3vii- Functionalisation via Silanisation

Silanisation protocols were performed using radio-labeled ligands, according to 2.3iv unless otherwise stated.

3.3viii- Cell Attachment Assessment- Immunocyochemistry.

The cell attachment assay outlined in 2.3v-2.3vii was performed. In brief, the cell area and the number of vinculin markers immuno-localised with anti-vinculin and quantified to calculate FA density, which was used as a measure of HDF attachment.

3.3ix- Statistics

Statistical analyses were performed according to Chapter 2.3x however; I have adjusted the *p-value* to account for the number of pair-wise comparisons being performed in this Chapter. Significance was now considered at 0.005 level, calculated by performing a Bonferroni correction thereby decreasing the probability of incorrectly rejecting the null hypothesis (Sedgwick, 2012).

3.4- Results

Study 1

In this section I investigated whether the addition of a Y residue would alter the effect of the RGD-polypeptide on HDF attachment. HDF attachment was observed on all substrates. A Kruskal-Wallis test demonstrated that the data for FA density were not from the same population distribution (p <0.05; Fig 3.02) and therefore pair-wise statistical analysis (MWU) was used to compare the means between treatments.

HDF attachment was highest on adsorbed RGD-polypeptide functionalised titanium alloy substrates, and significantly greater than controls (MWU p<0.05; Fig 3.02, Table 3.03. Adsorbed YRGD-polypeptide functionalised titanium alloy substrates significantly increased HDF attachment compared with controls (MWU p <0.05; Fig 3.01, Table 3.03).

There was no significant difference was observed in HDF attachment between either RGD or YRGD-polypeptide functionalised titanium alloy substrates (MWU p >0.05; Fig 3.02, Table 3.03) and so this indicates that incorporating the Y residue into RGD-polypeptide had no effect on the attachment of cells to functionalised surfaces.

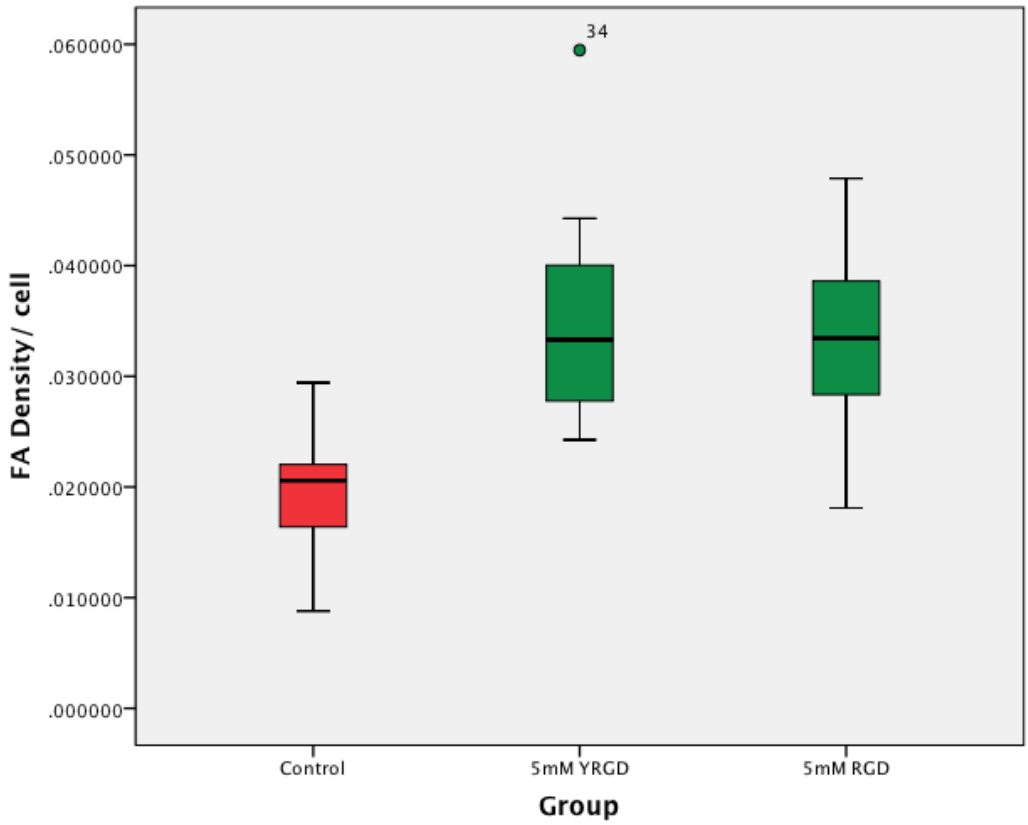

Fig 3.02 Box and Whisker plot demonstrating FA Density on adsorbed Linear (green) RGD functionalised titanium alloy substrates compared with controls (red) at 24 hours.

Table 3.03 Pair-wise (MWU) Compaisons

	Control	**5mM adYRGD**	**5mM adRGD**
Control		0.000	0.000
5mM adYRGD			0.975

Study 2

To avoid any errors pertaining to changes in half-life of I^{-125} a calibration of radio-activity, for both I^{-125}YRGD-polypetides and I^{-125}fibronectin was performed. Each radio-labelled ligand is presented in scatter plot were the Y-axis is defined by CMP and the X-axis is defined by concentration (Fig 3.03 and Fig 3.04). The radiochemical concentration of I^{-125}YRGD-polypetides was 4.5μCi/μg, with straight-line equation of **Y**=156326118**X** + 37970283.87 (Fig 3.03). The radiochemical concentration of ^{125}fibronectin was given at 4.30μCi/μg, with a straight-line equation of **Y**=91092**X** (Fig 3.04).

Calibration for each radio-labelled ligand demonstrated no errors relating to half-life or radiolysis and therefore subsequent experiments continued.

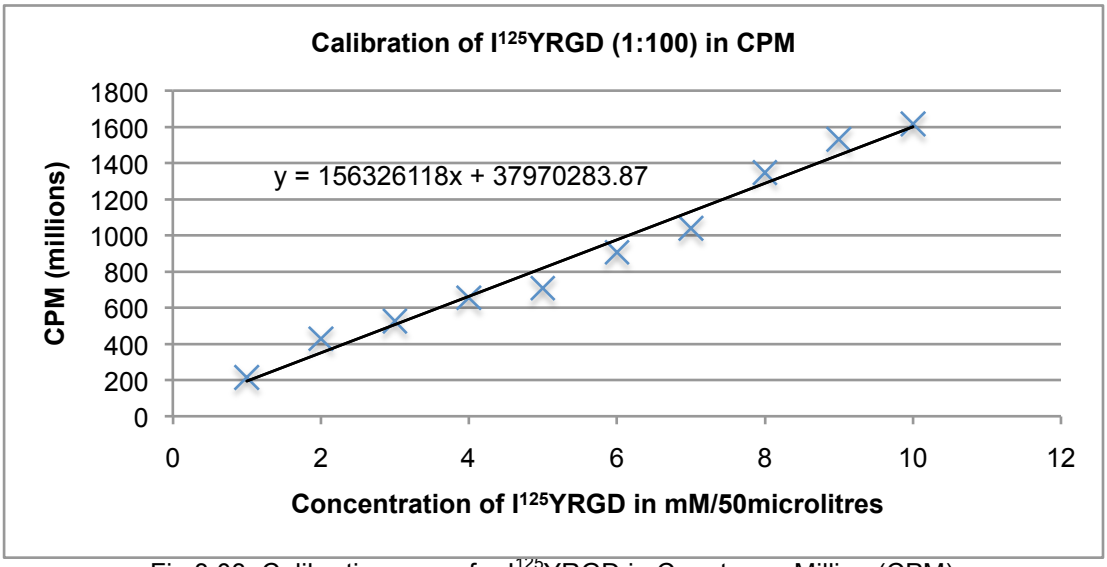

Fig 3.03. Calibration curve for I^{125}YRGD in Counts per Million (CPM)

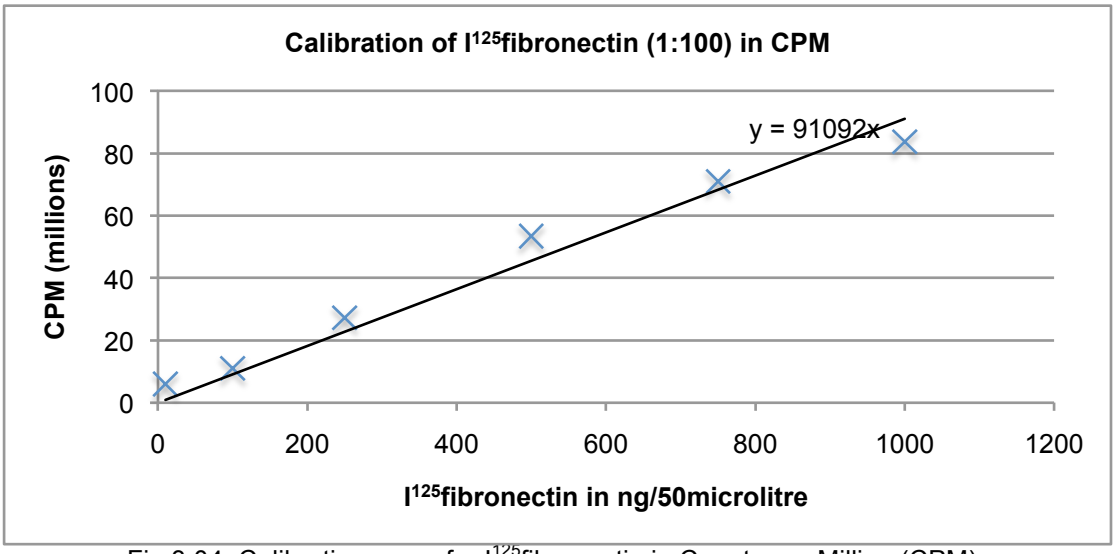

Fig 3.04. Calibration curve for I^{125}fibronectin in Counts per Million (CPM)

Study 3
Adsorbed YRGD

The data were not from the same population distribution (p <0.05). I^{-125}YRGD-polypetides were found to be present on all substrates (Fig 3.05).

For all adsorbed values of I^{-125}YRGD-polypetides, a lower concentration remained bound after the application phase. These values significantly increased as the initial concentration increased, up to 7mM (MWU p <0.005; Fig 3.05, Table 3.04). There were no significant differences in the amounts of adsorbed I^{-125}YRGD-polypetides remaining immobilized on the substrates between 7mM and 8mM (MWU p <0.005) and from 9mM and 10mM (MWU p >0.005). A significant difference in adsorbed I^{-125}YRGD-polypetides remaining immobilized on titanium alloy substrates was observed between from 8mM and 9mM (MWU p <0.005; Fig 3.05, Table 3.04).

Silanised YRGD

The data were not from the same population distribution (p <0.05) and silanised I^{-125}YRGD-polypetides were present on all substrates (Fig 3.06). For all initial amounts of I^{-125}YRGD-polypetides silanised, a lower concentration remained bound after the application phase. These values significantly increased with initial concentration, up to 7mM (MWU p <0.005; Fig 3.06, Table 3.05). There were no further significant differences observed thereafter (all p values > 0.005). 7mM was designated the point of substrate saturation, for silanised I^{-125}YRGD-polypetides, this represented approximately 60% of the original amount silanised onto the substrates (Fig 3.06, Table 3.05).

Fibronectin

The data were not from the same population distribution (p <0.05). I^{-125}fibronectin was present on all substrates (Fig 3.07).

For all concentrations of I^{-125}fibronectin used in the silanisation procedure, a lower amount remained bound after the application phase. These values significantly increased as the concentration increased, up until 80μg/mL I^{-125}fibronectin, which equates to 4000ng in weight (MWU p <0.005; Fig 3.07, Table 3.06).

There was no significant difference observed thereafter. 80μg/mL initially silanised, resulted in 946.9ng, approximately 23% of the original amount remaining on the substrates. This was designated the substrate saturation point (Fig 3.07, Table 3.06).

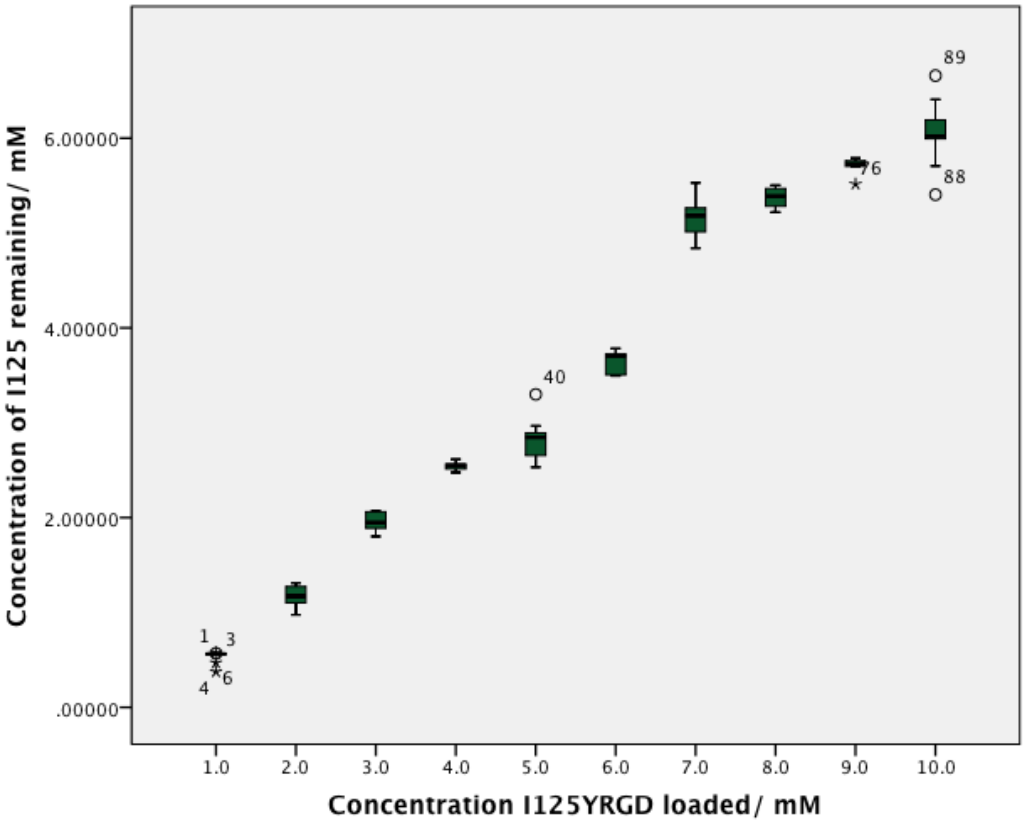

Fig 3.05. Box and Whisker plot of changes in concentration of I^{125}YRGD-polypetptides remaining adsorbed to titanium alloy substrates with increasing concentrations of I^{125}YRGD-polypeptides.

Table3.04 Pair-wise MWU comparisons

Initial Concentration of adsorbed I^{-} ^{125}YRGD-polypetides	**MWU**
1mM-2mM	0.000
2mM-3mM	0.000
3mM-4mM	0.000
4mM-5mM	0.002
5mM-6mM	0.000
6mM-7mM	0.002
7mM-8mM	0.024
8mM-9mM	0.000
9-mM10mM	0.024

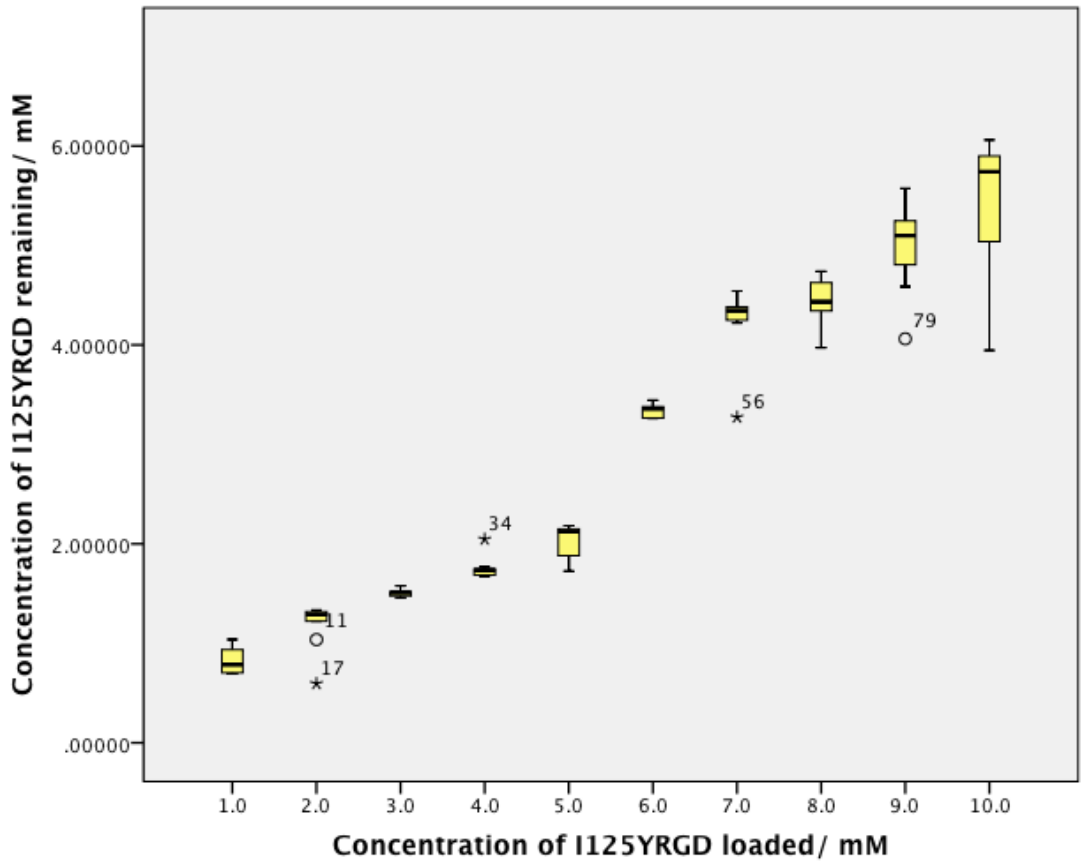

Fig 3.06. Box and Whisker plot of changes in concentration of I^{125}YRGD-polypeptides remaining silanised to titanium alloy substrates with increasing concentrations of I^{125}YRGD-polypeptides.

Table3.05 Pair-wise MWU comparisons

Initial Concentration of silanised I^{125}YRGD-polypetides	MWU
1-2	0.005
2-3	0.000
3-4	0.000
4-5	0.005
5-6	0.000
6-7	0.002
7-8	0.171
8-9	0.009
9-10	0.145

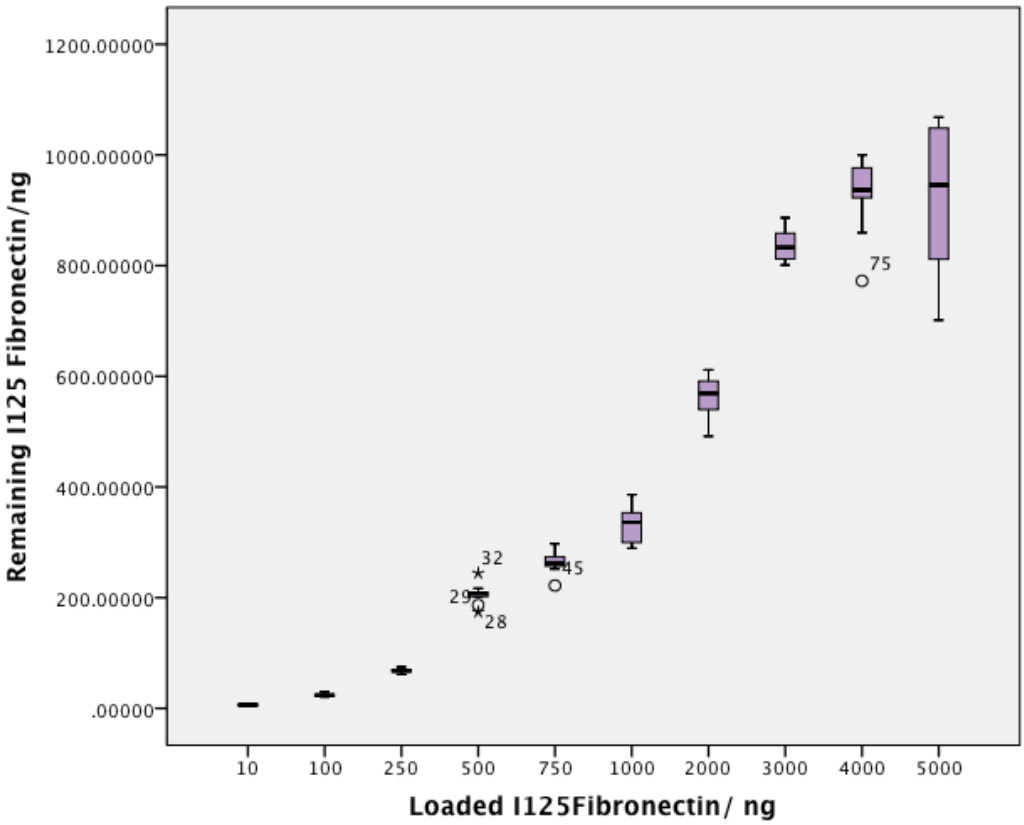

Fig 3.07. Box and Whisker plot of changes in amount of I^{125}fibronectin remaining silanised to titanium alloy substrates with increasing amounts of I^{125}fibronectin.

Table 3.06 Pair-wise MWU comparisons

Initial Concentration of silanised I^{125}fibronectin	**MWU**
10-100	0.000
100-250	0.000
25-500	0.000
500-750	0.000
750-1000	0.001
1000-2000	0.000
2000-3000	0.000
3000-4000	0.000
4000-5000	0.012

Study 4

The concentration of silanised I^{-125}YRGD-polypetides significantly increased over time up to 20-hours (MWN p <0.005), after which there were no further statistical differences (MWU p >0.005; Fig 3.08, Table 3.07). The amount of adsorbed I^{-125}YRGD-polypetides significantly increased between 5-mins and 2-hours (MWU p <0.005). No significant difference was observed in adsorbed I^{-125}YRGD-polypetides between 2-hours and 20-hours (MWU p >0.005). A significant decrease in adsorbed I^{-125}YRGD-polypetides between 20-hours to 140-hours was observed (MWU p <0.005; Fig 3.08, Table 3.07).

Comparisons made between functionalisation techniques showed that silanisation results in significantly more I^{-125}YRGD-polypetides coupled to titanium alloy over time compared with adsorption (MWU p <0.005), with the exception of 5-mins, were no statistical difference was observed (MWU p >0.005); Fig 3.08, Table 3.07).

The amount of silanised I^{-125}fibronectin significantly increased between 5-mins and 2-hours (MWN p <0.005), however, no further statistical differences were observed after that time (MWU p >0.005; Fig 3.09, Table 3.08). The amount of adsorbed I^{-125}fibronectin significantly increased at all time-points (MWU p <0.005; Fig 3.08, Table 3.08). Comparison of the silanised data with functionalised I^{-125}fibronectin showed significantly more silanised protein bound at all time-points compared with adsorbed I^{-125}fibronectin substrates (MWU p <0.005; Fig 3.09, Table 3.08).

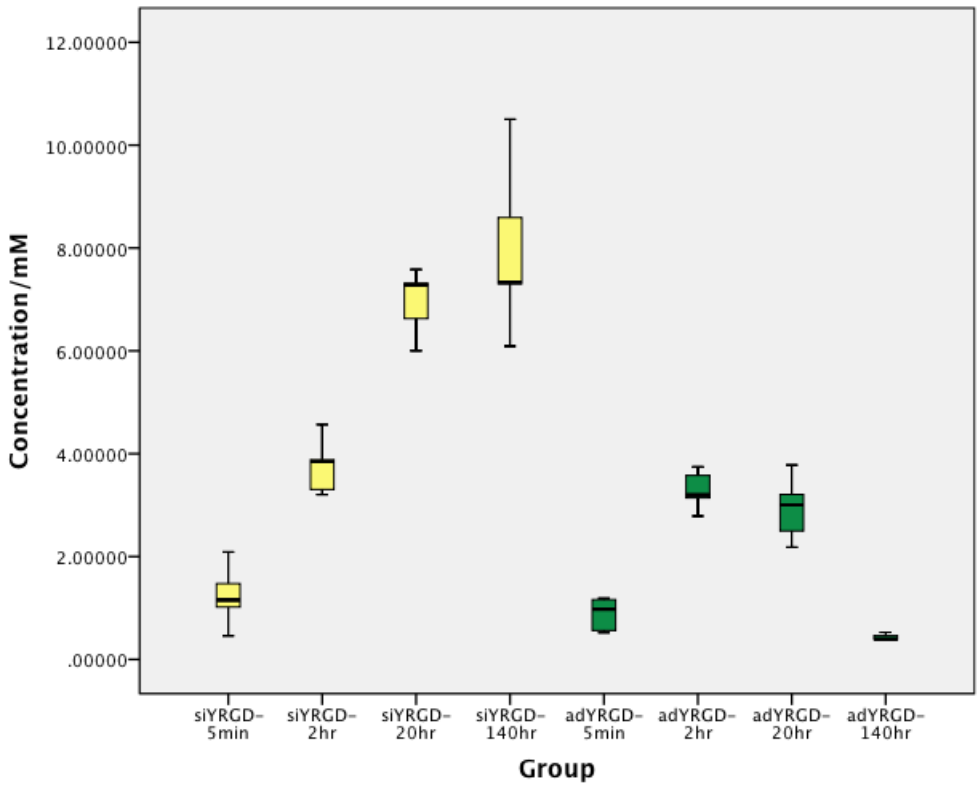

Fig 3.08 Box and Whisker plot of changes in concentration of silanised (yellow) and adsorbed (green) I^{125}YRGD functionalised titanium alloy substrates when washed in PBS after 5mins, 2, 20 and 140 hours.

Table 3.07 Pair-wise MWU Comparisons

	siYRGD 5mins	siYRGD 2hrs	siYRGD 20hrs	siYRGD 140hrs	adYRGD 5mins	adYRGD 2hrs	adYRGD 20hrs	adYRGD 140hrs
siYRGD 5mins		0.000			0.171			
siYRGD 2hrs			0.000			0.009		
siYRGD 20hrs				0.102			0.000	
siYRGD 140hrs								0.000
adYRGD 5mins						0.000		
adYRGD 2hrs							0.171	
adYRGD 20hrs								0.000

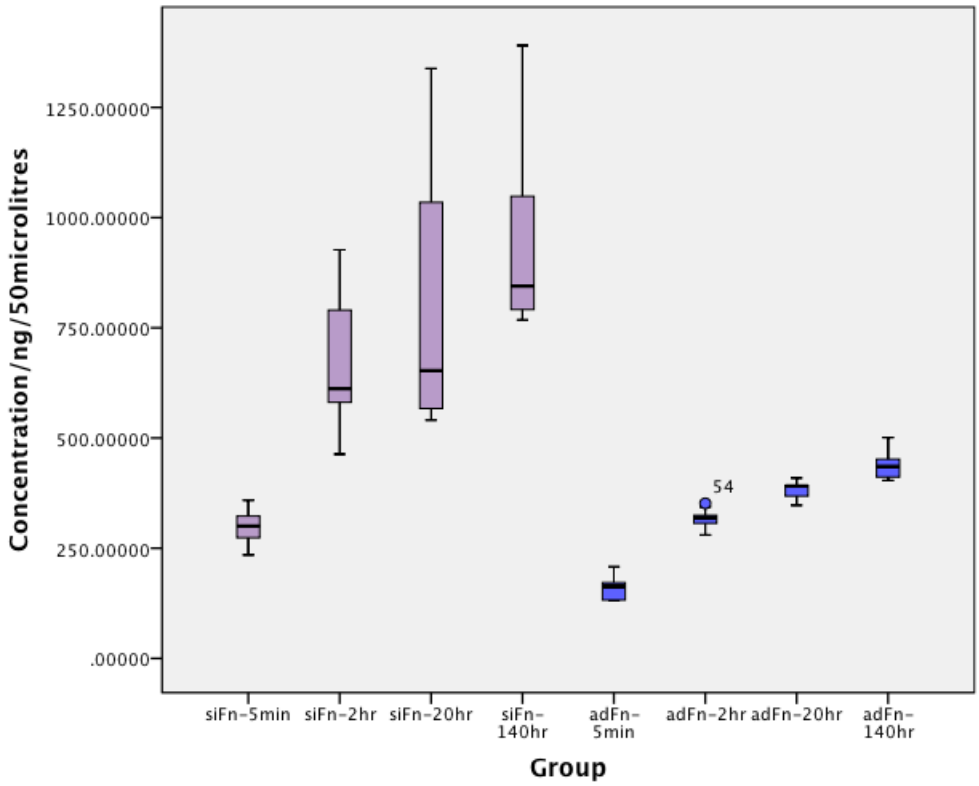

Fig 3.09. Box and Whisker plot of changes in concentration of silanised (purple) and adsorbed (blue) I^{125}fibronectin functionalised titanium alloy substrates were washed in PBS after 5mins, 2, 20 and 140 hours.

Table 3.08 Pair-wise MWU Comparisons

	Sifn 5mins	Sifn 2hrs	Sifn 20hrs	Sifn 140hrs	Adfn 5mins	Adfn 2hrs	Adfn 20hrs	Adfn 140hrs
Sifn 5 mins		0.000			0.000			
Sifn 2hrs			0.691			0.000		
Sifn 20hrs				0.085			0.000	
Sifn 140hrs								0.000
Adfn 5mins						0.000		
Adfn 2hrs							0.000	
Adfn 20hrs								0.000

Study 5

There was no significant decrease in silanised I^{-125}YRGD-polypetides between 5-mins and 2-hours soaked in FCS (MWU p >0.005). Thereafter significant decreases were observed (both MWU values p <0.005; Fig 3.10, Table 3.09). A significant reduction in absorbed I^{-125}YRGD-polypeptides was observed at all time-points (all MWU values p <0.005; Fig 3.10, Table 3.09).

Comparisons between silanised and adsorbed I^{-125}YRGD-polypetides substrates showed silanised I^{-125}YRGD-polypetides were significantly more durable compared with adsorbed functionalised substrates at all time-points (all MWU values p <0.005) with the exception of 5-min time-point, were no difference was observed (MWU p >0.005; Fig 3.10, Table 3.09).

There was a significant reduction in the amount of protein attached to the titanium alloy substrate between 5-mins and 2-hours for silanised I^{-125}fibronectin (MWU p <0.005), thereafter there were no significant differences (both MWU values p >0.005; Fig 3.11, Table 3.10).

For adsorbed I^{-125}fibronectin there was a significant reduction in the amount of attached protein after each time point. Values at each chronological point were significantly lower than the preceding time-point (all MWU values p <0.005; Fig 3.11, Table 3.10).

Comparisons between the functionalised I^{-125}fibronectin show silanisation produced a significantly more durable coating compared with adsorption at all time-points (all MWU values p <0.005; Fig 3.11,Table 3.10).

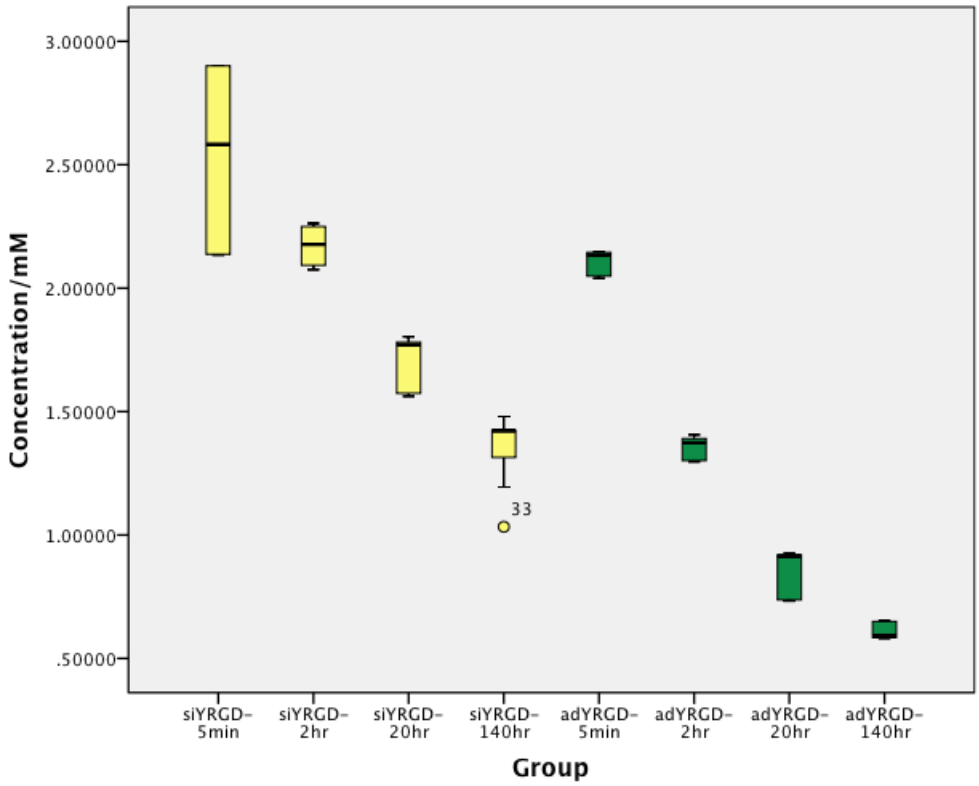

Fig 3.10. Box and Whisker plot of changes in concentration of silanised (yellow) and adsorbed (green) I^{125}YRGD functionalised titanium alloy substrates when soaked in FCS for 5mins, 2, 20 and 140-hours.

Table 3.09 Pair-wise MWU Comparisons

	siYRGD 5mins	siYRGD 2hrs	siYRGD 20hrs	siYRGD 140hrs	adYRGD 5mins	adYRGD 2hrs	adYRGD 20hrs	adYRGD 140hrs
siYRGD 5mins		0.047			0.012			
siYRGD 2hrs			0.000			0.000		
siYRGD 20hrs				0.000			0.000	
siYRGD 140hrs								0.000
adYRGD 5mins						0.000		
adYRGD 2hrs							0.000	
adYRGD 20hrs								0.000

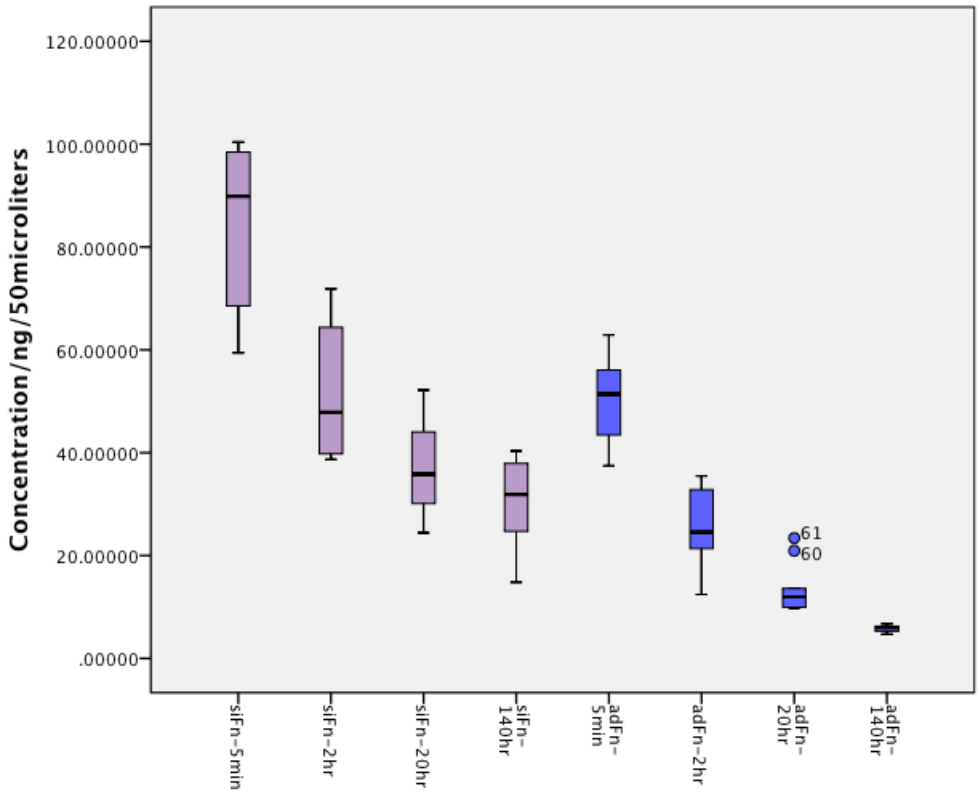

Fig 3.11. Box and Whisker plot of changes in concentration of silanised (purple) and adsorbed (blue) I^{125}fibronectin functionalised titanium alloy substrates when soaked in FCS for 5mins, 2, 20 and 140-hours.

Table 3.10 Pair-wise MWU Comparisions

	Sifn 5min	**Sifn 2hr**	**Sifn 20hr**	**Sifn 140hr**	**Adfn 5min**	**Adfn 2hr**	**Adfn 20hr**	**Adfn 140hr**
Sifn 5min		0.004			0.001			
Sifn 2hr			0.024			0.000		
Sifn 20hr				0.171			0.000	
Sifn 140hr								0.000
Adfn 5min						0.000		
Adfn 2hr							0.001	
Adfn 20hr								0.000

PBS Soak

The amount of silanised I^{-125}YRGD-polypetides decreased over time with PBS soaking. There was a significant decease in silanised I^{-125}YRGD-polypetides between 5-mins and 2-hours and 2-hours and 20-hours (both MWU values p <0.005), there was no significant decease thereafter (MWU p >0.005; Fig 3.12, Table 3.11).

Significant decreases in absorbed I^{-125}YRGD-polypeptides were observed at all time-points (all MWU values p <0.005; Fig 3.12, Table 3.11).

Comparison of the functionalisation techniques demonstrated that significantly more I^{-125}YRGD-polypetides remained bound with silanisation compared with adsorption at all time points (all MWU values p <0.005; Fig 3.12, Table 3.11).

There was a significant decrease observed between 5-mins and 2 hours for silanised I^{-125}fibronectin (MWU p <0.005), however, no significant differences were observed thereafter (both MWU values p >0.005; Fig 3.13, Table 3.12).

Significant decreases in absorbed I^{-125}fibronectin were observed at all time-points (all MWU values p <0.005; Fig 3.13,Table 3.12).

Comparisons between the functionalisation techniques showed that silanisation of I^{-125}fibronectin produced a more durable coating compared with adsorption at all time-points (MWU p <0.005), with the exception at the 2-hour time-point, where no significant difference was observed (MWU p >0.005; Fig 3.12, Table 3.11).

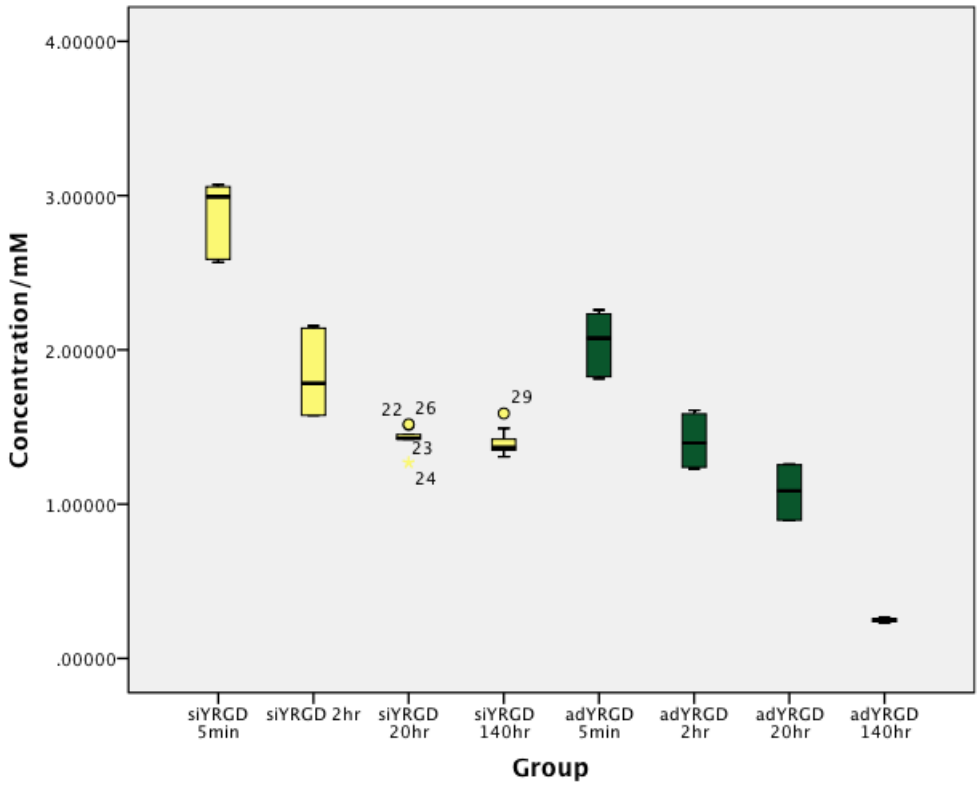

Fig 3.12 Box and Whisker plot of changes in concentration of silanised (yellow) and adsorbed (green) I^{125}YRGD functionalised titanium alloy substrates when soaked in PBS for 5mins, 2, 20 and 140-hours.

Table 3.11 Pair-wise MWU Comparisons

	siYRGD 5mins	siYRGD 2hrs	siYRGD 20hrs	siYRGD 140hrs	adYRGD 5mins	adYRGD 2hrs	adYRGD 20hrs	adYRGD 140hrs
siYRGD 5mins		0.000			0.000			
siYRGD 2hrs			0.000			0.004		
siYRGD 20hrs				0.387			0.000	
siYRGD 140hrs								0.000
adYRGD 5mins						0.000		
adYRGD 2hrs							0.004	
adYRGD 20hrs								0.000

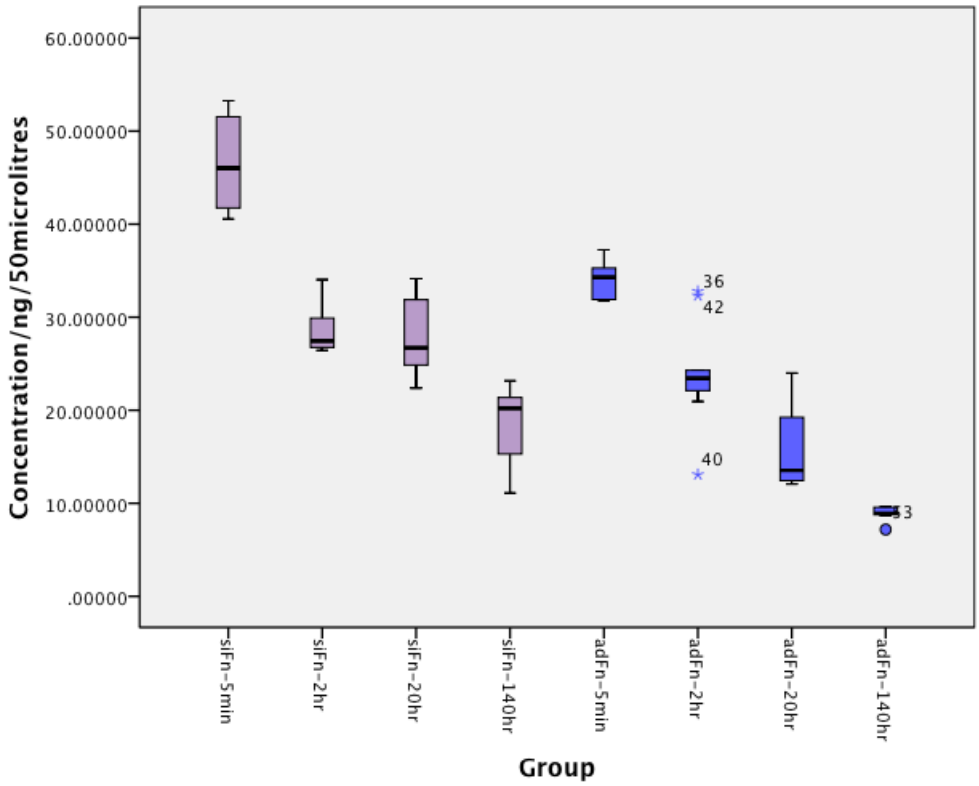

Fig 3.13. Box and Whisker plot of changes in concentration of silanised (purple) and adsorbed (blue) I^{125}fibronectin functionalised titanium alloy substrates when soaked in PBS for 5mins, 2, 20 and 140-hours.

Table 3.12 Pair-wise MWU Comparisons

	Sifn 5mins	Sifn 2hrs	Sifn 20hrs	Sifn 140hrs	Adfn 5mins	Adfn 2hrs	Adfn 20hrs	Adfn 140hrs
Sifn 5 mins		0.004			0.001			
Sifn 2hrs			0.522			0.045		
Sifn 20hrs				0.006			0.002	
Sifn 140hrs								0.001
Adfn 5mins						0.002		
Adfn 2hrs							0.005	
Adfn 20hrs								0.000

Study 6

HDF attachment was observed on all substrates, and the data were not parametrically distributed (p <0.05).

HDF attachment significantly increased on adsorbed fibronectin compared with controls at 1-hour (MWU p <0.005). There were no other significant differences in HDF attachment with other functionalised substrates compared with controls at this time-point (all MWU values p >0.005; Fig 3.14, Table 3.13).

At 4-hours, both adsorbed and silanised fibronectin significantly increase HDF attachment compared with controls (all MWU values p <0.005). HDF attachment on controls was significantly greater compared with YRGD-polypeptide functionalised titanium alloy substrates at this time-point (MWU p <0.005; Fig 3.14, Table 3.13). HDF attachment was significantly greater on all functionalised substrates compared with controls at 24-hours (MWU p <0.005; Fig 3.14, Table 3.13).

At 96-hours, HDF attachment was significantly greater on adsorbed and silanised fibronectin functionalised substrates compared with controls (MWU p <0.005). Adsorption of YRGD-polypeptides did not significantly alter HDF attachment compared with controls (MWU p >0.005). However, silanised YRGD-polypeptides did significantly increase HDF attachment compared with controls (MWU p <0.005; Fig 3.14, Table 3.13).

At 1 and 4-hours, HDF attachment significantly increased on adsorbed fibronectin substrates compared with adsorbed YRGD-polypeptide substrates (both MWU values p <0.005). However no significant differences were observed in HDF attachment between these functionalised substrates at 24 and 96-hours (both MWU values p >0.005; Fig 2.14, Table 2.13).

At 1, 24 and 96-hours, HDF attachment on silanised fibronectin and RGD-polypeptide functionalised substrates was not significantly different (all MWU

values p >0.005). However HDF attachment significantly increased on silanised fibronectin substrates compared with silanised RGD-polypeptides at 4-hours (MWU p <0.005; Fig 3.14, Table 3.13).

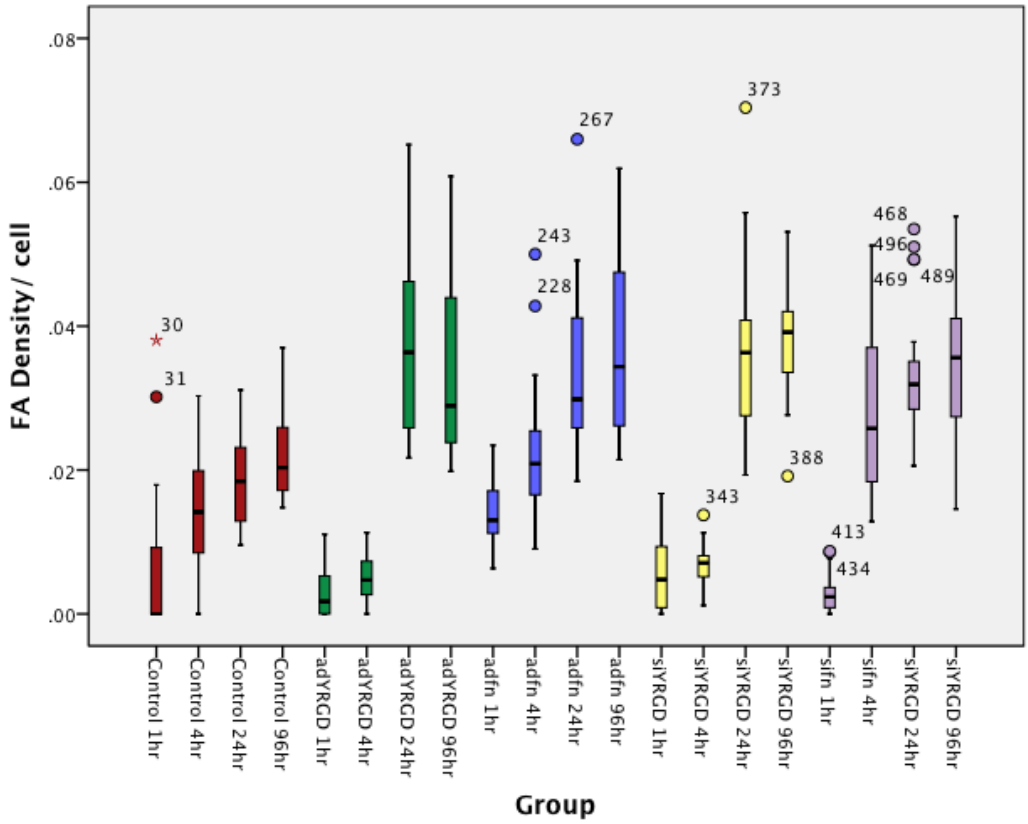

Fig 3.14. Box and Whisker plot demonstrating HDF attachment on adsorbed (green) and silanised (yellow) RGD functionalised titanium alloy substrates, adsorbed (blue) and silanised (purple) fibronectin functionalised titanium alloy substrates compared with controls (red) at 1, 4, 24 and 96-hours.

Table 3.13- Pair-wise MWU comparisons

	adYRGD 1hr	adYRGD 4hr	adYRGD 24hr	adYRGD 96hr
Control 1hr	0.669			
Control 4hr		<0.001		
Control 24hr			<0.001	
Control 96hr				0.01

	Adfn 1hr	Adfn 4hr	Adfn 24hr	Adfn 96hr
Control 1hr	<0.001			
Control 4hr		0.003		
Control 24hr			0.003	
Control 96hr				<0.001

	Adfn 1hr	**Adfn 4hr**	**Adfn 24hr**	**Adfn 96hr**
adYRGD 1hr	0.000			
adYRGD 4hr		0.000		
adYRGD 24hr			0.269	
adYRGD 96hr				0.425

	siYRGD 1hr	**siYRGD 4hr**	**siYRGD 24hr**	**siYRGD 96hr**
Control 1hr	0.225			
Control 4hr		<0.001		
Control 24hr			<0.001	
Control 96hr				<0.001

	sifn 1hr	**sifn 4hr**	**Adfn 24hr**	**Adfn 96hr**
Control 1hr	0.806			
Control 4hr		0.000		
Control 24hr			0.000	
Control 96hr				0.000

	sifn 1hr	**sifn 4hr**	**sifn 24hr**	**sifn 96hr**
siYRGD 1hr	0.024			
siYRGD 4hr		0.000		
siYRGD 24hr			0.273	
siYRGD 96hr				0.200

3.5- Discussion

In study 2 I demonstrated a linear relationship between the level of radioactivity and the concentration of either fibronectin or YRGD suggesting a stable coupling of the isotope had taken place and no radiolysis.

The first study in this chapter demonstrated that there was no detrimental effect on HDF attachment associated with the addition Y residue to the RGD-polypeptide and integrin affinity is maintained. Pierschbacher and Ruoslahti (1987) show flanking residues can influence integrin affinity but the uncharged, polar Y residue may stabilise the polypeptide within its local environment, aiding presentation to integrin cellular receptors. This work supports my first hypothesis. In a similar study, Jin et al. (2010) flanked their RGD-containing polypeptide with a Y residue. Integrin affinity for their RGD-containing polypeptides was achieved, albeit concentration dependent and not in an application with a metallic substrate. HDF attachment was significantly increased on RGD-polypeptide functionalised titanium alloy compared with controls. This is accordance with the findings of Chapter 2.

Study 3 demonstrated that there was a concentration of RGD or fibronectin, which resulted in the saturation of the titanium alloy substrate. Increasing the concentration beyond this level did not effectively increase the level of bound fibronectin or YRGD. Silanisation of 7mM of YRGD-polypeptide saturated the substrates surface with 60% (4.2mM) remaining covalently tether. Adsorbing the same ligand saturates the substrate surface at 7mM. However, a larger fraction of YRGD-polypeptide remained bound (5.0mM) compared with silanised substrates. This may be because of the additional chemistry associated with silanisation and the APTES/Glutaraldehyde complex spatial distribution.

Silanizing 4000ng of fibronectin to titanium alloy substrates yielded 946.9ng remaining covalently tether, approximately 23% of the original amount. This calculated coupling efficiency is less than Middleton et al (2007), who demonstrated 30% efficiency with 4000ng yielding 1218.40ng of silanised

fibronectin to titanium alloy substrates. Coupling efficiency is linked to bond formation between spacer (APTES/Glutaraldehyde complex) and ligand fibronectin or YRGD-polypeptides). It has been suggested that in the presence of increased number of ligands decreases the coupling efficiency. Increased ligands increases reaction products, which in turn inhibits the bond formation of a derivatised substrate (Gordon et al 2010). It is therefore important to understand the loading kinetic in the formation of a derivastised substrate, to make it as efficient as possible and have the most beneficial effect, in this case, on HDF attachment.

In study 4, I showed that YRGD-polypeptides required 20-hours to form covalent bonds the APTES/Glutaraldehyde complex linker on titanium alloy substrates. In contrast Davis et al. (2002) performed covalent coupling to APTES linkers for 2-hours however in this study regular sonication was performed, presumably to lower the activation energy of the chemical reaction. This may account for differences in reaction time used in the methodologies.

The use of radio-labelled ligands accurately quantified the presence of YRGD-polypeptides. I postulate that YRGD-polypeptides are successfully immobilized on the substrate surface. Unbound YRGD-polypeptides would be removed from the substrate surface by washing in PBS prior to radiation assessment and therefore the level of radiation would directly relate to immobilised ligands on the substrate surface. Davis et al. (2002) confirmed immobilisation of RGD-polypeptides with X-ray Photoelectron Spectroscopy elemental analysis (XPS). In short, relative changes in elemental composition of their substrates were attributed to covalent bond formation.

Based on my experimental findings in this study, the subsequent silanisation protocol was adapted to account for the time required for YRGD-polypeptide to couple to the APTES/Glutaraldehyde titanium alloy substrate. The time was increased from 4-hours to 20-hours. On the other hand fibronectin required only a minimum of 2-hours to covalently couple to APTES/Glutaraldehyde complexes on substrates whilst is a similar study, Gordon et al. (2010), demonstrated that laminin required 4-hours to silanised to titanium alloy

substrates, with no significant increase seen at 24-hours of reaction time. Middleton et al. (2007) observed 4-hours as the critical time for silanisation of fibronectin to titanium alloy substrates. So it appears that a difference exists in the time required for YRGD-polypeptides and fibronectin to couple to substrates. I suggest this may involve the number of reactions required to silanise YRGD-polypeptides, based upon the number of binding domains presented to the substrate surface. Furthermore, there may have been more free amine side chains ($-NH_3$) available in the each fibronectin protein compared with individual binding domains, increasing the opportunity for covalent bond formation between the aldehyde groups (-CHO) and subsequently reducing the time required to couple to the substrates.

In Study 5 I showed that silanised YRGD-polypeptides and fibronectin coatings are more durable compared with adsorbed substrates when soaked in PBS or FCS. Adsorption of biological material, be it polypeptides or large globular proteins such as fibronectin, will electrostatically bond to the surface of a substrate that possesses an amorphous oxide layer. (Discussed in Chapter 1.2 and 2.1) PBS is a buffered solution, which may interact with the electro-static surface bonds responsible for immobilization, irrespective to whether YRGD-polypeptides or fibronectin are adsorbed. The covalent bond formed during silanisation appears less susceptible to degradation from a buffered environment.

Soaking functionalised substrates in FCS creates an environment more representative of an *in vivo* environment. Serum proteins are expected to compete for the substrate surface *in vivo* and displace biological coatings. The electrostatic bonds associated with adsorbed substrates are insufficient to immobilise YRGD-polypeptide or fibronectin to the substrates. Larger serum proteins in the FCS may have replaced the coatings, as first described by Vroman et al (1980). However, further work would be needed to demonstrate this. By comparison, the covalent bonds created with silanisation can withstand surface competition from serum proteins in the FCS. This has been reflected in my results as significantly more YRGD-polypeptides and fibronectin remained immobilised on the silanised substrates, at all time points.

This may be beneficial for *in vivo* applications providing the coating remains biologically active.

These data support my hypothesis and are in accordance with others, who have also demonstrated the increased durability based on covalent tethering between metallic substrates and biological functionalisations within a PBS and FCS environment (Middleton et al 2007 and Gordon et al 2010).

The silanisation of YRGD-polypeptides significantly increased HDF attachment at 24 and 96-hours. These significant increases in HDF attachment to silanised YRGD-polypeptide substrates occur at the same time-points compared with Chapter 2, Study 5. No detrimental effects on HDF attachment were observed as a result of the changes to protocol between Chapter 2 Study 5 and Chapter 3 Study 6.

Silanisation of either YRGD-polypeptides or fibronectin show no significant difference on HDF attachment when compared to each other. Significant differences were observed in the comparison on HDF attachment on silanised RGD-polypeptides and fibronectin functionalised substrates in Chapter 2, Study 5. Amendments to the silanisation protocol in this chapter, based on the loading and released kinetics, may have created a more efficient, robust coating that aids HDF attachment. As a result, no significant difference was observed in HDF attachment when comparing silanised YRGD-polypeptides and fibronectin substrates.

Silanised fibronectin has increased soft tissue attachment to titanium alloy *in vivo* (Chimutengwende-Gordon et al 2011), yet its clinical use may be restricted due to regulatory issues and harsh sterilization techniques rendering it inactive. YRGD-polypeptides may provide an alternative solution to overcome these issues, particularly if this functionaliseation technique can functionalize the titanium alloy substrate.

It is possible that the silanisation techniques I have used do not result in the formation of covalent bonds between the RGD-polypeptides and the titanium

alloy substrates. Given the chemical structure of the APTES used, it is possible that it polymerises over the substrate surface, increasing the electrostatic forces of attraction, resulting in a more durable coating in the absence of the formation of covalent bonds. Puleo (1995) quantified the presence of $-NH_2$ groups using 2, 4, 6-trinitrobenzenesulfonic acid (TNBS) with the aim of demonstrating successfully derivatised metal substrates. Such a technique was used to quantify the presence of $-NH_2$ groups however; this does not conclusively show the formation of a covalently bonded APTES spacer to a metal substrate. Jose et al. (2007) performed a 2,2-Dihydroxyindane-1,3-dione (ninhydrin) assay to demonstrate the presence of $-NH_2$ groups on their titanium substrates, again, in an attempt to demonstrate a successfully derivatised metal substrate. These authors further demonstrated the presence of the chosen ligand (vancomycin) on titanium substrates by immunologically staining vancomycin with a fluorescence tag. Both techniques demonstrated the presence of silanised titanium substrates and localization of the ligands under fluorescent microscopy. In addition to using a biochemical method, and as discussed earlier, XPS has been used in an effort to confirm derivatised glass substrate with APTES (Davis et al 2002). Attenuated Total Reflection Fourier Transform Infrared Spectroscopy (ATR-FTIR) has also been used to demonstrate the formation of ligand bonding to polyurethane substrates (Lin et a 2001). None of these studies have conclusively demonstrated the formation of covalent bonds between ligands and their substrates however these methods have been used to demonstrate the formation of a durable, bioactive coating.

With regard to ITAP, a durable coating that could increase cell attachment strength for longer time periods of time would be ideal, however dermal cell attachment is the most critical in the first 24 hours, for successful ITAP device functioning *in vivo*. Despite the fact that covalent coupling of the RGD-polypeptides has not been unequivocally demonstrated here, the coatings have been shown to be more durable over 140 hours compared with adsorbed coatings, and moreover increased cell attachment strength to the substrates in the first 24 hours.

Conclusion

The aims of this chapter in my thesis was **to develop an understanding of the loading and release kinetics of linear RGD-polypeptides and fibronectin to titanium alloy substrates, through adsorption and silanisation, and to compare their effects on HDF attachment *in vitro.*** Silanisation of YRGD-polypeptides has been shown to produce robust coatings that withstand binding competition from serum proteins, and significantly increase HDF attachment between 24 and 96 hours.

The ITAP flange is design to provide an increased surface area for dermal cell and tissue attachment. Silanizing RGD-polypeptides to it may encourage earlier cell attachment to the ITAP flange, thus functionalising it. If achieved, a stable dermal seal will form and may help reduce downgrowth of the epithelium.

Chapter 4- Optimal Structure of Porous Implants for Soft Tissue Integration into ITAP.

Chapter 4

4.1- Introduction

"The critical part of the design of ITAP is a porous, subcutaneous flange that mimics the surface of the deer antler at the transcutaneous interface" (Quotation taken from Kang et al 2010) Perforating a flange with 700μm-diameter holes, and positioning it under the epidermal tissue layer has been shown to increase dermal soft tissue attachment, which acts as a physical barrier to limit epithelial downgrowth around ITAP. This implant design was based on the morphology of the bone at the skin-pedicle interface of deer antlers, which achieves an infection-resistant, and stable transcutaneous juncture without any evidence of downgrowth (Pendegrass et al 2006). When this is achieved clinically, it produced an effective seal preventing downgrowth and subsequent infection around transcutaneous implants (Kang et al 2010).

Loaded orthopaedic implants requiring bone fixation, such as massive endoprotheses, can be structurally adapted to selectively improve biocompatibility (Liu et al 2004). The mismatch in Young's Modulus between the metal implant and the bone can be reduced by manufacturing devices from metals and alloys with Young's Moduli closer to that of bone, for example titanium alloy (Ti_6Al_4V) compared with Cobalt Chrome, thus limiting stress shielding (Chapter 1.2). Bony fixation can be achieved by the in-growth and integration of osteoblasts forming bone tissue within and onto the implant structure. This is referred to as osseointegration. The surface structure of the implant effects the early cellular reaction, which leads to osseointegration (Simmons et al 1999).

Early porous coatings were manufactured using plasma spraying and sintering techniques. Plasma spraying involves introduction of powdered metal usually titanium or hydroxyapatite particle into a plasma flame. The particles are heated and accelerated onto the surface of the implant where they fuse to form a layer, which can be porous. This creates an efficient and low cost method of implant fabrication to create a biocompatible surface capable of being osseointegrated (Liu et al 2004). Sintering can also form

porous coatings and structures. Metal powders or beads can be heated and fused to each other and to a solid structure to create a porous surface in a process that is called sintering. Simmons et al. (1999) demonstrated that an interconnecting porous structure, achieved by sintering titanium alloy to titanium ally bulk implants, integrated into bone sites earlier and to a more stable degree. However, functionaliseation of bulk implant by sintering or plasma often creates non-uniform geometries layered onto a bulk implant, which makes defining the tissue infiltration with respect to the internal geometries difficult.

EBM was discussed, in brief, in Chapter 1. It is a rapid type of powder metallurical processing that fabricates highly specific microstructures, such as open-celled titanium alloy components (Heinl et al 2007). This technology was utilised by the aerospace industry in the fabrication of light-weight components. It is now being utilised in the orthopaedic implant market. (http://www.arcam.com/) It is thought that an open structure can act as a scaffold for the influx of new cells, supported by fluid and vascular delivery of nutrients (Heinl et al 2008).

Harnessed kinetic energy from an electron beam is transferred to thermal energy from a Tungsten filament (Parthasarathy et al 2010). Powdered titanium alloy is homogeneously applied layer-by-layer to form 3-dimensional porous structures. The EBM process has a greater energy density compared with laser manufacturing techniques. High scanning speeds and position accuracy can be achieved by focusing the electron beam through electromagnetic lenses, meaning this single step process has shorter build times and low manufacturing costs. Traditional manufacturing processes, such as those utilised in our laboratory can lower the purity of the metallic implant through adsorption of atmospheric gases, thus degrading the metal alloy. EBM maintains purity as the process occurs under vacuum (Heinl et al 2007, Heinl et al 2008 and Parthasarathy et al 2010).

Porous implant structures have been subject to much research, driven by the aim of developing biological fixation of load-bearing prosthesis in hard tissues.

Aspects from structure dimensions, through to biological response have all been investigated to ascertain optimal specifications (Black, 1992). The porosity of an open or cellular implant facilitates the influx of body fluid *in vivo*, supporting cellular attachment and ultimately tissue implant integration (Wen et al 2002).

The EBM process enables the fabrication of precise porous structures. The optimal porous structure for bone in-growth is yet to be defined (Ryan et al 2006). Internal geometries can be designed to support the Young's Modulus of the anchoring point (Li et al 2009), in an attempt to limit stress shielding. (Chapter 1.2) The flange, which is utilised for soft tissue in-growth, may be enhanced not only by functionaliseation using covalently bound proteins and peptides, which I have previously shown enhances cell attachment, but also by increasing the porosity, which would allow greater soft tissue in-growth. So for the subject of this thesis and the overall aim for ITAP devices, the effect of porous structures on soft tissue in-growth must be considered.

Porous structures aim to limit fibrous encapsulation of implant by providing a 3-D network in which host cells and tissue can invade, attach and integrate. If achieved, this can limit infection compared with bulk implants (Merrit et al 1979).

Neovascularisation throughout a porous structure impacts on connective soft tissue development, supporting collagen deposition and protecting against necrotic changes, based on the permeability of a porous implant. Capillary formation required larger pore diameter (250-488μm) compared with 18-62μm range (Taylor and Smith, 1972). Avascular tissue will impact on the long-term health and metabolism of that tissue.

It has been proposed that the internal architecture of a 3-D porous implant will allow soft connective tissue to infiltrate through a structure, increasing the attachment strength between tissue and implant interface. However porosity in these implants were created by sintering cobalt alloy beads to stainless steel bulk implants, meaning the surface was uneven with no well defined

pore dimension rather a range of 50-200μm which has been specified to enhance tissue in-growth (Bobyn et al 1982).

In contrast, however, La Berge et al. (1990) observed encapsulation, and no fibrous tissue infiltration with pore dimensions of 300μm (+/-15μm). Well vascularised fibrous tissue infiltration required pore dimensions of 900μm (+/-24μm). The manufacturing technique in their study produced a single-layer porous coating of cobalt-chrome alloy beads to bulk implant and the authors postulated that further infiltration could be achieved with a 3-D porous structure. In contrast titanium prostheses used for tendon re-attachment exhibited well-vascularised, fibrocartilage infiltration in porous structures of 400μm (Gottsauner-Wolf et al 1994).

Densely ordered, collagen rich, soft tissues have been observed at 4 weeks *in vivo* throughout interconnected and continuous porous tantalum structures. No specific details were offered in reference to pore dimensions, however SEM images suggested diameters of ~300μm (Hacking et al 2000).

The dental implant arena has also experimented with pore structure in an attempted to interface soft tissues with metal implants. Schroeder et al. (1981) describes the effect of a sintered titanium alloy porous coating on sub-epithelial (fibro-connective) soft tissue attachment *in vivo*. Internal pore geometries ranged between 25-100μm and facilitated dense collagen fibres at 90^0 anchoring to the implant without inflammation.

ITAP devices have been developed based on information obtained from studying the deer antler pedicle. These naturally occurring structures support a soft-hard tissue interface due to pores, which the soft tissues of the dermis and epidermis infiltrate and attach to. Interface characterisation, by Pendegrass et al. (2006), suggests a mean pore diameter of 217μm (+/-19.07μm).

The preceding paragraphs indicate that research on soft issue integration with metallic alloy implants has focused on discovering the optimal pores size. EBM technology allows me to design implants with a range of pore and strut sizes, to assess which is most beneficial for soft tissue integration. Soft tissue integration will be assessed subcutaneously in the belly of the para-spinal muscle in an ovine model. If successful, the findings will be applied to the ITAP flange to support dermal tissue integration.

4.2- Aims and Hypotheses

This chapter aims to **determine the effect of varying pore sizes of EBM porous titanium alloy on soft tissue in-filtration and re-vascularisation *in vivo.***

This chapter aims to test the following hypotheses:

1. Subcutaneous fibrous soft tissue will infiltrate all porous implant structures, but the larger pore sizes will facilitate significantly greater of infiltration compared with small pore sizes, *in vivo*.
2. Larger pores sizes will facilitate a significantly greater influx of cells and exhibit advanced vascularisation throughout the structure compared with the smaller pore sizes *in vivo*.

4.3- Material and Methods

4.3i- Study Design

Cylindrical, surgical grade titanium alloy (Ti_6V_4Al) implants, 20mm in height and 10mm in diameter, were manufactured using EBM techniques (Discussed in 5.2) by Stanmore Implants WorldWide (Stanmore Implants Worldwide, Elstree, UK). 9-implant groups were tested using various combinations of pore and strut sizes (Fig 4.01, Table 4.01), surgically implanted para-spinally into the soft tissue of an ovine model for 4-weeks. Implants were a 3-dimensional structure of circular pores (of constant diameter) and interconnecting struts, also of constant diameter.

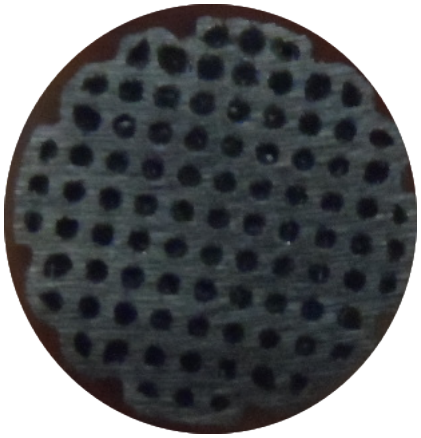

Fig 4.01 Example of Group 5 porous titanium alloy implant.

Table 4.01- Implant Dimensions

Group (n=6)	**Pore size/ μm**	**Strut size/ μm**
1	1000	400
2	1000	200
3	700	400
4	700	300
5	700	200
6	500	400
7	500	300
8	500	200
9	250	300

4.3ii- Implant Preparation

Implants were degreased in Decon 90 in an ultra-sonicator for 2-hours, rinsed extensively in dH_20 and cleaned in alcohol in an ultra-sonicator for 4-hours with hourly changes in alcohol.

4.3iii- Surgery

All surgery was carried out in accordance with the Animal (Scientific Procedures) Act 1986 (https://www.gov.uk/government/publications/animals-scientific-procedures-act-1986-amendment-regulations) and in conjunction with University College London's Statement of the Uses of Animals in Research (http://www.ucl.ac.uk/slms/research/animal-use).

Ovine adult, female Mules (breed) sheep were used for the *in vivo* study.

Premedication of 0.2mg/kg Xylazine, Rompun 2% (Bayer Healthcare, UK) was administered to each animal. Ketamine Hydrochloride (Ketaset, Fort Dodge Animal Health Ltd., UK) induced anesthesia at 2mg with 2.5mg of Midazolam Hypnovel (Roche Products Ltd., UK), both administered intravenously. Animal subjects were intubated, 5ml of Cefalexin Ceporex (Schering-Plough Animal Health, UK) was administered to achieve antibiotic prophylacsis and anesthesia was maintained by inhalation of Isofluorane at 2%.

Anesthetised animals were positioned in the ventral recumbencey and shaved centrally over the spinal region between T12 vertebrae and the Pelvic region in a $15cm^2$ area. The shaved area was washed and cleaned with Betadine-Povidine Surgical Scrub (Dynarex, Quick Medical, Washington, USA) and iodine solution (Dynarex, Quick Medical, Washington, USA), transferred into the operating theatre, draped and the prepared area treated with Chlorhexidine (Cardinal Health, Ohio, USA). All procedures were carried out using aseptic techniques. On the right side of the spine a proximal incision, of 5cm, 2cm below the T12 vertebrae was made in the longitudinal direction,

through the skin and fascia, exposing the para-spinal muscle. A smaller longitudinal incision was made into the muscle, and implants were pushed into the belly of the muscle above and below the incision. Implants sat in the saggital plane. The muscle and overlaying fascia were closed and sutured with absorbable 2-0 Vicryl (Ethicon Inc., New Jersey, USA) and the skin incision was closed using subcutaneous sutures of 1-0 Vicryl (Ethicon Inc., New Jersey, USA). A second skin incision was made, distally to the first. Implants were inserted by the same method, such that four implants were positioned in the right side of the para-spinal muscle. Each incision was sprayed with Opsite (Smith and Nephew plc, London, UK) dressing. The procedure was repeated on the left side of the spine.

4.3iv- Implant Retrieval and Histological Processing

Four weeks post implantation; animals were euthanized by intravenous injection of 0.7mg/kg IV Sodium Pentobarbitone (Pharmasol Ltd., Andover UK) into the jugular vein. All implants were surgically dissected out *en bloc* and placed in 10% formal saline, for 1-week. Then, over a 5-week period, all samples were serially dehydrated with IMS and defatted in Chloroform (full processing data is presented in Appendix 3).

Hard Grade Acrylic Resin (London Resin Company Ltd., London, UK) was given time to penetrate each sample, under vacuum and on a rotator over 2-weeks, with two resin changes.

Samples were cast in cold resin. Flexible casting moulds were lubricated with LR White Accelerator (London Resin Company Ltd, London, UK). Samples were placed in individual moulds and cold resin was mixed with accelerator (100:1). The moulds were filled with resin so the samples were covered and left to polymerise for a minimum of 4-hours in the freezer.

Sections were made, transversely, at the mid-point of each implant using an Exakt E310 diamond edged band saw (Mederex, Frame, UK). Sections were ground evenly using Exakt-Micro-Grinding System (Mederex, Frame, UK) to a

thickness of 100μm with ascending abrasive papers from P400 to P4000 and polished with a pad lubricated with AP-A Suspension, a 5μm agglomerate α alumina suspension (Struers Ltd., Solihull, UK). All sections were stained with Toluidine Blue, photographed with Carl Zeiss photomicroscope (KS300, Carl Zeiss, Oberkochen, Germany) and digital image processing software (Axiovision Rel 4.5, Carl Zeiss, Oberkochen, Germany).

4.3vi- Histological Analysis and Data Collection

Light Microscopy (Carl Zeiss photomicroscope (KS300, Zeiss, Germany)) was used to assess soft tissue morphology. Quantitative analysis, semi-quantitative analysis and qualitative analysis was carried out. The implants cross-section was divided in 3 Zones, both outer edges (Zones 1 and 2) and the central region (Zone 3), to ensure data was collected across the entire implant (Fig 4.02). Each outer Zone had data collected from 2 separate points with the average taken. 1 data collection point was taken in the central zone. A semi-quantitative percentage was assigned at each data collection point to represent the quality and maturity of the tissue infiltration within the pores. The percentage determined by comparison with healthy soft tissues surrounding the implant. A score of 100% would be assigned to a pore totally infiltrated with dense, well-ordered fibrous-connective tissue that was in intimate contact with the pore edge. 0% would indicate a pore devoid of soft tissue. Fig 4.03 represents typical histological sections that were scored by three, blinded independent assessors. These data were substantiated with a cell nuclei count within a measured area of each Zone to quantitatively assess the tissue maturation and viability, and a count of blood vessels to assess the extent of revascularization of the same area. These data were presented as a density per square millimeter.

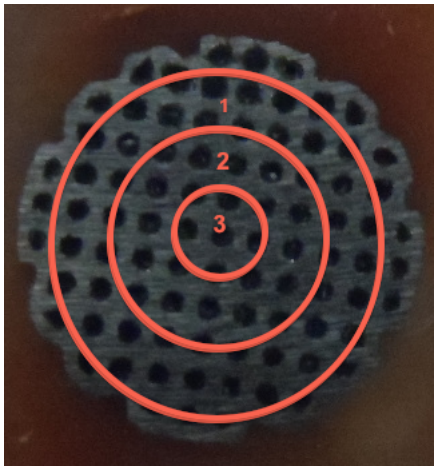

Fig 4.02. Implant cross-section for data collection; 1) Zone 1 First outer zone, 2) Zone 2 Second outer zone and 3) Zone 3 Central zone.

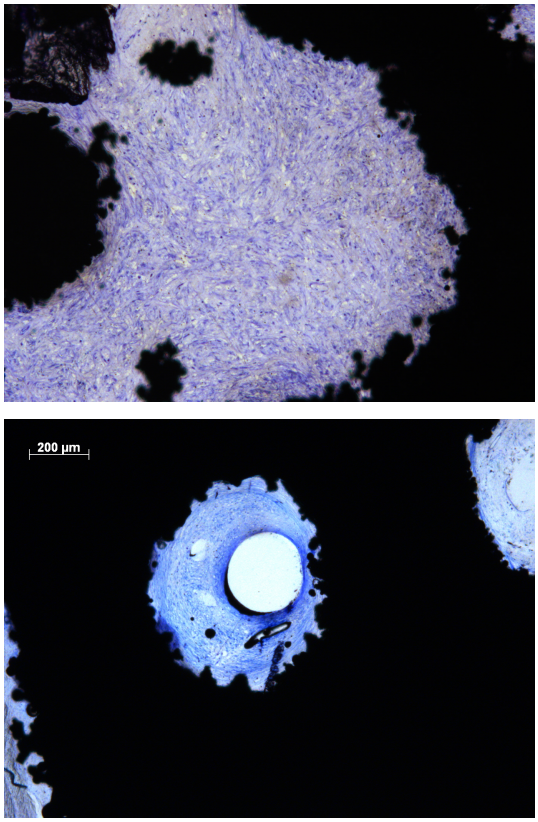

Fig 4.03. Typical examples of histological semi-quantitative scoring system used to calculate percentage of soft-tissue infiltration. A) 100% soft-tissue infiltration score. B) 50% soft-tissue infiltration score.

4.3vii- Statistics

Data are presented graphically in box and whisker plots for each Zone, where the X-axis represents the substrate groups (Table 4.01) and the Y-axis represents data collection made (Tissue infiltration, Cell Nuclei Density or

Blood Vessel Density). Data is presented as median (with 95% confidence intervals) and outliers are plotted as individual points outside the box and whiskers. Statistical analysis was performed in the same manner as discussed in Chapter 2.3x. Significance was considered at the 0.05 level.

4.4- Results

Data collection was not possible from Group 9 implants. No tissue was visible throughout the implant structure due to debris and artefacts infiltrating pores. These implants were therefore not represented in the result section but possible reasons for this are discussed in Section 4.5- Discussion.

Tissue Infiltration Zone 1

A Kruskal-Wallis test demonstrated that the data were not from the same population distribution (p <0.05). Statistical analysis shows that the greatest soft tissue infiltration occurred in Groups 1, 2 and 4 as all values were scored at 100% by each assessor. Significantly higher levels of tissue infiltration were observed in Group 1 compared with Group 3, Group 4 compared with Group 3 and Group 7 (MWU p <0.05) yet no difference was observed between Group 1 and Group 2 (MWU p >0.05; Fig 4.04, Table 4.02).

Group 3 and 6 showed the lowest levels of tissue infiltration at Zone 1, with median values of 40% and 27.5% respectively, yet, there were no significant differences between these groups (MWU p >0.05). Tissue infiltration was significantly lower in Group 3 compared with Group 5 (MWU p <0.05; Fig 4.04, Table 4.02).

Group 5 exhibited high levels of soft tissue in-filtration, median 88%. No significant difference existed between this group and Group 2 or Group 4 (MWU p >0.05; Fig 4.04, Table 4.02).

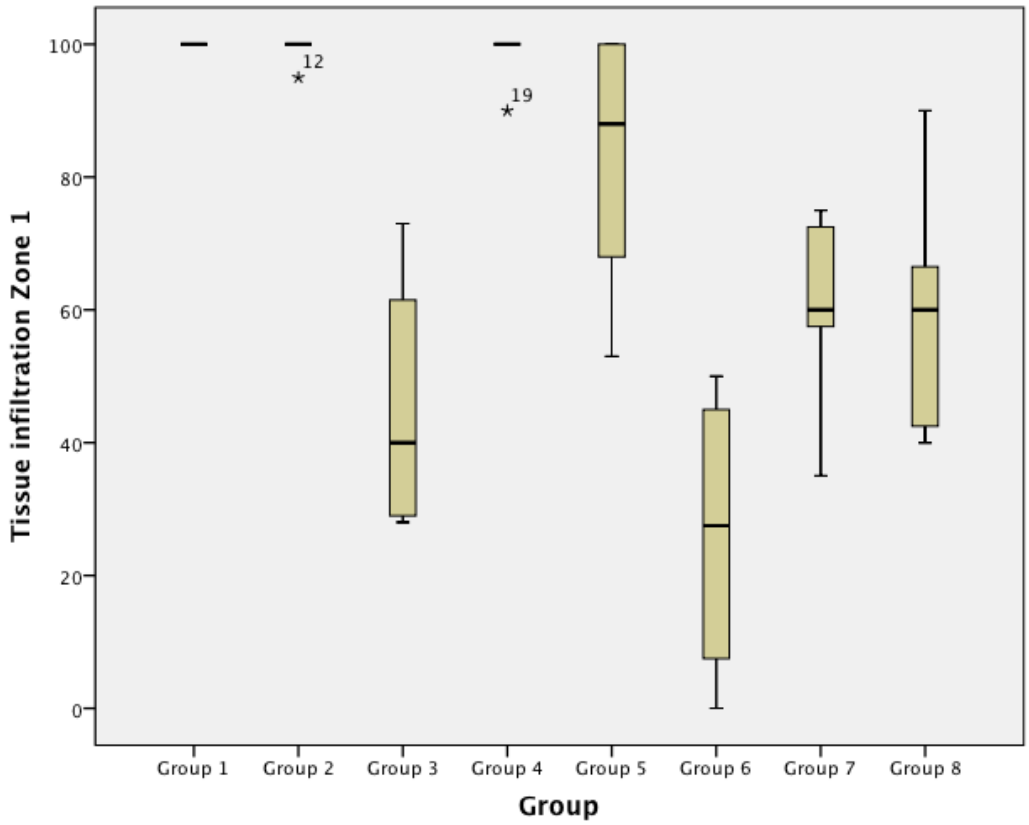

Fig 4.04. Box plot demonstrating the percentage of tissue infiltration of each porous implant group from the outer most zone, Zone 1.

Table 4.02- Pair-wise (MWU) Comparisons

	Group 1	Group 2	Group 3	Group 4	Group 5	Group 6	Group 7	Group 8
Group 1		0.355	0.004			0.003		
Group 2					0.051			0.001
Group 3				0.011	0.032	0.539		
Group 4					0.111		0.004	
Group 5								0.038
Group 6							0.073	0.220
Group 7								0.653
Group 8								

Tissue Infiltration Zone 2

Statistical analysis, using the Kruskal Wallis method, suggested that tissue infiltration data from Zone 2 was not from the same population (p <0.05). Results suggest that in this zone the more mature and denser soft tissue were seen in the implants with the larger pores sizes. This is similar to those results from Zone 1 but the variation of the data was greater, particularly for Groups 1,2 4 and 5. A description of the statistical differences follows.

Groups 1, 2 and 4 all exhibited median values of 98.5%, 100% and 95% soft tissue infiltration at Zone 2 respectively. Group 1 had significantly higher tissue infiltration compared with Group 3 and 6 (MWU p <0.05). Group 2 had significantly higher tissue infiltration compared with Group 8 (MWU p <0.05; Fig 4.04, Table 4.03). Group 5 exhibited a median value of 87.5% soft tissue infiltration, which was significantly higher than Group 3 (MWU p <0.05); Fig 4.05, Table 4.03). Group 3 and 6 exhibited the lowest levels of tissue in Zone 2, median value of 35% and 22.5% respectively. (Fig 4.05, Table 4.03) There were no other significant differences observed between Groups in this zone (MWU p >0.05; Fig 4.05,Table 4.03)

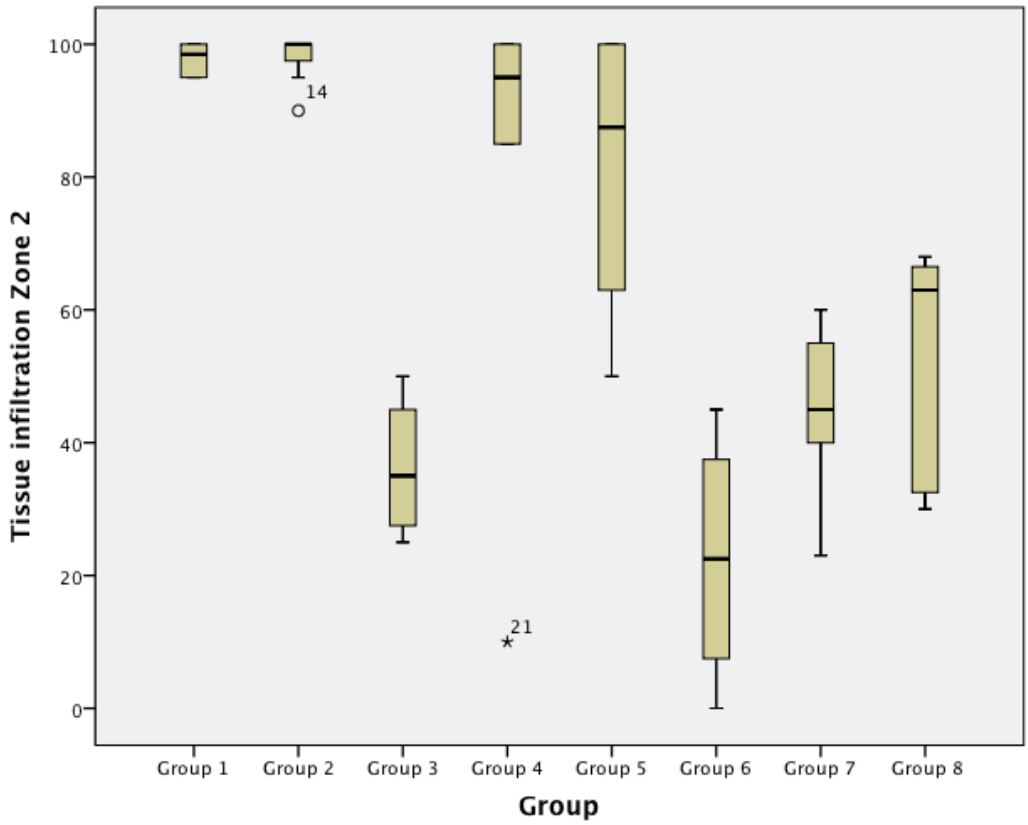

Fig 4.05. Box plot demonstrating the percentage of tissue infiltration of each porous implant group from Zone 2.

Table 4.03- Pair-wise (MWU) Comparisons

	Group 1	Group 2	Group 3	Group 4	Group 5	Group 6	Group 7	Group 8
Group 1		0.682	0.009			0.006		
Group 2					0.102			0.001
Group 3				0.140	0.014	0.712		
Group 4					0.779		0.086	
Group 5								0.052
Group 6							0.251	0.085
Group 7								0.368

Tissue infiltration Zone 3

Statistical analysis of this data set, using the Kruskal Wallis method, was significant (p <0.05). Group's 1, 2 and 4 all facilitated significantly high levels of tissue infiltration in Zone 3, as represented median values, all of 100%.
Significantly higher tissue infiltration was observed in Group 1 compared with Group's 3 and 6 (MWU p <0.05). Group 2 had significantly higher tissue infiltration compared with Group 8 (MWU p <0.05). Significantly higher levels of tissue infiltration were observed in Group 4 compared with Group's 3 and 7 (MWU p <0.05; Fig 4.06, Table 4.04). Group 5 facilitated high levels of tissue infiltration, median value 90%, which was significantly higher compared with Group 3 (MWU p <0.05; Fig 4.06, Table 4.04). The lowest levels of tissue infiltration in Zone 3 were observed in Group 6, median value 10% and Group 3, median value 25. (Fig 4.06, Table 4.04). There were no other significant differences observed in any other pair-wise comparisons between Groups in this Zone 3 (MWU p >0.05; Fig 4.06, Table 4.04).

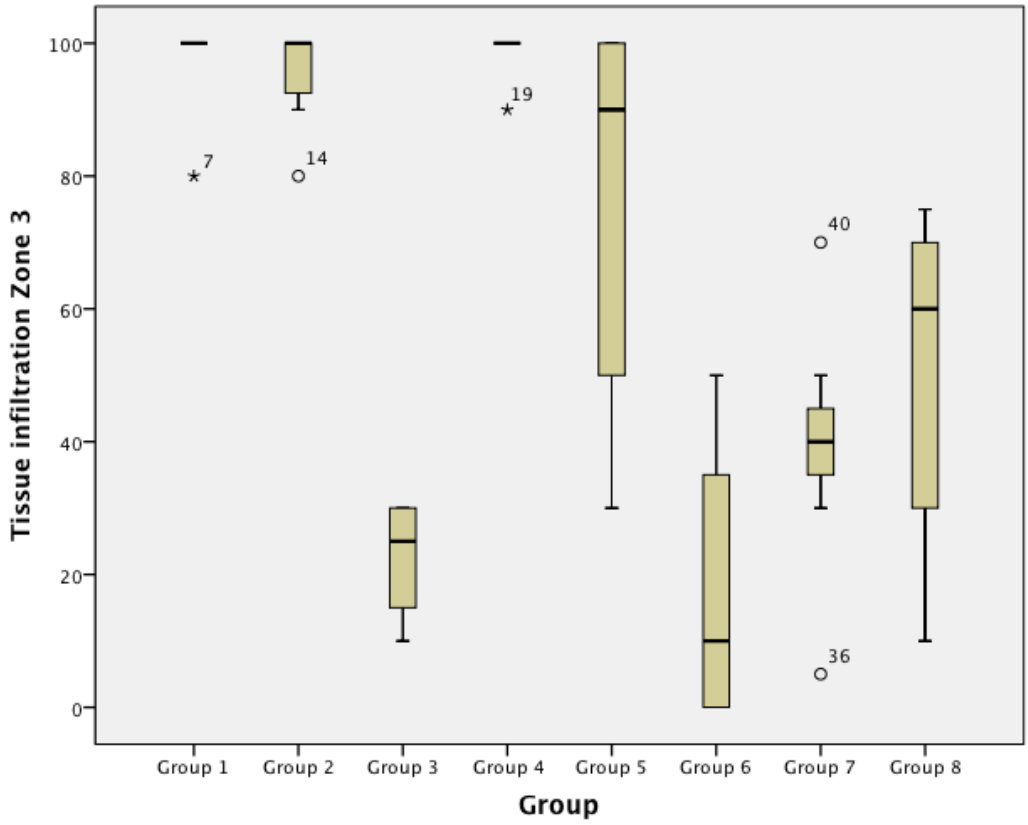

Fig 4.06. Box plot demonstrating the percentage of tissue infiltration of each porous implant group from inner most zone, Zone 3.

Table 4.04- Pair-wise (MWU) Comparisons

	Group 1	Group 2	Group 3	Group 4	Group 5	Group 6	Group 7	Group 8
Group 1		0.431	0.006			0.004		
Group 2					0.392			0.002
Group 3				0.010	0.016	0.901		
Group 4					0.205		0.004	
Group 5								0.083
Group 6							0.459	0.163
Group 7								0.476
Group 8								

Cell Nuclei Density Zone 1

Statistical analysis of this data set, using the Kruskal Wallis method, was significant (p <0.05). Unlike the semi- quantitative analysis of the percentage of soft tissue infiltration, a significant difference in the cell nuclei density could be detected between Groups 1 and 2. The median value for Group 2 (5059CN/mm^2), was significantly greater compared with Groups 1, 5 and 8 (MWU p <0.05; Fig 4.07, Table 4.05). Group 1 also had a high cell nuclei density (median value 3440.5CN/mm^2), which was significantly higher compared with Group 6 (MWU p <0.05; Fig 4.07, Table 4.05). There was no significant difference between Groups 3, 4 and 7 with median cell nuclei densities of 1190, 1389 and 1390CN/mm^2 respectively. Group 4 was significantly higher compared with Group 5 and Group 7 was significantly higher compared with Group 6 (MWU p <0.05; Fig 4.07, Table 4.05). There were no other significant differences observed in cell nuclei density in Zone 1 (MWU p >0.05: Fig 4.07, Table 4.05).

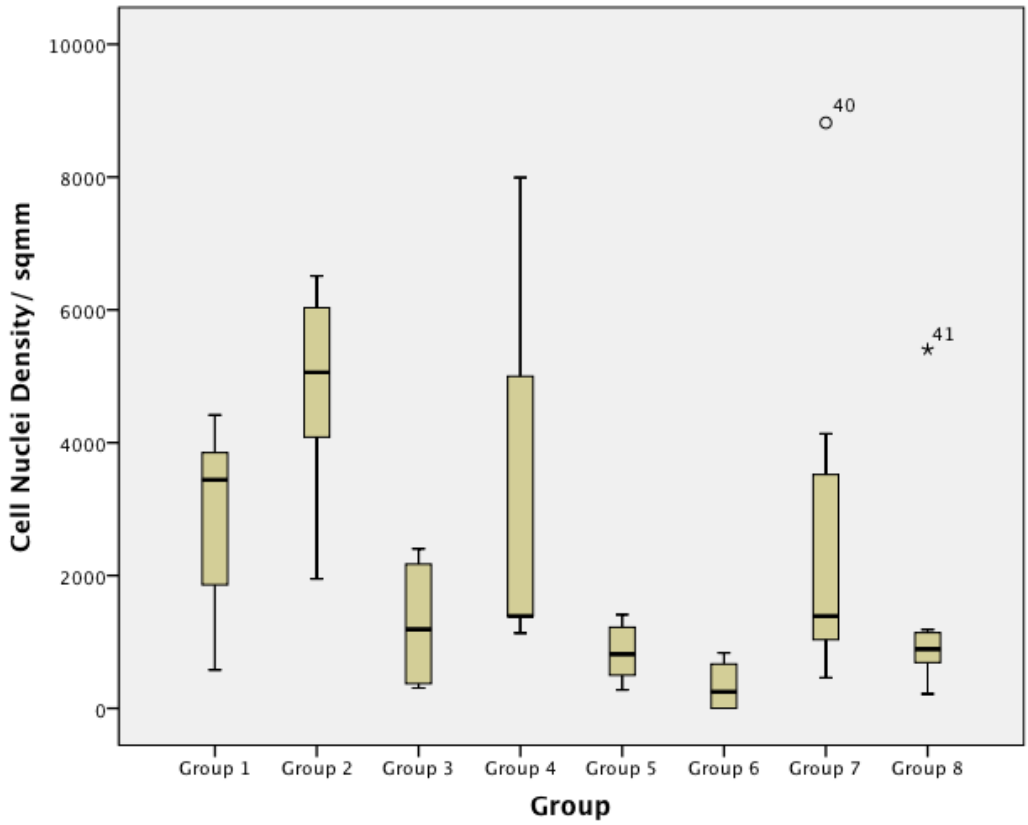

Fig 4.07 Box plot demonstrating the cell nuclei density/mm^2 of each porous implant group from the outer most zone, Zone 1.

Table 4.05- Pair-wise (MWU) Comparisons

	Group 1	Group 2	Group 3	Group 4	Group 5	Group 6	Group 7	Group 8
Group 1		0.046	0.088			0.019		
Group 2					0.003			0.009
Group 3				0.327	0.670	0.245		
Group 4					0.045		0.570	
Group 5								0.775
Group 6							0.023	0.058
Group 7								0.225
Group 8								

Cell Nuclei Density Zone 2

A significant difference was observed within this data population as demonstrated by the Kruskal Wallis method (p <0.05). Group 2 exhibited significantly higher cell nuclei density, (median value 4527CN/mm^2), compared with Groups 5 and 8 (MWU p <0.05; Fig 4.09, Table 4.06). Group 1 (median value 2846CN/mm^2) had a significantly greater cell nuclei density compared with Group 6 (MWU p <0.05), which had the lowest cell nuclei density (median value 268.5CN/mm^2) of all the Groups (Fig 4.08, Table 4.06). Group 4 did elicit a significantly higher cell nuclei density compared with Group 5 (MWU p <0.05; Fig 4.08, Table 4.06). No other significant differences presented themselves on a pair-wise basis (MWU p >0.05; Fig 4.08, Table 4.06).

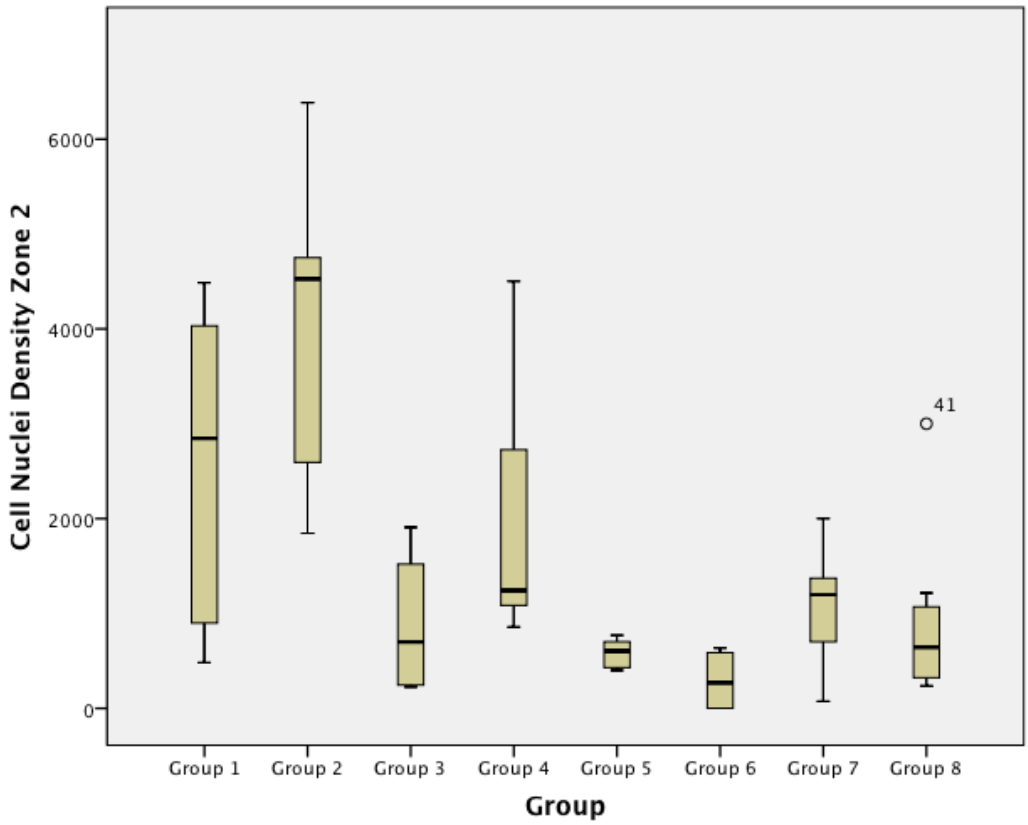

Fig 4.08. Box plot demonstrating the number of cell nuclei density/mm^2 of each porous implant group from Zone 2.

Table 4.06- Pair-wise (MWU) Comparisons

	Group 1	**Group 2**	**Group 3**	**Group 4**	**Group 5**	**Group 6**	**Group 7**	**Group 8**
Group 1		0.116	0.088			0.032		
Group 2					0.003			0.004
Group 3				0.221	1.000	0.245		
Group 4					0.006		0.291	
Group 5								1.000
Group 6							0.073	0.130
Group 7								0.482
Group 8								

Cell Nuclei Density Zone 3

Statistical analysis of this data set in Zone 3, using the Kruskal Wallis method, was significant, $p<0.05$. Groups 1, 2 and 4 facilitated the highest cell nuclei density; with median values were 3586.5, 5000 and 1306 CN/mm^2 respectively. (Fig 4.09, Table 4.07). Group 2 implants demonstrated significantly greater cell nuclei density compared with Groups 5 and 8 (MWU p <0.05; Fig 4.09, Table 4.07). Cell nuclei density of Group 1 was significantly increased compared with Group 6 (MWU p <0.05), the lowest observed median value, 251CN/mm^2 (Fig 4.09, Table 4.07). Significantly higher cell nuclei densities were observed in Group 4 compared with Group's 3 and 5 (MWU p <0.05; Fig 4.09, Table 4.07). Pair-wise statistical analysis saw no other significant differences (MWU p >0.05; Fig 4.09, Table 4.07).

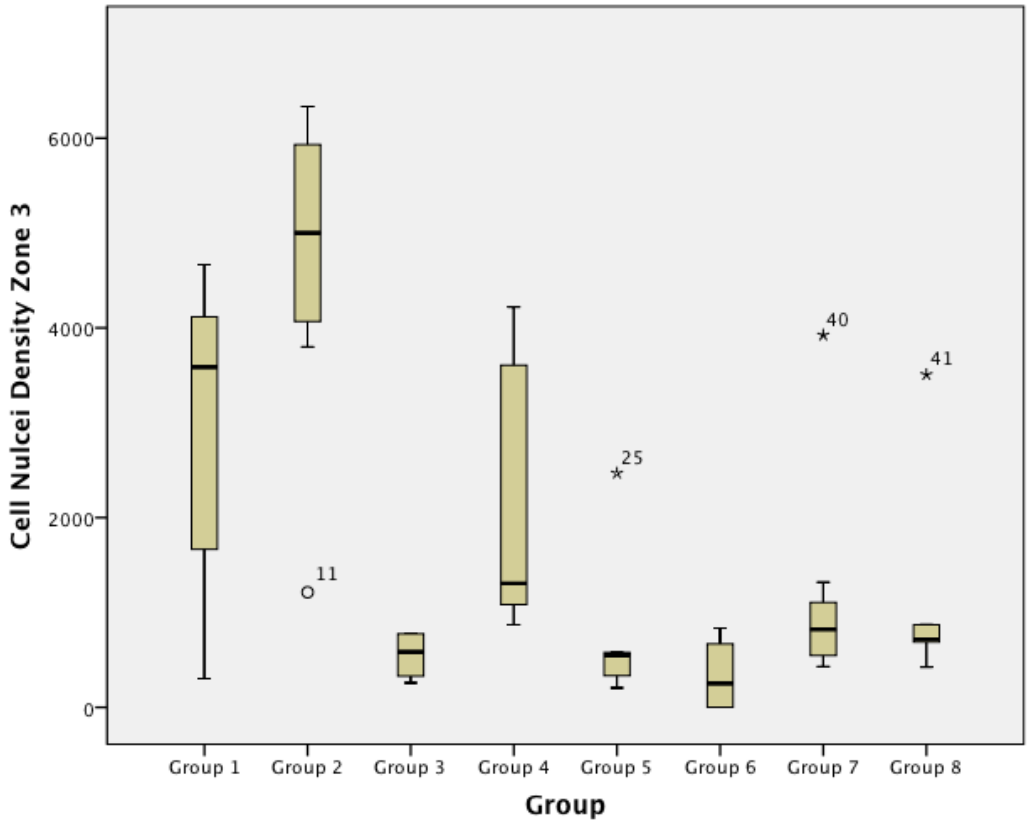

Fig 4.09. Box plot demonstrating the number of cell nuclei density/mm^2 of each porous implant group from inner most zone, Zone 3.

Table 4.07- Pair-wise (MWU) Comparisons

	Group 1	Group 2	Group 3	Group 4	Group 5	Group 6	Group 7	Group 8
Group 1		0.063	0.055			0.032		
Group 2					0.004			0.003
Group 3				0.014	0.831	0.561		
Group 4					0.028		0.123	
Group 5								0.086
Group 6							0.088	0.088
Group 7								0.848
Group 8								

Blood Vessel Density

The pore volume and the strut thickness influenced the blood vessel in-growth. As expected the overall highest blood vessel density was seen in Zone 1 and the lowest in Zone 3 this was also related to an increase in the variability in the measurement, which increased towards the inner porous structure.

Zone 1

A Kruskal-Wallis test demonstrated that the data from Zone 1 were not from the same population distribution (p <0.05). The pattern for the number of blood vessels within the porous structures also showed differences that were not discernable with semi quantitative analysis of percentage tissue infiltration. The Highest blood vessel density in Zone 1 was observed in Group 4, median value 15BV/mm^2, which was significantly higher compared with Group's 3 and 5 (MWU p <0.05; Fig 4.10, Table 4.08). Group 6 had the lowest blood vessel density, 0BV/mm^2, of all other implant groups. This was significantly lower compared to Groups 1, 7 and 8 (MWU p >0.05; Fig 4.10, Table 4.08). There were no significant differences apparent by pair-wise comparison of the data set (MWU p >0.05; Fig 4.010, Table 4.08).

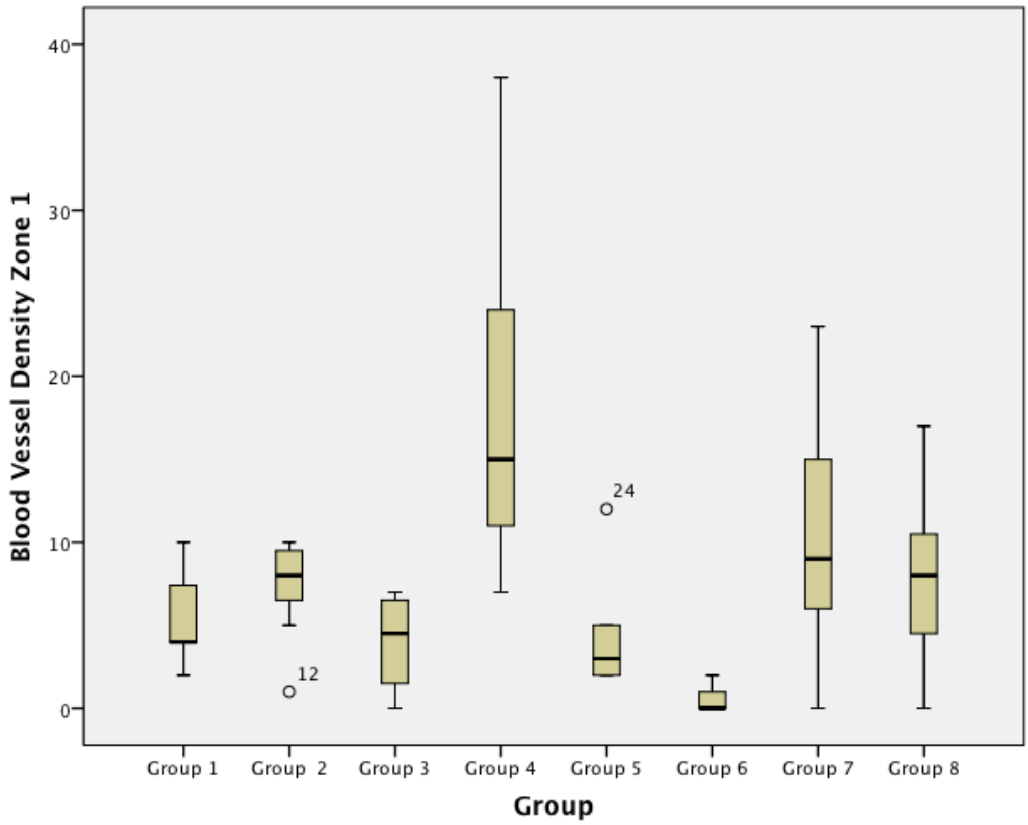

Fig 4.10. Box plot demonstrating the blood vessels density/mm^2 of each porous implant group from outer most zone, Zone 1.

Table 4.08 Pair-wise (MWU) Comparisons

	Group 1	Group 2	Group 3	Group 4	Group 5	Group 6	Group 7	Group 8
Group 1		0.286	0.461			0.017		
Group 2					0.221			0.897
Group 3				0.019	0.829	0.091		
Group 4					0.017		0.223	
Group 5								0.223
Group 6							0.026	0.026
Group 7								0.522
Group 8								

Blood Vessel Density Zone 2

Statistical analysis of the data set from Zone 2, using the Kruskal Wallis method, was significant, $p<0.05$.The highest blood vessel density was observed in Group 2, median value 10BV/mm^2, which was significantly higher compared with Group 5 only (MWU $p<0.05$; Fig 4.11, Table 4.09). Group 4 had high blood vessel density, median value 6BV/mm^2, this was significantly higher compared with Groups 3, 5 and 7 (MWU $p<0.05$; Fig 4.11, Table 4.09). Group 6 facilitated the lowest blood vessel density, median value 0BV/mm^2, which was significantly lower compared with Group 1 and 8 (MWU $p<0.05$; Fig 4.11, Table 4.09). Pair-wise statistical comparisons suggested there were no other significant differences in the data (MWU $p>0.05$; Fig 4.11, Table 4.09).

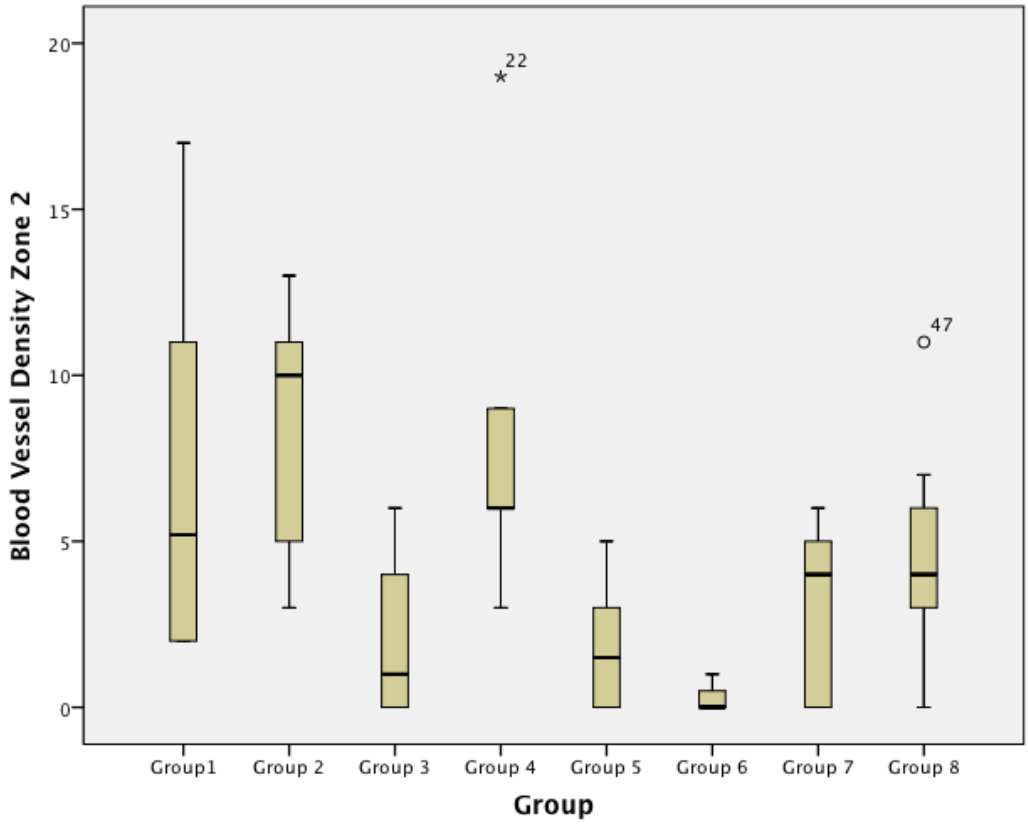

Fig 4.11 Box plot demonstrating the blood vessels density/mm^2 of each porous implant group from Zone 2.

Table4.09 Pair-wise (MWU) Comparisons

	Group 1	Group 2	Group 3	Group 4	Group 5	Group 6	Group 7	Group 8
Group 1		0.471	0.083			0.009		
Group 2					0.010			0.158
Group 3				0.045	0.912	0.321		
Group 4					0.013		0.039	
Group 5								0.113
Group 6							0.179	0.026
Group 7								0.434
Group 8								

Blood Vessel Density Zone 3

Statistical analysis of this data set from Zone 3, using the Kruskal Wallis method, was significant, $p<0.05$. Highest median value for blood vessel density was observed in Group 4, 11BV/mm^2, which was significantly higher compared with Group's 3, 5 and 7 (MWU p <0.05; Fig 4.12, Table 4.10). Groups 5 had low blood vessel density, medium value 0BV/mm^2. This was significantly lower compared with Group's 2, 3 and 8 (MWU p <0.05; Fig 4.12, Table 4.10). No other significant differences were observed with blood vessel density in Zone 3 (MWU p >0.05; Fig 4.12, Table 4.10). Groups 5 and 7 demonstrated no vessels within pores in Zone 3.

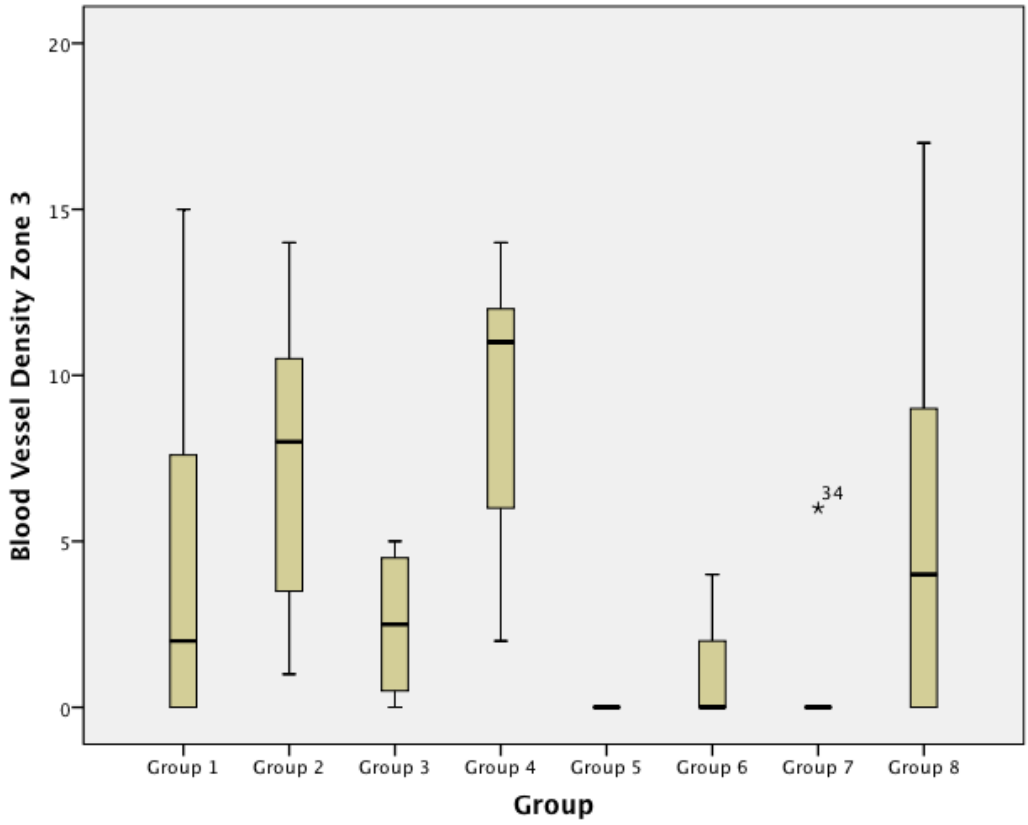

Fig 4.12 Box plot demonstrating the blood vessels density/mm^2 of each porous implant group from inner most zone, Zone 3.

Table 4.10 Pair-wise (MWU) Comparisons

	Group 1	Group 2	Group 3	Group 4	Group 5	Group 6	Group 7	Group 8
Group 1		0.197	0.914			0.225		
Group 2					0.002			0.403
Group 3				0.050	0.018	0.215		
Group 4					0.003		0.005	
Group 5								0.036
Group 6							0.779	0.215
Group 7								0.087
Group 8								

Qualitative Assessment

Light microscopy provided evidence to support the quantitative data. (Fig 4.13- 4.20) with Groups 1, 2 and 4 show dense, well order soft tissues filling the entire pore. Extensive infiltration across the entire implant was observed in these groups. These characteristics were consistent with tissue infiltration data (Fig 4.04, 4.05 and 4.06, Fig 4.13 and 4.14). Little open space was visible and intimate contact at the tissue implant interface suggested stable integration (Fig 4.15). Moreover, preferential collagen deposition appeared evident around interconnecting struts in these implants groups. No pro-inflammatory cells could be indentified (Fig 4.16). Large numbers of individual cells populated pores across the entire implant in Groups 1, 2 and 4, in support of the quantitative data (Fig 4.07, 4.08 and 4.09) (Fig 4.16). Blood vessels were clearly visible with endothelial nuclei punctuating in a ring creating a lumen. More of these vessels were observed in more open structures associated with Groups 2 and 4 (4.10, 4.11 and 4,12), suggestive of a capillary network throughout the implant. No necrotic tissue or degradation was evidenced (Fig 4.18).

Figs 4.19 and 4.20 show less dense soft tissue. These observations were associated with implant groups with a less open structure, which also correspond with lower cell nuclei densities (Fig 4.07, 4.08 and 4.09). Tissue integration within theses groups saw gaps with little interface formation between tissue and pore edge. Neovascularisation was not observed throughout implants in Groups 5, 6, and 7, supportive of the blood nuclei density data (Fig 4.10, 4.11 and 4.12), (Figs 4.19 and 4.20).

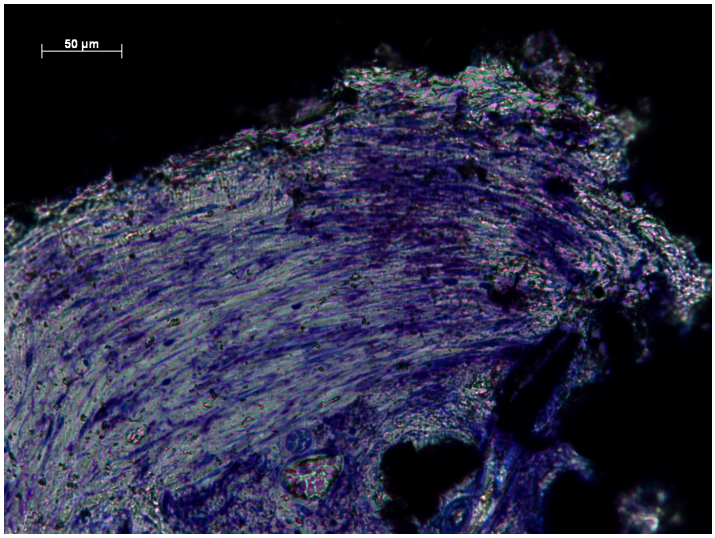

Figure 4.13. Light microscopy image sections stained with Toluidine blue of a Group 4 implant at Zone 1. High magnification image of dense, well-ordered soft tissue infiltration.

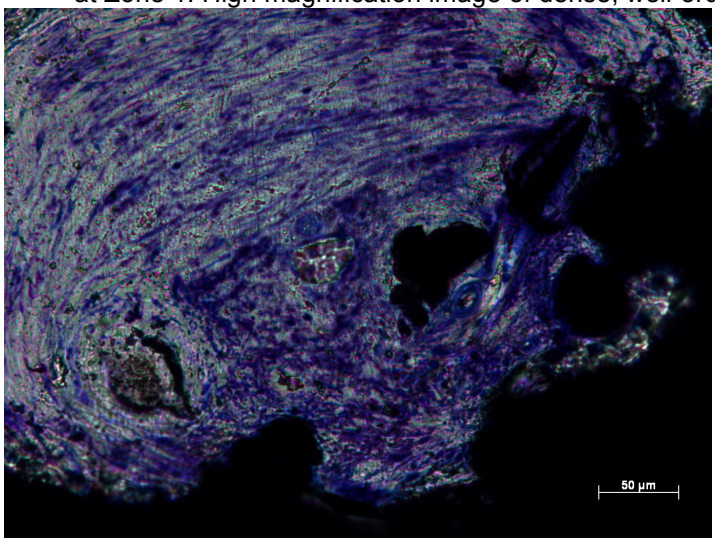

Figure 4.14. Light microscopy image sections stained with Toluidine blue of a Group 4 implant at Zone 1. High magnification image of dense, well-ordered soft tissue infiltration.

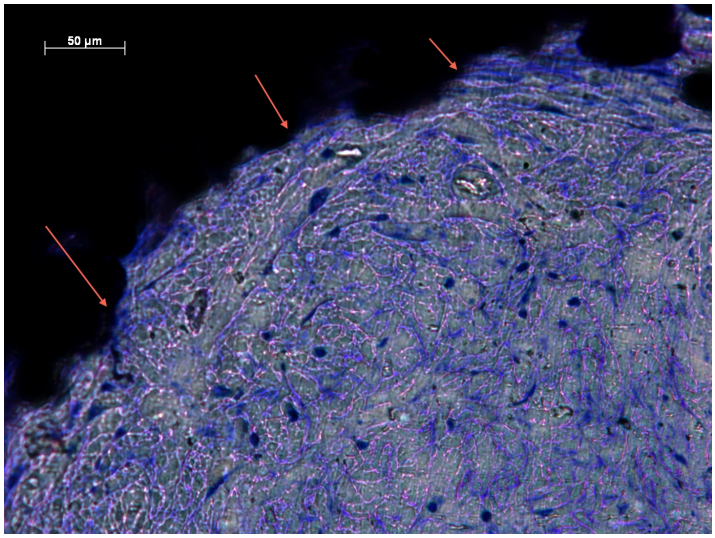

Figure 4.15 Light microscopy image sections stained with Toluidine blue of a Group 1 implant at Zone 2. High magnification image of dense, well-ordered soft tissue infiltration with intimate contact (arrows) between pore edge and soft tissues.

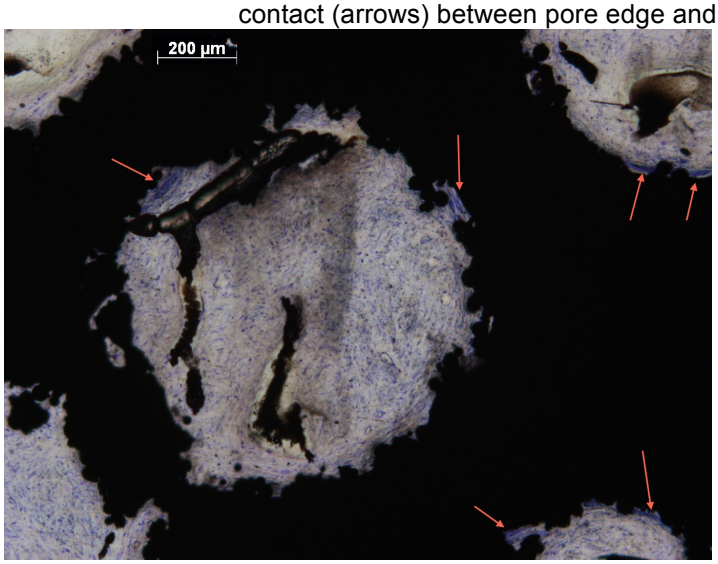

Figure 4.15 Light microscopy image sections stained with Toluidine blue of a Group 2 implant at Zone 3. Low magnification imagine of dense, well-ordered soft tissue preferentially depositing collagen around interconnecting struts (arrows).

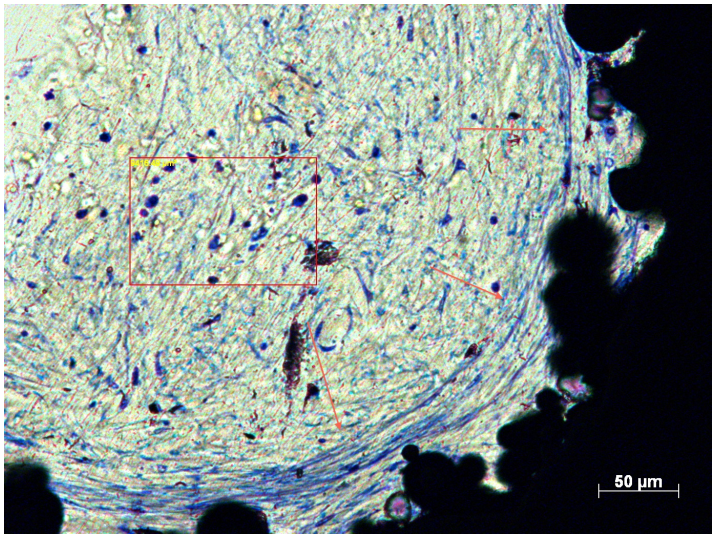

Figure 4.17 Light microscopy image sections stained with Toluidine blue of a Group 3 implant at Zone 1. Dense, well-ordered soft tissue, preferentially depositing collagen around interconnecting struts (arrows) with distinct cell nuclei populating the implant pore.

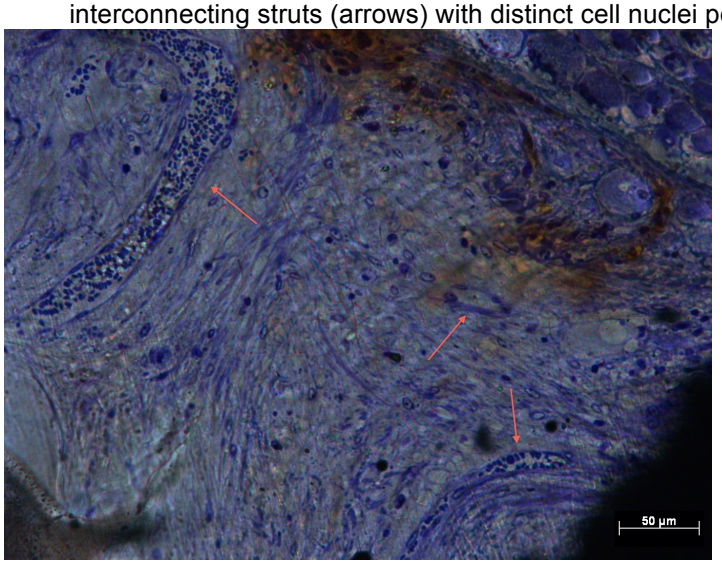

Figure 4.18 Light microscopy image sections stained with Toluidine blue of a Group 4 implant at Zone 1. High magnification image of dense, well ordered soft tissue with extensive blood vessel formation (arrows).

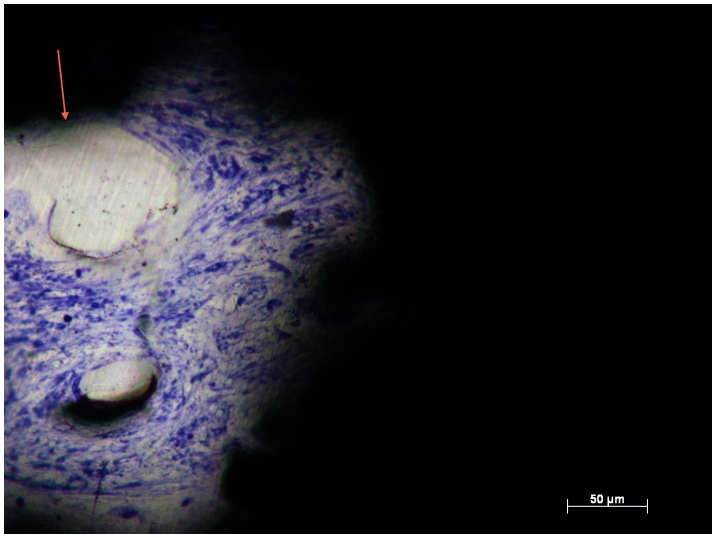

Figure 4.19 Light microscopy image sections stained with Toluidine blue of a Group 7 implant at Zone 2. High magnification image of less dense soft tissue with poor contact (arrows) between pore edge and soft tissues.

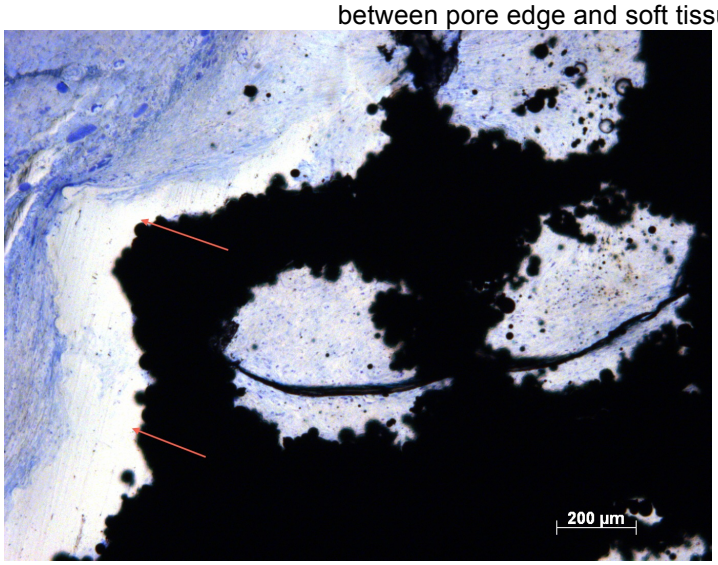

Figure 4.20 Light microscopy image sections stained with Toluidine blue of a Group 7 at Zone 1. Low magnification image of less dense soft tissues with poor contact (arrows) between pore edge and soft tissues.

4.5- Discussion

Subcutaneous soft tissue infiltrated throughout all porous implant groups after 4-weeks *in vivo* except Group 9. It has been hypothesised that the anatomical and physiological characteristics associated with soft tissues will require a more open structure to maintain viable tissue compared with bone tissues (Hacking et al 2000). Group 9 pore diameter was 250μm and therefore may have been too small to allow tissue infiltration. These data are in support of LaBerge et al. (1990) who observed fibrous encapsulation of implant with pore diameters of 300μm rather than infiltration. However others dispute this (Taylor and Smith 1972, Bobyn et al 1982, Hacking et al 2000) and, in contrast to my results, have observed soft tissues infiltrating structures with such diameters. A contributing factor to these results and my own may involve relative movement of the implant structures *in vivo*. Bobyn et al. (1982) secured implants into the subcutaneous soft tissue by suturing them, thereby decreasing relative movement *in situ* and allowing cell and tissue infiltration into significantly smaller pore dimensions. This was not performed in my study, nor by LaBerge et al. (1990), and both of these investigations showed little or no soft tissue infiltration with such dimensions.

Alternatively the successful implant groups in my study, when incorporated into an ITAP flange, may increase in the degree of dermal tissue infiltration, as the bone-anchored stem will limit relative implant movement *in vivo*. Pore diameters greater than 700μm supported extensive tissue infiltration compared with less open structures. Groups 1, 2 and 4 all demonstrated superior tissue infiltration compared with other groups across their entire structure. The open structure in these implant groups facilitated the flow of blood and body fluid into the structure which supports early attachment of cells.

Group 3 implant structures appeared not to follow the trend, observing lower soft tissue infiltration despite possessing large pore diameter of 700μm. The interconnecting strut dimension of 400μm in Group 3 implants may have detrimentally influenced tissue infiltration, creating a lower volumetric porosity.

The larger diameter of the strut will take up more free space within the 3-dimensional network of the implant structure, also taking up the free space created by the larger pore size.

Hacking et al. (2000) observed soft tissue infiltration throughout porous tantalum implants at 4-weeks. They also noted an increase in tissue infiltration over time and an associated increase in attachment strength by mechanical testing. If the degree of tissue infiltration is directly linked to tissue attachment strength, it could be suggested that the dimensions of Groups 1, 2 and 4 in my study support increased soft tissue attachment strength.

An ITAP patient has reported near normal functionality as a result of the treatment (Kang et al 2010). This increases the physical demand on the soft tissue implant interface and subsequently, a device that supports increased tissue attachment strength would be more favourable.

In my study, pore diameter of 500μm or larger was required to observed soft tissue infiltration as no data could be collected from implant Group 9. Interestingly bone tissue has been shown to infiltrate into defined pores below this diameter (Howe et al 1973), which is possibly associated with movement of the implants. For bone in-growth to occur micro-motion has to be minimal, however soft tissue implants (particularly those in muscle) will be subjected to the large movements associated with contraction of these muscles. Even if the implants were secured within the muscle, motion may be great due to the mismatch in modulus, which is so much greater between titanium alloy and soft tissues than with bone.

Hacking et al. (2000) suggested that soft tissues require larger area in which to infiltrate into and metabolise. This may account for unattainable results from Group 9 implants. Collagen appeared to preferentially deposit at the pore edges and interconnecting struts, extensively in Groups 1, 2 and 4. These features are indicative of soft tissue integration. Albrektsson et al. (1981) define tissue implant integration as the interaction of collagen and metal oxide. Howe et al. (1974) also noted these features in collagen

deposition around pore edges at the bone implant interface. Pendegrass et al. (2006) showed how collagenous Sharpey's fibres anchor dermal tissue to the deer antler pedicle.

It has been suggested that a lower volumetric porosity will take less time to infiltrate with bone tissue compare to an implant with a greater volumetric porosity (Bobyn et al 1980). This trend is not observed in my study as the larger pore diameters observed significantly increased soft tissue infiltration. Ponder et al. (2009) suggest successful infiltration with bone tissue can be achieve with a pore diameter of 450μm, which is significantly smaller to the 1000μm and 700μm diameter pores successful in this study. By comparison, there are obvious differences in tissue type between this study and mine. However, they went on to suggest that there could be a minimum size requirement to facilitate the influx of tissue. A much larger pore diameter may support vascularisation, allowing tissue respiration and promoting osteogenesis (Ponder et al 2009).

Groups 1 and 2 showed significantly increased cell nuclei density compared with other implant groups. Group 4 also exhibited a high level of cell nuclei density compared with Group 3 implant, significantly so in Zone 3, despite both possessing the same pore dimensions demonstrating the importance of the strut size. The cellular component of the many soft tissues, especially the subcutaneous tissue in this study, are fibroblasts (Alberts et al 2002) and are identifiable in the histological analysis. Toluidine blue stains nucleic acids within the cell nuclei, making fibroblasts easily identifiable.

It is my suggestion that the observed increases in cell nuclei density (seen in Groups 1 and 2, and to a lesser degree 4) can be linked to the structural dimensions possessed by the implant groups. The structural environment may support the chemotactic movement of fibroblasts across the entire implant.

Fibroblast migration across porous titanium alloy has been demonstrated, in limited fashion, *in vitro* (Cheung et al 2007) and can be controlled *in vivo* by

decreasing the free space between pores (Vrana et al 2011). Cell nuclei densities between Zone 1 and 3 were not significantly different for Groups 1, 2 or 4. This suggests a uniform movement of cells across the entire implant structures. Surface roughness on EBM implants increases, compared to more established fabrication methods (Koike et al 2011), which may support fibroblast migration throughout the implant surface. Contact guidance and micro-structured surfaces may aid fibroblast migration along the interconnecting strut network (Walboomers et al 1999). The increases in cell nuclei density may result in an increase in collagen deposition, discussed earlier, as fibroblasts are well established as a collagen secreting cell type (Alberts et al 2002).

Long-term *in vivo* success relies on the early formation of an extensive vascular network (Nelson et al 1983). Undoubtedly cell density will be associated with the invasion of blood vessels. Blood vessels were observed across the entire implant structure in Groups 1, 2, 3, 4 and 8. Groups 2 and 4 saw the highest blood vessels densities, with no significant differences between Zones. The 400μm strut dimension, of Groups 1 and 3, may have detrimentally influenced the vascularisation in these implant groups by lowering the volumetric porosity, taking up free space. The biological impact of re-vascularisation provides nutrients and facilitates the removal of metabolic products, supporting healthy soft tissue (Taylor and Smith, 1972). Porous titanium implants with much smaller inter-porous spaces (150μm) fail to support blood vessel formation (Schultz et al 2007). Hypoxic conditions associated with the lack of blood vessels may have detrimentally affected soft tissue growth within less open structures, conversely, the more open structures of implant Groups 2 and 4 allow soft tissue to flourish as a well-oxygenated environment was present.

My study differentiates itself from others in the quantification of soft tissue infiltration. I accept that I have not performed any mechanical testing on the strength of tissue attachment to the implant, where other studies have (Bobyn et al 1982, LaBerge et al 1990, Hacking et al 2000). Mechanical strength of

attachment positively correlates with pore size (Bobyn et al 1982) and time *in vivo* (LaBerge et al 1990). I have extensively quantified the tissue within my implant structures, I believe the data are robust and can be compared with others (Bobyn et al 1982, LaBerge et al 1990, Hacking et al 2000), who have suggested strength of attachment and tissue infiltration positively correlate. To my knowledge these studies have not quantified tissue infiltration, rather qualitatively described it. Therefore I can postulate that in the groups where I have observed significant increases in soft tissue infiltration and vascularisation, it is likely that those structures would demonstrate a significantly higher degree of attachment strength. Should they be implanted for longer time periods (to potentially increase dermal tissue integration to ITAP devices) can also be suggested that mechanical strength would increase. Furthermore, the EMB technique employed in my study created continuous 3-D porous structure compared with single (LaBerge et al 1990) or several (Bobyn et al 1982) layered porous coating. Hacking et al. 2000 demonstrated an increase in mechanical fibrous tissue attachment strength to continuous porous tantalum implants compared with these authors.

4.6- Conclusion

Owing to my methods of data collection I have met the pre-determined hypotheses of this experimental chapter, with the exception of implant group 9. The results from my study allow soft tissue infiltration to be optimised as a function of pore and strut diameter. These implant dimensions were made possible by the EBM process, which would otherwise be unachievable in our laboratory. Group 4 exhibited significantly higher blood vessel densities across the entire implant structure compared with other implant groups and this structure was taken forward in my next chapter where I investigate the *in vivo* soft tissue in-growth. If successful in this study this structure should also be considered for a clinical ITAP flange. The formation of blood vessels, re-vascularising the soft tissues surrounding the skin implant interface will be beneficial in the long-term stability of the skin seal. The incorporation of a flange structure to and ITAP device may provide an opportunity to control the

soft tissue interface and in turn develop a stable, biological seal at the transcutaneous point.

The ultimate goal for ITAP devices is clinical longevity; the use of an EBM ITAP flange must be tested *in vivo* long-term to characterise the transcutaneous implant interface and observe any changes.

Chapter 5- An *in Vivo* Assessment of Functionalised ITAP Flanges in a Long-term Amputation Model.

Chapter 5

5.1- Introduction

Soft tissue attachment and integration *in vivo* is critical for the long-term success of ITAP devices. Failure modalities are characterised by the upper layers of the skin dividing down along the implant shaft in an attempt to re-establish continuity (discussed in Chapter 1.2). Dermal attachment to ITAP devices physically hinders epidermal downgrowth and promotes clinical longevity (Kang et al. 2010).

In vivo implantation of transcutaneous devices, such as ITAP, breaks the skin barrier. In doing so, they trigger a wound healing cascade (Chapter 1.2vi) as the skin reacts against the foreign body and attempts to re-establish skin continuity. The initial reaction or early phase acts to plug the wound space, to manage homeostasis. This is followed by the cellular phase, where various cell types migrate to the site and act to limit infection, re-cellularise and remodel the tissue (Lanza et al 2000).

With the failure modalities of transcutaneous devices linked to wound healing mechanisms the functionalisation of devices act to aid these mechanisms and allow the foreign body to successfully interface with the soft tissues of the skin. Chimutengwende-Gordon et al. (2011) have shown silanised fibronectin to titanium alloy substrates implanted in subcutaneous soft tissue in an ovine model had a positive effect at the tissue implant interface. I have developed an *in vitro* functionalisation technique using silanised RGD-polypeptides, which increases HDF attachment strength compared with polished titanium alloy substrates. Furthermore, results showed no significant difference in HDF attachment compared with substrates functionalised with silanised fibronectin, as described by Chimutengwende-Gordon et al. (2011). The implants used in this study were not subject to axial load nor were they in a transcutaneous setting, both critical features of an ITAP model (Chimutengwende-Gordon et al 2011).

Sterilization techniques, such as those implicated by the National Institute of Health an Excellence (NICE) including gamma irradiation, will degrade the quaternary structure of fibronectin and render it ineffective. This will limit fibronectin's use clinically, despite the biological gains. Synthetic RGD-polypeptides, such as those used in the development of my functionalisation technique, are not subject to the same degree of degradation as their structures are in primary form. They, therefore, may be able to overcome these issues and have a long-term clinical application. This however has not so far, been tested.

Porous implants promote tissue integration as they support the influx of cells *in vitro* and tissue *in vivo* (Cheung et al. 2007 and Chapter 4). I have shown that varying pore and strut dimensions can optimise soft tissue integration. Cells can infiltrate across the entire implant allowing intimate tissue contact and revascularisation of the tissue. A pore diameter of 700μm and strut diameter of 300μm were observed in Chapter 4 to facilitate optimal subcutaneous soft tissue integration compared with other larger and small dimensions tested. Porous titanium alloy transcutaneous implants support skin integration *in vivo* with varying degrees of infiltration dependent on structure and implantation time. Epidermal downgrowth was still observed in this study (Farrell et al 2013). Squier and Collins (1981) observed an inverse relationship between epidermal downgrowth and pore size. They defined the critical feature of a transcutaneous implant to be its ability to support connective tissue, which can infiltrate and anchor into pore spaces.

A combination of proteins with a porous structure has previously been investigated. Keratin has been covalently coupled to a porous coated transcutaneous device with varied success. No fibrous capsule presented after 3-months *in vivo* yet epidermal downgrowth was still observed (Jeyapalina et al. 2013). Laminin-5 has also been used in conjunction with porous structures in an attempt to attach the migrating epithelium to dental implants. Histological comparisons offered no discernable difference between biological functionalised porous implants and uncoated porous controls

(Werner et al 2009). Laminin-5 is present in the hemidesmosome complex that attaches the oral epithalium to basal lamina and Keratin is a structural protein on the outmost layer of the skin, not present in the dermis (Chapter 1.2v and Alberts et al 2002).

RGD-polypeptides are ubiquitous in cell attachment mechanisms in the dermis (Chapter 1.2v and Alberts et al 2002). Attachment of the dermis to implant shafts increases longevity by way of a physical blockage to the migrating epidermis. RGD-polypeptides may provide that opportunity to functionalise the ITAP transcutaneous portion to increase the early attachment of the dermis and support the formation of a tight biological seal at the transcutaneous interface.

The ITAP flange is designed to mimic the transcutaneous interface of the deer antler. A highly porous pedicle allows dermal tissue infiltration over its' increased surface area. This creates a tight biological seal at the transcutaneous interface. The ITAP flange promotes soft tissue integration by providing an increased surface area for dermal soft tissue to attach and significantly reducing epidermal downgrowth. To achieve this, it follows the mechanism described above, where connective fibres anchor perpendicular to the porous pedicle (Pendegrass et al 2006). Porous titanium coatings on flanged implants at the soft tissue interface have been shown to reduced infection compared with uncoated controls in a bone-anchored, transcutaneous amputation model (Isackson et al 2011 and Jeyaplina et al 2012), which suggests a tight seal at the transcutaneous interface. HA coating of the ITAP flange further increases soft tissue integration by providing a biocompatible surface in which to allow soft tissue to attach. This has been shown to support clinical longevity (Kang et al 2010).

Despite numerous attempts, epidermal downgrowth has yet to be completely eradicated in bone-anchored, transcutaneous devices *in vivo*. There is no study that biologically functionalised a totally porous flange with RGD-polypeptides, in a long-term bone-anchored transcutaneous *in vivo* model.

This chapter aims to combine the techniques developed in my thesis thus far in an ITAP device and application.

5.2- Aims and Hypotheses

This chapter aims **to determine the effect of functionalising the ITAP flange on the skin implant interface in a long-term *in vivo* model.**

More specifically I aim to compare the effects of a porous EBM flange with the current discoid flange perforated with drilled holes on soft tissue integration at the transcutaneous interface. I also want to observe the effect of biologically functionalising the ITAP flange (either porous or non-porous) with silanised RGD-polypeptides with the current clinical standard, a HA coated transcutaneous portion.

This chapter aims to test the following hypotheses:

An RGD-polypeptide functionalised porous flange will support dermal interface formation and limit epidermal downgrowth compared with the HA coated non-porous flange.

5.3- Material and Methods

5.3i- Study Design

Table 5.01 outlines the 4 experimental groups tested in this study. ITAP devices were designed to incorporate structural and biological functionalisations developed in my previous experimental chapters. Implants were manufacture from titanium alloy ($TiAl_6V_4$), the alloy used throughout my thesis. A 3-D porous structure was incorporated into the flange. This was based on the successful dimensions observed in Chapter 4, which were a pore diameter of 700μm and strut diameter of 300μm. A discoid collar perforated with 24, drilled holes acted as the control (detailed dimensions published in Appendix 4). Implants were biological functionalised by silanising 7mM of RGD-polypeptides, as observed as the optimal concentration for HDF attachment *in vitro* for Chapter 3. HA coated structures were used as controls for both porous and non-porous flanges. ITAP devices were implanted trans-tibially into an ovine model for a period of 5-months.

Table 5.01 Study Description

Group (n=6)	**Functionalisation**	**Experimental Details**
Flange Control	Flange perforated with 24 drilled holes, 0.7mm in diameter. HA-coated (5.3ii). This is the **current clinical standard** (Kang et al 2010).	5-months *in vivo*. Removed en bloc and processed for hard-grade resin histology and interface characterisation.
Flange RGD	Flange perforated with 24 drilled holes, 0.7mm in diameter. The drilled flange silanised with RGD polypeptide (based on results of Chapter 3).	5-months *in vivo*. Removed en bloc and processed for hard-grade resin histology and interface characterisation.
Porous Control	Porous Flange with pore and strut dimensions of 700 and 300 respectively. HA-coated (5.3ii).	5-months *in vivo*. Removed en bloc and processed for hard-grade resin histology and interface characterisation.

Porous RGD	Porous Flange with pore and strut dimensions of 700 and 300 respectively. The Porous flange silanised with RGD polypeptide (based on results of Chapter 3).	5-months *in vivo*. Removed en bloc and processed for hard-grade resin histology and interface characterisation.

5.3ii- Implant Preparation

Bone-anchored portion of the ITAP implant shaft were all HA-coated (Plasma Biotel, Derbyshire, UK), irrespective of their design features. Those implants that acted as controls to the biologically functionalised implants, had the flange structure HA-coated in the same manner. Full implant dimensions are published in Appendix 4 but in brief, the bone-anchored portion extended over 29mm and tapered from a diameter of 5mm to the base of 4mm diameter (Fig 5.01 B and D).

Biological functionalisation of the ITAP flanges was achieved by silanisation of RGD-polypeptides to the titanium alloy implant surface. The protocol was based upon the results of Chapter 3, as used in Chapter 3 Study 6.

5.3iii- Surgery

All surgery was carried out in accordance with the Animal (Scientific Procedures) Act 1986 (https://www.gov.uk/government/publications/animals-scientific-procedures-act-1986-amendment-regulations) and in conjunction with University College London's Statement of the Uses of Animals in Research (http://www.ucl.ac.uk/slms/research/animal-use).

Ovine adult (fully mouthed and skeletally mature), female Mules (breed) were used for the *in vivo* study.

Premedication of 0.2mg/kg xylazine, Rompun 2% (Bayer Healthcare, UK) was administered to each animal subject with dose based on weight at time of

procedure. Ketamine hydrochloride (Ketaset, Fort Dodge Animal Health Ltd., UK) induced anesthesia at 2mg with 2.5mg of midazolam hypnovel (Roche Products Ltd., UK), both were administered intravenously. Animal subjects were intubated, 5ml of cefalexin ceporex (Schering-Plough Animal Health, UK) was administered to achieve antibiotic prophylaxis and anesthesia was maintained by inhalation with isoflurane at 2%.

During anaesthesia, each animal was positioned in the dorsal recumbency. The skin overlaying the medial aspect of the tibia and surrounding area were shaved, bi-laterally, and treated with betadine-povidine scrub solution and iodine aspetic solution (Dynarex, Quick Medical, Washington, USA) followed by alcoholic chlorhexidine scrub (Cardinal Health, Ohio, USA) preoperatively.

The tibial tuberosity was palpated through the skin and the first incision was made approximately 3cm distally to the tuberosity over the medial aspect of the left tibia, this became the proximal position. The soft tissue was dissected off the bone to expose it for ease of drilling. A 4mm diameter hole was drilled through both tibial cortices and enlarged to 4.8mm at the top end to construct a tapered structure. The construct was reamed to accommodate each implant individually and then press fitted in such that no micro-movement was apparent and the base of the flange was 3mm from the bone. The dermal tissue and fascia was draped over the flange and sutured with absorbable 1-0 Vicryl (Ethicon Inc., New Jersey, USA). The uppermost layers of the skin were also sutured with 2-0 Vicryl (Ethicon Inc., New Jersey, USA) around the uppermost stem of the ITAP device creating a transcutaneous portion. Wounds were coated in excess with Opsite (Smith and Nephew plc, London, UK) and bandaged. This process was repeated for all 4-sites per animal. Distal sites were created relative to proximal sites in the given tibia, such that the original incision was made approximately 3-cm below the first site. Intra-operative images can be observed in Fig 5.01, A and C.

Table 5.02 in vivo Implant Position

Animal 6034	**Right Leg**	**Left Leg**
Proximal site	Flange RGD	Porous Control

Distal site	Flange Control	Porous RGD

Animal 6064	**Right Leg**	**Left Leg**
Proximal site	Flange Control	Porous Control
Distal site	Porous RGD	Flange RGD

Animal 6046	**Right Leg**	**Left Leg**
Proximal site	Porous RGD	Porous Control
Distal site	Flange RGD	Flange Control

Animal 6073	**Right Leg**	**Left Leg**
Proximal site	Flange RGD	Porous Control
Distal site	Flange Control	Porous RGD

Animal 6059	**Right Leg**	**Left Leg**
Proximal site	Porous RGD	Flange Control
Distal site	Flange RGD	Porous Control

Animal 6027	**Right Leg**	**Left Leg**
Proximal site	Flange RGD	Porous Control
Distal site	Porous RGD	Flange Control

5.3iv- Histological Processing

Implants remained *in situ* for 5-months, at which point animal subjects were euthanized by intravenous injection of 0.7mg/kg IV Sodium Pentobarbitone (Pharmasol Ltd., Hampshire, UK) into the jugular vein. All implants were retrieved, taking care to remove all local tissue to the implant without disruption. Following retrieval, implants were immediately housed in 10% formal saline, for 1-week.

All samples were prepared for hard grade resin histology is the same manner outlined in Chapter 4.3iv. A full laboratory log can be observed in Appendix 4. Longitudinal sections were cut, through the centre of each implant and associated tissues, ground and polished to a thickness of < 100μm and stained with Toluidine Blue.

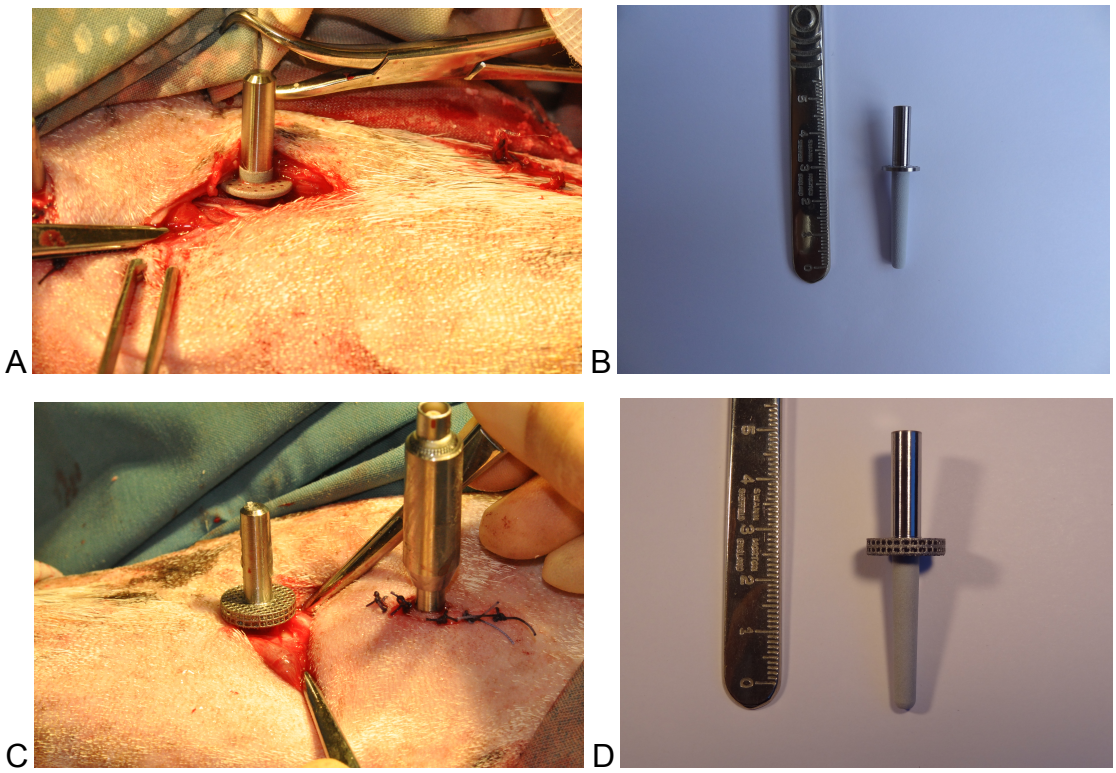

Fig 5.01 Functionaliseed Implant Groups; A) Flange Control, intra-operative, B) Flanged RGD pre-silanisation, C) Porous Control intra-operative (Right), Porous RGD intra-operative (Left) and D) Porous RGD pre-silanisation.

5.3vi- Histological Analysis and Data Collection

Light Microscopy was used to characterise the soft tissue implant interface. To assess the soft tissue implant interface 4 parameters were measured as described below.

1) Epidermal downgrowth was measured by length, using the intercept method, described by Pendegrass et al. (2006)
2) The percentages of epidermal attachment to the implants were calculated, based on measurements of epidermis peri-implant (Pendegrass et al 2006).
3) The degree of dermal tissue infiltration was measured within central pores or drilled holes within the flange structures of each implant by the number of cell nuclei as a function of area (μm^2)
4) The number of blood vessels within the pores as a function of area (μm^2), as described in Chapter 4.3vi, was also measured.

Additionally a semi-quantitative percentage fill score was assigned to the amount of tissue infiltration with a pore or drilled hole within flange structure, also described previously (Chapter 4.3vi).

5.3vii- Statistics

Statistical analysis was performed in the same manner as discussed in Chapter 2.3x with significance considered at the $p = <0.05$ level.

5.4- Results

Animal 6034

This animal subject showed gross signs of impaired locomotion and appeared lame on the back, right leg.

The right leg proximal implant site presented with an excess of strong smelling exudate. Microbiology analysis of cultures from the wound exudate concluded moderate severity of *Escherichia. coli, Corynebacterium, Peptostreptococcus spp,* and *Bacteriodes spp.* Radiographs suggested no bone trauma. Both investigations are present in Appendix 4.

It was also noted that this animal had sustained weight loss of 10kg from initial implantation surgery to this point. Early euthanasia was agreed and achieved by the method discussed in 5.3iv.

This animal subject was repeated in order to limit the effect on statistical analysis.

Epidermal Downgrowth

Statistical analysis by the Kruskal-Wallis method demonstrated no significant differences between the 4 implant devices, p >0.05, Fig 5.02. Table 5.03 displays the median downgrowth values and 95% confidence intervals for all implant groups. Median downgrowth lengths associated with RGD-polypeptide functionalised implants were higher compared with control implants, though these differences were not significant (Fig 5.02, Table 5.03).

Table 5.03 Median Downgrowth Figures for ITAP Devices.

Group	Median/ μm	95% Confidence Intervals
Flange Control	7185.5	5941.3-7900.87
Flange RGD	8178.0	6255.14-11299.41
Porous Control	5359.0	4646.77-10409.23
Porous RGD	7878	5702.48-9195.52

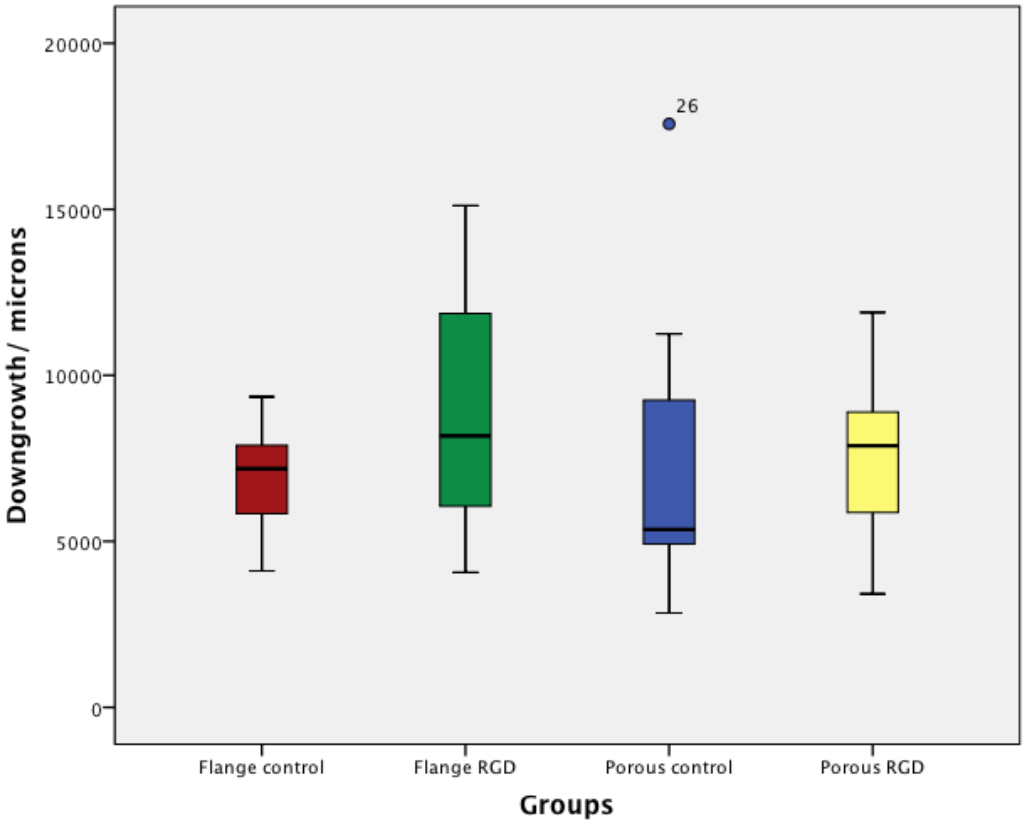

Fig 5.02. Box and Whisker plot demonstrating the length of Downgrowth (μm) for functionalised ITAP flanges by drilling (red), drilling and silanised with RGD-polypeptides (green), porous (blue) and porous silanised with RGD-polypeptide (yellow).

Epidermal Attachment

No significant difference was observed in the epidermal attachment between the 4 implant devices, a Kruskal-Wallis test demonstrated p >0.05, Fig 5.03. Table 5.04 displays the median percentages for epidermal attachment and 95% confidence intervals for all implant groups. Median percentage values associated with RGD-polypeptide functionalised implants were lower compared with control implants, though these differences were not significant (Fig 5.03, Table 5.04).

Table 5.04 Median and 95% Confidence Intervals for Percentage Epidermal Attachment.

Group	Median/ Percentage	95% Confidence Intervals
Flange Control	50.9	32.47-63.73
Flange RGD	44.54	17.16-58.67
Porous Control	39.4	22.0-57.63
Porous RGD	27.2	21.81-49.02

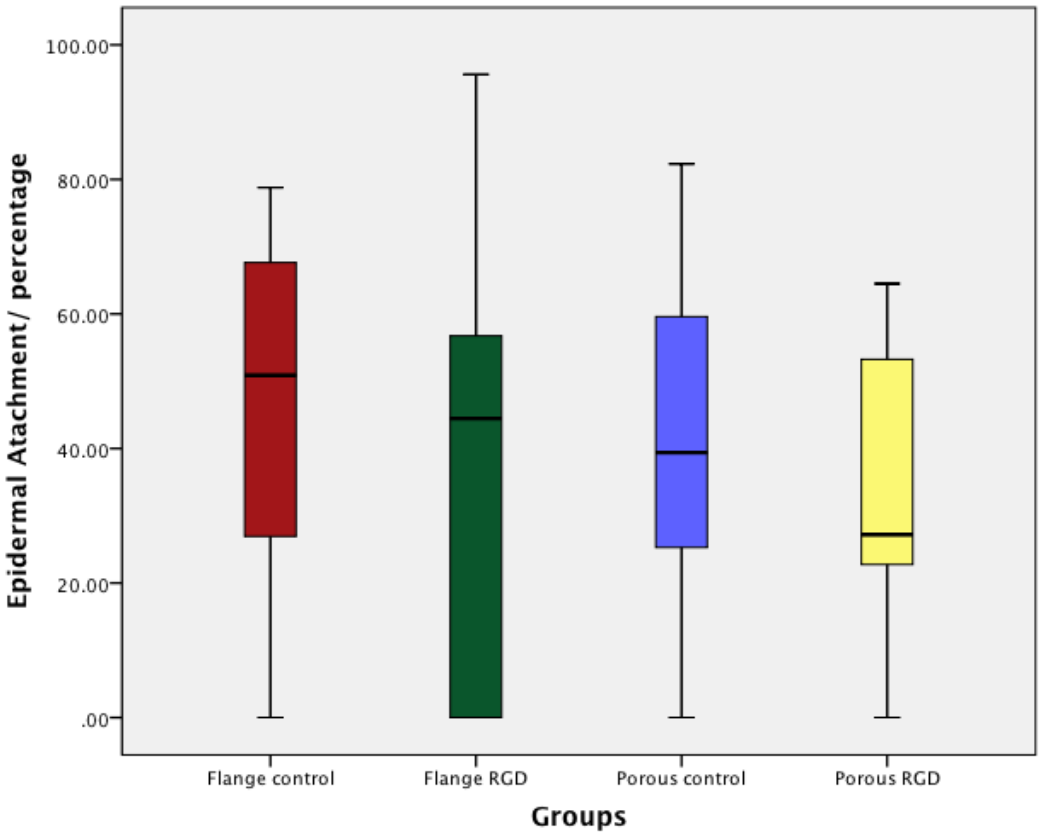

Fig 5.03. Box and Whisker plot demonstrating the percentage of Epidermal Attachment for functionalised ITAP flanges by drilling (red), drilling and silanised with RGD-polypeptides (green), porous (blue) and porous silanised with RGD-polypeptide (yellow).

Blood Vessel Density

A Kruskal Wallis test demonstrates the data were from different populations as p <0.05. Highest blood vessel density was observed in soft tissue within porous controls. These data were significantly higher compared with flange control implants (MWU p <0.05; Fig 5.04, Table 5.05). Significantly increased blood vessel density was also observed in soft tissue within porous RGD implants compared with flange RGD implants (MWU p <0.05; Fig 5.04, Table 5.05). There was no significant difference in blood vessel density between flange controls and flange RGD implant groups or porous controls and porous RGD implant groups (both MWU p >0.05; Fig 5.04, Table 5.05). These data suggest that the porous structures promote better invasion of blood vessels from the surrounding tissues.

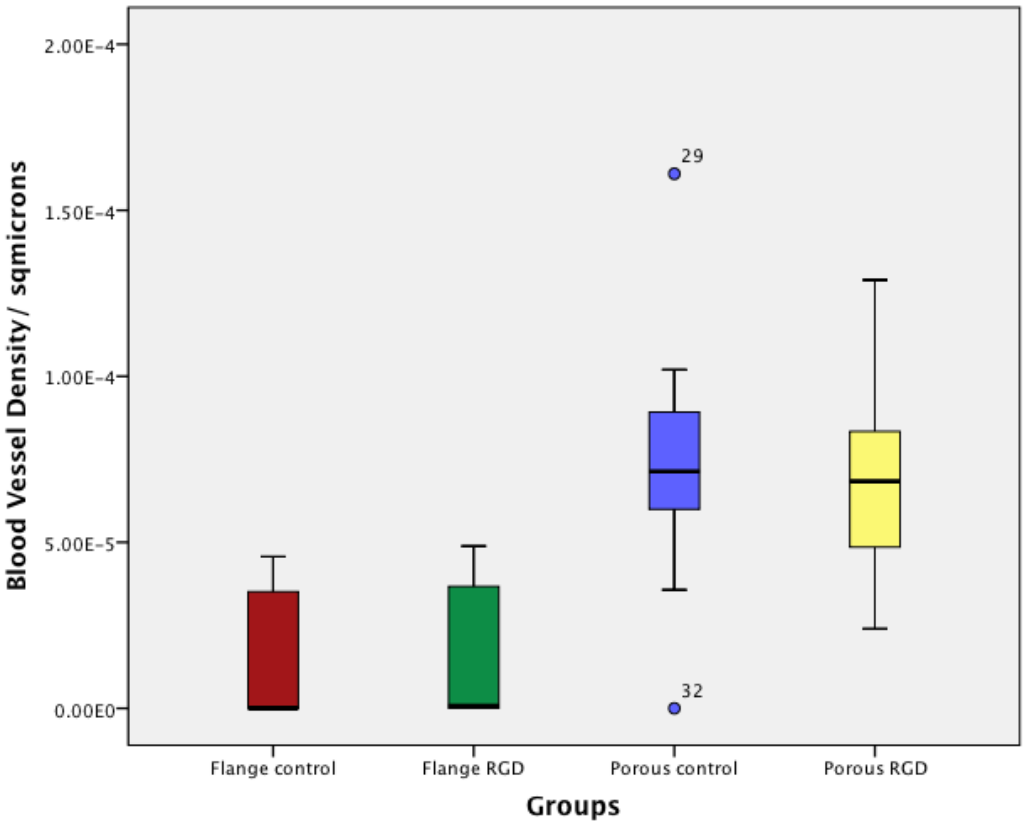

Fig 5.04. Box and Whisker plot demonstrating the blood vessel density of soft tissue with functionalised ITAP flanges by drilling (red), drilling and silanised with RGD-polypeptides (green), porous (blue) and porous silanised with RGD-polypeptide (yellow).

Table 5.05- Pair-Wise (MWU) Comparisons

	Flange Control	**Flange RGD**	**Porous Control**	**Porous RGD**
Flange Control		0.594	0.001	
Flange RGD				0.001
Porous Control				0.854

Cell Nuclei Density

These data were from the same population as a Kruskal Wallis test was not significant, p >0.05. Table 5.06 displays the median percentages for cell nuclei density and 95% confidence intervals for all implant groups. All cell nuclei densities remained consistent despite functionalisation of the implant flanges (Fig 5.05, Table 5.06).

Table 5.06 Median and 95% Confidence Intervals for Cell Nuclei Density.

Group	Median/ Percentage	95% Confidence Intervals
Flange Control	0.000585	0.000254 – 0.00152
Flange RGD	0.000301	0.0000648 – 0.000813
Porous Control	0.000513	0.000385 – 0.000675
Porous RGD	0.00054	0.000386 – 0.000735

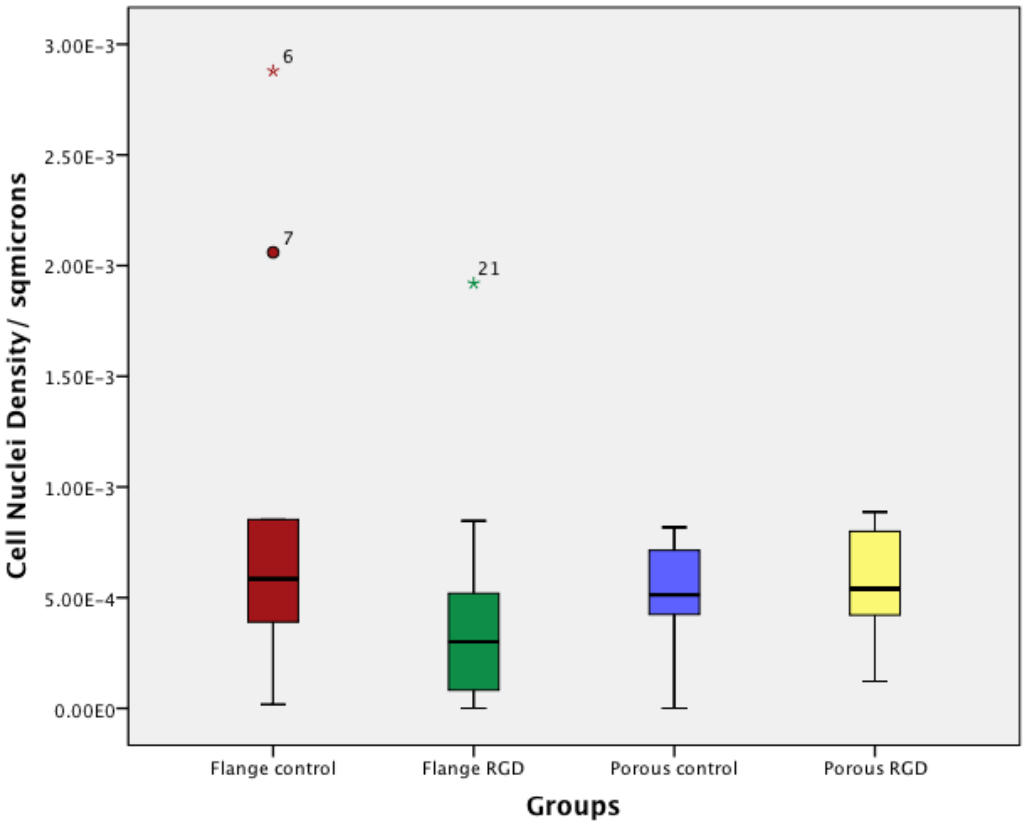

Fig 5.05. Box and Whisker plot demonstrating cell nuclei density of soft tissue with functionalised ITAP flanges by drilling (red), drilling and silanised with RGD-polypeptides (green), porous (blue) and porous silanised with RGD-polypeptide (yellow).

Dermal Tissue Infiltration

Statistical analysis by the Kruskal-Wallis method demonstrated a significant difference between the 4 implant devices; p <0.05 Fig 5.06. Percentage of dermal tissue infiltration was significantly increased in porous RGD implant structures compared with flange RGD, MWU p <0.05. These data were also significantly higher compared with porous control implants, MWU p <0.05; Table 5.06, Fig 5.06. There were no other significant differences observed in percentage of dermal tissue infiltration (Table 5.06, Fig 5.06). Again, these data suggest that porous flanges promote better soft tissue integration and that is increased further when the alloy surface is enhanced with RGD-polypeptide.

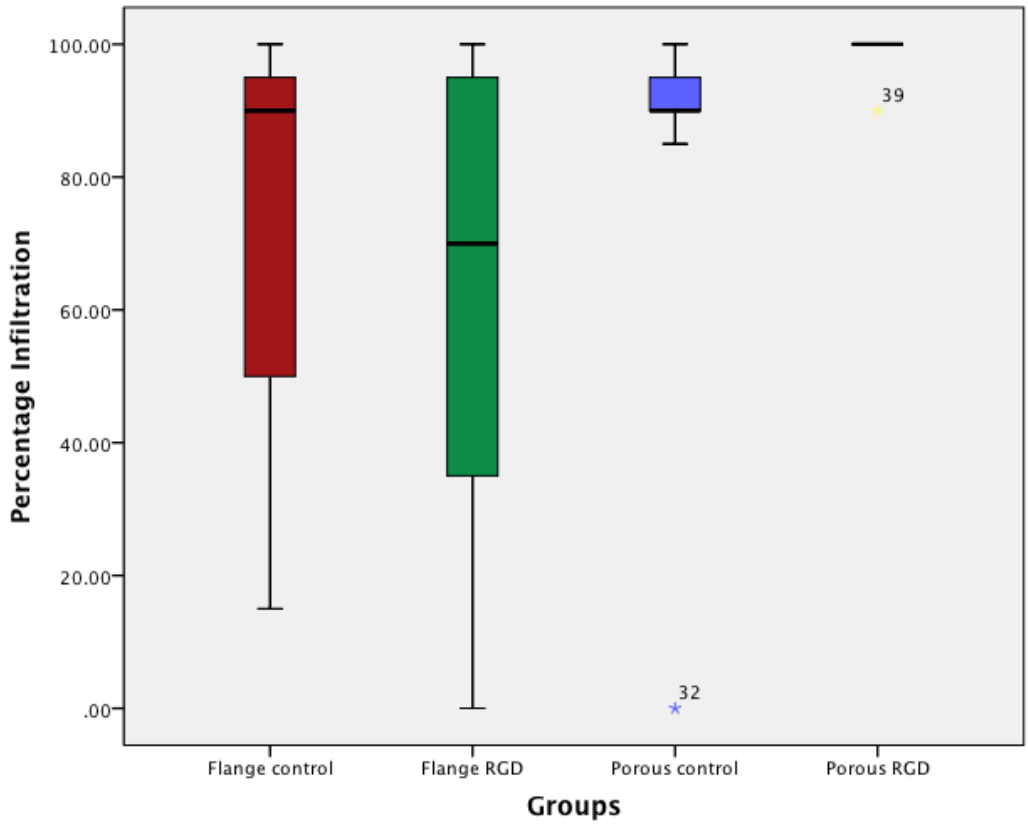

Fig 5.06. Box and Whisker plot demonstrating percentage of dermal tissue infiltration with functionalised ITAP flanges by drilling (red), drilling and silanised with RGD-polypeptides (green), porous (blue) and porous silanised with RGD-polypeptide (yellow).

Table 5.06- Pair-Wise (MWU) Comparisons

	Flange Control	**Flange RGD**	**Porous Control**	**Porous RGD**
Flange Control		0.565	0.637	
Flange RGD				0.000
Porous Control				0.001

Qualitative Assessment

Downgrowth was evident, characterised by the epidermal cell layer tracking down along the implant shaft. Distinct gaps were observed under light microscopy between the implant shaft and soft tissue. This in conjunction with the downgrowth data suggested it was not in response to a specific functionalised group. In some instances downgrowth led to defined pockets forming (Fig 5.07). Wound debris, such as clots, necrotic tissue and exduates, collected between implant and tissue at the transcutaneous portion. This presented in a majority of instances, impeding interface formation (Fig 5.08). Where epidermal downgrowth was limited, intimate contact between tissue and implant shaft suggested a stable transcutaneous interface well above the flange structure (Fig 5.09). Wide ranging epidermal attachment data was collected due to epidermal soft tissue tracking down to the flange (Fig 5.10). Artifacts were common observations during the histological analysis resulting from histological processing.

Soft tissue of the dermis integrated well within porous structures, infiltrating throughout the interconnecting frameworks of titanium alloy structures in many instances (Fig 5.11). Ordered collagen formation was observed in intimate contact with implant structures including natural recesses, created by the underside of the flange.

Soft tissue present within porous structures was well vascularised with rounded lumens and individual cells (Fig.12 and Fig 5.13). Where soft dermal tissue infiltration was poor, gaps at the tissue implant interface could be observed (Fig 5.14).

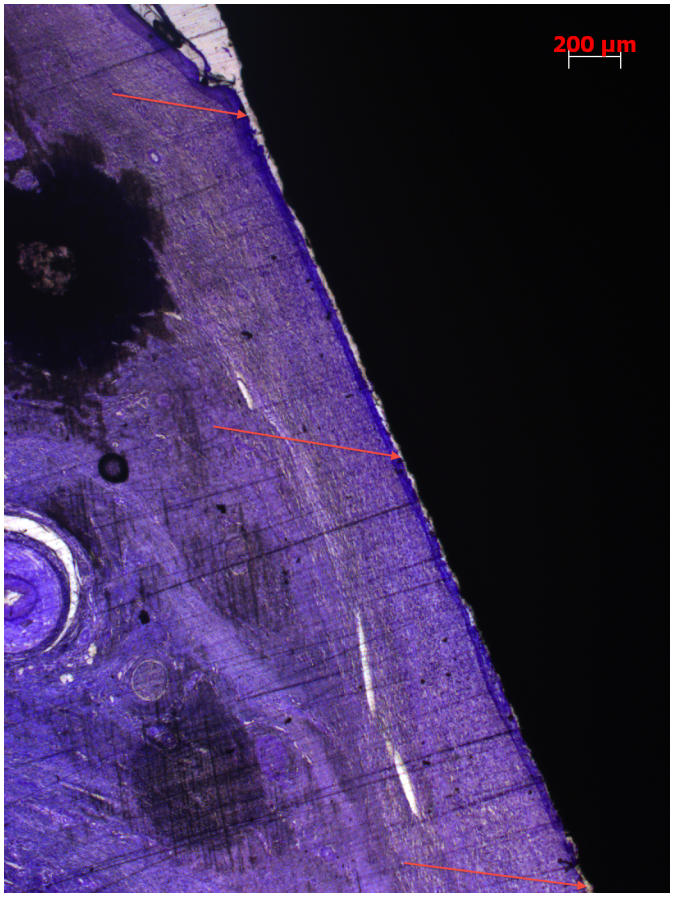

Fig 5.07. Light microscopy image of a transcutaneous section stained with Toluidine blue of a Group 4 implant at Zone 1. Low magnification image of epidermal downgrowth and sinus track formation along the implant shaft (arrows).

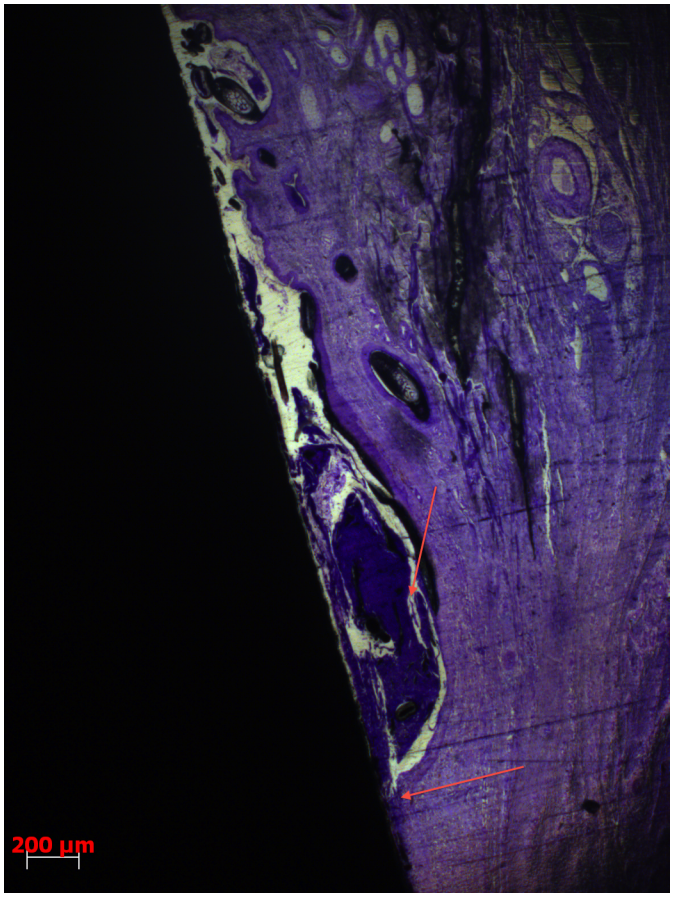

Fig 5.08. Light microscopy image of a transcutaneous section stained with Toluidine blue of a Group 4 implant at Zone 1. Low magnification image of wound debris impeding epidermal attachment, forcing the cell sheet underneath the blockage before interfacing with the implant

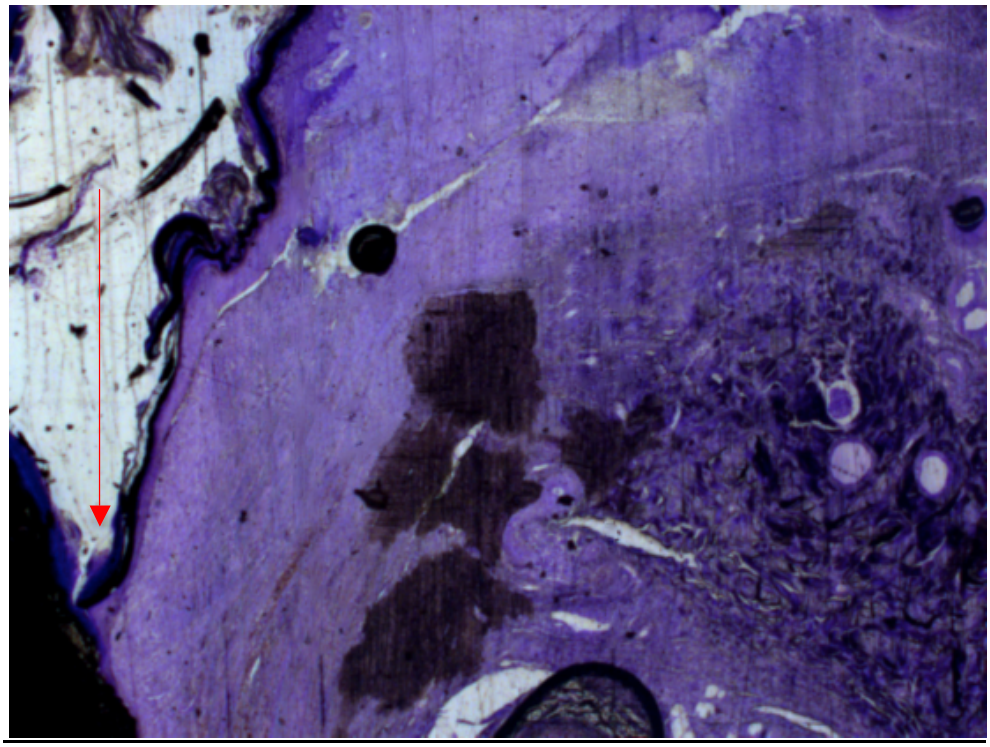

Fig 5.09. Light microscopy image of a transcutaneous section stained with Toluidine blue of a Group 3 implant. Low magnification image of epidermal attachment, with limited downgrowth.

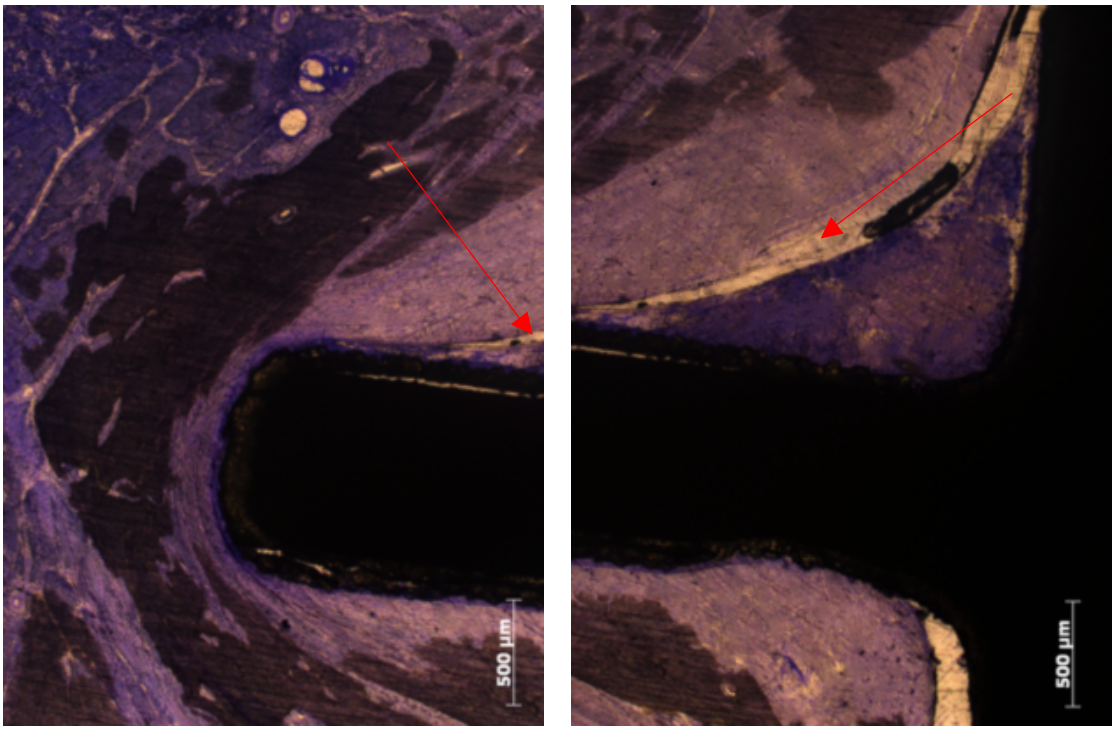

Fig 5.10. Light microscopy image (split in two) of a transcutaneous section stained with Toluidine blue of a Group 1 implant. Low magnification image of epidermal attachment taking place at the flange (red arrows).

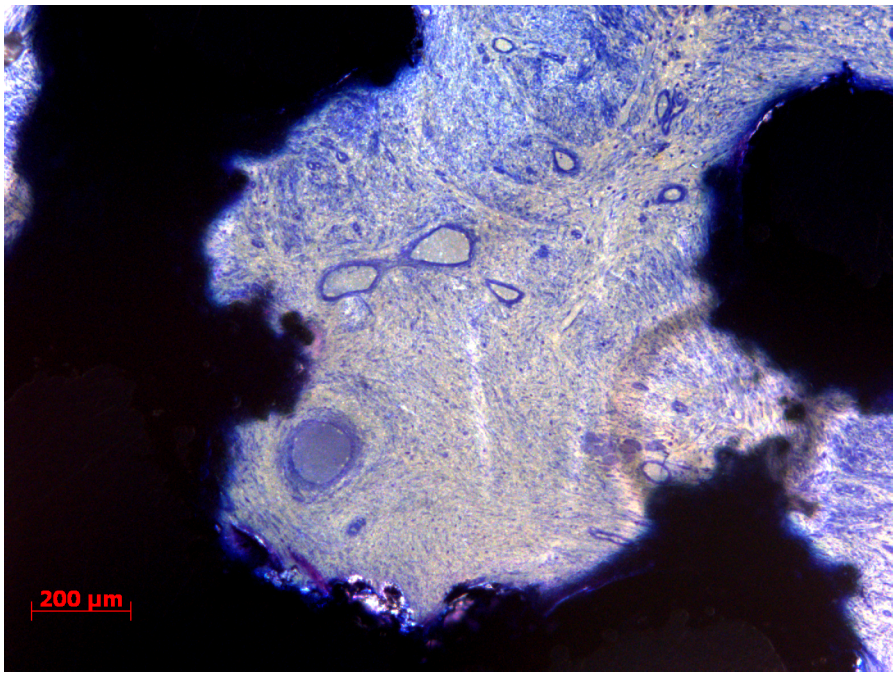

Fig 5.11. Light microscopy image of a transcutaneous section stained with Toluidine blue of a Group 4 implant. Low magnification image of dermal tissue infiltration within a porous flange

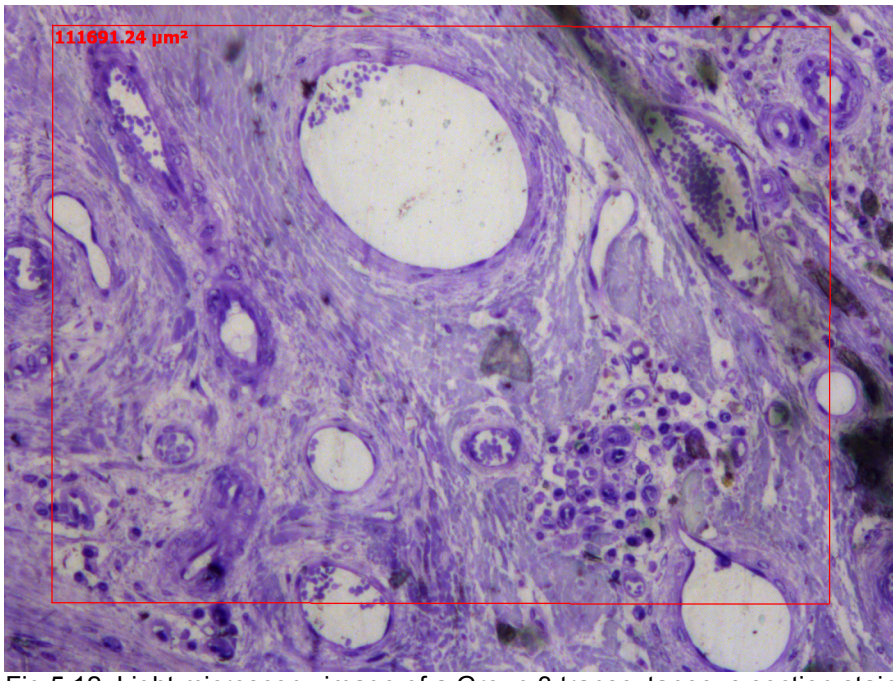

Fig 5.12. Light microscopy image of a Group 3 transcutaneous section stained with Toluidine blue. High magnification image of dense, well-ordered dermal tissue with a number of blood vessels formed within a pore.

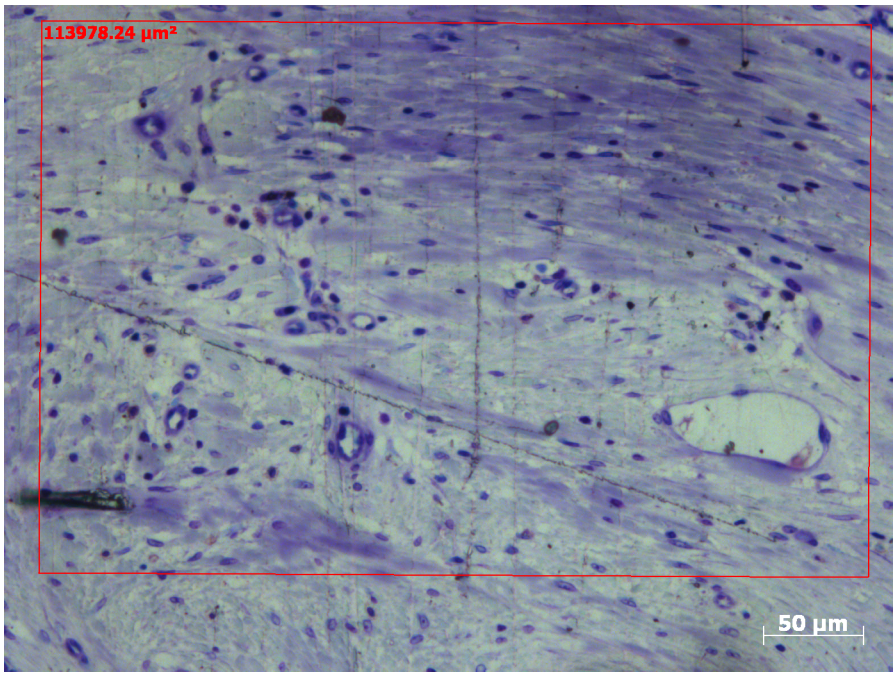

Fig 5.13. Light microscopy image of a Group 4 transcutaneous section stained with Toluidine blue. High magnification image of dense, well-ordered dermal tissue with a number of blood vessels formed within a pore.

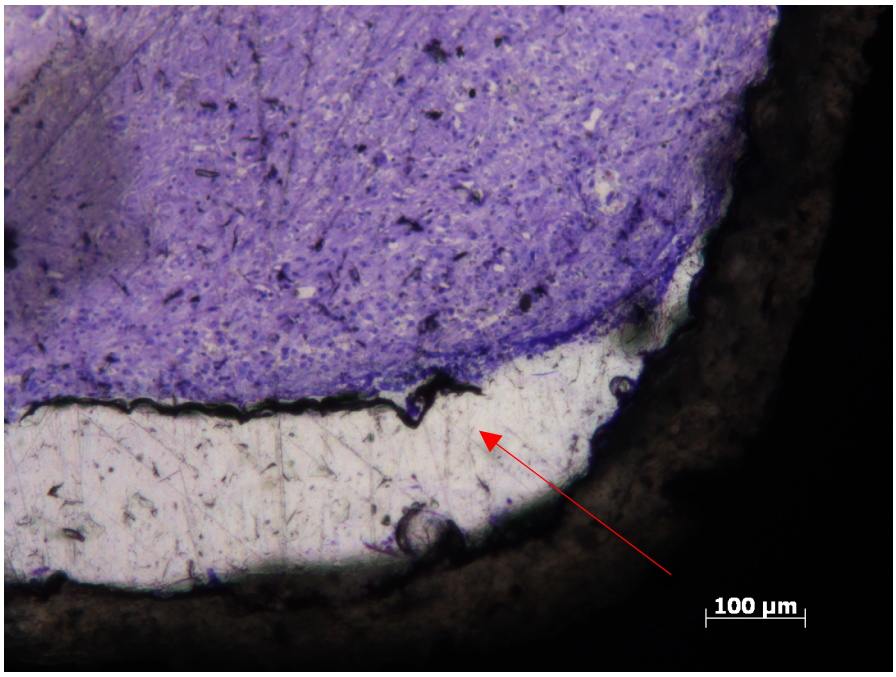

Fig 5.14. Light microscopy image of a transcutaneous section stained with Toluidine blue of a Group 1 implant. Low magnification image of dermal tissue infiltration within a drilled flange, poor contact at dermal tissue implant interface (red arrow).

5.5- Discussion

Epidermal Downgrowth presented in all implanted groups after a 5-month period *in vivo*. No significant reduction in downgrowth could be attributed to any of the functionalisation techniques employed in my study. The percentage of epidermal attachment also observed no significant difference between the various functionalised ITAP flanges. Despite the lack of significant difference between these data, the functionalisation techniques tested in my study had no detrimental effect on the performance of the transcutaneous implant devices compared with current clinical standard (Kang et al 2010). Immediately after implantation *in vivo* the early phase of wound healing begins. This is characterised by an increase in bleeding in the local area, delivering clotting factors to plug the wound space. The fibrinogen and fibrin rich clot acts to provide a provisional matrix to structurally support the migration of cells during later wound healing cascades (Lanza et al. 2000).

Wound debris was clearly visible at the transcutaneous interface both macro- and microscopically of my retrieved implants. Farrell et al. (2013) describe a serocellular crust presenting at the epidermal-implant junction with their porous transcutaneous implants.

Epidermal cell sheet followed the course of the debris before interfacing with the implant shaft or flange. Farrell et al. (2013) observed downgrowth of “a few millimeters”- but no specific data was offered in this regard. My study was performed over 5-months, which could account for larger measurements of epidermal downgrowth compared with these comments. I postulate that this presenting debris could have increased the degree of epidermal downgrowth, as it physically impeded the epidermal-implant interface.

Epidermal keratinocytes do not express integrin $alpha_V beta_3$ receptors that have affinity for fibrinogen and fibrin within the clot (Kubo et al 2001). Without receptor interaction with the fibrinogen/fibrin rich clot, which sits between the epidermal-implant interface, the epidermis will have no way of physically attaching to it therefore forcing the entire cell sheet to migrate under it. No

debris or physical impedance was noted by Al-Ajam et al. (2013), which allowed keratinized epithelium (epidermal layer) to interface with implant, stably. To decrease epidermal downgrowth, limiting debris coagulating in the wound space is of paramount importance. Surgical technique is an obvious factor that can be controlled, to limit the local trauma to skin and keep the wound space as small as possible. This may prevent build up of clots, potentially responsible for increasing the degree of epidermal downgrowth.

The wound care of a human ITAP recipient contributed to stable transcutaneous interface, as no obvious evidence of debris, serocellular crust or exudates presented 2-years post implantation. The care regime involved daily cleaning and re-dressing (Kang et al 2010). The same standards are unachievable within an ovine model, which may have contributed to the formation of wound debris that ultimately increased epidermal downgrowth in my study, irrespective of the functionalisation techniques employed.

There are obvious differences in skin anatomy of a human compared with an ovine model. Farrell et al. (2013) observed no significant difference, at 6-weeks, on porous transcutaneous implant performance between haired and hairless *in vivo* models. Despite these data the authors questioned the likelihood of loose hairs collecting between epidermal-implant interface over time. This may have been a contributing factor in my study, in the collection of debris in such a long-term haired model, a factor that would not influence the human recipient to such a degree.

Blood vessel density significantly increased within porous flanges compared with drilled flanges with RGD-polypeptides appearing to have no effect on vascularisation of the soft tissue. 3-D porous structures can support the formation blood vessels, which in turn, can provide an innervating network for healthy soft tissue metabolism as results from Chapter 4 of my thesis showed. Extensive blood vessel formation was observed throughout porous structures with the same dimensions as the porous flanges in this chapter. These implants were not functionalised with RGD-polypeptides and still exhibited significantly increased blood vessel formation. Vascularisation relies on

endothelial cell migration and subsequent attachment. Sprouting blood vessels express the integrin alpha$_V$beta$_3$ receptors as endothelial cells attach to form a new lumen (Brooks et al 1994). Feng et al. (1999) demonstrate how an engineered ECM structure can influence integrin alpha$_V$beta$_3$ receptor expression of endothelial cells, thereby regulating blood vessel formation. A 3-D fibrin matrix significant increased mRNA levels of integrin alpha$_V$beta$_3$ receptors over single layer ECM protein coats.

I postulate that the 3-D porous flange may act as the provisional matrix thereby inducing integrin alpha$_V$beta$_3$ receptor expression on endothelial cells to a greater degree than drilled flange structures, implicating the structural environment created by the porous flange rather than the biological functionalisation with RGD-polypeptides. The cascades of events that define wound healing occur over time. From vascularisation to be possible, biological cues must be in place first and in theory will not occur on day 4, post implantation.

Results from Chapter 3 of my thesis suggested that silanised RGD-polypeptides have the potential to remain immobilised on the implant *in vivo* up to this time-point. However I suggest that RGD-polypeptide cell attachment points, by this time period, will have bound ligands during early interface formation and therefore be unable to directly influence blood vessels formation, as observed.

Cell density as determined by counting nuclei saw no significant differences across all functionalised structures. Both structural functionalised flanges incorporated a 700μm diameter pore space for tissue to infiltrate. During the cellular phase of wound healing an influx of fibroblasts occurs to initiate the ECM formation by secreting collagen. As the wound becomes stable with structural support by a collagen matrix, the requirement for fibroblasts decreases and wound healing enters the maturation phase. This is known as tissue re-modeling, the collagen ECM is maintained and there becomes less of a requirement on fibroblasts.

Implant retrieval occurred 5-months post implantation in my study, by which time the wound healing process must have entered its maturation phase. I postulate that no significant difference in cell nuclei density was observed between my functionalised devices was because the tissue had entered the maturation phase. Equilibrium had been achieved in the number of cells required to maintain collagen matrix.

Farrell et al. (2013) saw significant differences in soft tissue infiltration to various porous transcutaneous structures between 3-weeks and 4-6-weeks *in vivo*. However, no significant differences were observed between the various porous structures at the end time-point (4-6-weeks). Sufficient time had elapsed for cell migration *in vivo* to even out as wound healing had entered the maturation phase, despite the porosity differences.

A combination of RGD-polypeptides and porous flange significantly increased soft tissue infiltration compared with all other implant groups. Early phase of wound healing aims to regulate homeostasis in response to skin breakage and lay down a basic structural framework in which to support the influx of cells during the cellular phase of wound healing (Lanza et al. 2000). I postulate that the 3-D porous flange silanised with RGD-polypeptides provides a provisional wound matrix to support the cellular phase of wound healing, which has translated in a significant increase in soft tissue infiltration compared with the other functionalised devices.

The RGD-polypeptides will stimulate migrating fibroblasts to express integrin receptors, responsible for attachment. Xu and Clark (1996) demonstrated up-regulation of integrin $alpha_3beta_1$ and $alpha_5beta_1$ receptors on fibroblasts *in vitro*. These receptors have a high affinity for the RGD binding domain and therefore it is logical to suggest the same up-regulation may occur within the 3-D porous flange silanised with RGD-polypeptides that observed a significant increase in dermal tissue infiltration in this study. Silanised RGD-polypeptide substrates enhanced cell attachment *in vitro* (Chapter 2 and 3) and I expected favorable reaction *in vivo* as they have the potential to remain immobilised to the implant (Chapter 3) and support the influx of fibroblasts.

I hypothesized, at the beginning of this chapter, that a combination of silanised RGD-polypeptides with a porous flange would support the formation of a stable transcutaneous interface. Jeyapalina et al. (2013) described the covalent coupling of keratin to porous titanium transcutaneous implants. They observed no impaired wound healing between 3- and 6-months *in vivo* despite the additional chemistry associated with the coating. Warner et al. (2009) suggest to observed differences attributed to the biological functionalisation with Laminin-5 would require experiments that could account for the early wound healing cascades. I suggest that my data shows that silanised RGD-polypeptides had a transient effect *in vivo*. Significant increases were observed in dermal tissue infiltration when in combination with a porous flange, which support my hypothesis.

This form of analysis assessed early effects to the wound-healing cascade, as cells migrated into the provisional wound matrix post clotting events. Subsequent events were, therefore, unable to benefit from the potential effects of functionalisation with RGD-polypeptides as they were utilised in this preceding event.

RGD-polypeptides have a positive effect on early transcutaneous interface formation. However these positive effects were not represented in all the measurable outcomes. Significant differences in HDF attachment to titanium alloy substrates functionalised with RGD-polypeptides were observed in Chapter 2, but were concentration dependent. It may be possible to increase the apparent transient effect of RGD-polypeptides *in vivo* so that later wound healing events can exploit their presence by altering the concentration. This may involve optimising concentrations *in vivo*.

Porous structures alone did not suffer from loss of activity in this manner and were utilised in later wound healing events, such as significant increases in blood vessel formation compared with drilled flanged implants.

No other significant increases were observed to prove or dispute my hypothesis. Moreover, the functionalisation techniques used had no

detrimental effect and demonstrated no significant differences when compared to functionalisation techniques currently used in clinical settings.

The functionalisation techniques investigated in this study had no significant positive impact of epidermal downgrowth and epidermal attachment. These data do not support my hypothesis, in that RGD-polypeptide functionalised porous flange will limit epidermal downgrowth compared with the HA coated non-porous flange.

However, a significant increase was observed in dermal tissue infiltration and the density of blood vessels in infiltrated dermal tissue in RDG-polypeptide functionalised porous flanged implants compared with controls. This supports my hypothesis. A good blood supply is essential for formation of a healthy dermal tissue interface, and it is postulated that this increase in blood vessel density will be essential in maintaining the interface long-term. It has been demonstrated that the infiltration of highly vascularised dermal tissue at the transcutaneous interface of a bony deer antler is the prerequisite to a long-term stable transcutaneous interface in nature (Pendegrass et al 2006).

Fitzpatrick et al. (2011) noted soft tissue infiltration to possess high numbers of dermal fibroblasts and epidermal keratinocytes at the interface of functioning ITAP devices in clinical veterinary cases after 8-, 12- and 17-months. To facilitate this, there must have been good vascular infiltration to support tissue and cell viability. Despite the fact that after 5-months there was no significant difference in downgrowth or epidermal attachment between implant types in my study, the results suggest that improved vascular infiltration has occurred in silanised RGD-polypeptide functionalised porous titanium alloy flanges. This may be critical to the maintenance of a healthy dermal interface over time periods extending beyond 5-months. It should also be noted that downgrowth was not eliminated in the veterinary clinical cases reported by Fiztpatrick et al. (2011) using a solid flanged device. It is possible that with RGD-polypeptide functionalisation combined with porous implants may eliminate downgrowth and support vascular infiltration capable of supporting a long-term biologically sealed transcutaneous interface.

5.6- Conclusion

The aim of this final experimental chapter of my thesis was **to determine the effect of functionalising the ITAP flange on the skin implant interface in a long-term *in vivo* model.**

Functionalisation techniques employed in this study did not eradicate the failure modalities of ITAP devices, however they did not detrimentally affect the formation of a stable transcutaneous interface compared with current clinical standards. Indeed positive and significant effects were observed, with the biological functionalisation using RGD-polypeptides and structural functionalisation with EBM fabricated porous flanges, on the long-term stability of the transcutaneous interface.

Chapter 6- The Final Discussion

Chapter 6

Discussion and Future Work

The aim of my thesis was **to develop functionalisation techniques that will enhance dermal cell and tissue attachment, in order to enhance a seal and reduce infection of implant biomaterials used for ITAP**.

The first chapter in my thesis reviewed the current literature surrounding bone-anchored transcutaneous implant devices. Based on the understandings from this review I formulated a general hypothesis: **Soft tissue attachment to ITAP will be improved using a protein coated porous implant compared with surfaces that are currently used for ITAP.** In order to achieve my pre-determined aim and test my hypothesis, a number of experimental chapters were devised, each of which were designed to answer specific research questions relating to the general hypothesis.

The first experimental chapter of my thesis, Chapter 2, focused on HDF attachment *in vitro* to titanium alloy substrates, the material of choice for ITAP devices. More specifically, the effect of functionalising ITAP substrates with RGD-polypeptides on HDF attachment was investigated. These experiments were also performed in relation to established techniques, using fibronectin, the whole molecule counterpart of RGD-polypeptides. Previous work by Middleton et al. (2007) has shown that using silanised fibronectin enhances the attachment of these cells. The distinct advantage of being able to use synthetic RGD-polypeptides means that regulatory complications associated with medical devices and harsh sterilizations treatments may be avoided compared with the clinical use of fibronectin. It was hypothesized that RGD-polypeptides would elicit a similar up-regulatory effect on HDF attachment compared with fibronectin coatings *in vitro*. For significant increases in HDF attachment to occur RGD-polypeptides had to be successfully immobilised onto the substrate. This was achieved through both adsorption and silanisation protocols. The degree of HDF attachment varied with concentration but did elicit comparable responses to fibronectin substrates. The essential feature in this chapter was HDF attachment was observed to

significantly increase on RGD-polypeptide substrates by 24-hours. Functionalisation with RGD-polypeptides *in vitro*, as demonstrated an increases in HFD attachment strength to titanium alloy substrates. 24-hours is the critical timeframe in which soft tissue must attach to ITAP devices *in vivo*. These data suggested that RGD-polypeptide coating could have potential use *in vivo*, however aspects of the functionalisation protocol had to be optimised first and this was investigated in Chapter 3. Despite optimizing the protocol, the functionalisation of titanium alloy had to increase dermal cell attachment strength to be a viable technique for ITAP use.

Chapter 3 aimed to quantify the loading and release kinetics of RGD-polypeptides to ITAP substrates, in an attempt to control the concentration dependent variations in HDF attachment, observed in Chapter 2. This chapter also tested the durability of the functionalisation technique as the *in vivo* environment is far removed from that of cell culture studies. Silanisation of titanium alloys substrates with RGD-polypeptides resulted in a more robust coating. After challenging with FCS, significantly higher levels of silanised RGD-polypeptides remained on the substrate compared with absorbed coatings. Silanised substrates also significantly increased HDF attachment by 24-hours compared with controls. Evidence from Chapter 3 suggested that functionalising ITAP substrates with silanised RGD-polypeptides increased cell attachment and could remain attached when incubated with serum proteins. Therefore I postulated that this technique may have provided an opportunity to functionalise an ITAP device *in vivo* by increasing dermal tissue attachment to the ITAP flange. This functionalised substrate may enhance the formation of a stable biological seal at the transcutaneous interface *in vivo*.

Chapter 4 concentrated on the structural functionalisation of the ITAP flange. The ITAP flange was designed to increase the surface area for dermal soft tissue attachment *in vivo*, a characteristic possessed by a natural transcutaneous structure- the antler of a deer. The EBM technique used to construct the novel porous titanium alloy created precise 3-D structures. The aim of this chapter was to test the hypothesis that a more open structure would lead to significant increases in soft fibrous connective tissue infiltration

and vascularisation throughout the implant. Results suggested that varying the pore and strut diameters could lead to an optimal structure that supports significant increases in tissue infiltration and vascularisation. This is the first time that the optimal pore and strut diameters have been systematically investigated *in vivo* for soft tissue attachment. Bobyn et al. (1982), LaBerge et al. (1990), Hacking et al. (2000) all investigated the mechanical strength of soft tissue attachment of various porous implant structures but did not quantify soft tissue in-growth. Dimensions of 700μm pore diameter and 300μm strut diameter observed consistently high soft tissue infiltration and vascularisation. In light of the results, I went on to hypothesize that if these dimensions were incorporated into the ITAP flange, dermal tissue may have more opportunity to attach, thereby forming a stable skin seal at the transcutaneous interface.

Chapter 5 was devised to assess the functionalisation techniques developed in previous chapters in an ITAP *in vivo* transcutaneous model. No previous ITAP experimental study had been documented *in vivo* for longer than 4-weeks. This final experimental study aimed to assess the effect on the formation of the transcutaneous implant interface over a long-term study. It was hypothesized that a combination of a porous flange silanised with RGD-polypeptides would significantly increase interface formation. My functionalised ITAP devices were compared against the current clinical implant for 5-months. The transcutaneous interface was quantitatively characterized by length of epidermal downgrowth and the percentage of epidermal attachment. Data was also collected on the percentage of dermal tissue infiltration to the flange and density of blood vessels and cell nuclei within the infiltrated tissue. The functionalisation techniques developed in my thesis and those used in ITAP clinical practice (Kang et al 2010) did not eradicate epidermal downgrowth, as no significant difference was observed between groups. Although there was no statistical significance demonstrated between the functionalised implant groups with regard to epidermal downgrowth and epidermal attachment, there were significant increases observed in blood vessel density and dermal tissue infiltration. These were attributed to porous flanges silanised with RGD-polypeptides. Overall this

chapter demonstrated that my functionalisation techniques had no detrimental effect on the formation of transcutaneous interface.

There are a number of bone-anchored transcutaneous devices in clinical and preclinical use, including ITAP devices (Pitkin, 2013). This form of treatment eradicates many of the clinical and psychological issues observed with conventional treatment and care of amputations. Un-natural pressure distribution between the stump and prosthesis leads to soft tissue injuries, often chronic (DesGroseilliers et al 1978, Dudek et al 2005, Koc et al 2008, Lyon et al 2000, Portnoy 2009 and Schmalz et al 2002). Bypassing these soft tissues of the stump with a bone-anchored transcutaneous device alleviates such problems. Load from locomotion can be directly transferred from bone, through the device, to prosthesis. Such a device can be donned and doffed by the user with ease and locomotion itself can be more efficient through osteoperception (Kang et al 2010).

The aim of this thesis was to contribute to the longevity of these devices by developing techniques that could allow a skin implant interface to form. If this is achieved early and skin seals around the implant shaft, continuity of the skin is maintained, the passage of invading pathogens will be curtailed and unable to enter the body. Dermal cell attachment, to titanium alloy substrates *in vitro*, can be significantly up-regulated by biological functionalisation with RGD-polypeptides. When combined with porous titanium alloy structures dermal tissue infiltration and blood vessel density can also be significantly up-regulated *in vivo*.

To represent my experimental work I devised a flow diagram at the end of Chapter 1 (Fig 1.06). The questions outlined in my flow diagram were experimentally answered. In summation of my thesis it is important see how my work contributes in the wider landscape of dermal cell and tissue attachment and how it may be translated in the clinical locale.

The current epidemiology of amputation suggests incidence of dysvascular related amputation is rising due to the prevalence of diabetes

(http://www.bbc.co.uk/news/health-17270379). With compromised vascularity of the soft tissues in the stump, bone-anchored transcutaneous devices may not be a viable treatment option for such individuals as long-term skin implant interface may not formed due to the lack of blood supply. Results of my thesis have the potential to increase the number of viable candidates that could benefit from such novel therapies, should it be incorporated into clinical practice. The porous flanged silanised with RGD-polypeptides facilitated significant increases in dermal tissue infiltration and blood vessel density.

Large numbers of service men and women are returning from recent warzones suffering from traumatic amputation (Wallace, 2012). Porous titanium alloy structures silanised with RGD-polypeptides support the formation of well vascularised healthy soft tissues (as shown in Chapter 5). These functionalised techniques may, therefore, provide a viable treatment option for such traumatic injuries where soft tissues have been heavily damaged or scarred. In turn this may positively impact long-term stump heath and increase quality of life for another patient group.

This technology has the potential of many benefits, including those of the emerging discipline of intuitive neuromuscular control of prostheses, where ITAP devices (Al-Ajam et al 2013) or other bone anchored transcutaneous devices (Pitkin et al 2012) act as conduits to house electrodes capable to transmitting signals in and out of the body. The most inspiring benefits are the well-documented increases to quality of life to users of such devices (Kang et al 2010 and Lundberg et al 2011). Such devices also benefit veterinary cases (Fitzpatrick et al 2011). Results of Chapter 4 are being used in “second generation” of a more successful ITAP device used in veterinary cases, where a porous flange is made by selective laser sintering. Dimensions of the pores were selected as a result of my study (Oral Communication; Combine Orthopedic Research Society: Venice 2013, Symposium Chaired by Prof G Blunn (UCL), speaker N Fitzpatrick) (Fig 6.01).

Fig 6.01. PerFiTS device (Percutaneous Fixation To Skeleton) courtesy of Fitzbionics (Patents PCT/GB2013/052639 and 1317782.9) “Second Generation” ITAP device used in Veterinary cases.

My findings suggest it is possible to engineer an environment that does promote a long-term stable skin seal, which prevents harmful pathogens entering the internal environment. It is hoped that these functionalisation techniques will be incorporated into further pre-clinical and clinical studies of ITAP devices and continue to improve the lives of many amputees currently suffering with conventional treatment.

It is hoped that further work will continue to understand the mechanisms of dermal cell and tissue attachment to implant biomaterials used for ITAP, and make a significant contribution to science. In light of the early reported successes with direct skeletally attached prostheses to human and animal subjects using ITAP devices (Fitzpatrick et al 2011 and Kang et al 2010), the EBM manufacturing technique utilized in Chapter 4 highlighted the dexterity and precision achievable in implant structures. This application may be extended to subjects who are not fully-grown, because the porous metals may be able to accommodate changes in musculature size and soft tissue growth. Winter (1974) originally stated that if a porous structure could support the influx of dermal fibroblasts during wound healing transcutaneous integration

might be achievable. It therefore may be of interest to use EBM to create a totally porous titanium alloy device and test it in a transcutaneous *in vivo* environment.

One particular area of work that I believe logically follows on from the biological functionalisation technique developed in my thesis is the transfer of this into a clinical setting. Preparing a sterile, functionalised, titanium alloy substrate that could be applied to ITAP is of particular interest. Understanding how the biological activity of silanised RGD-polypeptides to titanium alloy substrates (in terms of cell attachment *in vitro*) would be influenced by harsh and stringent medical sterilisation protocols, such as ethylene oxide, gamma-irradiation and heat treatment is important. How long could such a substrate remain biological active for? Is it possible to freeze dry substrates to increase shelf life? These are all valid questions that would need to be experimentally tested and would be the first steps in designing an "off the shelf ITAP device" which then may provide the opportunity for ITAP devices to become a wide spread treatment option for amputees. Alternatively it may possible to functionalise ITAP devices with RGD-polypeptides in an aseptic environment just before implantation.

In vivo testing of my functionalisation techniques was an important aspect in relation to the application of ITAP devices. Chapters 2 and 3 investigated cell attachment strength *in vitro*. I aimed to up-regulate HDF attachment strength using biological functionalisation of titanium alloy. Although cell attachment is a critical requirement for ITAP (Pendegrass et al 2006 and Kang et al 2010), it is only one aspect of cellular function. Further work could include the investigation of more cellular responses, including proliferation, migration and possible differentiation of HDFs on the functionalised substrates to further characterise the effects of the RGD-polypeptides.

Fibroblast migration through porous structures *in vivo* must result from the contractile elements of the cellular cytoskeleton (Alberts et al 2002). Information about the cellular cytoskeleton in cells migrating on RDG

functionalised and non-treated titanium alloy surfaces both *in vitro* and *in vivo* would also be of interest.

Chapter 3 was designed to develop a functionalisation technique that could withstand *in vivo* implantation and provide a more durable coating long-term. My *in vitro* experiments were all 2D culture systems, despite trying to create a competitive environment with serum proteins and PBS. The silanisation of RGD-polypeptides to titanium alloy was then tested in a 3D system *in vivo* over 5-months. This is an environment far removed from the *in vitro* experiments I had performed in Chapters 2 and 3. The use of a 3D cell culture systems may "bridge the gap" from *in vitro* environments to long-term *in vivo* environments. Fibroblast morphology has been shown to differ from 2D to 3D systems (Sheez et al 2005), which may result from different attachment proteins secreted *in vivo*.

It may be of interest to develop a 3D porous substrate, such as those used in Chapter 4, functionalise it by silanisation of RGD-polypeptides and introduce dermal fibroblasts into a bioreactor. This may provide the opportunity to observe how biologically functionalised porous titanium alloy (such as the group 4 in Chapter 5) behave in a 3D culture system.

In order for ITAP to be transferable into widespread clinical use, further research has to be done. Although the promising results of the functionalisation techniques tested in Chapter 5, some consideration must be given to the animal model used. ITAP devices were orientated perpendicular to the bone in a trans-tibial plane. Designing and implementing a full amputation model may provide more realistic conditions for ITAP devices to be tested in. This is currently unachievable in this country due to the terms of the Animals under the Animals (Scientific Procedures) Act 1986. http://www.legislation.gov.uk/ukpga/1986/14/pdfs/ukpga_19860014_en.pdf

Appendix

Appendix 1

Substrate Surface Profilometry Analysis

Par.	Value	Tol +	Tol -
Ra	0.026 µm		
Rz	0.16 µm		

Par.	Value	Tol +	Tol -
Ra	0.03 µm		
Rz	0.221 µm		

Par.	Value	Tol +	Tol -
Ra	0.021 µm		
Rz	0.138 µm		

Study 1

Cell Area

	Median cell area/μm^2	**95% confidence intervals**
Controls	2141	2043.51-2439.22
0.1mM Linear RGD 1h	2162	2111.55-2602.72
0.1mM Linear RGD 4h	2272.4	1854.21-2940.6
0.1mM Cyclic RGD 1h	2409.5	2197.9-2657.92
0.1mM Cyclic RGD 4h	2167	1763.76-3025.44

Vinculin Markers

	Median	**95% confidence intervals**
Controls	36	35.2-49.2
0.1mM Linear RGD 1h	45.5	39.3-50.7
0.1mM Linear RGD 4h	94	82.4-109.1
0.1mM Cyclic RGD 1h	46.5	45.6-59.9
0.1mM Cyclic RGD 4h	88	77.2-112.2

Density of Vinculin Markers

	Median	**95% confidence intervals**

Controls	0.0163	0.0161-0.0219
0.1mM Linear RGD 1h	0.0163	0.0173-0.0218
0.1mM Linear RGD 4h	0.0398	0.0357-0.0529
0.1mM Cyclic RGD 1h	0.0214	0.0192-0.0262
0.1mM Cyclic RGD 4h	0.0446	0.0392-0.07

Study 2

Cell Area

	Median cell area/μm^2	**95% confidence intervals**
Controls	2076.7	1738.1-2242.3
0.1mM Linear siRGD	2018.5	1835.2-2156.4
0.1mM Cyclic siRGD	2251.5	2101.5-2828.5

Vinculin Markers

	Median	**95% confidence intervals**
Controls	63	52.7-70.7
0.1mM Linear siRGD	85	71.1-93.9
0.1mM Cyclic siRGD	79.5	70.8-97.5

Density of Vinculin Markers

	Median	**95% confidence intervals**
Controls	0.032	0.0273-0.037
0.1mM Linear siRGD	0.0439	0.0363-0.0476
0.1mM Cyclic siRGD	0.0326	0.0303-0.0394

Study 3

Cell area

	Median	**95% confidence intervals**
Control	2145	1931-2498.3
Ad RGD	2160	1966.9-2317.6
Ad fn	2767.7	2567.8-3085.9
Si RGD	2173.6	1865.6-2683
Si fn	2287.5	2035-2546.4

Vinculin markers

	Median	95% confidence intervals
Control	30	28.3-38.1
Ad RGD	68	63.2-81.2
Ad fn	101	87.6-113.8
Si RGD	61.5	53.7-76.2
Si fn	88.5	78.6-103.8

Density of Vinculin Markers

	Median	95% confidence intervals
Control	0.0159	0.0129-0.0186
Ad RGD	0.0334	0.0301-0.0382
Ad fn	0.0339	0.0312-0.0417
Si RGD	0.0295	0.0256-0.0378
Si fn	0.0428	0.0357-0.0454

Study 4

Cell area

	Median	95% confidence intervals
Control	2145	1931-2498.3
5mM adRGD	2160	1966.9-2135.6
10mM adRGD	2105.9	1897-2395.8
25mM adRGD	2236	2074.6-2473.3
50mM adRGD	2768	2251.2-3111.8
100mM adRGD	2080	1809.5-2199.7

Vinculin marker

	Median	95% confidence intervals
Control	30	28.3-38.1
5mM adRGD	68	63.2-81.2
10mM adRGD	64.5	61-78
25mM adRGD	60	66.1-69
50mM adRGD	51	45.2-65.4
100mM adRGD	49	43-54.4

Density of Vinculin Markers

	Median	95% confidence intervals
Control	0.0159	0.0129-0.0153
5mM adRGD	0.0334	0.0301-0.0382
10mM adRGD	0.0344	0.0286-0.0389
25mM adRGD	0.0273	0.0248-0.0313
50mM adsorbed RGD	0.0202	0.0179-0.0245
100mM adsorbed RGD	0.0246	0.0214-0.0285

Study 5

Cell Area

	Median	95% Confidence Interval
Control 1h	189.1	170.2-230.7
Control 4h	1173.7	931.3-1304
Control 24h	1134.	1038.4-1456.7
Control 96h	1619.9	1378.9-1801.3
AdRGD 1h	1119.5	1119.9-1595.1
AdRGD 4h	1083.6	939.9-1484.6
AdRGD 24h	2142.2	1959.2-2594.1
AdRGD 96h	1271.7	1090.2-1609.7
Adfn 1h	1227.8	1038.6-1344.6
Adfn 4h	1032.3	819.4-1232
Adfn 24h	2086	1637.6-2181.4
Adfn 96h	1740.6	1400.2-2102.5
siRGD 1h	1166.5	470.4-2085.9
siRGD 4h	2144.5	1461.9-2466.2
siRGD 24h	1932.9	1822.8-2175.7
siRGD 96h	1429.9	1322.5-1863
Sifn 1h	731.4	584.4-1176.3
Sifn 4h	1912	1644.9-2158.9
Sifn 24h	1818.7	1537.8-2250.5
Sifn 96h	1339.6	1018.4-1710.5

Vinculin Markers

	Median	95% Confidence Interval
Control 1h	2	1.1-3.3
Control 4h	20	16.4-23.6

Control 24h	25	19.7-27.4
Control 96h	29.5	27.8-35.1
AdRGD 1h	23	21.3-31.9
AdRGD 4h	30	28.5-34.4
AdRGD 24h	74	66.4-85.5
AdRGD 96h	85	82.1-108
Adfn 1h	22	18.7-25.4
Adfn 4h	24	21-29.9
Adfn 24h	47	40-56.8
Adfn 96h	87	75.7-98.5
siRGD 1h	18	5.8-35.5
siRGD 4h	44	30.2-52.5
siRGD 24h	70.5	60.6-78.5
siRGD 96h	65	58.3-72.8
Sifn 1h	13	11.3-23.3
Sifn 4h	30.5	27.9-37
Sifn 24h	48	38-56.5
Sifn 96h	58.5	55.8-74.5

Density of Vinculin Markers

	Median	**95% Confidence Interval**
Control 1h	0.0099	0.0054-0.0203
Control 4h	0.0194	0.0138-0.0241
Control 24h	0.0206	0.0164-0.0229
Control 96h	0.018	0.017-0.0265
AdRGD 1h	0.0195	0.0174-0.0216
AdRGD 4h	0.0286	0.0238-0.0329
AdRGD 24h	0.0333	0.0303-0.0391
AdRGD 96h	0.0734	0.0668-0.0785
Adfn 1h	0.0177	0.017-0.0212
Adfn 4h	0.0251	0.0217-0.0299
Adfn 24h	0.0261	0.022-0.0285
Adfn 96h	0.0508	0.0453-0.0625
siRGD 1h	0.0174	0.0122-0.0192
siRGD 4h	0.0206	0.0193-0.0228
siRGD 24h	0.0333	0.0303-0.0391
siRGD 96h	0.0447	0.0381-0.0498
Sifn 1h	0.0181	0.0167-0.0231

Sifn 4h	0.0178	0.0153-0.0205
Sifn 24h	0.0247	0.0221-0.0291
Sifn 96h	0.0447	0.0381-0.0498

Appendix 2

YRGD-polypeptide synthesis data provided by AltaBioscience.

AltaBioscience

While the science may be challenging, our vision is simple:
to support research and discovery in academia and industry.

Peptide data sheet

Printed 27/01/2012
M2481 dowling

Client Name : **Robert Dowling**
Order Number : **HQ809608**

Peptide code	Sequence
M2481	YRGD

Weight of peptide **14mg**

Peptide purity **>95%**

Molecular weight **510**

Special amino acids:

Peptide salt form:-	Peptides are normally supplied as their TFA salts.
Analytical HPLC:-	Column = Waters XBridge C18 3.5µm, 50 x 4.5 mm Buffer A = 0.05% TFA in water Buffer B = 0.05% TFA in 100% MeCN Gradient = 0% B to 55% B in 7 minutes, 80% B for 1 minutes Flow rate = 1.5 ml / min Wavelength = 215 nm
Mass spectrometry:-	MALDI-TOF with gentisic acid or α-cyano hydroxy cinnamic acid as matrix.
Storage:-	Best stored at -20°C
Warning:-	The biological effects of these materials are not known. Exercise care in handling and use. For research use only. Not for humans or clinical diagnosis.

Page 1 of 1

For conditions of sale, please refer to our Brochure and Price List or our website at
www.altabioscience.bham.ac.uk/about/conditions.shtml

Template 'pure peptide template'
V2, 3 September 2009

	Pk No.	Name	Time	Height	Area	Area %
1	1		2.0	0.18	0.718	1.1
2	2		2.2	15.44	63.250	98
3	3		2.3	0.18	0.277	0.43

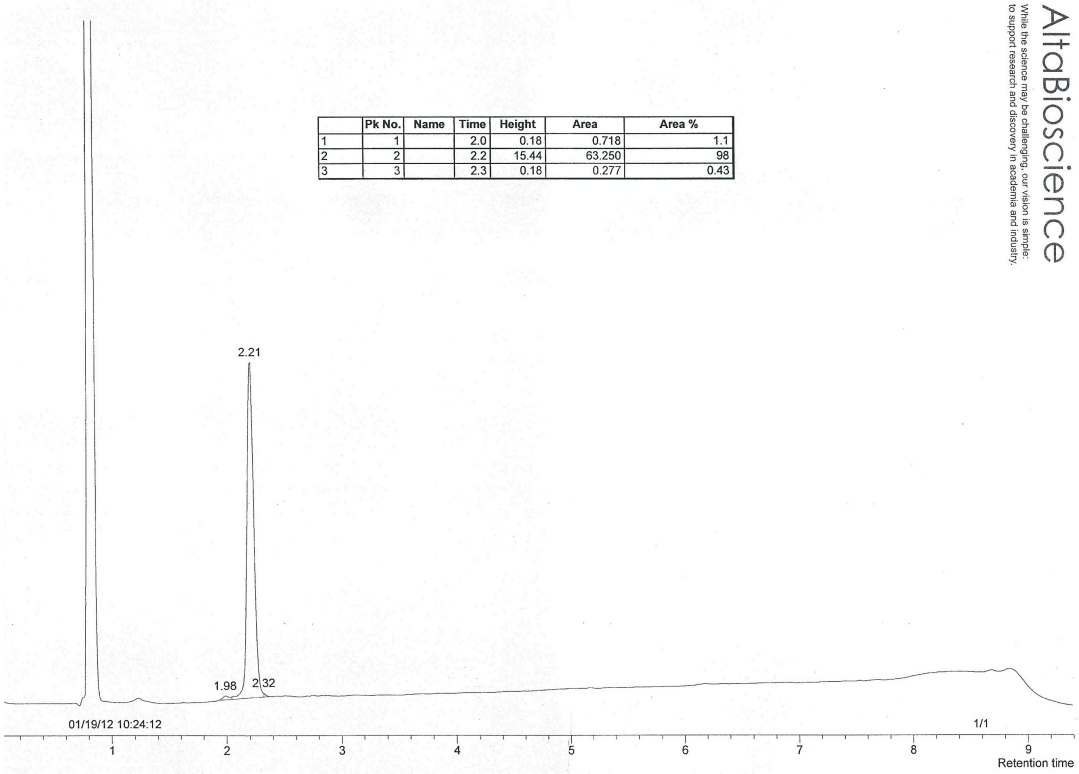

AltaBioscience
While the science may be challenging, our vision is simple:
to support research and discovery in academia and industry.

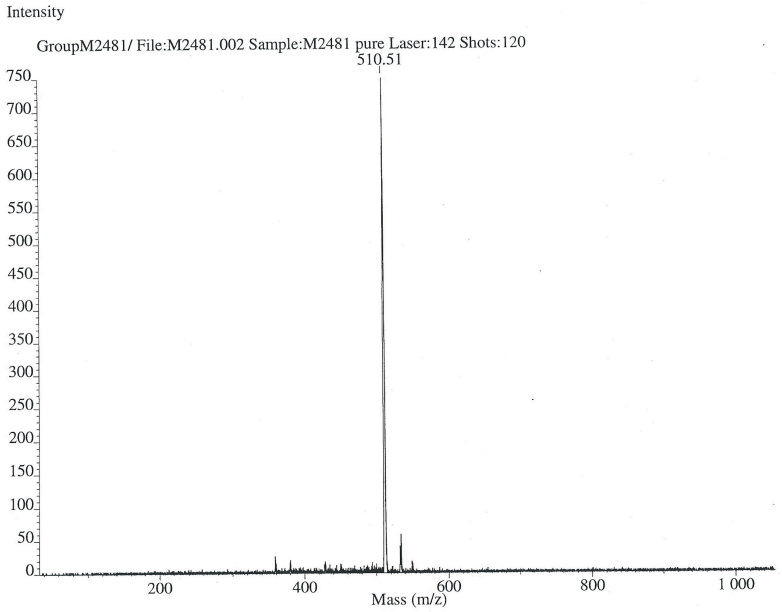

Technical Data for the iodination of YRGD-polypeptide and Fibronectin.

^{125}I Technical Data Certificate of Analysis

Caution: For Laboratory Use. A research chemical for research purposes only.

Custom Iodination Services

NEX083 **Iodination with Lactoperoxidase**

[^{125}I]-*Fibronectin*

LOT SPECIFIC INFORMATION

Calculated as of:	**05-Jan-2012**
Lot Number:	**CIS10521**
Specific Activity:	**70.0 TBq/mmol**
	1892 Ci/mmol
Radiochemical Concentration	**0.16 MBq/µg**
	4.30 µCi/µg
	11.1 MBq/ml
	300 µCi//ml
Radiochemical Purity:	**< 5%**

Package Size Information

Total Activity	**1.5 mCi**
Package Size(s)	**1.5 mCi**
Volume	**5.0 mL**

PACKAGING: [^{125}I] – Fibronectin is frozen in 50mM sodium phosphate pH 7.2 80mM sodium chloride, and 0.1% BSA. It is shipped on dry ice.

STORAGE: Storage is at customer's discretion. Refer to back page of this sheet for further instructions on stability and storage.

SPECIFIC ACTIVITY: Determined by percent incorporation of ^{125}I into the product. Specific activity decays with time.

RADIOCHEMICAL PURITY: Initially less than 5% unbound iodide as determined by instant thin layer chromatography.

PREPARATIVE PROCEDURE: Radioiodination is performed with no carrier added ^{125}I using a lactoperoxidase procedure and is purified by open column chromatography. This method predominantly labels tyrosine residues.

www.perkinelmer.com

^{125}I Technical Data Certificate of Analysis

Caution: For Laboratory Use. A research chemical for research purposes only.

Custom Iodination Services

NEX084 **Iodination with Chloramine-T**

[^{125}I]-*YRGD*

LOT SPECIFIC INFORMATION

Calculated as of:	**05-APR-2012**
Lot Number:	**CIS40521**
Specific Activity:	**57 MBq/mmol**
	1.6 Ci/mmol
	166 kBq/µg RGD
	4.5 µCi/µg RGD
Radiochemical Concentration	**11.1 MBq/ml**
	0.3 mCi/ml
Radiochemical Purity:	**>95%**

Package Size Information

Total Activity	**1.5 mCi**
Package Size(s)	**2 x 0.75 mCi**
Volume	**5 ml**

PACKAGING: [^{125}I]-Packaged in solution containing 10% RGD buffer and 90% PBS: 10 mM phosphate buffer (pH 7.4), 2.7 mM potassium chloride, 137 mM sodium chloride. It is shipped on dry ice.

STORAGE: Store at -20°C. Refer to back page of this sheet for further instructions on stability and storage.

SPECIFIC ACTIVITY: The initial specific activity is 2200 Ci/mmol. Preparative HPLC separates unlabeled from [^{125}I]-labeled product. Upon decay, the iodinated product undergoes decay catastrophe, and the specific activity remains constant with time. However, it is not known what molecular fragments are generated from the decay event or what functional activity these fragments may have in different assays.

RADIOCHEMICAL PURITY: Initially found to contain >95% radiochemical purity by reversed phase HPLC.

PREPARATIVE PROCEDURE: Radioiodination is performed with no carrier added ^{125}I using a chloramine-T procedure and is purified by reversed phase HPLC. This method predominantly labels tyrosine.

HAZARD WARNING: This compound contains a chemical(s) known to the state of California to cause cancer.

www.perkinelmer.com

Study 1

Cell Area

	Median	95%Confidence Intervals
Control	1247.5	1038.4-1456.7
5mM YRGD	2276.6	1959.2-2594.1
5mM RGD	2142.2	1966.9-2317.6

Vinculin Markers

	Median	95%Confidence Intervals
Control	23.53	19.71-27.35
5mM YRGD	75.94	66.43-85.46
5mM RGD	72.2	63.2-81.2

FA Density

	Median	95%Confidence Interval
Control	0.0196	0.0164-0.0229
5mM YRGD	0.0303	0.0303-0.0391
5mM RGD	0.0341	0.0300-0.0382

Study 3

Adsorbed I^{125} YRGD-Polypeptide

	Median	95% Confidence Interval
1	0.56	0.48-0.58
2	1.17	1.08-1.26
3	1.95	1.88-2.02
4	2.55	2.51-2.58
5	2.85	2.65-2.99
6	3.7	3.55-3.73
7	5.18	4.99-5.33
8	5.39	5.30-5.45
9	5.73	5.65-5.78
10	6.023	5.77-6.35

Silanised I^{125} YRGD-Polypeptide

	Median	95% Confidence Intervals
1	0.79	0.72- 0.92
2	1.29	1.00-1.37
3	1.51	1.47-1.53
4	1.74	1.67-1.84
5	2.12	1.88-2.16
6	3.36	3.29-3.40
7	4.35	3.95-4.54
8	4.43	4.25-4.63

9	5.1	4.62-5.35
10	5.74	4.88-5.95

Silanised I^{125} Fibronectin

	Median	**95% Confidence Intervals**
10	6.30	5.09-7.15
100	23.93	21.81-26.22
250	68.02	64.98-71.07
500	207.83	191.31-221.18
750	262.07	247.43-282.87
1000	336.24	308.82-363.89
2000	569.02	533.88-591.40
3000	833.11	814.96-859.99
4000	936.81	870.63-980.66
5000	946.02	808.41-1027.23

Study 4

I^{125} YRGD-Polypeptide

Group	**Median**	**95% Confidence Interval**
Si I^{125}YRGD 5-mins	1.16	0.83-1.56
Si I^{125}YRGD 2-hours	3.85	3.42-4.12
Si I^{125}YRGD 20-hours	7.28	6.51-7.4
Si I^{125}YRGD 140-hours	7.33	6.73-9.07
Ad I^{125}YRGD 5-mins	0.97	0.64-1.11
Ad I^{125}YRGD 2-hours	3.2	3.04-3.54
Ad I^{125}YRGD 20-hours	3.01	2.45-3.35
Ad I^{125}YRGD 140-hours	0.39	0.39-0.46

I^{125} Fibronectin

Group	**Median**	**95% Confidence Interval**
Si I^{125}fibronectin 5-mins	300.06	269.9-330.22
Si I^{125}fibronectin 2-hours	612.06	561.93-794.98
Si I^{125}fibronectin 20-hours	652.65	563.39-1031.81
Si I^{125}fibronectin 140-hours	844.55	769.251144.06
Ad I^{125}fibronectin 5-mins	163.52	139.07-178.68
Ad I^{125}fibronectin 2-hours	319.33	297.69-334.54

Ad I^{125}fibronectin 20-hours	391.26	368.75-399.99
Ad I^{125}fibronectin 140-hours	435.18	411.44-465.42

Study 5

PBS Soak

I^{125} YRGD-Polypeptide

Group	Median	95% Confidence Interval
Si I^{125}YRGD 5-mins	2.99	2.7 - 3.05
Si I^{125}YRGD 2-hours	1.78	1.64 - 2.03
Si I^{125}YRGD 20-hours	1.43	1.35 - 1.49
Si I^{125}YRGD 140-hours	1.37	1.33 - 1.47
Ad I^{125}YRGD 5-mins	2.08	1.90 - 2.19
Ad I^{125}YRGD 2-hours	1.4	1.29 - 21.53
Ad I^{125}YRGD 20-hours	1.09	0.96- 1.19
Ad I^{125}YRGD 140-hours	0.25	0.24 - 0.26

I^{125} Fibronectin

Group	Median	95% Confidence Interval
Si I^{125}fibronectin 5-mins	46.02	40.59- 52.45
Si I^{125}fibronectin 2-hours	27.44	25.69- 31.7
Si I^{125}fibronectin 20-hours	26.71	23.14 - 32.42
Si I^{125}fibronectin 140-hours	20.19	13.85 - 23.26
Ad I^{125}fibronectin 5-mins	34.29	32.52 - 35.68
Ad I^{125}fibronectin 2-hours	23.44	19.47 - 28.56
Ad I^{125}fibronectin 20-hours	13.53	12.69 - 19.56
Ad I^{125}fibronectin 140-hours	8.92	8.33- 9.48

FCS Soak

I^{125} YRGD-Polypeptide

Group	Median	95% Confidence Interval
Si I^{125}YRGD 5-mins	2.58	2.28 - 2.79
Si I^{125}YRGD 2-hours	2.18	2.11 - 2.23

Si I^{125}YRGD 20-hours	1.77	1.63- 1.79
Si I^{125}YRGD 140-hours	1.42	1.24- 1.46
Ad I^{125}YRGD 5-mins	2.13	2.07 - 2.14
Ad I^{125}YRGD 2-hours	1.37	1.32- 1.39
Ad I^{125}YRGD 20-hours	0.91	0.79 - 0.93
Ad I^{125}YRGD 140-hours	0.59	0.58 - 14

I^{125} Fibronectin

Group	**Median**	**95% Confidence Interval**
Si I^{125}fibronectin 5-mins	89.87	70.24 - 98.14
Si I^{125}fibronectin 2-hours	47.85	42.42 - 62
Si I^{125}fibronectin 20-hours	35.83	30.43 - 44.5
Si I^{125}fibronectin 140-hours	31.87	23.49 - 37.01
Ad I^{125}fibronectin 5-mins	51.42	44.59 - 57.83
Ad I^{125}fibronectin 2-hours	24.55	19.881651 - 31.47
Ad I^{125}fibronectin 20-hours	11.98	9.93 - 17.59
Ad I^{125}fibronectin 140-hours	6.01	5.28 - 6.28

Study 6

Cell Area

	Median	**95% Confidence Interval**
Control 1h	254	244.4-321.7
Control 4h	344.5	321.8-442.7
Control 24h	1026	999.4-1303.1
Control 96h	1401	1288.1-1806.1
AdYRGD 1h	377.5	354.7-496.4
AdYRGD 4h	667	516.2-756.4
AdYRGD 24h	1508.5	1280.3-1778.8
AdYRGD 96h	2017.5	1053-2393.3
Adfn 1h	914.5	828.4-1096.4
Adfn 4h	1072	937.4-1198.1
Adfn 24h	1500	1310.8-1676.4
Adfn 96h	1346	1287.5-1705.3
siYRGD 1h	375	358.3-578.7
siYRGD 4h	942	879.9-1330.9
siYRGD 24h	1558	1359.1-1797.2

siYRGD 96h	1575	1419.1-1794.7
Sifn 1h	1133.5	945.4-1220.5
Sifn 4h	1010	987.8-1303.7
Sifn 24h	1817	1606.6-2009.8
Sifn 96h	2006.5	1865.4-2373.2

Vinculin Markers

	Median	**95% Confidence Interval**
Control 1h	0	0.6-2
Control 4h	5	3.8-5.8
Control 24h	19	17.3-23.2
Control 96h	31	27.8-36.4
AdRGD 1h	1	0.6-1.7
AdRGD 4h	4	2.4-4.7
AdRGD 24h	52	46.6-61.8
AdRGD 96h	50	37.1-61.4
Adfn 1h	11	10.7-15.6
Adfn 4h	23	19.4-25.7
Adfn 24h	47	41-52.5
Adfn 96h	50	46.9-55.7
siRGD 1h	2	1.8-3.2
siRGD 4h	7	5.3-10.2
siRGD 24h	52.5	47.6-5.9
siRGD 96h	64	52.6-6.8
Sifn 1h	2.5	1.9-3.4
Sifn 4h	30.5	26.4-35.1
Sifn 24h	58	52.4-62.8
Sifn 96h	70	62.1-79.1

FA Density

	Median	**95% Confidence Interval**
Control 1h	0	0.003-0.009
Control 4h	0.01	0.01-0.02
Control 24h	0.02	0.02-0.02
Control 96h	0.02	0.02-0.02
AdRGD 1h	0.002	0.002-0.004
AdRGD 4h	0.005	0.004-0.006
AdRGD 24h	0.04	0.03-0.05

AdRGD 96h	0.03	0.02-0.05
Adfn 1h	0.01	0.01-0.02
Adfn 4h	0.02	0.02-0.03
Adfn 24h	0.03	0.03-0.04
Adfn 96h	0.03	0.03-0.04
siRGD 1h	0.005	0.004-0.007
siRGD 4h	0.007	0.006-0.008
siRGD 24h	0.04	0.03-0.04
siRGD 96h	0.04	0.04-0.04
Sifn 1h	0.002	0.002-0.004
Sifn 4h	0.03	0.02-0.03
Sifn 24h	0.03	0.03-0.04
Sifn 96h	0.04	0.03-0.04

Appendix 3

Histological Processing

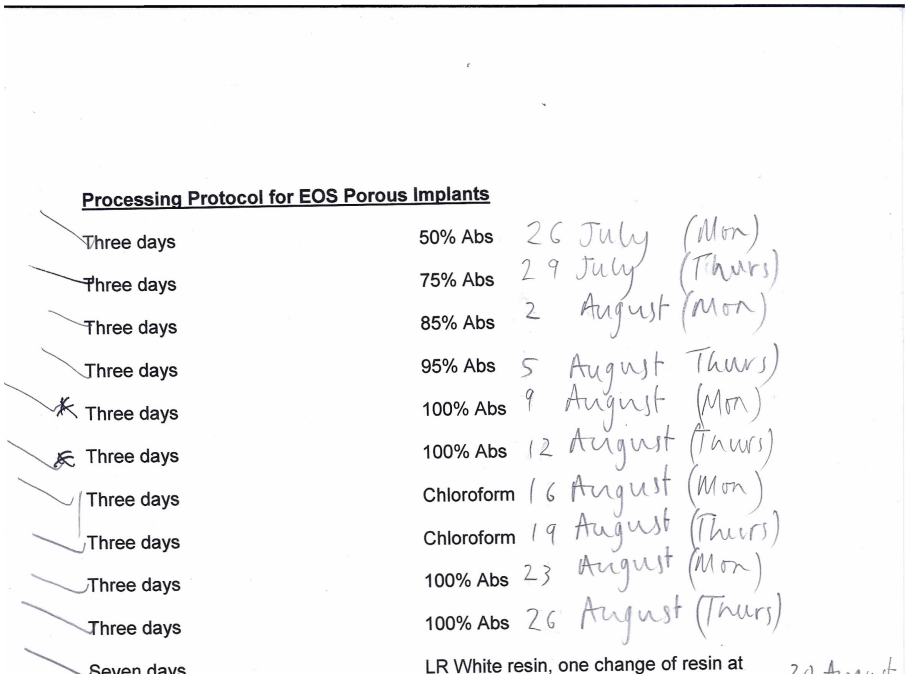

Processing Protocol for EOS Porous Implants

Three days	50% Abs	26 July (Mon)
Three days	75% Abs	29 July (Thurs)
Three days	85% Abs	2 August (Mon)
Three days	95% Abs	5 August Thurs)
Three days	100% Abs	9 August (Mon)
Three days	100% Abs	12 August (Thurs)
Three days	Chloroform	16 August (Mon)
Three days	Chloroform	19 August (Thurs)
Three days	100% Abs	23 August (Mon)
Three days	100% Abs	26 August (Thurs)
Seven days	LR White resin, one change of resin at	

Percentage Fill Score

Group	Median Zone 1/%	95% Confidence Intervals	Median Zone 2/%	95% Confidence Intervals	Medan Zone 3/%	95% Confidence Intervals
1	100		98.5	95.23-100.44	100	88.1-105.24
2	100	97.54-101.03	100	94.22-101.5	100	87.94-102.06
3	40	11.84-78.66	35	18.61-53.89	25	7.27-37.73
4	100	92.48-103.55	95	30.19-125.81	100	92.45-103.55
5	88	62.09-103.57	87.5	59.3-103.36	90	45.07-108.26
6	27.5	-10.14-62.64	22.5	-8.31-53.31	10	-20.1-55.1
7	60	48.43-74.43	45	33.44-57.41	40	21.09-57.48
8	60	41.43-75.14	63	34.17-68.40	60	25.64-72.93
9	N/A	N/A	N/A	N/A	N/A	N/A

Cell Nuclei Density

Group	Median Zone 1/mm^2	95% Confidence Intervals	Median Zone 2/mm^2	95% Confidence Intervals	Median Zone 3/mm^2	95% Confidence Intervals
1	3440.50	1407.93-4453.4	2846	800.64-4397.02	3586.50	1246.15-4728.85
2	5059	3330.45-6312.7	4527	2402.37-5439.06	5000	3004.61-6293.96
3	1190	-409.57-2953.57	700	-392.4-2157.9	584.50	131.82-970.68
4	1389	-390.62-7151.82	1243	172.19-3993.41	1306	266.55-4168.65
5	815	363.3-1315.36	604	420.53-749.47	551.50	-99.65-1662.32
6	250	-317.35-985.35	268.50	-249.1-835.11	251	-316.48-984.48
7	1390	110.59-5540.55	1199	478.45-1641.83	821	71.18-2351.4
8	890	-187.08-3091.36	645	53.6-1850.68	720	122.22-2097.78
9	N/A	N/A	N/A	N/A	N/A	N/A

Blood Vessel Density

Group	Median BV Zone1/mm^2	95% Confidence Intervals	Median BV Zone2/mm^2	95% Confidence Intervals	Median BV Zone3/mm^2	95% Confidence Intervals
1	4	1.52-9.43	5.20	0.73-13.4	2	-1.77-10.64
2	8	4.28-10.29	10	4.52-12.05	8	2.83-11.74
3	4.50	-1.03-9.03	1	-2.5-6.5	2.5	-1.29-6.29
4	15	3.67-34.3	6	0.92-16.28	11	2.92-15.08
5	3	0.48-8.52	1.5	-0.2-3.88	0	
6	0	-1.09-2.09	0	-0.55-1.05	0	-2.18-4.18
7	9	3.25-17.9	4	0.33-5.39	0	-1.24-2.95
8	8	2.75-12.96	4	1.44-8.0	4	-0.42-11.56
9	N/A	N/A	N/A	N/A	N/A	N/A

Appendix 4

Implant Dimensions

Porous Implant Dimension/μm- Control and RGD

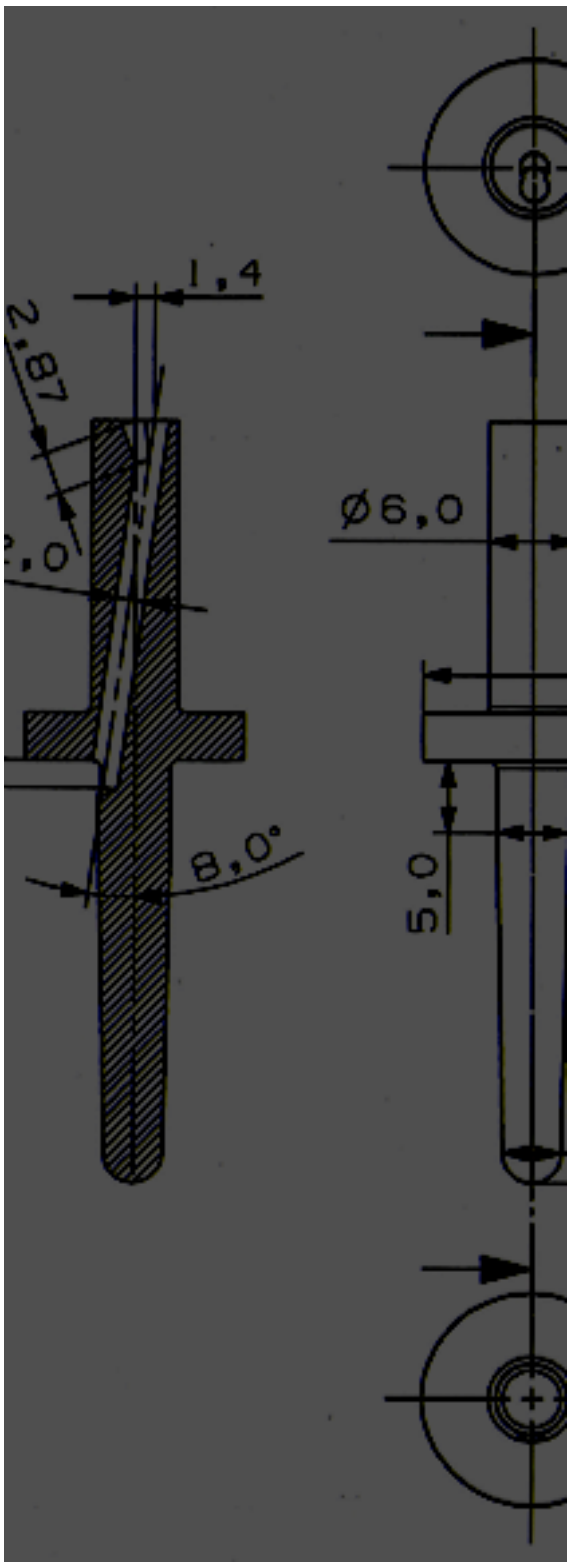

Drilled Implant Dimension/μm- Control and RGD

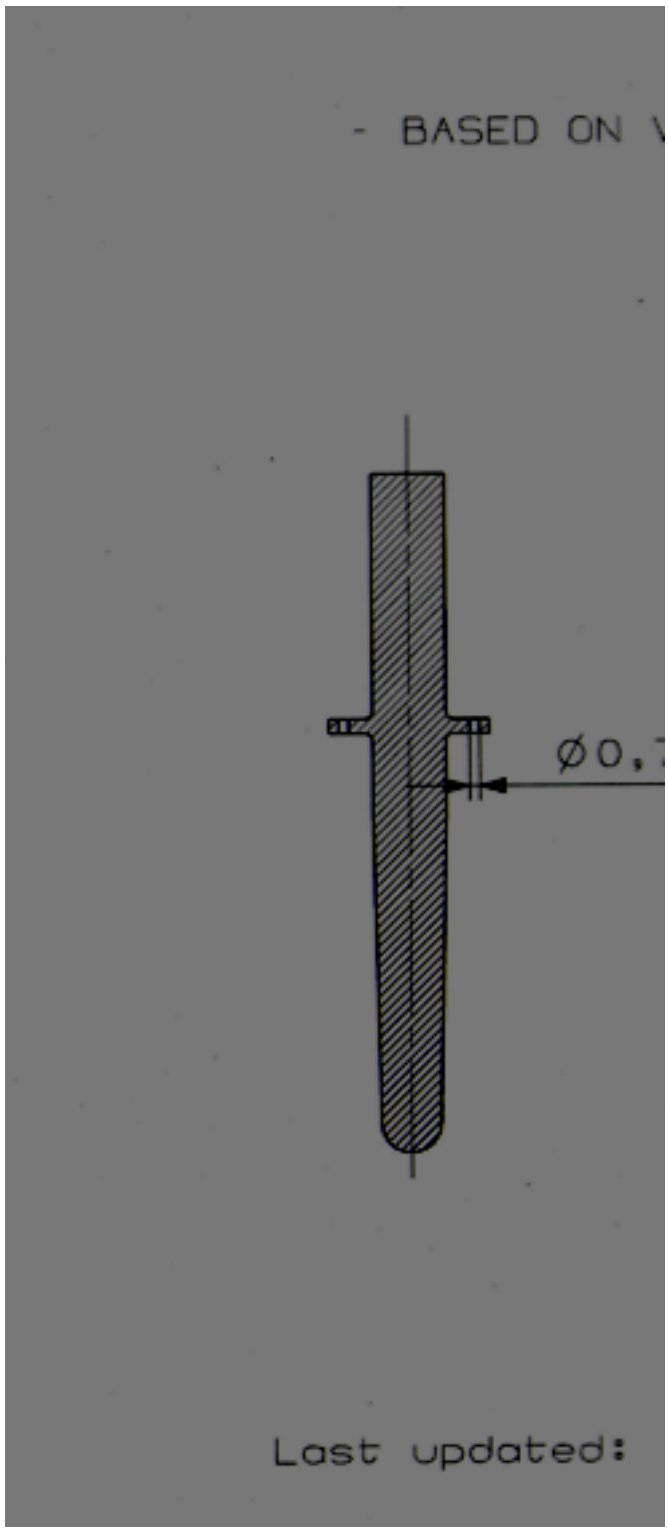

Histological Processing

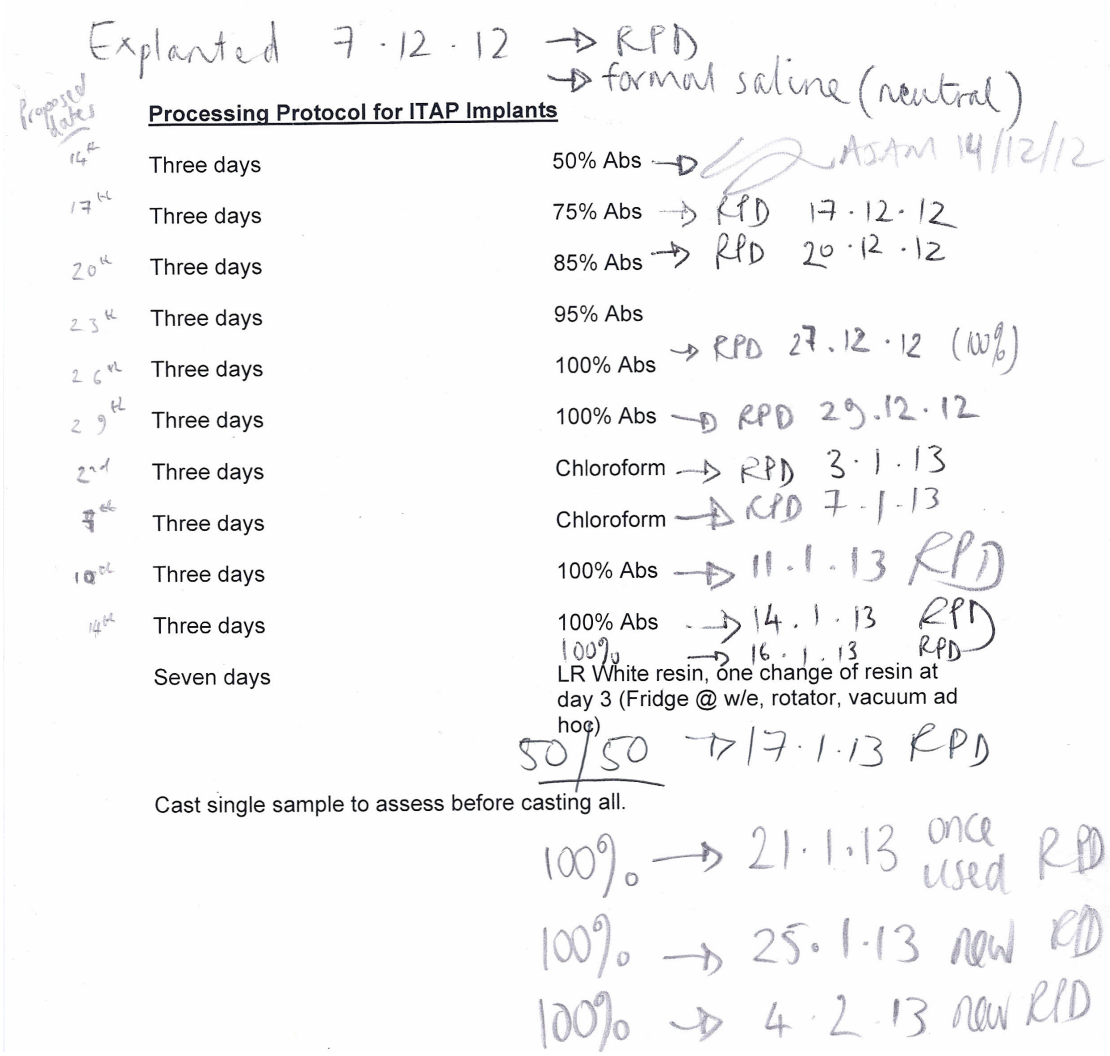

Explanted 7·12·12 → RPD
→ formal saline (neutral)

Proposed dates

Processing Protocol for ITAP Implants

14th	Three days	50% Abs → ASAM 14/12/12
17th	Three days	75% Abs → RPD 17·12·12
20th	Three days	85% Abs → RPD 20·12·12
23rd	Three days	95% Abs
26th	Three days	100% Abs → RPD 27·12·12 (100%)
29th	Three days	100% Abs → RPD 29.12.12
2nd	Three days	Chloroform → RPD 3·1·13
5th	Three days	Chloroform → RPD 7·1·13
10th	Three days	100% Abs → 11.1.13 RPD
14th	Three days	100% Abs → 14.1.13 RPD
		100% → 16.1.13 RPD
	Seven days	LR White resin, one change of resin at day 3 (Fridge @ w/e, rotator, vacuum ad hoc)

50/50 → 17·1·13 RPD

Cast single sample to assess before casting all.

100% → 21·1·13 once used RPD

100% → 25·1·13 new RPD

100% → 4·2·13 new RPD

6036 Nana Explanted 20-2-13

↳ Formal saline (neutral)

Processing Protocol for EOS Porous Implants

27th	Three days	50% Abs 27/2/13 RPD
4th	Three days	75% Abs 4/3/13 RPD
7th	Three days	85% Abs 7/3/13 RPD
11th	Three days	95% Abs 12/3/13 RPD
14th	Three days	100% Abs 14/3/13 RPD → 18/3/13 IMS
18th	Three days	100% Abs ? → VAZAN → 21/3/13 (Chloroform)
21st	Three days	Chloroform → 22/3/13
RPD Holiday 25th	Three days	Chloroform → 25/3/13 RPD
28th	Three days	100% Abs → 27/3/13 RPD
1st	Three days	100% Abs → 3/4/13 RPD → IMS 4/4/13 RPD → IMS
	Seven days	LR White resin, one change of resin at day 3 (Fridge @ w/e, rotator, vacuum ad hoc)

5/4/13 → Resin Vacuum RPD.

6/4/13 → Rotator

9/4/13 → Vacuum.

16-4-13 → change resin 100%

17-4-13 → Cast.

Cast single sample to assess before casting all.

Animal 6034

RVC Diagnostic Laboratories University of London

Laboratory Results

Diagnostic Laboratories

The Royal Veterinary College

Hawkshead Lane, North Mymms, Herts, AL9 7TA

Tel: 01707 666208 Fax: 01707 661464

Owner: CRU
Ref.: 6034
6034
Ovine Mule
Age unknown F

Path No: P225005
Clinician:
Dept./Practice: Biological Services Uni C/T (BSU)

Received: 14/09/12

Reported: 21/09/12 11:0

Microbiology

1120901313 Site: SWAB Detail: Wound

Test	Result	Range	Units
Culture:	Moderate, mixed growth of 1. E. coli, 2. Coryneform, 3. Peptostreptococcus spp. and 4. Bacteroides spp.		
SENSITIVITY	1 2 3 4		
Streptomycin	R R R R		
Ampicillin	R S S S		
Ceftiofur	S S R S		
Cloxacillin	R S S R		
Metronidazole	R R S S		
Neomycin	R R R R		
Oxytetracycline	S S S S		
Penicillin G	R S S S		
Sulphonamide/Trimeth	S R S R		

Microbiology swab results taken from exduate of back right leg in the proximal position from animal 6034.

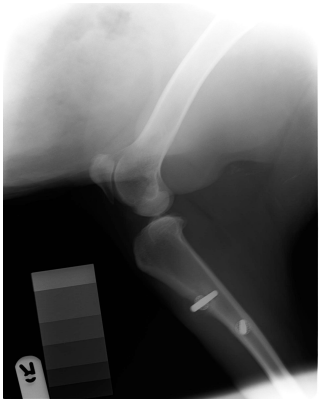

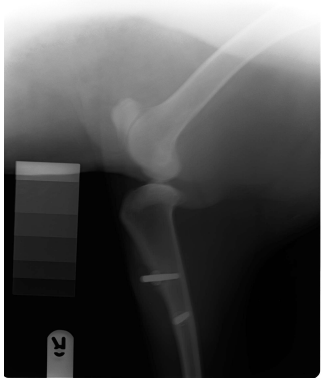

Radiograph images of right hind leg of animal 6034

Experimental Data

	Median	**95% Confidence Intervals**
Epidermal Downgrowth (μm)		
Flange Control	7185.5	5941.3-7900.87
Flange RGD	8178.0	6255.14-11299.41
Porous Control	5359.0	4646.77-10409.23
Porous RGD	7878	5702.48-9195.52
Epidermal Attachment (%)		

Flange Control	50.9	32.47-63.73
Flange RGD	44.54	17.16-58.67
Porous Control	39.4	22.0-57.63
Porous RGD	27.2	21.81-49.02
Blood Vessel Density (mm^2)		
Flange Control	0.00	-0.000001-0.000028
Flange Porous	0.000001	0.000003-0.000031
Porous Control	0.000071	0.000049-0.000098
Porous RGD	0.000068	0.000048-0.000092
Cell Nuclei Density (mm^2)		
Flange Control	0.000585	0.000254 – 0.00152
Flange RGD	0.000301	0.0000648 – 0.000813
Porous Control	0.000513	0.000385 – 0.000675
Porous RGD	0.00054	0.000386 – 0.000735
Dermal Tissue Infiltration (%)		
Flange Control	90	49.31-96.24
Flange RGD	70	38.35-88.01
Porous Control	90	67.76-102.24
Porous RGD	100	97.07-101.12

Reference List

Reference List

Acram AB. 2013 **EBM in Aerospace**. [ONLINE] http://www.arcam.com/

Al-Ajam, Y., Lancashire, H., Pendegrass, C., Kang, N., Dowling, R., Taylor, S., Blunn, G. 2013 **The Use of a Bone-Anchored Device as a Hard-Wired Conduit for Transmitting EMG Signals From Implanted Muscle Electrodes.** *Biomedical Engineering, IEEE*. 60(6), pp.1654-1659.

Alberts, B., Johnson, A., Lewis, J., Raff, M., Roberts, K., Walter, P. 2002 **Molecular Biology of the Cell**. 4th Ed. New York: GS Garland Science

Albrektsson, T., Branemark, P.-I., Hansson, H.-A., Lindstrom, J. 1981 **Osseointgerated titanium implants.** *Acta Orthop. Scand.* 52, pp.155-170.

Aschoff, H. H. 2011 **The Endo-Exo-Femoral Prosthesis.** pp.101-105.

Aschoff, H. H., Kennon, R. E., Keggi, J. M., Rubin, L. E. 2010 **Transcutaneous, Distal Femoral, Intradmedullary Attachment for Above-thee-Knee Prostheses: An Endo-Exo Device.** *The Journal of Bone and Joint Surgery, Incorporated.* 92(2), pp.180-186.

Black, J. 1992 **Biological Performances of Materials: Fundamentals of** Biocompatibility. *2nd Ed.* PLACE: Marcel Dekker, Inc.

Baier, R. E. and Dutton, R. C. 1969 **Initial events in interactions of blood with a foreign surface.** *Journal of Biomedical Materials Research.* 3(1), pp.191–206.

Balaban, N. Q., Schwartz. U. S., Riveline. D., Goichberg. P., Tzur. G., Sabanay. I., Mahalu. D., Safran. S., Bershadsky. A., Addadi. L., Geiger. B. 2001 **Force and Focal Adhesion assembly: A Close Relationship Studied** using Elastic Micropatterned Substrates. *Nature Cell Biology.* 3, pp.466-472.

Bershadsky, A. D., Tint, I. S., Neyfakh, A. A., Vasiliev, J. M. 1985 **Focal Contacts of Normal and RSV-transformed Quail Cells: Hypothesis of the Transformation-induced deficient Maturation of Focal Contacts**. *Experimental Cell Research.* 158(2), pp.433–444.

Buetner, E., H. and Jorden, R., E. 1964 Demonstration of Skin Antibodies in Sera of Pemphigus Vulgaris Patients by Indirect Immunoflourescent Staining. *Society for Experimental Biology and Medicine.* 117(2), pp.505-510.

Bobyn, J. D., Pilliar, R. M., Cameron, H. U., Weatherly, G. C. 1980 **The Optimum Pore Size for the Fixation of Porous-Surfaced Metal Implants by the Ingrowth of Bone.** *Clinical Orthopaedics & Related Research.* 150, pp.263-270.

Bobyn, J. D., Wilson, G. J., MacGregor, D. C., Pilliar, R. M., Weatherly, G. C. 1982 **Effect of Pore Size on the Peel Strength of Attachment of Fibrous Tissue to Porous-surfaced Implants**. *Journal of Biomedical Materials Research.*16(5), pp.571–584.

Bothe, R.T., Beaton, L.E., Davenport, H.A., (1940) **Reaction of bone to multiple metallic implants**. *Surgery, Gynecology, and Obstetrics* 71. pp598-602

Brånemark, P.-I., Breine, U., Adell, R., Hansson, B. O., Lindström, J., Ohlsson, A. 1969 **Intra-Osseous Anchorage of Dental Prostheses: *Experimental Studies*.** *Journal of Plastic and Reconstructive Surgery and Hand Surgery*. 3(2), pp.81-100.

Brånemark, P.-I., Albrektsson, T., 1982 **Titanium Implants Permanently Penetrating Human Skin.** *Scandinavian Journal for Plastic and Reconstructive Surgery*. 16, pp.17-21.

Brånemark, R., Brånemark, P-I., Rydevik, B., Myers, R. R., 2001 **Osseointegration in Skeletal Reconstruction and Rehabilitation: A Review.** *Journal of Rehabilitation Research and Development.* 38(2), pp.175-181.

British Broadcasting Corporation. 2012 [ONLINE] http://www.bbc.co.uk/news/health-17270379.

Brooks, P. C., Clark, R. A., Cheresh, D. A. 1994 **Requirement of vascular integrin alpha v beta 3 for angiogenesis.** *Science.* 264(5158), pp569-571.

Brunette, D. M. 1986 **Fibroblasts on Micromachined Substrata Orient Hierarchically to Grooves of Different Dimensions**. *Experimental Cell Research.* 164, pp.11-26.

Butts, T. E., Peterson, L. J., Allen, C. M., 1989 **Early Soft Tissue Ingrowth onto Porous Block Hydroxyapatite.** *Journal of Oral and Maxilllofacial Surgery*. 47, pp.475-479.

Chapman, D. I., 1975 **Antlers- Bones of Contention.** *Mammal Review.* 5(4), pp.122-1172.

Chehroudi, B., Brunette, D. M., 2002 **Subcutaneous Microfabricated Surfaces Inhibit Epithelial Recession and Promote Long-term Survival of Percutaneous Implants.** *Biomaterials.* 23, pp.229-237.

Chen, C. S., Mrksich, M., Huang, S., Whitesides, G. M., Inger, D. E., 1997 **Geometric Control of Cell Life and Death**. *Science*. 276(5317), pp.1425-1428.

Cheung, S., Gauthier, M., Lefebvre, L-P., Dunbar, M., Filiaggi, M. 2007 **Fibroblastic interactions with high-porosity Ti-6Al-4V metal foam**. *Journal of Biomedical Materials Research Part B: Applied Biomaterials*. 82(B),

pp.440–449.

Chimutengwende-Gordon, M., Pendegrass, C., Blunn, G. 2011 **Enhancing the Soft Tissue Seal Around Intraosseous Transcutaneous Amputation Prostheses Using Silanised Fibronectin Titanium Alloy.** *Biomedical Materials*. 6(2),

Cochrane, H., Orsi, K., Reilly, P., 2001 **Lower Limb Amputation Part 3: Prosthetics- a 10 Year Literature Review.** *Prosthetics and Orthotics International.* 25, pp.21-28.

Compact Oxford English Dictionary For current Englsih (2005) 3rd Ed. Oxford: Oxford University Press

Davis, D. H., Giannoulis, C. S., Johnson, R. W., Desai T. A. 2002 **Immobilization of RGD to <1 1 1> silicon surfaces for enhanced cell adhesion and proliferation**. *Biomaterials.* 23(19), pp.4019–4027.

DesGroseilliers, J. P., DesJardins, J. P., Germain, J. P., Krol, A. L. 1978 **Dermatologic problems in amputees.** *Canadian Medicine Association Journal.* 118(5), pp.535–537.

Ducheyne, P., Hench, L. L., Kagan, II A., Marten, M., Bursens, A., Mulier, J. C., 1980 **Effect of Hydroxyapetite Impregnation on Skeletal Bonding of Porous Coated Implants.** *Journal of Biomedical Materials Research.* 14, pp.225-237.

Dudek, N., Marks, M., Marshall, S., Chardon, J., 2005 **Dermatologic conditions associated with the use of lower extremity prosthesis.** *Archives of Physical Medicine and Rehabilitation*. 86(4), pp.659-663.

El-Ghanna, A., Starr, L., Jones, J., 1997 **Laminin-5 Coating Enhances Epithelial Cell Attachment, Spreading and Hemidesmosome Assembly**

on Ti-Al_6-V_4 Implant Material *in vitro*. *Jounral of Biomedical Material Research*. 41, pp.30-40.

Elmengaard, B., Bechtold, E., Søballe, K. 2005 **In vivo Study of the Effect of RGD Treatment on Bone Ingrowth on Press-fit Titanium Alloy Implants.** *Biomaterials*. 26(17), pp.3521–3526.

Farrell, B. J., Prilutsky, B. I., Ritter, J. M., Kelley, S., Popat, K., Pitkin, M. **Effects of Pore Size, Implantation Time, and Nano-surface Properties on Rat Skin Ingrowth into Percutaneous Porous Titanium Implants.** *Journal of Biomedical Materials Research Part A.* 00(A), pp.000–000.

Fath, K. R., Edgell, C. J., and Burridge, K. 1989 **The Distribution of Distinct Integrins in Focal Contacts is Determined by the Substratum Composition.** *Journal of Cell Science*. 92, pp.67-75.

Ferris, D. M., Moodie, G. D., Dimond, P. M., Giorani, C. W. D., Ehrlich, M. G., Valentini, R. F. 1999 RGD-coated titanium implants stimulate increased bone formation in vivo. Biomaterial. 20(23-24), pp.2201-2460.

Fitzpatrick, N., Smith, T. J., Pendegrass, C. J., Yeadon, R., Ring, M., Goodship, A. E., Blunn, G. W. 2011 **Intraosseous Transcutaneous Amputation Prosthesis (ITAP) for Limb Salvage in 4 Dogs**. *Veterinary Surgery*. 40(8), pp.909-925.

Gardner., W, D and Osburn., W, A., (1973) **Structure of the Human Body**. 2nd Ed. St. Lewis: W.B Saunders Company

Gordon, D, J., Bhagawati, D. D., Pendegrass*, C. J., Middleton, C. A., Blunn. G. W. 2010 **Modification of Titanium alloy Surfaces for Percutaneous Implants by Covalently Attaching Laminin**. *Journal of Biomedical Materials Research.* 94A(2), pp.586–593.

Gottlie, B. S., Leventhal, G.S. 1951 Titanium, a metal for surgery, *Journal of Bone and Joint Surgery* 33(A), pp.473-474.

Green, K. J., Jones, J. C. R., 1996 **Desomsomes and Hemidesmosomes: Structure and Function of Molecular Components.** *The FASEB Journal.* 10, pp.871-881.

Grinnell, F., 1984 **Fibronectin and Wound Healing.** *Journal of Cellular Biochemistry*. 26, pp.107-116.

Gottsauner-Wolf, F., Egger, E. L., Schultz, F. M., Sim, F. H., Chao, E. Y. S. 1994 **Tendons attached to prostheses by tendon-bone block fixation: An experimental study in dogs.** *Journal of Orthopaedic Research.* 12(6), pp.814-821.

Grosse-Siestrup, C., Affled. K., 1984 **Design Criteria for Percutaneous** Devices. *Journal of Biomedical Material Research.* 18, pp.357-382.

Gupta, A., Pollock, R., Cannon, S. R., Briggs, T. W. R., Skinner, J., Blunn, G. **A Knee-Sparing Distal Femoral Endoprosthesis using Hydroxyapatite-coated Extracortical Plates**. *Journal of Bone and Joint Surgery*. 88B(10), pp.1367-1372

Hacking, S. A., Bobyn, J. D., Toh, K.-K., Tanzer, M., Krygier, J. J., 2000 **Fibrous Tissue Ingrowth and Attachment to Porous Tantalum.** *Journal of Biomedical Material Research.* 52, pp.631-638.

Hall, C. W., Adams, L. M., Ghidoni, J. J., 1975 **Development of Skin Interfacing Cannula.** *Transactions - American Society for Artificial Internal Organs.* XXI, pp.281-288.

Harrison, R. G. 1912 **The Cultivation of Tissues in Exteneous Media as a Method of Morphogenetic Study.** *The anatomical Record.* 6, pp.181-193.

Hautanen, A., Gailit, J., Mann, D. M., Ruoslahti, E. 1989 **Effects of Modifications of the RGD Sequence and its Context on Recognition by the Fibronectin Receptor.** *The Journal of Biological Chemistry*. 264, pp.1437-1442.

Hayakawa, T., Yoshinari, M., Nemeto, K. 2003 **Direct Attachment of Fibronectin to Tresyl Chloride-activated Titanium.** *Journal Biomedical Material Research*. 67(A), pp.684 – 688.

Heinl, P., Muller, L., Korner, C., Singer, R. F., Muller, F. 2008 **Cellular Ti-6Al-4V Structures with Interconnected Macro Porosity for Bone Implants Fabricated by Selective Electron Beam Melting.** *Acta Biomaterialia.* 4, pp.1536-1544.

Heinl, P., Rottmair, A., Korner, C. and Singer, R. F. 2007 **Cellular Titanium by Selective Electron Beam Melting.** *Advanced Engineering Materials.* 9(5), pp.360-364.

Hersel, U., Dahmen, C., Kesseler, H. (2001) **RGD Modified Polymers: Biomaterials Stimulated for Cell Adhesion and Beyond.** *Biomaterials.* 24(24), pp. 4385–4415.

Hess, C. T., and Kirsner. R. S. 2003 **Orchestrating Wound Repair: Assessing and Preparing the Wound Bed.** *Advances in Skin and Wound Care.* 16(5), pp.246-257.

Holgers, K. M., Thomsen, P., Tjellstrom, A., Ericson, L. E. 1995 **Electron Microscopic Observation on the Soft-Tissue Around Clinical Long-Term** Percutaneous Titanium Implants. *Biomaterials.* 16, pp.83-90.

Holland, J., Hersht, L., Bryhant, M., Onyiriuka, E., Ziegler, L. 1996 **Culture of Human Vascular Endothelial cells on an RGD-containing Synthetic Peptide Attached to a Starch-coated Polystyrene Surface: Comparison with Fibronectin-coated Tissue Grade Polystyrene.** *Biomaterials.* 17, pp.

2147-2156.

Hormia, M. and Kononen, M. 1994 **Immunolocalization of Fibronectin and Vitronectin Receptors in Human Gingival Fibroblasts Spreading on Titanium Surfaces.** *Journal of Periodontal Research.* 29(2), pp.146–152.

Howe, D. F., Svare, C. W., Tock, R. W. 1974 Some Effects of Pore **Diameter on Single Pore Bony Ingression Patterns in Teflon**. *Journal of Biomedical Materials Research*. 8(6), pp.399–406.

Hunter, W. M., Greenwood, F. C. 1962 **Preparation of Iodine-131 Labelled Human Growth Hormone of High Specific Activity.** *Nature.* 194(4827), pp.495-496.

Hunter, A., Archer, C. W., Walker, P. S., Blunn, G. W. 1994 **Attachment and Proliferation of Osteoblasts and Fibroblasts on Biomaterials for Orthopaedic Use.** *Biomaterials*. 16(4), pp.287–295.

Irvine, D. J., Hue, K. A., Mayes, A. M., Griffith, L. G. 2002 **Simulations of Cell-Surface Integrin Binding to Nanoscale-Clustered Adhesion Ligands**. *Biophysical Journal.* 82(1), pp.120-132.

Iscackson, D., McGill, L. D., Bachus, K. N. 2011 **Percutaneous Implants with Porous Titanium Dermal Barriers: An *in vivo* Evaluation of Infection** Risk. *Medical Engineering and Physics.* 33, pp.418-426.

Jarcho, M., Kay, J. F., Gumaer, K. I., Doremus, R. H., Drobeck, H. P. 1977 **Tissue, Cellular and Subcellular Events at a Bone-ceramic Hydroxylapatite Interface.** *Journal of Bioengineering.* 1(2), pp.79-92.

Jeyapalina, S., Beck, J. P., Bachus, K. N., Williams, D. L., Bloebaum, R. D. 2012 Efficacy of a Porous-structured Titanium Subdermal Barrier for **Preventing Infection in Percutaneous Osseointegrated Prostheses**.

Journal of Orthopaedic Research. 30(8), pp.1304–1311.

Jeyapalina, S., Van Dyke, M., Sampson, A., Betz, D. H., Bloebaum, R. D. 2013 **Investigating Keratin as a Biomimetic Coating for Percutaneous Device Applications**. *Society for Biomaterial: Boston 2013.* #70

Jin, Z-H., Furukawa, T., Waki, A., Akaji, K., Coll, J-L., Saga, T., Fujibayashi, Y. 2010 **Effect of Multimerization of a Linear Arg-Gly-Asp Peptide on Integrin Binding Affinity and Specificity**. *Biological Pharmaceutical Bulletin.* 33(3), pp.370—378.

Jones, J. C. R., Hopkinson, S. B., Goldfinger, L. E. 1998 **Structure and Assembly of Hemidesmosomes.** *Bioassays.* 20, pp.488-494.

Jose, B., Antoci, Jr. V., Zeiger, A. R., Wickstrom, E., Hickok, N. H. 2005 **Vancomycin Covalently Bonded to Titanium Beads Kills *Staphylococcus aureus.*** *Chemistry & Biology*. 12, pp.1041-1048.

Kämmerer, P. W., Heller, P., Brieger, J., Klein, M. O., Al-Nawas, B., Gabriel, M. 2011 **Immobilization of Linear and Cyclic RGD-peptides on Titanium Surfaces and their Impact on Endothelial Cell Adhesion and Proliferation.** *European Cells and Materials.* 21, pp.364-372.

Kang, N., Pendegrass, C., Blunn, G. 2010 **Osseointegration of an ITAP used in a Reconstruction of a Transhumeral Amputee: Case Report.** *Journal of Hand Surgery.* 35(A), pp.1130-1134.

Kanitakis, J. 2002 **Anatomy, Histology and Immunohistochemistry of Normal Human Skin.** *European Journal of Dermatology.* 12(4), pp.390-401.

Kasemo, B. and Gold, J. 1999 **Implant Surfaces and Interface Processes.** *Journal of Dental Research.* 13(1), pp.8-20.

Kantlehner, M., Schaffner, P., Finsinger, F., Meyer, J., Jonczyk, A.,

Diefenbach, B., Nies, B., Hölzemann, G., Goodman, S. L., Kessler, H. 2000 **Surface Coating with Cyclic RGD Peptides Stimulates Osteoblast Adhesion and Proliferation as well as Bone Formation**. *ChemBiochem.* 1, pp.107-114.

Kasemo, B., Gold, J. 1999 **Implant Surfaces and Interface Processes.** *Journal of Dental Research.* 13(1), pp.8-20.

Klebe, R. J. 1974 **Isolation of a collagen dependent cell attachment factor.** *Nature.* 221, pp. 248-251

Koc, E., Tunca, M., Akar, A., Erbil, A. H., Demiralp, B. and Arca, E. 2008 **Skin problems in amputees: a descriptive study.** *International Journal of Dermatology.* 47, pp.463–466.

Kohler, P., Lindh, L., Bjorklind, A., 1989 **Bacteria on stumps of amputees and the effects of antiseptics.** *Prosthetics and Orthotics International*. 13, pp.149-151.

Koike, M., Martinez, K., Guo, L., Chahine, G., Kovacevic, R., Okabe, T. 2011 **Evaluation of Titanium Alloy Fabricated using electron Beam Melting System for dental Applications.** *Journal of Materials Processing Technology*. 211, pp.1400–1408.

Koivunen, E., Wang, B., Ruoslahti, E. 1994 **Isolation of a Highly Specific Ligand for the Alpha5Beta1 Integrin from a Phage Display Library.** *The Journal of Cell Biology.* 124(3), pp.373-380.

Krawczyk, W. S. and Wilgram, G. 1973 **Hemidesmosome and Desmosome Morphogenesis during Epidermal Wound Healing.** *Journal of Ultrastructure Research.* 45, pp.93-101.

Kroese-Deutman H. C., Van Den Dolder, J., Spauwen, P. H. M., Jansen, J. A.

2005 **Influence of RGD-Loaded Titanium Implants on Bone Formation *in Vivo***. *Tissue Engineering.* 11(11/12), pp. 1867-1875.

Kubo, M., Van De Water, L., Plantefaber, L. C., Mosesson, M. W., Simon, M., Tonnesen, M. G., Taichman, L., Clark, R. A. F. 2001 **Fibrinogen and Fibrin are Anti-Adhesive for Keratinocytes: A Mechanism for Fibrin Eschar Slough During Wound Repair.** *The Journal of Investigative Dermatology.* 117, pp.1369-1381.

LaBerge, M., Bobyn, J. D., Rivard, C. H., Drouin, G., Duval, P. 1990 **Study of Soft Tissue Ingrowth into Canine Porous Coated Femoral Implants Designed for Osteosarcomas Managemen**t. *Journal of Biomedical Materials Research.* 24(7), pp.959–971.

Landete-Castillejos, T., Estevez, JA., Ceacero, F., Garcia, AJ., Gallego, L. 2012 **A Review of Factors Affecting Antler Composition and Mechanics.** Frontiers in Bioscience. E4, pp.2328-2339.

Lanza, R. P., Langer, R., Vacanti, J. 2000 **Principles of Tissue Engineering.** *2nd Ed.* Waltham: Academic Press

Le Gros Clark., W. E. 1946 **The Tissues of the Human Body.** *2nd Ed.* Oxford: Oxford at the Clarendon Press.

Leventhal, G. S., 1951 **Titanium, A Metal for Surgery**. *The Journal of Bone and Joint Surgery.* 33(2):473-474

Levy, S. 1956 **Skin problems of the lower extremity amputee.** *Artificial Limbs.* 3, pp.20-35

Levy, S. 1980 **Skin problems of the leg amputee.** *Prosthetics and Orthotics International.* 4, pp.37-44.

Li, C., Mackintosh, C. G., Martin, S. K., Clark, D. E. 2007 **Identification of Key Tissue Type for Antler Regeneration Through Pedicle Periosteum Deletion.** *Cell Tissue Research*. 328, pp.65-75.

Li. C., Sutteie. J., Clark. D. 2005 **Histological Examination of Antler Regeneration in Red Deer (*Cervus elaphus*).** *The Anatomical Record.* 282(A), pp.168-174.

Lin. Y-S., Wang, S-S., Chung, T-W., Wang, Y-H., Chiou, S-H., Hsu, J-J., Chou, N-K., Hsieh, K_H., Chou, S-H. 2001 **Growth of Endothelial Cells on Different Concentrations of Gly-Arg-Gly-Asp Photochemically Grafted in Polyethylene Glycol Modified Polyurethane.** *Artificial Organs.* 25(8), pp. 617-621.

Lodish, H., Berk, A., Kaiser, C., Krieger, M., Scott, M., Bretscher, A., Ploegh, H., Matsudaira, P. 2008 **Molecular Biology of the Cell.** *6th Ed.* New York: W.H Freeman and Company.

Luff, R. **Amputee statistical Database for the United Kingdom: 2006/07 Report**

Liu, X., Chu, P. K., Ding, C. 2004 **Surface Modification of Titanium, Titanium Alloys, and Related Materials for Biomedical Application.** *Materials Science and Engineering: R: Reports.* 47(3-4), pp.49-121.

Lundberg, M., Hagberg, K., Bullington, J. 2011 **My Prosthesis as a part of me: a qualitative analysis of living with an osseoinegratd prosthetic limb.** *International Society for Prosthetcis and Orthotics.* 35(2), pp.207-214.

Lundborg, G., Branemark, P-I., Rosen, B. 1996 **Osseointegrated Thumb Prostheses: A Concept for Fixation of Digit Prosthetic Devices.** *Journal of Hand Surgery*. 21(A), pp.216-221.

Lyon, C., Kulkarni, J., Zimersonc, E., Van Ross, E., Beck, M. 2000 **Skin**

Disorders in Amputees. *Journal of the American Academy of Dermatology*. 42(3), pp.501–507.

McDonald, J. H. 2009 **Handbook of Biological Statistics**. 2nd ed. Baltimore: Sparky House Publishing.

Main, A. L., Harvey, T. S., Baron, M., Boyd, J., Campbell, I. D. 1992. **The Three-dimensional Structure of the tenth Type III Module of Fibronectin: An Insight into RGD-mediated Interactions.** *Cell.* 71, pp.671–678

Malone, J., Moore, W., Leal, J., Childers, S. 1981 **Rehabilitation for Lower Extemity Amputation.** *Arch Surg.* 116, pp.93-98.

Marchalonis, J. J. 1969 **An Enzymatic Method for the Trace Iodination of Immunoglobunlins and Other Proteins.** *Journal of Biochemistry.* 113, pp.299-305.

Martin. P., 1997 **Wound Healing- Aiming for Perfect Skin Regeneration.** *Science.* 276, pp.75-80.

Merritt, K., Shafer, J. W., Brown, S. A. 1979 **Implant Site Infection Rates with Porous and Dense Materials.** *Journal of Biomedical Materials Research.* 13, pp.101-108.

Middleton, C., Pendegrass, C., Gorden, D., Jacob, J., Blunn, G., (2007) **Fibronectin silanised titanium alloy: A bioinductive and Durable Coating to Enhance Fibroblast Attachment *in vitro*.** *Journal of Biomedical Materials Research.* 83(A), pp.1032-1038.

Nagai, M., Hayakawa, T., Fukatsu, A., Yamamoto, M., fukumoto, M., Nagahama, F., Mishima, H., Yoshinari, M., Nemoto, K. 2002 ***In Vitro* Study of Collagen Coating of Titanium Implants for Initial Cell Attachment.** *Dental Materials Journal*. 21(3), pp.250-260.

Nanci, A., Wuest, J. D., Peru, L., Brunet, P., Sharma, V., Zalzal, S., McKee, M. D. 1988 **Chemical Modification of Titanium Surfaces for Covalent Attachment of Biological Molecules.** *Journal of Biomedical Material Research.* 40, pp.324-335.

Niessen, C, N. 2007 **Tight Junction/Adherens Junctions: Basic Structure and Function.** *Journal of Investigative Dermatology.* 127, pp.2525-2532.

Nelson, R. J., Goldberg, L., White, R. A., Shors, E., Hirose, F. M. 1983 **Neovascularity of a Tracheal Prosthesis/tissue Complex.** *The Journal of Thoracic and Cardiovascular Surgery.* 86(6), pp.800-808.

Nygren, H., Eriksson, C., Lausmaa, J. 1997 **Adhesion and Activation of Platelets and Polymorphonuclear Granulocyte Cellsat TiO_2 Surfaces**. *Journal of Laboratory and Clinical Medicine*. 129, pp.35-46

Obara, M., Yoshizato, K. 1995 **Possible Involvement of the Interaction of the α5 Subunit of α5β1 Integrin with the Synergistic Region of the Central Cell-binding Domain of Fibronectin in Cells to Fibronectin Binding**. *Experimental Cell Research.* 216, pp.273–276.

Obara, M., Kang, M., Yamada, K. 1988 **Site-Directed Mutagenesis of the Cell-Binding Domain of Human Fibronectin: Separable, Synergistic Sites Mediate Adhesive Function.** *Cell Press*. 53, pp.649-657

Parthasarathy, J., Starly, B., Raman, S., Christensen, A. (2010) **Mechanical Evaluation of Porous Titanium (Ti6Al4V) structures with electron beam melting.** *Journal of the Mechanical Behaviur o f Biomedical Materials.* 3 pp249-259

Patel, P. R., Kiser, R. C., Lu, Y. Y., Fong, E., Ho, W. C., Tirrell, D. A., Grubbs, R. H. 2012 **Synthesis and Cell Adhesive Properties of Linear and Cyclic RGD Functionalized Polynorbornene Thin Films.** *Biomacromolecules.* 13, pp.2546−2553.

Pendegrass, C., Goodship, A., Blunn, G. 2006 **Development of a soft tissue seal around bone-anchored transcutaneous amputation prostheses**. *Biomaterials*. 27, pp.4183-4191.

Pendegrass, C., Goodship, A., Price, J., Blunn, G. 2006 **Nature's answer to breaching the skin barrier: an innovative development for amputees.** *Journal Anatomical Society.* 209, pp.59-67.

Pendegrass, C., Middleton, C., Gorden, D., Jacob, J., Blunn, G. 2008 **Measuring the strength of dermal fibroblast attachment to functionalized titantium alloys *in vitro.*** *Journal of Biomedical Materials Research.* 92(A), pp.1028-1037.

Pettersson, E., Luning, B., Mickos, H., Heinehard, D. 1991 **Synthesis, NMR and Function of an O-Phosphorylated Peptide, Comprising the RGD-Adhesion Sequence of Osteopontin.** *Anta Chemica scandinavica.* 4, pp.604-608.

Pierschbacher, M. D., Ruoslahti, E. 1984a. **The Cell Attachment Activity of Fibronectin can be Duplicated by Small Fragments of the Molecule**. *Nature* 309, pp.30–33.

Pierschbacher, M., Ruoslahti, E. 1987 **Influence of Stereochemistry of the Sequence Arg-Gly-Asp-X on Binding Specificity in Cell Adhesion**. *The Journal of Biological Chemistry.* 262(36), pp.17294-17298.

Pitkin, M., Cassidy, C., Muppavarapu, R., Edell, D. 2012 **Recording of Electric Signal Passing Through a Pylon in Direct Skeletal Attachment of Leg Protheses With Neuromuscular Control.** *IEEE Transcations on Biomedical Engineering.* 59(5), pp.1349-1353.

Pitkin, M. 2013 **Design features of implants for direct skeletal attachment of limb prostheses**. *Journal of Biomedical Materials Research.* 00(A),

pp.000-000. [only available on-line] http://onlinelibrary.wiley.com/doi/10.1002/jbm.a.34606/abstract?deniedAccessCustomisedMessage=&userIsAuthenticated=false

Pohjolainen, T., Alaranta, H., Urkuinen, M. 1990 **Prosthetic Use and Functional and Social Outcome Following Major Lower Limb Amputation.** *Prosthetics and Orthotics International.* 14, pp.75-79**.**

Pollack, S. 1984 **The Wound Healing Process.** *Clinics in Dermatology.* 2(3), pp.8-16.

Ponader, S., von Wilmowsky, C., Widenmayer, M., Lutz, R., Heinl, P., Korner, C., Singer, R. F., Nkenke, E., Neukam, F. W., Schlegel, K. A. 2010 ***In vivo*** **Performance of Selective Electron Beam-melted Ti-6Al-4V Structures.** *Journal of Biomedical Material Research.* 92(A), pp.56-62.

Porte-Durrieu, M. C., Guillemot, F., Pallu, S., Labrugere, C., Brouillaud, B., Bareille, R., Amedee, J., Barthe, N., Dard, M., Baquey, C. 2004 **Cyclo-(DfKRG) Peptide Grafting onto Ti–6Al–4V: Physical Characterization and Interest Towards Human Osteoprogenitor Cells Ahesion.** *Biomaterials*. 25, pp.4837–4846.

Portnoy, S., Siev-Nev, I., Yizhar, Z., Kristal, A., Shabshin, N., Gefen, A. 2009 **Surgical and Morphological Factors that Affect Internal Mechanical Loads in Soft Tissues of the Transtibial Residuum.** *The Journal of the Biomedical Engineering Society.* 37(12), pp.2583-2605.

Price, J. S., Allen, S., Faucheux, C., Althnaian, T., Mount, J. G. 2005 **Deer antlers: a Zoological Curiosity or the Key to Understanding Organ Regeneration in Mammals?** *Journal of Anatomical Society*. 207, pp.603-618.

Puleo, D. A. 1995 **Activity of Enzyme Immobilized on Silanised Co-Cr-Mo.** *Journal of Biomedical Materials Research*. 29, pp.951-957.

Pytela, R., Pierschbacher, M. D., Ruoslahti, E. 1985a. **Identification and Isolation of a 140 Kilodalton Cell Surface Glycoprotein with Properties of a Fibronectin Receptor.** *Cell.* 40, pp.191–98.

Pytela, R., Pierschbacher, M. D., Ruoslahti, E. 1985b**. A 125/115 KD Cell Surface Receptor Specific for Vitronectin Interacts with the Arg-Gly-Asp Adhesion Sequence Derived from Fibronectin.** *Proceedings of the National Academy of Sciences USA.* 82(57), pp.66–70.

Rao, S. S. and Winter, J. O. 2009 **Adhesion Molecule-Modified Biomaterials for Neural Tissue Engineering.** *Frontiers in Neuroengineering.* 2(6), pp.1-14.

Reed, J., Hull, W. E., von der Lieth, C.-W., Kiibler, D., Suhai, S.,& Kinzel, V. 1988 **Secondary Structure of the Arg-Gly-Asp Recognition Site in Proteins Involved in Cell-surface Adhesion.** *European Journal of Biochemistry.* 178, pp.141-154.

Ruoslahti, E., Vaheri, A. 1974 **Novel Human Serum Protein from Fibroblast Plasma Membrane.** *Nature (London).* 248, pp.789-791.

Ruoslahti, E., Vaheri, A., Kuusela, P., Linder, E. 1973 **Fibroblast Surface Antigen: A new Serum Protein.** *Biochimica et Biophysica Acta.* 322, pp.352-358.

Rouslahti, E. 1996 **RGD and Other Recognition Sequences For Integrins.** An*nual Review of Cell and Developmental Biology.* 12, pp.697-715.

Roy, D. M. and Linnehan, S. K. 1974 **Hydroxyapeptite Formed from Coral Skeletal Carbonate by Hydrothermal Exchange.** *Nature: Letters to Nautre*. 247, pp.220-222.

Saligo, C. and Muller, A. E. 1999 **Nails and Claws in Primate Evolution.** *Journal of Human Evolution.* 36, pp.97-114.

Sauberlich, S., Klee, D., Richer, F-J., Hocker, H., Spiekermann, H. 1999 **Cell Culture Tests for Assessing the Tolerance of Soft Tissue to Variously Modified Titanium Surfaces.** *Clinical Oral Implant Research.* 10, pp.379-393.

Schmalz, T., Blumentritt, S., Jarasch, R. 2002 **Energy Expenditure and Biomechanical Characteristics of Lower Limb Amputee Gait: The Influence of Prosthetic Alignment and Different Prosthetic Components.** *Gait and Posture.* 16, pp.255- 263.

Schroeder, A., *van der Zypen, E., Stich, H., Sutter, F.*1981 **The Reactions of Bone, Connective Tissue, and Epithelium to Endosteal Implants with Titanium- Sprayed Surfaces.** *Journal of Maxillofacial Surgery.* 9, pp.15-25.

Schultz, P., Vautier, D., Charpiot, A., Lavalle, P., Debry, C. 2007 **Development of Tracheal Prostheses made of Porous Titanium: a Study on Sheep.** *European Archives of Otorhinolaryngology.* 264, pp.433–438.

Sedgwick, P. 2012 **Multiple Significance Tests: the Bonferroni Correction**. *British Medical Journal.* 344(e509)

Sheez

Shin, H., Jo, S., Mikos, A. G. 2003 **Biomimetic Materials for Tissue Engineering: Review**. *Biomaterials.* 24, pp.4353–4364.

Singer, I. I., Scott, S., Kawka, D. W., Kazazis, D. M., Gailit, J., Ruoslahti E. 1988 **Cell Surface Distribution of Fibronectin and Vitronectin Receptors Depends on Substrate Composition and Extracellular Matrix Accumulation.** *The Journal of Cell Biology*. 106, pp.2171-2182.

Simmons, C. A., Valiquette, N., Pilliar, R. M. 1999 **Osseointegration of Sintered Porous-surfaced and Plasma Spray–coated Implants: An Animal Model Study of Early Postimplantation Healing Response and**

Mechanical Stability. *Journal of Biomedical Material Research.* 47, pp.127–138.

Soligo, C., Muller, A. E. 1999 **Nails and claws in primate evolution.** *Journal of Human Evolution.* 36, pp.97–114.

Squier, C. A., Collins, P. 1981 **The Relationship Between Soft Tissue Attachment, Epithelial Downgrowth and Surface Porosity.** *Journal of Peridontal Research.* 16, pp.434-440.

Stoker, M., O'Neill, C., Berryman, S., Waxman, V. 1968 **Anchorage and Growth Regulation in Normal and Virus-Transformed Cells.** *International Journal of Cancer.* 3, pp.683-693.

Sullivan, J., Uden, M., Robinson, K. P., Soorriakumaran, S. 2003 **Rehabilitation of the Trans-femoral Amputee with an Osseoinegrated Prostheis: The United Kingdom Experience.** *International Society for Prosthetcis and Orthotics*. 27, pp.114-120.

Suzuki, S., Oldberg, A., Hayman, E. G., Pier-Schbacher, M. D., Ruoslahti, E. 1985. **Complete amino Acid Sequence of Human Vitronectin Deduced from cDNA. Similarity of Cell Attachment Sites in Vitronectin and Fibronectin.** *European Molecular Biology Organization Journal.* 4, pp.2519–2524.

Takahashi, S., Leiss, M., Moser, M., Ohashi, T., Kitao, T., Heckmann, D., Pfeifer, A., Kessler, H., Takagi, J., Erickson, H. P., fassler, R. 2007 **The RGD Motif in Fibronectin is Essential for Development but dispensable for Fibril Assembly.** *The Journal of Cell Biology.* 178(1), pp.167-178.

Taylor, D. F. and Smith, F. B. 1972 **Porous methyl methacrylate as an Implant Material.** ***Journal of Biomedical Materials Research.*** **6(1)**, **pp.467–479.**

Thurston, A. 2007 **Pare and prosthetics: the early history of artificial limbs.** *ANZ Journal of Surgery.* 77(12), pp.1114-1119.

Truskey, G. A. and Pirone, J. S. 1990 **The Effect of Fluid Shear Stress Upon Cell Adhesion to Fibronectin-Treated Surfaces.** *Journal of Biomedical Materials Research.* 24, pp.1333-1353.

University College London. 2013 **UCL Safety Services, Ionizing Radiations.** [ONLINE] http://www.ucl.ac.uk/estates/safetynet/guidance/radiation/ionising/index.htm

University College London. 2013 **UCL School of Life and Medical Sciences: Statement on the Uses of Animals in Research.** [ONLINE] http://www.ucl.ac.uk/slms/research/animal-use

Unwin, N. 2000 **Epidemiology of lower extremity amputation centres in Europe, North America and East Asia.** *British Journal of Surgery.* 87(3), pp.328-337.

Van Ness, J., Kalbfleisch, S., Petne, C. R., Reed, M. W., Tabone, J. C., Vermeulen, N. M. J. 1991 **A Versatile Solid Support System for Oligodeoxynucleotide Probe-based Hybridization Assays.** Nucleic. Acids Research. 19 (12), pp.3345-3350

Van Noort, R. 1987 **Titanium: The Implant Material of Today**. *Journal of Material Science.* 22, pp.3801-3811.

von Recum., A. F. 1984 **Applications and Failure modes of Percutaneous Devices: A Review.** *Journal of Biomedical Material Research.* 18, pp.323-336.

Vrana, N. E., Dupret, A., Coraux, C., Vautier, D., Debry, C., Lavalle, P. 2007 **Hybrid Titanium/Biodegradable Polymer Implants with an Hierarchical**

Pore Structure as a Means to Control Selective Cell Movement. *Public Library of Science.* 6(5), pp.1-10.

Vroman, L., Adams, A. L., Fischer, G. C., Munoz, P. C. 1980 **Interaction of High Molecular Weight Kininogen, Factor XII, and Fibrinogen in Plasma at Interfaces.** *Blood.* **55**(1), pp.156–159.

Walboomers, X. F., Monaghan, W., Curtis, A. S. G., Jansen, J. A. 1999 **Attachment of Fibroblasts on Smooth and Microgrooved Polystyrene.** *Journal of Biomedical Material Research.* 46, pp.212–220.

Wallace, D. 2012 **Trends in traumatic limb amputation in allied forces in Iraq and Afghanistan.** *Journal of Military and Veterans Health*. 20(2), pp.31-35.

Webster, J. B., Levy, C. E., Bryant, P. R., Prusakowski, P. E. **2001 Sports and Recreation for Persons with Limb Deficiency.** *Achieves of Physical Medicine and Rehabilitation.* 82(3,1), pp.S34-S38.

Weiss, P. 1945 **Experiments on the Cell and Axon Orientation *In Vitro* The role of Colloidal Exudates in Tissue Organisation.** *Journal of Experimental Zoology.* 100, pp.353-386.

Wen, C. E., Yamada, Y., Shimojima, K., Chino, Y., Asahina, T., Mabuchi, M. 2002 **Processing and Mechanical Properties of Autogenous Titanium Implant Materials.** *Journal of Materials Science: Materials in Medicine.* 13, pp. 397-401.

Werner, S., Huck, O., Frisch, B., Vautier, D., Elkaim, R., Voegel, J-C., Brunel, G., Tenenbaum, H. 2009 **The Effect of Microstructured Surfaces and Laminin-derived Peptide Coatings on Soft Tissue Interactions with Titanium Dental Implants.** *Biomaterials.* 30(12), pp. 2291–2301

Wilson, C. J., Clegg, R. E., Leavesley, D. I., Pearcey, M. J. 2005 **Mediation of Biomaterial–Cell Interactions by Adsorbed Proteins: A Review**. *Tissue Engineering.* 11(1/2), pp.1-18.

Winter. G. W. 1974 **Transcutaneous Implants: Reactions of the Skin-Implant interface.** *Journal of Biomedical Material Research Symposium.* 5(1), pp.99-113.

Xu, J., Clarke, R. A. F. 1996 **Extracellular Matrix Alters PDGF Regulation of Fibroblast Integrins.** *The Journal of Cell Biology.* 132(1&2), pp.239-249.

Yamada, K., Yamada, S., Pastan, I. 1976 **Cell Surface Protein Partially Restores Morphology, Adhesiveness, and Contact Inhibition of Movement to Transformed Fibroblasts.** *Proceedings of the National Academy of Science of the USA*. 73(4), pp.1217-1221.

Yamada, K. M. and Kennedy, D. W. 1984. **Dualistic Nature of Adhesive Protein Function: Fibronectin and its Biologically Active Peptide Fragments can Autoinhibit Fibronectin Function.** *Journal of Cell Biology.* 99, pp.29–36.

Yang, Y., Cavin, R., Ong, J. L., 2003 **Protein Adsorption on Titanium Surfaces and their Effect on Osteoblast Attachment.** *Journal of Biomedical Materials Research.* 67A(1), pp.344–349.